Facing Global Warming for Water Resources in Semi-Arid Areas

Essaouira coastal zone case study in Morocco

Mohammed BAHIR

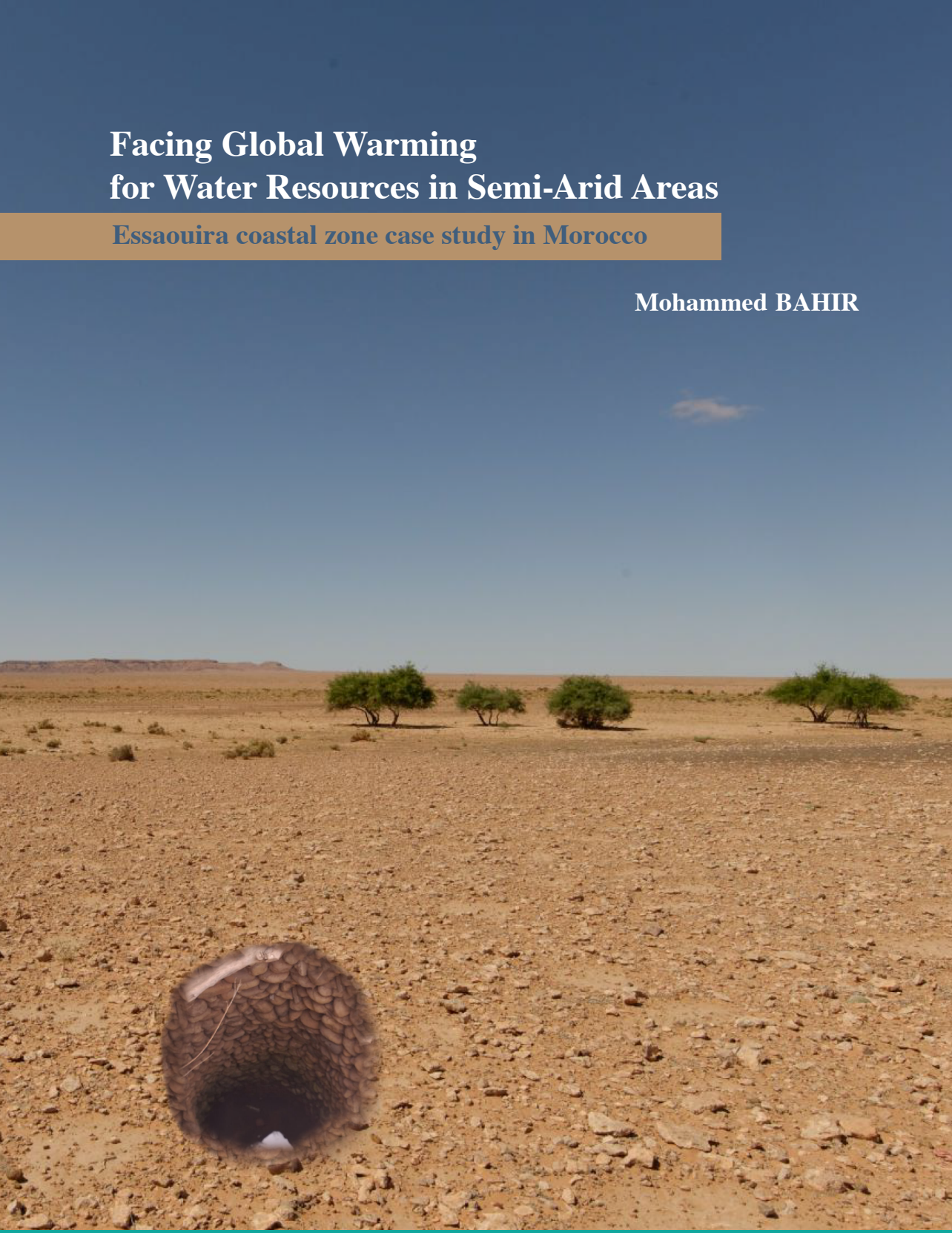

Photo première page de couverture :
http://atlas-sahara.org/milieux/daya/daya.html?cat=milieux
Puits : crédit M. Mohammed BAHIR

Facing Global Warming for Water Resources in Semi Arid Areas

A case study in a coastal zone of Morocco

Académie Hassan II des Sciences et Techniques
Km 4, Avenue Mohammed VI (ex Route des Zaers)
Rabat, Royaume du Maroc

Dépôt Légal : 2022MO4654
ISBN : 978-9954-716-20-5

Réalisation : **AGRI-BYS S.A.R.L.**

Achevé d'imprimer : novembre 2022
Imprimerie ELP Print

Mohammed Bahir

Facing Global Warming for Water Resources in Semi Arid Areas

A case study in a coastal zone of Morocco

Preface

Water is a fundamental constituent of life and is required for a wide range of economic activities. Unfortunately, this is also a limited resource, as it is frequently reminded by the tragic effects of droughts. Over-use and exploitation, and mismanagement of water have created severe constraints on its availability aggravated by the accelerating demand on freshwater.

Groundwater in particular plays an important role of water supply for drinking, agricultural and industrial purposes, exclusively in the arid and semi-arid regions.

Hydrogeological systems differ greatly due to the complex geological formations, environmental, and climatic variations. They are very often extremely complex to understand and hence, the characterization and assessment of aquifer systems can be a very time-consuming process. Improved monitoring is playing a crucial role for establishing the evidence base to support groundwater overall management.

Assessment and monitoring of groundwater quality is by no means a trivial task, as the resource:

- is often distributed over tens to hundreds of meters below our feet.
- is heavily depends on the geological formations whose structure conditions their dynamics.
- Its renewal period can range from a few months for water tables with low reserves and high flow rates to several thousand years for deep, quasi-fossil water tables.
- its dynamics timescale is ranging from a few years to millennia.
- is threatened by many potentially polluting activities.
- is deteriorating due to contaminant loading from the land surface.

Leading to high monitoring difficulties for the specification of appropriate management and protection measures and for their effectiveness.

The author of this book Prof.Dr.Eng. Mohamed Bahir, expert in the field, has been striving for more than a decade to collect state-of-the-art information on the Essaouira basin, providing further stimulation to the work of all stakeholders involved in the huge challenges of sound groundwater management.

This book first of a series dedicated to water resources issues, within the framework of the Science and Technology of Environment, Earth and Sea College of Hassan II

Academy of Science and Technology is devoted to groundwater monitoring and management within a semi-arid basin in Morocco.

Morocco has experienced long and unusual periods of droughts, with a dramatic drop piezometric levels, the drying up of many sources, the reduction of Wadi's flows, and saltwater intrusion to some extent.

Through the Plio-quaternary aquifer of Essaouira basin, one of the most important basins of Morocco; containing 10% of the total aquifer at the national level (8 aquifers over 80), the author is developing a rational methodology for improving the management of water resources within the context of semi-arid climate and in terms of climate change, and vulnerability to potential seawater intrusion.

One of the main objectives is to understand the main process controlling groundwater mineralization. High salinity contents occurring from evaporated mineral dissolution (halite, gypsum, and anhydrite), agricultural and industrial activity, evaporation phenomenon and climate change are also examined. A detailed geochemical study was carried out for years to understand the whole groundwater dynamics.

The logical sequence of the book is described through:

– Introduction: The author gives a general overview of this so-called hidden asset i.e. groundwater in the world with a focus for Morocco providing an insight into stakeholder's involvement in water resources management.

– Evolution of historical and future precipitations and temperatures within Essaouira basin under climate change effect: The analysis consisted in the treatment of (i) climatic parameters (temperature and precipitation), (ii) groundwater level, salinity, (iii) isotopic composition of groundwater. The author carefully described the data issues, statistical tools and tests, hydrologic models, methods, and climate scenarios according to IPCC studies.

– Assessment the climate change impact on the past and future evapotranspiration and flows from a semi-arid environment: the Essaouira Basin is experiencing a decrease in precipitation because of climate change. As flows and rainfalls within these basins are causally related, the investigations aimed to evaluate the climate change impact on the hydrological regime within the Essaouira basin for the period 2020-2050.

– Groundwater level evolution: The drop in water level varies between 5 and 17 meters and this decline in the piezometric level could be explained by the decrease in precipitation during the last decades because of climate change and by over-exploitation to meet the drinking water needs.

– Quantitative and qualitative assessment of groundwater in semi-arid zones in the context of climate change, example of Essaouira region, morocco: The study of the spatio-temporal evolution of the groundwater quality in the area shows a gradual

deterioration in time and space. In addition, the Essaouira basin is more vulnerable to climate change because its recharge is entirely dependent on meteoric waters.

– Behavior of the isotopic signature of groundwater facing climate change within a semi-arid environment: The correlation between the deuterium and oxygen-18 contents of the groundwater of the Cenomanian-Turonian and Plio-Quaternary aquifer highlighted that the recharge of these waters is ensured by the precipitations of Atlantic origin without significant evaporation.

– Seawater intrusion into coastal aquifers in semi-arid environments, Case study of the alluvial aquifer of Essaouira basin: The crossing of the different results obtained provide clearer information on the origin of the groundwater salinization in the study area. This intrusion is probably caused by the decline in the piezometric level due to the decrease in precipitation.

– Conclusions and perspectives: The deterioration of water quality in recent decades is a result of climate change and by over-exploitation. Ionic ratios and use of stable isotopes show a significant marine intrusion, and this intrusion is probably caused by the decline in the piezometric level due to the decrease in precipitations. Furthermore, stable isotopes approach highlights that the recharge of Essaouira basin is ensured by precipitations of Atlantic origin without significant evaporation. The region of Essaouira, on the Atlantic coast of Morocco, illustrates the multiple problems encountered in semi-arid zones. To manage these groundwater resources, decision-makers must solve these problems by building hillside dams, mixing desalinated seawater with the available resource and reusing treated wastewater.

This book is firmly based, well-illustrated and contains a blend of professional practice and scientific information, and an ideal reference methodology work for those undertaking fieldworks. It is more than opportune, as it will serve as a detailed guide for water-sector professionals on the methodology and practice of groundwater quality assessment and monitoring at the level required by regulations if any.

This book can also serve to students, engineers and professionals, researchers within geoscience, environmental science, geological engineering, and civil engineering interests.

Driss Ouazar,
Professor of Water Resources Engineering
Resident member, Hassan II Academy of Science and Technology

Contents

This book first of a series dedicated to water resources issues, within the framework of the Science and Technology of Environment, Earth and Sea College of Hassan II Academy of Science and Technology is devoted to groundwater monitoring and management within a semi-arid basin in Morocco.

Introduction

Groundwater is the main commodity/source of water supply for drinking, agricultural and industrial purposes, exclusively in the arid and semi-arid regions of many countries. Globally, 65% of groundwater is used for drinking purposes, 20% for irrigation and livestock, and 15% for industry and mining. As an important water resource, groundwater has a series of advantages over surface water, i.e. having a wide distribution, good stability, natural regulation, good water quality and not easy to be contaminated. However, groundwater also has some disadvantages for exploitation, such as being more difficult to be accessed than surface water due to being buried underground, and requiring full understanding of the distribution rules prior to use. In recent decades, however, with the continuous development of cities and the continuous improvement of life quality, the demand for groundwater resources is increasing and groundwater resources are facing greater pressure than ever. The groundwater that feeds 2.5 billion people on Earth is in danger of drying up, according to a study recently published in "Science" by two researchers at the University of California, Santa Barbara. "Up to 20 percent of the world's wells are no more than five meters below the water table. This means that millions of them could dry up if groundwater levels drop due to global warming or over-abstraction," says Debra Perrone, co-author of the analysis.

In Africa, there are about eighty transboundary river and lake basins, and at least forty transboundary aquifer basins. The Africa Water Vision 2025 points out that groundwater is the main, and often the only, source of drinking water for more than 75% of the African population. Groundwater constitutes more than 95% of Africa's freshwater resources, and the pollution and salinization of this resource is often irreversible on a human scale.

In North African arid/desert lands, groundwater (depth > 500 m) is the only source of water supply for most of the local demand (agricultural, industry, tourism, and domestic). Just like most of the countries in the world, the populations in southern Mediterranean countries live under water stress (< 450 l/person/year), defined as those using more than 20% of their renewable water resources, while the withdrawal of over 40–50% mean serious water stress. Currently the ONU estimates that in 2025,

25 African countries are expected to suffer from water scarcity or water stress. Also, according to UNEP (2006, 2010, 2011), about 1100 million people do not have access to clean drinking water (surface and/or groundwater), and contaminated water is the direct cause of 5 million deaths every year, most of them occurring in sub-desertic Africa.

At the national level, water issues, especially groundwater salinization, has become the center of interests of scientific researchers and managers. It has been raised by several studies across the country. Morocco, like the Mediterranean countries, have suffered from several periods of drought since the beginning of the 1980s of the previous century. Its water resources are limited; they are estimated at 20 billion cubic meters, or an average of 700 m3/year/inhabitant, which corresponds to a situation of fairly high water stress. The number of years in rainfall de!cit is greater than the number of wet years, with a general downward trend of 23%.

One of the most important aquifers in Morocco, according to its extension and its location is the Plio-quaternary aquifer of the Essaouira basin, located in the western of the kingdom. In order to assess the quality evolution of this vital resource, especially groundwater, within areas under semi-arid climate and in terms of climate change, the Essaouira basin is used as an example. In last decades, this basin has experienced a succession of drought periods leading to a degradation of their groundwater quality. The Essaouira basin is one of the most important basins of Morocco; it contains 10% of the total aquifer at the national level (8 aquifers out of 80). Therefore, to improve the management of water resources in these regions, it is important to understand the main process controlling groundwater mineralisation. The coastal aquifers, especially shallow aquifers, are often vulnerable to the seawater intrusion. Not only is seawater mixing responsible for degradation of water resources, but also the high salinity encountered may come from evaporated mineral dissolution (halite, gypsum, and anhydrite), agricultural and industrial activity, evaporation phenomenon and climate change. The Essaouira basin, part of the Atlantic coast of Morocco, was selected for a geochemical study that will be discussed in the present work. Inhabitants of Essaouira basin mostly depend on groundwater as their main source of water supply and for irrigation. The findings of this study will be very useful to improve management strategies to protect scarce groundwater resources in the region, as well as to deepen the knowledge on the status of coastal aquifers in the in the Atlantic basin.

Morocco has experienced in recent decades fairly long and unusual periods of drought until then, which have resulted in generalized drops in especially free piezometric levels, the drying up of many sources, and the reduction in wadi's flows. The mobilization of the resource has reached its limits and the best locations for the dams are already used. In this context, it will be more and more difficult to mobilize

the resource and meet an ever-increasing demand. This is the end of the system said "OFFERTA (OFFER)" by our Spanish friends.

One of the latest recommendations from the Higher Council for Water and Climate, stipulates that groundwater reserved as a priority for drinking water supply, will become difficult to achieve in the future, due to recharging of bad to worst water quality as a result of water stress and wastewater discharges into the surrounding environment of major urban and rural settlements.

The potential of groundwater resources is estimated to 4x109 cubic meters and distributed over approximately 80 surfaces and deep aquifers of the nine basins in the country, regularly monitored by the Hydraulics Directorate and the National Water Office. Cadi Ayyad University is working on a certain number of basins, including that of Essaouira, in consultation with the public authorities. This is the main subject of this book.

Groundwater is part of both the water cycle and the subsoil. They are linked to surface water and continuously interpenetrate in space and time through infiltration and drainage. They are renewed by a fraction of the rainwater which infiltrates and is subject to the effects of the atmosphere where part of it returns by direct or indirect evaporation.

They are intimately linked to the subsoil of which they are an essential and active constituent. They cannot be considered either as a separate resource or as a natural soil resource comparable to others. They constitute stocks of water and circulating flows like surface water. Their renewal is affected by the infiltration of rainwater, and this supply maintains its flow rate.

Their distribution in space, is much more continuous than that of surface water, and heavily depends on the geological formations whose structure conditions their dynamics.

Thus, groundwater flows very slowly and offers great inertia. If on the surface, water flows at speeds of the order of m3/s, in the subsoil, on the other hand, the speed varies depending on the case from a few meters per day in porous media, to around ten kilometers per day in cracked environments. The renewal period can range from a few months for water tables with low reserves and high flow rates to several thousand years for deep, quasi-fossil water tables.

While a surface water reserve can take a few days or at most a few months to fill and/or empty, for an underground reserve, these times are expressed in years, with a few more seasonal "sub-fluctuations". Taking into account previous criteria the recharge of the aquifer allows for long-term management.

The groundwater resource is both a relative and multidimensional concept (Castany 1982):

- Relative to the space scale, the reference period and the evaluation criteria
- Multidimensional because it is expressed in terms of flow, stock, renewal regime, quality, access and cost conditions, and internal and external constraints to the system.

At the physical level, the first characteristic that is specific to groundwater is the coexistence of flow and stock, and consequently impacts specifically the distribution between renewable and non-renewable resources. The respective assessments of these two terms depend both on natural conditions and socio-economic objectives of water use.

On the socio-economic level, the user's concern boils down to the production of catchment works including the local resource, the exploitation and conservation of which unfortunately take precedence over its protection.

At the macroeconomic level, managers place themselves at the regional resource level. They are equipped with technical means of study, evaluation and management, but without direct means of action on groundwater (El Hebil, 1995).

This difference in perception of the resource depending on the level at which one places oneself leads to a distinction between:

- The local resource relating to a catchment or group of catchments as an element ensuring the sustainability of production with an assessed risk of failure.
- The regional potential of an aquifer system as a resource in the economic sense.

Groundwater constitutes in Morocco an important part of the hydraulic heritage because of its geological constitution: sedimentary basins with groundwater and captive water tables (Sous, Tadla, Haouz, Saiss), karstic limestone massifs with large sources (causes of the middle atlas), alluvial valleys with tablecloths closely linked to surface flows (Ziz valley, Draa valley). The country has about fifty surface aquifers and about thirty semi-deeps to deep aquifers.

Estimates based on 40 years of observation give an average of seven and a half billion cubic meters (reduced by a third during the last drought) to the share of infiltrated rainwater contributing to the renewal of groundwater. Slow renewal reserves represent a few billion m3 in stock.

These groundwaters play an important role in socio-economic development. The total withdrawal is estimated to 3 billion cubic meters / year. These samples are taken more and more by pumping to the detriment of gravity flows (Khettaras, springs, emergences). Of these three billion, 85% is intended for irrigation, an average

comparable to the Mediterranean average, or 27% of the water resource used by this sector. On the other hand, groundwater accounts for 55% of drinking and industrial water supply needs.

Between 1970 and 2016, withdrawals more than tripled in certain large aquifers (Fig. 1).

Figure 1

Growth in withdrawals in many times from the large aquifers of Morocco vs. regions

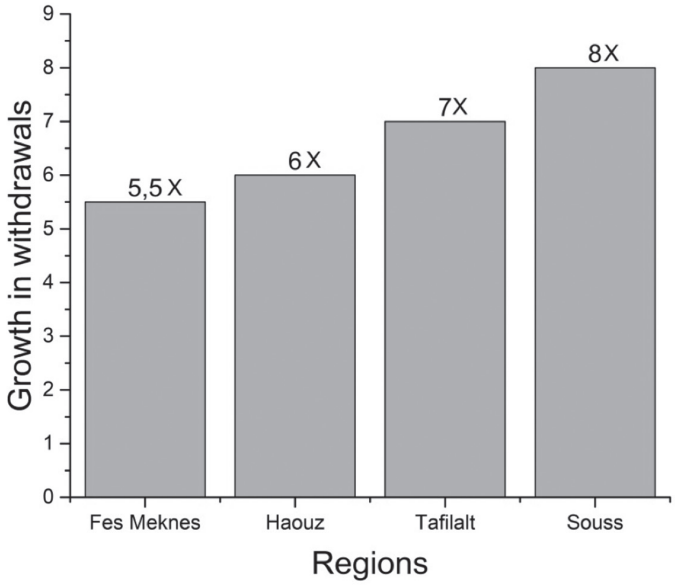

Regardless of any climate change, water management is one of the major issues that condition the future of Morocco. The country is expected to be in a situation of water stress and will find itself in a situation of water scarcity by 2030 horizon, as significant quality problems will arise with erosion, salinization, and pollution.

Climate change could exacerbate the negative impacts of spatio-temporal scarcity and the strong degradation that characterizes water resources on socio-economic development.

An analysis of the change in temperature as well as the temporal variability of rainfall has been carried out in recent decades for several stations by the national meteorology department (Agoumi 1999). It shows a temperature rise of around 2 °C as

well as a very significant drop of about 30% in cumulative precipitation during 1978-1994 compared to the period 1961-1977. The 1994-1995 season was the driest of the century in Morocco (Hassani et al. 1998).

The examination of droughts experienced by Morocco during the twentieth century shows a higher frequency and a greater spatial extension of droughts between 1982 and 2000: five episodes of droughts in Morocco out of the 11th century took place during this period.

Overall, the average annual rainfall over the entire territory is estimated at 150 billion cubic meters, very unevenly distributed over the different regions of the country. About 15% of the area receives more than 50% of the rainfall. Of these usable inputs, rain represents only 20%, or 29 billion cubic meters, including 16 billion from surface water and 4 billion from groundwater.

Given its main characteristic in terms of accessibility and/or supply namely, and its distribution in space, groundwater is subject to an infinite number of operating intervenant.

These very numerous and differentiated economic intervenant have either the legal capacity, or the economic power, or both to directly exploit groundwater.

Thousands of drinking water production units supplying populations in rural and urban areas are subdivided between:

- The National Drinking Water Office (ONEP) responsible for supplying cities and major centers.
- Water distribution boards operating only in urban and peri-urban areas.
- Local communities: 30% of the rural population is supplied by underground water collected by wells and boreholes.

Since 1997, the authorities have delegated the distribution of water to multinationals in large Moroccan cities such as Casablanca, Rabat, and Tangier, due to the increasing cost of infrastructure.

For agriculture, using groundwater, the following statistics are noted as significant indicators (Fig. 2):

Figure 2

Number of pumping stations vs. regions in Km² for agriculture use

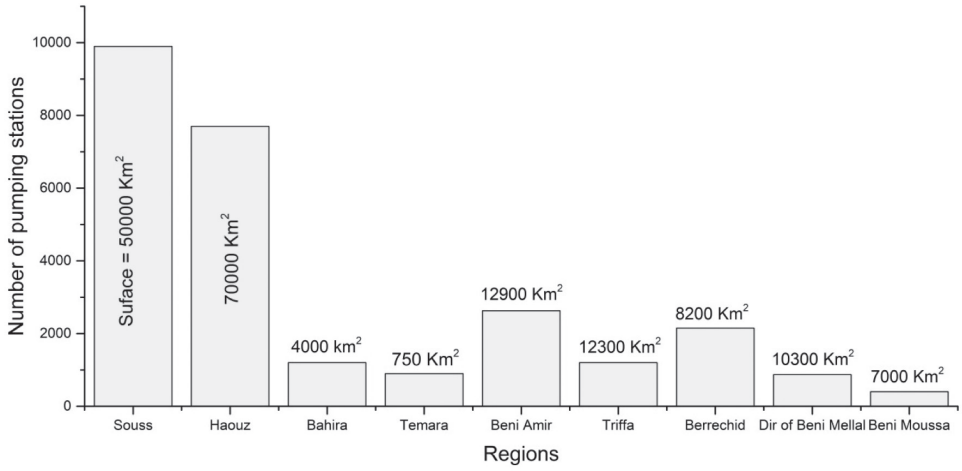

Mining operations also use groundwater either for industrial ore processing purposes or for operating constraints on mineral deposits (dewatering), and phosphate washing.

The signs of the actions of all these agents can interfere, leading to problems of various kinds and magnitudes, but can be summed up in three essential impacts:

– Excessive groundwater drops in intensely exploited sectors (Haouz, Souss, Sahel), leading to decreases in productivity, and increases in production costs
– Current reversal mainly along the coast causing an invasion of marine water and destruction of the hydraulic potential
– Conflicts between usages, mainly between drinking water supply and irrigation.
– Water quality degradation.

On a theoretical level, the groundwater exploitation results in the modification of the state of the water table and its dynamics in a more or less extended space according to the pressures impulses exerted and the nature and parameters of the water aquifer. These modifications affect the water levels (drop), the point flows (decrease in productivity) or the limit flows which can sometimes go as far as the inversion of surface flows towards the subsoil or (vice versa) or between contiguous aquifers, or between seawater and groundwater.

On a concrete level, studies of the history of piezometric changes in water tables monitored for 20 to 35 years show that the state of overexploitation has been reached for several aquifers in the country (withdrawals greater than the renewal contributions).

While in some cases this state is not so alarming, some of the most heavily used or sensitive aquifers are prone to harmful effects such as:

- Drying-up or reduction in the productivity of structures, forcing operators to periodically deepen them and consequently leading to production losses due to insufficient irrigation (case of certain sectors of Souss and Haouz).
- Dewatering of productive levels (case of Temara, Tafilalt, Beni Amir, Beni Moussa, Dir of Beni Mellal).
- The intrusion of marine water in the coastal zone where the swamp is very developed (Case of the Sahel, between Oualidia and Casablanca).
- Drop in the productivity of collective use structures used to supply water, leading to chronic shortages (Imintanout, Essaouira, Jbel Hamra in Oujda, water production field for the cities of Marrakech, Agadir, Oujda, Fez, etc...)

The development of groundwater exploitation is subordinated to the control of available resources, a prerequisite for good management of this heritage. This mastery not only supposes a very in-depth knowledge of the natural physical environment, of the laws and mechanisms that govern their formation and renewal, of their evolution in time and space, but also the identification of all the often existing operations, numerous and diverse and correct forecasting of the evolution of water demand.

The purpose of controlling the resource is to orient and organize both in time and in space "at scales appropriate to the physical conditions of the resource and to the economic conditions of the demands for use" actions development and operation in accordance with the objectives set. And all the parameters that come into play continually require reconsideration due:

- The inherent uncertainties in the inaccuracies of all the measurements necessary for a quantitative approach of the mechanisms governing flows and underground storage
- To climatic hazards
- The lack of knowledge of the samples and the behavior of operating agents.
- The unidentified water demands such as quantity and quality in an urgent way.

The location of the actual exploitation of groundwater is subject to often restrictive conditions: some are linked to the structure of the environment, others to the types of operating structures and finally to the structure of water use.

Hydrogeological conditions are obviously involved by the nature and structure of aquifers and by the distribution of productivities, but also by that of water qualities. But in addition to these conditions, the exploitation of groundwater is subject to economic criteria which also entail constraints:

- Maximum depth deemed acceptable either to reach the reservoir and put it into production (borehole depth), or to pump water, which translates into production costs that must be accepted by the user.
- Limitations imposed on exploitation to minimize the consequences on the flow rates of emergences, on the regime of other catchments, or even other aquifers.
- The operating structures require very different site conditions depending on their type and according to demand.

For groundwater, management is applied across the resource system as a common good offered and determined by natural conditions. This implies a condition between the objectives of exploitation and the objectives of allocation and conservation of the resource in the general interest.

As groundwater is interdependent with surface water, its management is integrated into water management as a whole. It presupposes objectives, stakeholders, and instruments.

Given their scale, the objectives in themselves constitute constraints on the exploitation of groundwater. They are multiple and must be reconciled to:

- Satisfy the demands for underground water in quantity and quality
- Allocate the resource according to priorities
- Keep the potential resource in quantity and quality
- Keep the productivity and accessibility of groundwater, especially when it is intended for collective use
- Intensify the use of the resource deemed to be underexploited.
- Avoid conflict interests between stakeholders

Thus, these management objectives are in the common interest of both users and the community.

The objectives listed above lead to the following question: “the management of groundwater is under whose responsibility?”.

It is the business of managers but still the business of everyone since groundwater is a common good; it is also the business of the state since groundwater is part of the hydraulic domain (1995 Morocco Water Law). It is of interest to those to whom it

offers an accessible resource from which they benefit as well as to those who represent and reconcile multiple and often conflicting interests.

With money and investigation aspects actions are associated. Actions consist in investments for investigations. Direct actions on groundwater are of interest to operators who are numerous and diversified because of:

- The extension of aquifers
- That the operation does not require public utility development like surface reservoirs.
- That the occupants of the land see themselves as "rights holders" over groundwater.

At the level of these farmers, microeconomic objectives predominate. They individually manage their production according to their criteria, but not the resource itself. They are normally united since their actions interfere, but paradoxically do not care much about the effects of their actions which accumulate within the same aquifer system.

On the other hand, the authority emanating from public power or management authority has no means of direct action on groundwater before the promulgation of the water law of 1995. It does not have the appropriate power to intervene. on the behavior of operators. It only intervenes through various traditional indirect management instruments.

This responsibility lies with the Ministry of Public Works, certain powers of which are delegated concerning agricultural water to the Regional Offices for Agricultural Development. Note that Thermo mineral waters are under the responsibility of the Ministry of Energy and Mines.

As for the water law, nine years after its promulgation, stipulating among other things the creation of hydraulic basin agencies, its effective application is still progressing slowly.

In general, three major constraints affect water resources in Morocco: The scarcity of resources, their irregularity in time and space (Nadifi 1998).

Concerning groundwater resources, there are more exactly 32 deepwater tables (depth ranging from 200 m to more than 1000 m) and 48 surface water tables (shallow water level). The former is difficult to access with a high economic cost, the latter is more accessible, but also more vulnerable to pollution and drought, such as the case of the Plio-Quaternary aquifer in the Essaouira basin (Bahir et al. 2001) ensuring the supply of drinking water to the city (198400 inhabitants in 2014) and the surrounding rural agglomerations.

During the last decades, the exploitation of groundwater has continued to grow under the combined effects of demographic pressure, the search for satisfactory food self-sufficiency, industrialization, and the political will for balanced regional development.

This growth is due not only to new drilling techniques and ever more efficient means of dewatering, but also an unfavorable climatic situation leading to an acceleration of groundwater operations to compensate for deficits in surface flow and rainwater.

The combined effects of intensive operating conditions and unfavorable climatic conditions have led to hydrodynamic imbalance regimes which have almost generally caused alarming reductions in reserves (Haouz, Sous, Angads, Tafilalt) and consequently productivity losses of collective or individual collection works, dewatering of traditional works (Khettaras, shallow wells), and reduction in emergence flows.

But one can wonder if these worrying reductions are the result of a provisional state of groundwater and its capacity to regulate and if the more favorable climatic conditions were correcting the broken equilibria. Should we curb and advise against an intensification of these exploitations by freezing this precious natural "capital"? On the contrary, should we encourage, guide, organize the exploitation of groundwater and take actions accordingly for a better valuation of this natural resource while avoiding irreversible disruption of the balance?

It is legitimate for those responsible for the planning and management of water resources, academics, and those responsible for economic development to ask these questions and seek appropriate answers. Be that as it may, and given the level of exploitation of our groundwater, we will agree that a period of rigorous management of these resources, whether renewable or not, is now required, to best adapt quantity, quality, and users in a context where all the natural, socio-economic parameters are not completely mastered, nor controllable. This is what motivated the selection of the Essaouira basin as a case study for both its complexity and fragility.

In arid and semi-arid environments, the precipitations and temperatures are determining parameters for climatic characterization. Studying the evolution of recent climate variability, which is essential for better management of water resources, remains an essential tool for overcoming the problems resulting from the relationship between water needs and their availability.

Climate change is a global phenomenon. In the long term, it involves complex interactions between environmental factors and economic and social conditions,

leading to significant regional effects (Vennetier et al. 2005; Filho 2012; Misra 2014), including the Maghreb (El Kharraz, 2012).

Morocco, like Algeria (Elouissi et al. 2017) and other Mediterranean countries (Nassopoulos 2012; Taabni and El Jihad 2012) have suffered from several periods of drought accompanied by a water shortage. Over the past decades, numerous studies have shown a downward trend in precipitation and an upward trend in temperatures across North Africa (Meddi and Meddi, 2007; Sebbar 2013). Morocco, in particular, has experienced a drop in the average annual precipitation and remarkable warming that began since the late 1970s (Driouech 2010; Babqiqi 2014; Sebbar 2013). The changes in climate parameters mentioned above are not the same for all areas and the intensity should be quantified locally to manage natural resources, in particular water resources.

Due to its geographic location and context, Morocco remains one of the countries most vulnerable to the effects of climate change. The first signs of climate change are already manifesting in changing temperatures and precipitations. The precipitations show an overall fluctuating decrease depending on the region, between 3 and 30% (Babqiqi 2014). Temperatures display an average increase of +0.6 to +1.4 °C depending on the region (DMN 2007). ESCWA (2017) forecasts a reduction in precipitation of 8 to 10 mm/month depending on the scenarios, by the end of the century over Morocco. This reduction is accompanied by an increase in temperature expected to reach 4 °C.

These changes will undoubtedly have harmful effects on the water resource already characterized by scarcity and a spatio-temporal irregularity. HCP (2013) indicates that Morocco would be exposed to move from a situation of water stress (<1000 m3/inhabitant/year) to a situation of water scarcity (<500 m3/inhabitant/year) by the 2030 horizon. This situation requires the rational exploitation of available water resources; its recycling, and the use of water-saving techniques. Existing studies on the assessment of the climate change impact on water resources in Morocco remain very rare, general, and regional. It is therefore essential to move towards local studies, otherwise, on the “hydrological and hydrogeological basins” scale. This makes it possible to specify the effects on this vital resource and to recommend the necessary adaptation measures.

In this context, this book is dedicated to the study of the behavior of water resources within the Essaouira basin facing climate change. To this end, several approaches are used combing climatological, hydrological, piezometric, hydrochemical, and isotopic studies.

Evolution of historical and future precipitations and temperatures within Essaouira basin under climate change effect

Data Issues

1. Introduction

In recent decades, global warming has been a real threat to humanity. Morocco, specifically with an arid and semi-arid climate, remains one of the most vulnerable to the effects of climate change (Boko et al. 2007; Kuriqi 2014; Kuriqi et al. 2016). It is characterized by a spatiotemporal irregularity of rainfall with further decrease towards the south (Driouech et al. 2013; Babqiqi 2014).

The IPCC's Fourth Climate Change Report (IPCC 2007) has shown that Morocco will likely experience a decrease in precipitations that could reach 20% and a rise in temperatures that are expected to reach 2.5 °C to 5.5 °C at the end of the century. However, the global climate models used to date by the IPCC are of low resolution and do not include very precise information on topography, vegetation, and soil. Assessing the impact of climate change on socio-economic sectors such as agriculture and water resources, requires indeed high-resolution climate change scenarios.

Several studies on rainfall in Morocco have shown that the number of years with a rainfall deficit is greater than the number of surplus years, with a general downward trend between 12 to 23% depending on the region (Stour and Agoumi 2009; Driouech 2010; Sebbar et al. 2011; Driouech et al. 2013; Ouhamdouch et al. 2016; Ouhamdouch and Bahir 2017). By comparing the mean annual temperatures over two periods 1971-1980 and 1998-2007, an upward trend with warming varying from 0.3 ° C to 2.5 ° C depending on the region has been observed (Babqiqi 2014; Blunden and Derek 2015; Bahir et al. 2016). This situation makes water resources limited; they are estimated to 20 billion cubic meters corresponding to an average of 700 m3/person/year, which corresponds to a situation of high-water stress.

The main objective herein is to evaluate the groundwater state in a semi-arid environment in Morocco and their relationship with global warming, by taking the Essaouira Basin as an example. In order to achieve this objective, we have analysed and treated the evolution of:

– climatic parameters (temperature and precipitation),
– groundwater level, salinity,
– isotopic composition of groundwater.

The Essaouira Basin is located on the Atlantic coast of Morocco, at the western end of the High Atlas. This Basin occupies an area of 6000 km^2. It includes several aquifer systems belonging to two synclinal units: the Bouabout unit (eastern part of the Basin) and the synclinal unit of Essaouira (western part of the Basin). These two units are separated by the outcrop of the Triassic formations (Tidzi diapir) (Fig. 1).

On the geological and structural framework, the Triassic and Jurassic formations have only very small outcrops and are located in the center of anticlines (Jbel Hadid NW, Jbel Amsitene SW, and diapir Tidzi), while the formations of the tertiary and quaternary occur in the synclinal Basin as depicted in (Fig. 1).

The Triassic formations consist of saliferous red clays, doleritic basalts, and sandstone pelites. The Jurassic formations are composed of carbonate deposits (limestones and dolomites) and marls rich in gypsum and anhydrite. As for the lower Cretaceous, it is formed of marls and limestones with an average thickness of 200m (Duffaud et al. 1966); the middle Cretaceous begins with martian-sandstone deposits of the Aptian with an average thickness of 60 m, followed by pyritic marl of the Albian with a thickness of about 100 m). Marls also dominate the Cenomanian (thickness of about 200 m); they are rich in anhydrites and are interbreed with past some limestone units. These marls constitute the bedrock of the Turonian aquifer with fractured flint, 60 m thick on average. The Cretaceous is completed by dolomitic marls and limestones surmounted by gypsiferous and siliceous gray marls interspersed with Senonian sandstone which separate the two Turonian and Plio-Quaternary aquifers of the synclinal zone of Essaouira (Duffaud et al. 1966).

Tertiary age compression (Souid 1983; Amghar 1995) and distasic tectonics of Triassic and Jurassic age (Duffaud et al. 1966; Souid 1983; Broghton and Trepanier 1993) gave the study area architecture in the form of anticlines and synclines. This architecture allows having several aquifers distributed as follows: In the upstream part, we find aquifers housed in the limestone and dolomitic limestones of the Cenomanian-Turonian. The impermeable base and the roof of the system are ensured respectively by the gray clays of the Lower Cenomanian and the Senonian white marls (Bahir et al. 2007). While in the downstream part, groundwater resources are contained in

two main reservoirs: the Plio-quaternary with marine calcareous sandstone matrix containing phreatic aquifers, and the Turonian which contains a water table quickly captive under the Senonian marls probably in direct contact with the Plio-quaternary on the borders of this structure (Bahir et al. 2007; Jalal et al. 2001).

2. Data and Methods

The climatic data (precipitations and temperatures) used in this work have been made available by the Hydraulic Basin Agency of Tensift (ABHT) (Annex I). Several series of precipitation measurements have also been made available. For the climatic study, the data of the Adamna, Igrounzar and Essaouira stations were used to study the precipitation and only the last two stations were used to study the temperatures, because they are the only ones for which precipitations and temperatures are available. In order for a series of measurements to be usable to study climate change, the observation period must be long enough to represent the climate of the region. According to the World Meteorological Organization (WMO), the observation period should be more than 30 years. The three stations mentioned in our case, above satisfy this criterion for precipitation and for temperatures.

The maximum daily temperatures, daily minimum temperatures and daily precipitations measured during the period 1987-2004 and the period 1978-2011 in the Igrounzar station were used as predictands for this study. The model used in this study is the second-generation Canadian Earth System Model (CanESM2) developed by the Canadian Centre for Climate Modeling and Analysis (CCCma) of Environment Canada. The primary reason behind using this model in this study is that it is the only model that made daily predictor variables available to be directly fed into SDSM (Statistical DownScaling Model). SDSM is a decision support tool for assessing local climate change impacts using a robust statistical downscaling technique.. The CanESM2 outputs were downloaded for three different climate scenarios, viz. RCP 2.6, RCP 4.5 and RCP 8.5, and were used in this study. The RCP 2.6 was developed by the IMAGE modeling team of the PBL Netherlands Environmental Assessment Agency (Thomson, et al. 2011; Wayne 2013). This RCP is representative of the mitigation scenarios which aims to limit the increase of global mean temperature to 2 °C. The important assumption in this scenario is that new energy efficient technologies can be rapidly transferred to all over the world and implement immediately. The RCP 4.5 was developed by the GCAM modeling group at the Pacific Northwest National Laboratory ‘s Joint Global Change Research Institute (JGCRI) in the United States. It is the stabilization scenario (Wayne 2013) in which radiative forcing stabilizes at 4.5 W/m2 in 2100 without ever exceeding that value (Thomson et al. 2011). The major assumptions of this scenario are that the global population reaches a maximum

of more than 9 billion by 2065 and then declines to 8.7 billion in 2100, declines in energy consumption, increase in fossil fuel consumption, substantial increase in renewable energy and large increase in forest area as a mitigation strategy. The RCP 8.5 was developed by Integrated Assessment Framework by the International Institute for Applied System Analysis (IIASA) using MESSAGE model (Thomson, et al. 2011; Wayne 2013).This RCP is representative of high emission scenarios and characterized by increasing GHG emission over time (Riahi et al. 2011).The important assumptions in this pathway are continuous increase in global population reaching 12 billion by 2100, slow income growth with modest rates of technological progress, long-term high energy demand, moving towards coal intensive technologies and high emission in the absence of climate change policies (Riahi et al. 2011).

Beside these, large scale atmospheric variables from National Center for Environmental Prediction (NCEP) and National Center for Atmospheric Research (NCAR) reanalysis project were used for establishing a statistical relationship with the observed station data. CCCma provided the NCEP/NCAR predictor variables in addition to the large-scale atmospheric variables from CanESM2. We selected the same time frame from 1961-2005 and also the same variables from NCEP/NCAR to have consistency with the atmospheric variables available from CanESM2 outputs. Both the CanESM2 output and NCEP/NCAR reanalysis project data (Box_126x_44y) have provided the same set of 26 predictor variables (Table 1) which were downloaded from Canadian Climate Data and Scenarios website (http://ccds-dscc.ec.gc.ca/) and were used for this study. These outputs were then processed by the SDSM and XLSTAT® software to predict climate change in the Essaouira basin during the future period 2018-2050. The SDSM model seems to be the best model of projection of the local climate change (Gagnon et al. 2005; Rashid and Mukand 2012; Parvase et al. 2016).

The selection of predictors for this study requires the use of a combination of the correlation coefficient (R), the coefficient of determination (R^2) and the p-value between them and the predictands (Table 2). After a routine screening procedure for the selection of predictors, the calibration and validation phase take place. The 28 years (1978-2005) series of observation of precipitations and the 18 years (1987-2004) series of observations of temperatures were divided into two groups. For precipitations, the first 22 years (1978-1999) were used for calibration and the remaining 6 years (2000-2005) were used for validation. As for temperatures, the calibration was made over the first 13 years (1987-1999) and the validation was realized over the 5 remaining years (2000-2004). In this study, the SDSM was developed with selected NCEP predictors using annual and monthly sub-models.

For the description of the historical and future temporal series of local climatic parameters, two methods were used: a graphical method based on the analysis of the

evolution of future weighted rainfall index and a statistical method based on the use of the statistical test, viz. Pettitt's test (detection of the break) and Mann-Kendall test (detection of trend). The rainfall index was calculated by the Nicholson method, and the statistical tests have been applied using the XLSTAT® software.

2.1. Rainfall Index (RI)

The rainfall index measures the deviation from the average of the future rainfall series obtained from the SDSM model of the Igrounzar station. The annual rainfall index "RI" is the reduced centered variable of the annual rainfall. It is obtained by the Eq. (1) (Nicholson 1986):

$$RI = \frac{X_i - X_m}{\sigma} \tag{1}$$

where: x_i is the rainfall of the year i; x_m is the series average; and σ is the standard deviation.

To better visualize the interannual fluctuation in the pluviometry, the seasonal variations are eliminated by weighting the annual pluviometric totals through Eqs. (2) to (6) recommended by Assaini (1999):

$$x_t = 0.06x_{(t-2)} + 0.25x_{(t-1)} + 0.38x_{(t)} + 0.25x_{(t+1)} + 0.06x_{(t+1)} \tag{2}$$

where: $3 \leq t \leq (n-2)$; x_t is the total weighted rainfall of the t term; $x_{(t-2)}$ and $x_{(t-1)}$ are the observed rainfall totals immediately preceding the t term; and $x_{(t-2)}$ and $x_{(t-1)}$ are the observed rainfall totals of two terms immediately following the t term.

The weighted rainfall totals of the first two ($x_{(1)}$ and $x_{(2)}$) and the last two ($x_{(n-1)}$ and $x_{(n)}$) terms in the series are calculated as follows:

$$x_{(1)} = 0.54x_{(1)} + 0.46x_{(2)} \tag{3}$$

$$x_{(2)} = 0.25x_{(1)} + 0.50x_{(2)} + 0.25x_{(3)} \tag{4}$$

$$x_{(n-1)} = 0.25x_{(n-2)} + 0.50x_{(n-1)} + 0.25x_{(n)} \tag{5}$$

$$x_{(n)} = 0.54x_{(n)} + 0.46x_{(n-1)} \tag{6}$$

2.2. Pettitt's Test

The Pettitt's test (1979) is a non-parametric test that requires no assumption about the distribution of data. It examines the existence of a break at an unknown moment

in the series from a formulation derived of that by the Mann-Whitney test. This test is more particularly sensitive to a change of average and, if the H0 hypothesis of homogeneity of the series is rejected, it proposes an estimation of the date of break. This test rests on the calculation of the variable UtT defined by Eq. (7):

$$U_{tT} = \sum_{i=1}^{T} \sum_{i=i+1}^{T} Dij \quad (7)$$

where: Dij = –1 if $(x_i - x_j)>0$, $D_{ij} = 0$ if $(x_i - x_j) = 0$, $D_{ij} = 1$ if $(x_i - x_j)>0$.

2.3. Mann-Kendall Test

The Mann-Kendall test (Mann 1945; Kendall 1975) is a non-parametric statistical test used to detect the presence of a linear trend (upward or downward) within a time series. For the series Xi (x_1, x_2... x_n), this method defines the standard normal multi-variable U_{MK} as follows:

$$U_{MK} = \frac{S}{\sqrt{var\,(S)}} \quad (8)$$

Where: $S = \sum_{i=1}^{n-1} \sum_{j=i+1}^{n} sgn(x_j - x_i)$; $var(s) = \frac{n(n-1)(2n+5)}{18}$; and n is the number of data in the series.

In this test, the null hypothesis H_0 "absence of trend" is accepted if the p-value is greater than the alpha significance level. The trend direction is defined by the statistical coefficient of Mann-Kendall "U_{MK}". The trend is upward if $U_{MK} > 0$ and downward if $U_{MK} < 0$.

3. Historical evolution

3.1. Rainfall

Monitoring the average annual rainfall has shown that Essaouira basin is between 300 and 375 mm/year isohyets with an average of 343 mm/year (Fig. 1). These rains consist generally of short and violent thunderstorms and are distributed irregularly throughout the year. The interannual map of isohyets (1975-2004 period) shown in (Fig. 1) are drawn using ABHT data. Generally, this shows that the rainfall increases towards the outside of the basin. This can be explained by the Foehn effect since this basin is located at the foothills of the High Atlas (Western Atlas).

Figure 1

Isohyets map for the period 1978-2004 within Essaouira basin

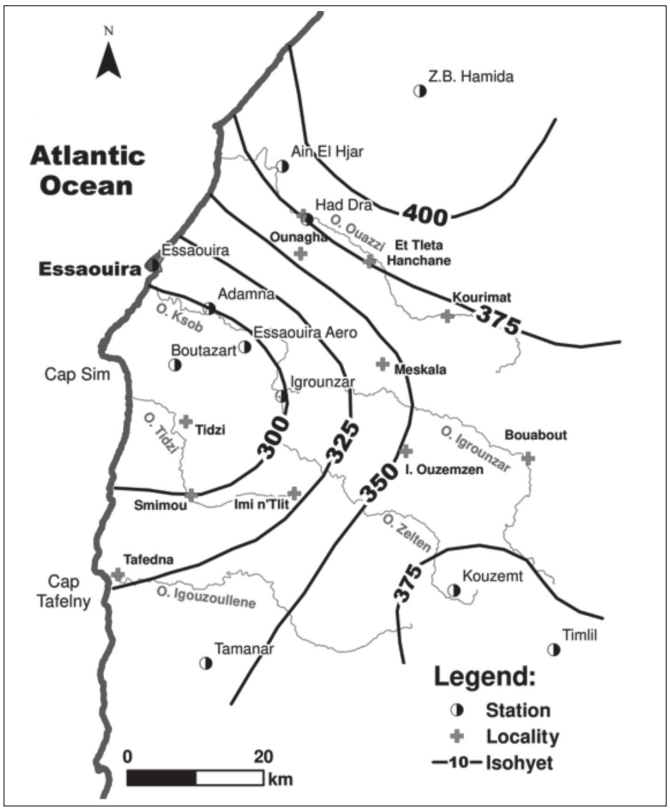

Precipitation is the most important climatic parameter, especially in arid and semi-arid zones. It also constitutes the essential factor of the hydrological regime.

Analysis of rainfall data relating to a 38-year observation period from 1977/78 to 2014/15 for the three stations Igrounzar, Adamna, and Essaouira (Fig. 2), reveals significant variability in the annual scale. Indeed, this rainfall is subject to wide fluctuations from one year to another, with rainy periods and dry periods of two to five consecutive years. The precipitation rate oscillates between a minimum of 98 mm/year, measured at Essaouira station during the hydrological year 2007/08; and a maximum of 758 mm, recorded at Adamna station during the year 1995/96.

The calculation of the standard deviation and the variation coefficient (%) for each station (Table 3) shows that the annual variation coefficient is relatively the same for

the three stations. This is probably due to the small difference in altitude between the three stations.

Figure 2

Analysis of interannual precipitation

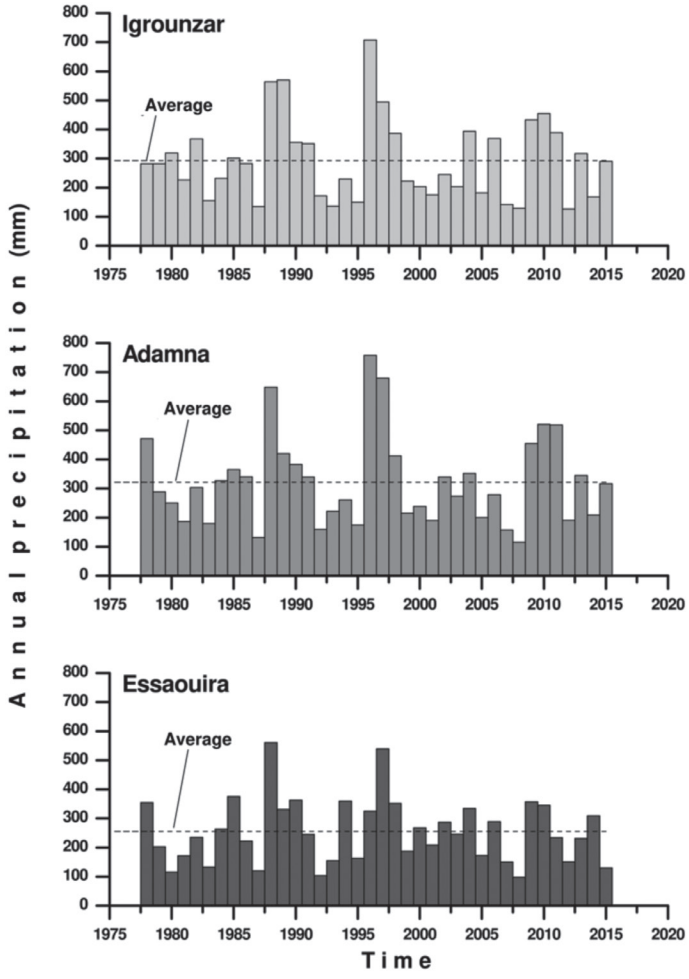

The graphical method based on the analysis of the rainfall indices evolution (reduced centered variable) made it possible to differentiate between a rainy year and dry year. Figure 3a shows the variation in the rainfall indices of the average annual precipitation for the Igrounzar, Adamna, and Essaouira stations. It shows that the

indices are mostly below zero indicating the existence of more dry years than wet years for the three stations. To better visualize the interannual precipitation fluctuation, the seasonal variations are eliminated by weighting the annual rainfall totals through the equations (Eq 2 to 6).

Figure 3

Evolution of (a) rainfall indices and (b) weighted rainfall indices at the Igrounzar, Adamna and Essaouira stations (1978-2015). DP = dry period, WP = wet period, NP = normal period

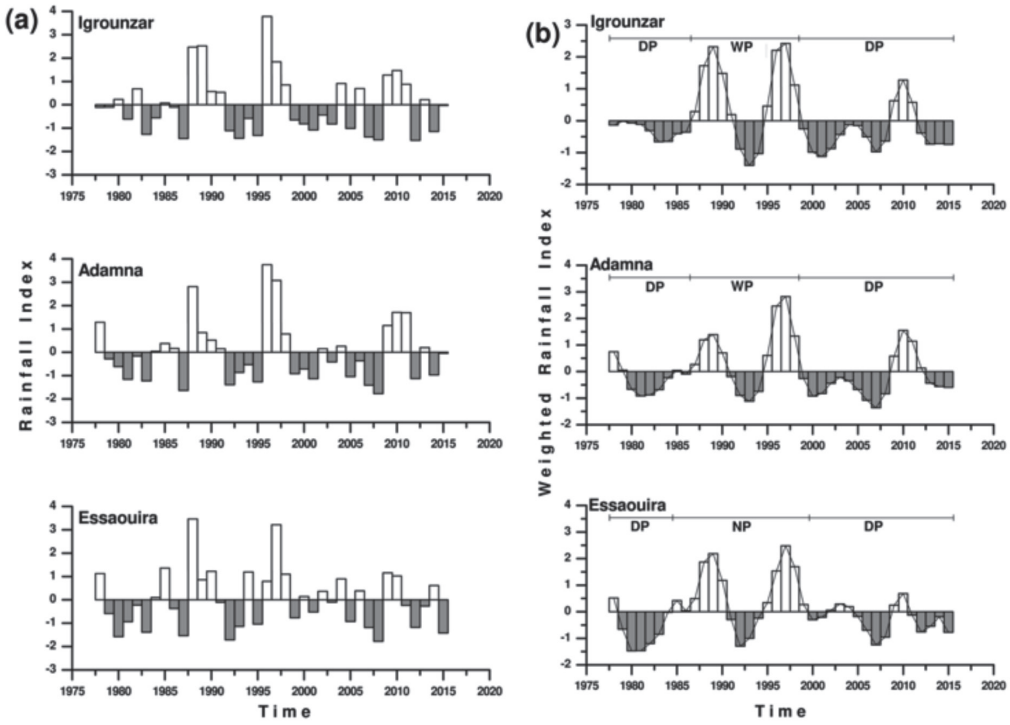

For Igrounzar station (Fig. 3b), the series studied presents a 12 years wet period from 1986/78 to 1997/98 separating two dry periods. The first began in 1977/78 and ended in 1985/86 over 9 years. Regarding the second, it spans 17 years from 1998/99 until 2014/15, the end of the study period.

For Adamna station (Fig. 3b), the weighted rainfall indices evolution shows the same pattern as that observed at Igrounzar station. The wet period began in 1986/87 and ended in 1997/98. For the first deficit period, it spans from the series start until

1985/86, and this over 9 years. Beyond 1998/99, the second deficit period takes place, until the end of the studied series, over 17 years.

At the Essaouira station (Fig. 3b), the same evolution occuring at Adamna and Igrounzar stations was observed at this station with a replacement of the wet period with a normal period and a shortening of the two dry periods. The normal period started in 1984/85 and ended in 1998/99, either 15 years. As for the first dry period, it spans 7 years from the start of the series until 1983/84. Beyond 1999/00, the second dry period takes place until the end of the series, over 16 years.

Generally, the same evolution is observed for the three series of rainfall indices with a remarkable dominance of dry periods over wet periods. To get an idea about the homogeneity and the trend of the rainfall series, we used the conventional robust statistical tests of Pettitt and that of Mann-Kendall trend.

The Mann-Kendall and Pettitt trend test results are reported in Table 4 and Figure 4.

For Igrounzar station, the application of the Pettitt test, with a confidence degree of 90%, reveals the presence of a break in the pluviometric series in 1998/97. The average annual rainfall before and after this break is 313.83 and 263.40 mm, respectively. This allows us to estimate a rainfall deficit of 16.06% and confirms the results obtained by the rainfall index method. The results of the Mann-Kendall trend test (Table 4) show that the calculated multivariable standard normal U_{MK} is less than zero with a value equal to -1.09 reflecting a downward trend in precipitation and confirming the results of the Pettitt test and those of the rainfall indices.

As for the Adamna station, the Pettitt test applied with a 90% confidence level shows the presence of a break in the pluviometric series in 1997/98. The annual average rainfall before and after this break is 342.52 and 292.90 mm, respectively. This allows us to estimate a rainfall deficit slightly lower than that the one calculated for the Igrounzar station and which is 14.48%. The results of this test corroborate the results of the rainfall index technique where long dry spells begin after this break. The Mann-Kendall test applied to the same series shows a downward trend in precipitation (U_{MK} = -0.44) by confirming the results obtained by the Pettitt test and those of the rainfall index.

With an alpha significance level equal to 5%, the Pettitt test applied to the rainfall series observed at the Essaouira station shows the presence of a rupture in 2003/04. The annual average before and after this change is respectively 265.30 and 232.51 mm. The deficit calculated in this time is lower than that estimated for the two stations Igrounzar and Adamna, and represents 12.35%. This deficit confirms the results of the rainfall indices calculated for these series. The Mann-Kendall test applied with a confidence degree equal to 95% shows a downward trend in precipitation observed at the Essaouira station (U_{MK} = -0.24) by confirming the results of the Pettitt test and rainfall index.

Figure 4

Evolution of annual precipitation at the station of Igrounzar, Adamna, and Essaouira (1975-2015)

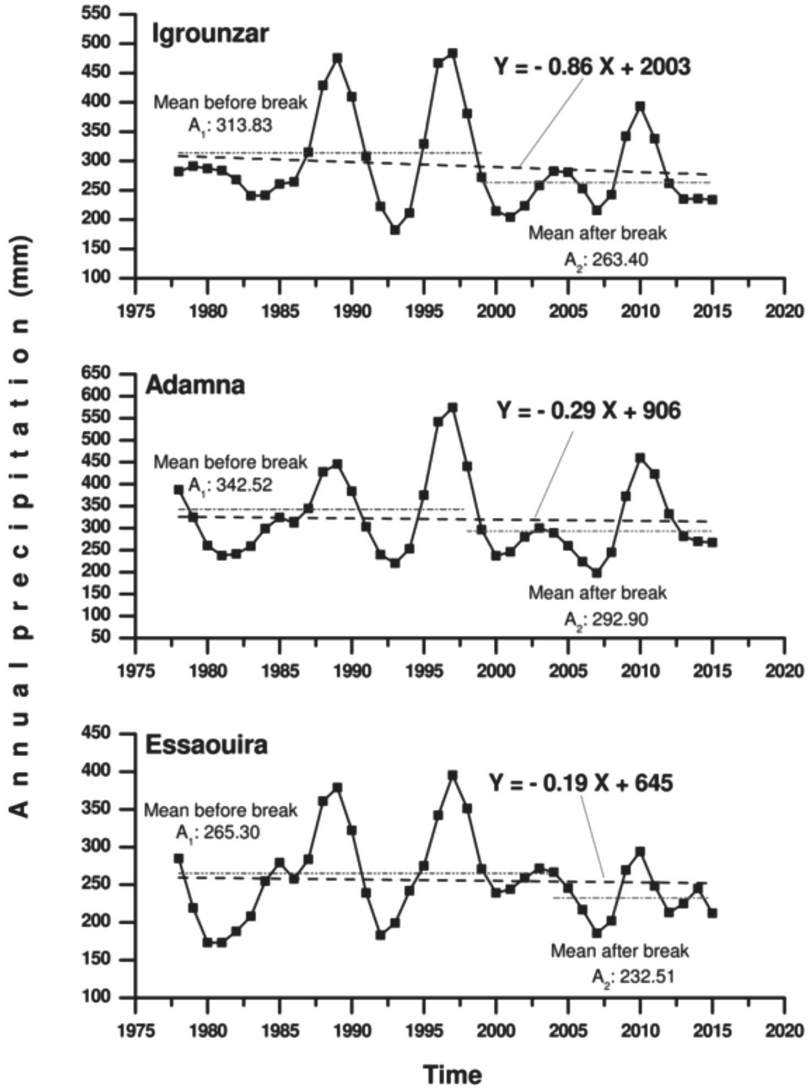

However, the results of the rainfall index and statistical tests allow us to conclude that annual precipitation has a general downward trend with a deficit varying from 12.35 to 16.06% for the study period spanning 1978 / 77 to 2014/15, and this following

the impact of climate change on this parameter. This deficit becomes more and more high going from the ocean towards the continent reflecting the continentality effect on the precipitations. Thus, it can be said that the climate change effect on precipitation becomes more important as it moves away from the ocean.

According to the results of IPCC (2014) and the national study by Babqiqi (2014), the results showed a general downward trend in annual precipitation, following the climate change effect, which is consistent with those obtained in this study.

3.2. Temperature

In this study, we have temperature data from the Igrounzar and Essaouira stations, for 28 years (1987-2014) for Igrounzar and 29 (1987-2015) for Essaouira. For these two stations, a study of the maximum, average, and minimum annual temperatures is presented (Fig. 5 and Table 5).

Figure 5

Annual maximum, mean, and minimum temperatures at the Igrounzar and Essaouira stations

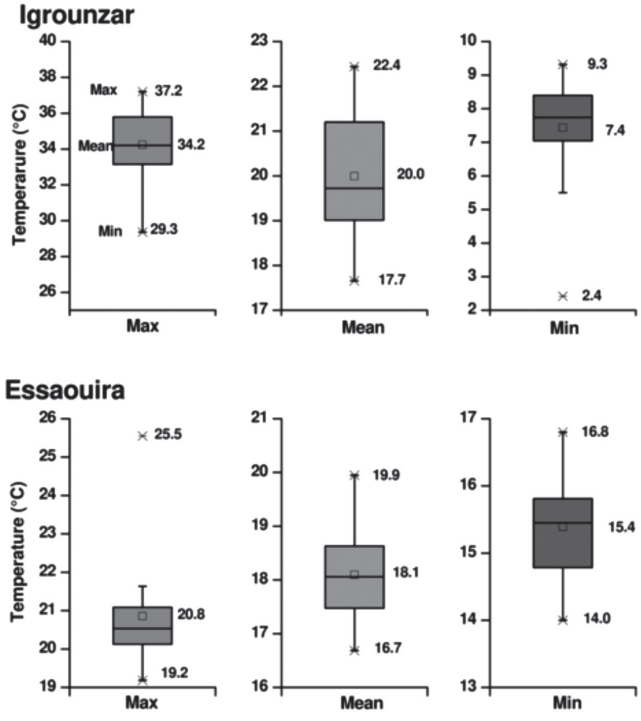

At Igrounzar station, the maximum annual temperatures vary between 29.3 and 37.2 °C, with an average of 34.2 °C. The minimum annual temperatures range between 2.4 and 9.3 °C, with an average of 7.4 °C. While annual average temperatures, they vary between 17.7 and 22.4 °C, with an average of 20 °C. As for the Essaouira station, the maximum annual temperatures range between 19.2 and 25.5 °C, with an average of 20.8 °C. The annual minimum temperatures vary between 14.0 and 16.8 °C with an average of 15.4 °C. While the annual average temperatures, vary between 16.7 and 19.9 °C with an average of 18.1 °C. From these results, it can be seen that the maximum and average annual temperatures recorded at the Igrounzar station are higher than those observed at the Essaouira station. The minimum temperatures show an opposite trend. This could be explained by the effect of the distance to the ocean. The temporal evolution of temperatures was done in two stages, in the first stage we have based the calculation from the deviation from the mean, and in the second stage through a statistical approach. Compared to the average (Fig. 6), the series can be subdivided into two periods; a first with negative anomalies and a second with positive anomalies. Positive anomalies have been observed in recent years, for the maximum, average and minimum temperatures recorded at the Igrounzar station and for the maximum temperatures observed at the Essaouira station. On the other hand, the minimum temperatures recorded in recent years at the Essaouira station show negative anomalies.

Figure 6

Anomalies in annual maximum, mean and minimum temperatures compared to the average at the Igrounzar and Essaouira stations

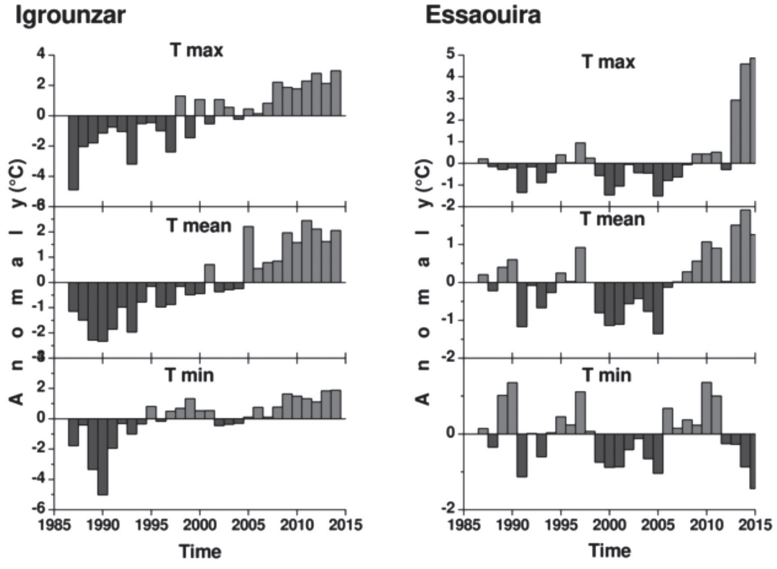

To verify the presence or absence of a trend within the temperature series as well as their meaning, the Pettitt and Mann-Kendall statistical tests were applied and the results obtained are grouped in Figure 7, 8 and Table 5.

For the Igrounzar station, the application of the Pettitt test with a significance level of 5% shows the presence of a significant break in the series of annual maximum, average, and minimum temperatures, in 1999, 2000, and 1994, respectively. The average before and after the break is equal to 32.75 and 35.53 °C for the maximum annual temperatures, either warming of 2.8 °C. As for average annual temperatures, the mean before and after the break is 18.85 and 21.13 °C, respectively, with an increase of 2.3 °C. For the minimum annual temperatures, the means before and after the break are 5.66 and 8.14 °C, meaning a warming of 2.5 °C. This upward trend is corroborated by the Mann-Kendall test with a standard multivariable standard UMK equal to +5.24 for annual maximum temperatures, +5.65 for annual average temperatures, and +4.65 for minimum temperatures annual (Table 5).

Figure 7

Temporal evolution of annual maximum, average and minimum temperatures at the Igrounzar station (1987-2014). A1 = mean before break, A2 = mean after break

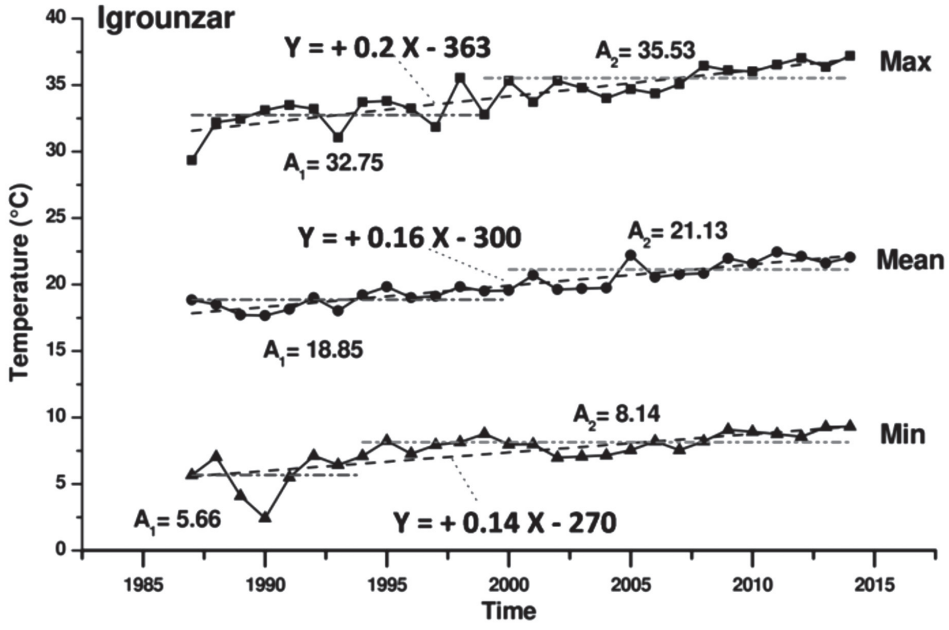

Concerning the Essaouira station, only the series of annual maximum and mean temperatures show a break using the Pettitt test. The series of annual minimum temperatures are homogeneous. For annual maximum temperatures, the means before and after the break are 20.28 and 22.37 °C, with warming of 2.09 °C. As for the annual mean temperatures, the meanq before and after the break are respectively 17.72 and 18.93 °C, i.e. a warming of 1.2 °C. This upward trend is confirmed by the Mann-Kendall test. The calculated UMK equal to +1.72 for the series of annual maximum temperatures and +2.06 for the series of annual average temperatures.

Figure 8

Temporal evolution of annual maximum, average and minimum temperatures at the Essaouira station (1987-2014). A1 = mean before break, A2 = mean after break

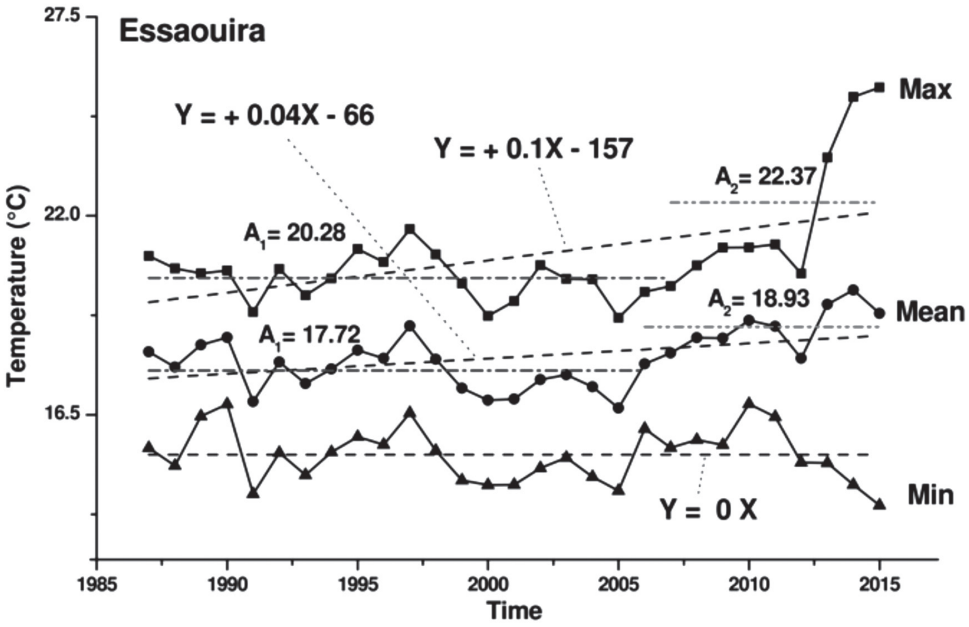

However, the annual temperatures recorded within the Essaouira basin show generally upward trend and this remains perfectly consistent with the upward trend in temperature observed on a national scale (Babqiqi 2014) and worldwide (IPCC 2014).

4. Future evolution

4.1. Selected Predictor Variables

The predictor variables available from NCEP/NCAR reanalysis data were selected for calculating the correlation coefficient (R) following the preliminary analysis of the determination coefficient (R^2) of all the predictor variables. The final set of predictor variables were selected after analyzing the correlation coefficient, and checking the association of predictors and predictands via scatter plots. The dominant predictor variables selected for minimum and maximum mean of temperature were 6 and 26 respectively. Similarly for mean precipitation were 4 and 22 respectively. Minimum and maximum mean temperatures have always higher correlation coefficients ranging from 0.60 to 0.83, 0.60 to 0.90 and 0.59 to 0.83, respectively. For precipitation, these correlation coefficients ranged from 0.60 to 0.78. The list of selected predictor variables, their R, R^2 and p-value for all the climatic variables are given in Table 2. The surface-specific humidity and the surface temperature were most commonly selected predictor variables for maximum and minimum temperature, whereas for precipitation, these are surface precipitation and relative vorticity of wind. The predictor variables selected in this study for temperature and precipitation are common with other studies, such as those by Nigatu (2013) in Ethiopia, Rifai et al. (2014) in Morocco, and Dorji et al. (2017) in Sri Lanka.

4.2. Evaluation, Calibration and Validation

The performance of the SDSM model was evaluated based on different statistical criterias such such as RMSE (Root Mean Square Error), R, R^2 and DW (coefficient of Durbin-Watson) value. The results obtained from these evaluation criteria revealed that the SDSM performed well for downscaling maximum mean and minimum temperature. The lower RMSE and DW value and higher R and R2 value clearly demonstrated the better efficiency of SDSM in simulating the daily temperature data (Table 6).

The RMSE and DW values ranged from 1.68 °C to 3.28 °C and 1.37 to 1.87, respectively, for calibration and validation period of maximum mean and minimum temperature. For precipitation, the RMSE and DW values ranged from 3.37 mm to 4.87 mm and 1.47 to 1.85, respectively. The R and R^2 values ranged from 0.69 to 0.94 for the three temperature variables and 0.67 to 0.85 for precipitation showing better efficiency of SDSM in generating the daily temperatures and precipitations data.

Based on the visual presentations, the simulated maximum and minimum temperature have shown good agreement with the observed data (Fig. 9). The

simulated mean monthly precipitation was able to capture well the observed data but was not able to capture well the rainfall characteristics, such as the mean wet and dry-spell length. However, the results can be considered as satisfactory for simulating future data, as several other studies have pointed out similar discrepancies between simulated and observed precipitations and still moved forward using the model for downscaling future data despite of these discrepancies (Chen et al. 2012; Fiseha et al. 2012; Zulkarnain et al. 2014).

4.3. Projection of Temperature and Precipitation

The climate projections of this study were based GCM model CanESM2 which is one of the participating models in CMIP5. This study used three scenarios, i.e., RCP 2.6, 4.5 and 8.5, which were used in IPCC 5th Assessment Report. The weighting is a technique allowing to visualize better the periods of deficit and excess precipitation.

Figure 9

Validation of SDSM performance for precipitation (a) Maximum (b) mean (c) and minimum (d) temperatures by comparing monthly mean for observed and simulated data for the period of 2000-2005

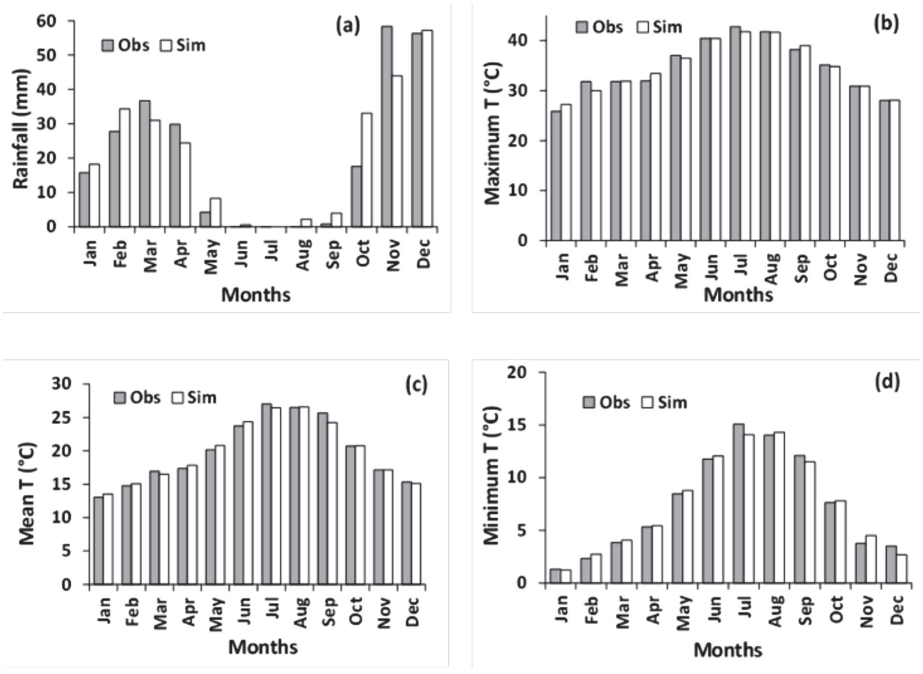

4.3.1. Temperature Variables

For the same period, the annual maximum, average and minimum temperatures show an upward trend for the three scenarios RCPs 2.6, 4.5 and 8.5. By the end of the study period (middle of the century), the maximum temperature will increase by 1.26 °C, 1.32 °C and 1.51 °C for Essaouira basin under the RCPs 2.6, 4.5 and 8.5 scenarios, respectively (Fig. 10). Alike the maximum temperature, the projection showed the increasing trend of the mean temperature. The average annual increase will be 0.72 °C, 0.57 °C and 0.69 °C under the RCPs 2.6, 4.5 and 8.5 scenarios, respectively. Similarly for the minimum temperature, there will be an increase by 0.67 °C, 0.60 °C and 0.63 °C under the RCPs 2.6, 4.5 and 8.5 scenarios, respectively. This increase is confirmed by the Mann-Kendall trend test whose results are reported in Table 7. The maximum increase under the RCP 8.5 compared to the RCP 4.5 scenario is also true based on the storylines of the scenarios where RCP 8.5 is considered as the emission scenario featured by increasing greenhouse gases (GHGs) emission (Riahi et al. 2011) and RCP 4.5 considered as the stabilization scenario which assumes generally less emission than RCP 8.5 (Thomson et al. 2011).

Figure 10

Annual variation of the future maximum (a) mean (b) and minimum (c) temperature under RCP 2.6, 4.5 and 8.5 scenarios for the period 2018-2050

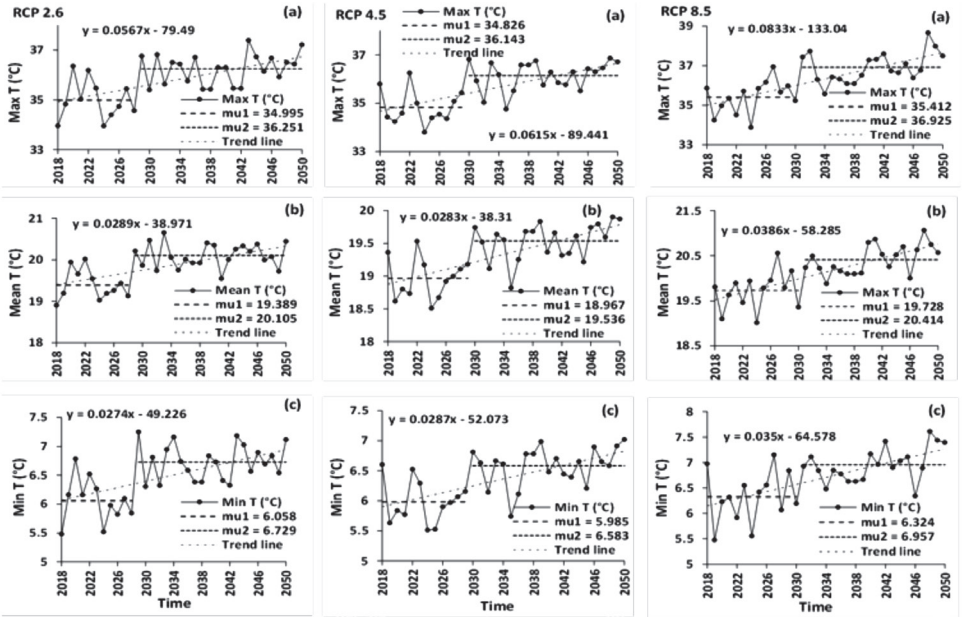

Though the increase in mean temperature obtained in this study is slightly higher than most of the earlier studies, it is still comparable to the earlier studies on changes in temperature in Morocco, as the earlier studies were based on the old scenarios AR4, while this study is projecting the trend in the 21st century and is based on the new scenarios AR5. The study by Babqiqi (2014) and by Ait Brahim et al. (2017) found increases by 0.8 °C to 1.2 °C till 2020s and by 1 °C to 2 °C till 2050s under B2 scenario. But under A2 scenario, this increase is about of 1°C to 1.2°C till 2020s and 2 °C to 2.3 °C till 2050s.

4.3.2. Precipitation

Under RCP 2.6 scenario, for the period 2018-2050, the precipitation shows significant fluctuations from year to year (Fig. 11a). Based on the weighted rainfall index, future rainfall also has modest fluctuations that allow the study period to be subdivided into the following three periods, which follow one another: the first is a normal period of 19 years (2018-2036), followed by a dry period of 6 years from 2037 to 2042. The third is a humid period of 7 years, thus marking the return of precipitation at the end of the study period (middle of the century) (Fig. 11b). The application of Pettitt's test, with a confidence level of 95%, reveals the presence of a break in the future precipitations in 2042 (Fig. 11c). This break confirms the limit between the dry and wet period determined by the method of the weighted rainfall index. The rainfall averages before and after the break allowed to estimate an excess of the order of 12.50%. The Mann-Kendall trend test results are reported in Table 7. Since the calculated p-value is less than the alpha significance threshold (0.05), we must retain the hypothesis of the existence of a trend in the series studied. The calculated normal multivariable standard UMK is positive, which reflects an upward trend of precipitation.

According to scenario RCP 8.5 based on the weighted precipitation index (Fig. 11b), the evolution of future precipitation shows two periods: the first one is a dry period going from 2018 to 2023, and the second is a normal period beginning in 2024. Pettitt's test shows in this case an early break in 2022, instead of 2042 quoted for RCP 2.6, with an excess of 21.33% almost doubled compared to that obtained under RCP 2.6. The multivariable standard UMK is greater than zero indicating an upward trend in precipitation (Table 7). However, the results of the statistical tests lead to the conclusion that future precipitation under RCPs 2.6 and 8.5 will show a general upward trend with an excess of 12.50% and 21.33% for the study period 2018-2050.

Figure 11

Annual variation of the future RI (a) RWI (b) and ARW (c) under RCP 2.6, 4.5 and 8.5 scenarios for the period 2018-2050

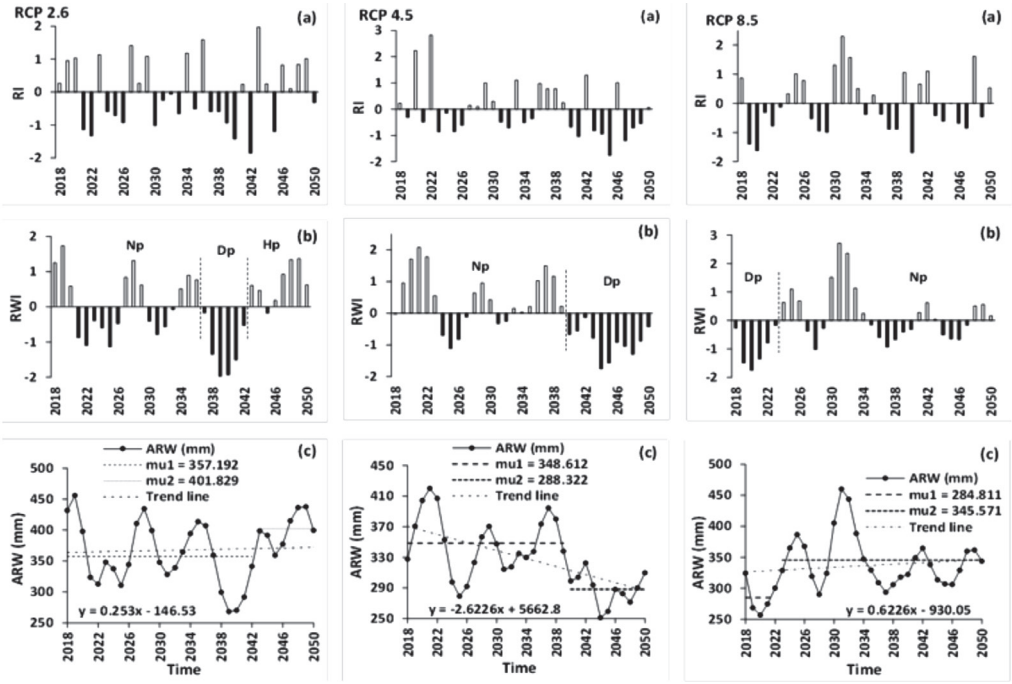

In contrast to the both scenarios RCPs 2.6 and 8.5, the future precipitation series under scenario RCP 4.5 shows a downward trend with a deficit of 17.29%. As shown in Figure 11c, the break year will be 2039. The calculated UMK is negative, reflecting a downward trend (Table 7).

The temperature and rainfall data collected by the Tensift Hydraulic Basin Agency (ABHT) at the Igrounzar station for the period 1988-2004 and those forecasted under the RCPS 2.6, 4.5 and 8.5 scenarios for the period 2018-2050 make possible the preparation of ombrothermic diagrams (Fig. 12). The comparison of the two diagrams confirms the upward trend of temperature and the downward trend of precipitation. Indeed, a significant reduction in precipitation is predicted for the months October, November, December and January accompanied by an increase in temperature. Given that the study area is characterized a semi-arid climate, the expected return of rainfall during the period 2018-2050 for April, May, June, July, August and September will likely be in the form of storms, because these months represent the dry season of the semi-arid zones. Under

the three scenarios RCP 2.6, 4.5 and 8.5, November which was part of the wet season during the period 1988-2004, will be counted in the dry season during the period 2018-2015. Also, the two months November and December during the period 2018-2050, will be colder compared to the period 1987-2004 under the three scenarios. The projected months from January to August will be warmer under RCP 8.5 scenario compared to the same period in 1987-2004, while both September and October will remain similar to those of the 1987-2004 period. Under the RCP 4.5 scenario, months April to July are projected to be warmer than those of the 1987-2004 period, while the three months August, September and October will remain similar to those of the 1987-2004 period. For the RCP 2.6 scenario, the four months February, March, September and October will remain similar to those of the 1987-2004 period, but April through August will be warmer compared to the 1987-2004 period. In general, it can be concluded that there will be a shortening of the wet season from five months (November to March) to four months (December to March) for the Essaouira basin. Due to similarity of climatic conditions, this situation may also characterize other semi-arid zones of the globe.

Figure 12

Ombrothermic diagram of Igrounzar station for the period 1987-2004 (in blue) and the period 2018-2050 (in red) according to (a) RCP 2.6, (b) RCP 4.5, and (c) RCP 8.5 senarios

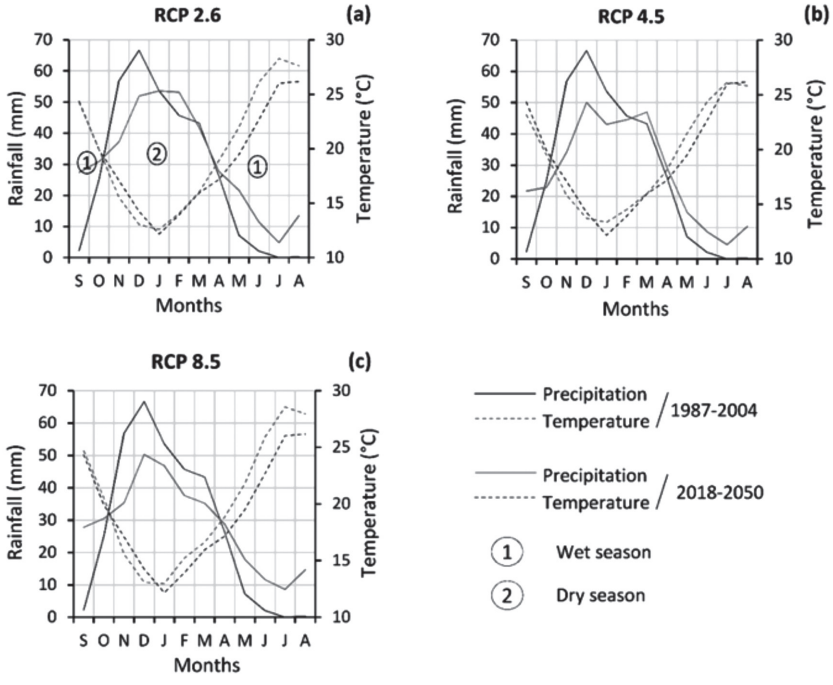

5. Conclusion

Analysis results of the annual precipitation using the Nicholson rainfall index graphical method and statistical tests, namely t Pettitt and Mann-Kendall tests, revealed an overall negative trend of the basin of 12 to 16% for the period 1978-2015. This decrease in average annual precipitation is accompanied by an increase in temperatures with a very significant extent of warming of 1.2 °C in the downstream part of the study area and 2.3 °C in its upstream part. This reflects the effect of continentality of temperatures in the study area.

Statistical downscaling was used to downscale future temperature variables and precipitation based on the statistical relationship between large scale atmospheric variables called predictor variables and observed temperature and precipitation data called predictands. The application of these models in a semi-arid area, such as the case of the Essaouira basin in western Morocco, has led to the conclusion that the maximum and minimum temperatures are sensitive to the surface wind direction, meridional velocity at 500 hPa, geopotential height at 500 hPa, specific near surface humidity and mean temperature at 2m predictors, while precipitation is influenced by the predictors surface meridional velocity, air flow strength at 850 hPa, zonal velocity at 850hPa and surface precipitation.

The combined use of this model and the Nicholson rainfall index, as well as Pettitt's and Mann-Kendall statistical tests have projected the significantly increasing trend of temperature variables. They showed the possibility of increase in mean temperature by up to 0.72 °C by the middle of the century (end of the study period) under the RCP 2.6 scenario, and by 0.57 °C and 0.69 °C under the RCP 4.5 and RCP 8.5 scenarios.

The precipitation is projected to be different in different time slices and under the three scenarios. Under scenarios RCP 2.6 and 8.5, the precipitation is peredicted to increase significantly with an excess of 12.50 % and 21.33 %, respectively. This predicted return of precipitation under these two scenarios is likely to be in the form of storms, a phenomenon that characterizes precipitation in semi-arid areas today. This return will be in summer as indicated by the presented ombrothermic diragrams. On the other hand, the RCP 4.5 scenario projected a decrease in mean annual precipitation during the study period of the order of 17.29 %. The ombrothermic diagrams show a shortening of the wet season from five (November to March) to four months (December to March). As a result, the climate of semi-arid areas, such as the one of this study, tends towards aridity with warmer and dryer conditions. Thus, urgent actions need to be undertaken at both the national and the global levels. It is recommended for the local and global policy to include the reduction of greenhouse gas emissions, the use of clean and renewable energy, and educating the population to adopt as soon as possible adapted behaviors towards a warmer and drier climate, especially people living in areas under semi-arid, arid and saharan climate.

Table 1

Predictor variables of the Global Climate Model (GCM) and the National Center for Environmental Prediction (NCEP)

#	Predictor	Description	#	Predictor	Description
1	mslp	Mean sea level pressure	14	p8_f	850 hPa air flow strength
2	p1_f	Surface air flow strength	15	p8_u	850 hPa zonal velocity
3	p1_u	Surface zonal velocity	16	p8_v	850 hPa meridional velocity
4	p1_v	Surface meridional velocity	17	p8_z	850 hPa vorticity
5	p1_z	Surface vorticity	18	p8_th	850 hPa wind direction
6	p1_th	Surface wind direction	19	p8_zh	850 hPa divergence
7	p1_zh	Surface divergence	20	p500	500 hPa geopotential height
8	p5_f	500 hPa air flow strength	21	p850	850 hPa geopotential height
9	p5_u	500 hPa zonal velocity	22	prcp	Surface precipitation
10	p5_v	500 hPa meridional velocity	23	s500	Specific humidity at 500 hPa height
11	p5_z	500 hPa vorticity	24	s850	Specific humidity at 850 hPa height
12	p5-th	500 hPa wind direction	25	shum	Surface-specific humidity
13	p5_zh	500 hPa divergence	26	temp	Surface mean temperature

Table 2

Selected set of predictor variables

Predictand	Predictor	R	R^2	p-value
Precipitation	p1_v	0.606	0.367	<0.0001
	p8_f	0.633	0.4	<0.0001
	p8_4	0.518	0.268	<0.0001
	prcp	0.786	0.619	<0.0001
Maximum Temperature	p1_th	0.605	0.366	<0.0001
	p5_v	0.628	0.395	<0.0001
	p500	0.743	0.552	<0.0001
	shum	0.757	0.573	<0.0001
	temp	0.832	0.692	<0.0001
Mean Temperature	p1_th	0.604	0.365	<0.0001
	p5_v	0.669	0.448	<0.0001
	p500	0.831	0.691	<0.0001
	shum	0.84	0.706	<0.0001
	temp	0.903	0.816	<0.0001
Minimum Temperature	p1_th	0.593	0.351	<0.0001
	p5_v	0.641	0.411	<0.0001
	p500	0.76	0.577	<0.0001
	shum	0.788	0.62	<0.0001
	temp	0.835	0.696	<0.0001

Note: R = correlation coefficient; R^2 = coefficient of determination

Table 3

Statistical evaluation of SDSM performance for calibration (1987-1999 for temperature and 1978-1999 for precipitation) and validation (2000-2005 for temperature and 2000-2004 for precipitation) at Igrounzar station

RMSE		R		R^2		DW	
1987-99	**2000-04**	**1987-99**	**2000-04**	**1987-99**	**2000-04**	**1987-99**	**2000-04**
Maximum Temperature							
3.28	2.78	0.86	0.89	0.74	0.79	1.37	1.87
Mean Temperature							
2	1.68	0.91	0.94	0.84	0.88	1.77	1.68
Minimum Temperature							
3.14	1.73	0.83	0.94	0.69	0.88	1.5	1.85
1978-99	**2000-05**	**1978-99**	**2000-05**	**1978-99**	**2000-05**	**1978-99**	**2000-05**
Precipitation							
4.87	3.37	0.82	0.85	0.67	0.72	1.85	1.47

Table 4

Analysis of interannual precipitation

Station	X	Y	Z	Max	Mean	Min	SD	VC
	km			mm				%
Igrounzar	103.5	91.3	205	707.6	293.2	126.5	139.04	47.4
Adamna	92.9	104.15	70	757.6	321.4	115.4	152.98	47.5
Essaouira	84.5	110.5	5	561.0	255.4	98.1	110.70	43.4

SD = Standard Deviation; VC = Variation Coefficient

Table 5

Analysis of interannual precipitation

Pettitt test					
	p-value	**Alpha**	**Beak date**	**Deficit (%)**	
Igrounzar	0.08	0.1	1998/99	16.06	
Adamna	0.09	0.1	1997/98	14.48	
Essaouira	0.001	0.05	2003/04	12.35	
Mann-Kendall test					
	p-value	**Alpha**	**H0: no trend**	**UMK**	**Trend sense**
Igrounzar	0.07	0.1	no	-1.09	Decrease
Adamna	0.09	0.1	no	-0.44	Decrease
Essaouira	0.02	0.05	no	-0.24	Decrease

Table 6

Results of the statistical tests applied to the temperature series (1987-2015)

Pettitt test					
Station	**p-value**	**Alpha**	**Break date**	**Warming (°C)**	
Maximum temperature					
Igrounzar	<0.0001	0.05	1999	2.8	
Essaouira	0.01	0.05	2007	2.1	
Mean temperature					
Igrounzar	<0.0001	0.05	2000	2.3	
Essaouira	0.001	0.05	2006	1.2	
Minimum temperature					
Igrounzar	<0.0001	0.05	1994	2.5	
Essaouira	0.50	0.05	-	-	
Mann-Kendall test					
Station	**p-value**	**Alpha**	**H0: no trend**	**UMK**	**Trend sense**
Maximum temperature					
Igrounzar	<0.0001	0.05	no	+5.24	Increase
Essaouira	0.03	0.05	no	+1.72	Increase
Mean temperature					
Igrounzar	<0.0001	0.05	no	+5.65	Increase
Essaouira	0.02	0.05	no	+2.06	Increase
Minimum temperature					
Igrounzar	<0.0001	0.05	no	+4.65	Increase
Essaouira	0.75	0.05	yes	-	-

Table 7

Results of the Mann-Kendall test applied to future annual precipitations, maximum temperatures, minimum temperatures and mean temperatures of Essaouira basin for the period 2018-2050 according to RCPs 2.6, 4.5 and 8.5 scenarios

Variable	p-value	Alpha	H0: no trend	UMK	Trend sense
RCP 2.6					
Precipitation	0.03	0.05	no	+0.68	Upward
Maximum T	0.001	0.05	no	+3.23	Upward
Mean T	0.001	0.05	no	+3.27	Upward
Minimum T	0.001	0.05	no	+3.24	Upward
RCP 4.5					
Precipitation	0.01	0.05	no	-3.16	Downward
Maximum T	0.0001	0.05	no	+3.86	Upward
Mean T	<0.0001	0.05	no	+4.26	Upward
Minimum T	0.0003	0.05	no	+3.64	Upward
RCP 8.5					
Precipitation	0.02	0.05	no	+0.99	Upward
Maximum T	<0.0001	0.05	no	+4.69	Upward
Mean T	<0.0001	0.05	no	+4.63	Upward
Minimum T	<0.0001	0.05	no	+3.92	Upward

Assessment the climate change impact on the past and future evapotranspiration and flows from a semi-arid environment

1. Introduction

Access to drinking water for the greatest number of populations, securing this often over-exploited and poorly managed resource, controlling agricultural and industrial use of water, and environment represent major challenges. Among other stakes, we can mention the probable transformations of increasingly anthropised natural environments, the collective management of natural risks (floods, drought, salinisation of groundwater) and the prospect of global warming during this century and beyond (Bahir et al. 2016; El Gayar and Hamed 2018; Mokadem et al. 2018; Theodossiou 2016).

The stakes of water and its management are problems that condition the future of thie Maghreb region (Agoumi et al. 1999). Regardless of any climate change, the high sensitivity of watersheds to small variations in climate variables implies that the volume of water available for mobilization will be strongly affected by the decrease in runoff.

Like countries under Saharan, arid and semi-arid climate, Morocco suffers from a recurrence of drought periods since the beginning of the 80s of the previous century. These episodes had obviously an impact on water availability (Bahir and Mennani 2002). These environments are characterized by scarcity, or surface water resources absence, so the term entering the water balance in these environments is summarized with the rains. However, the decrease in rainfall has an effect on flows.

In recent decades, several studies on climate change impact on water resources in arid and semi-arid zones have been conducted (Bahir et al. 2016; Kour et al. 2016; Ouhamdouch et al. 2018; Meddi et al. 2009; Theodossiou 2016; Belarbi et al. 2015). They show a quantitative and qualitative degradation that is manifested by the water quality and the decline in the level of groundwater and surface water. However, this situation is a warning that suggests an adequate intervention, particularly by

academics, university researchers and politicians, to control, protect and develop this resource. This intervention, therefore, requires beforehand a good knowledge in the functioning of these resources.

Numerous hydrological models have been developed in recent decades, especially those that look at the rain-flow relationship, offering a great deal of flexibility in handling, a lot of time and material gain. Among these models, the Rural Genius (RG) model developed by CEMAGREF is to be mentioned. This model is a tank model, which works for different annual time steps GR1A, monthly GR2M, and daily GR4J. This model has been used by several authors and has given very satisfactory results (Dezetter et al. 2008; Belarbi et al. 2015; Mouelhi et al. 2017; Rwasoka et al. 2014). A rainfall model is very important; it allows estimating the available resource for a development, as it also allows the development of this resource in the years and the future decades by combining it with the data and the climatic scenarios.

The Essaouira basin seves as a case study. A rainfall-flow model to characterize the sub-basin of Essaouira (Igrounzar, Zelten, and Ksob sub-basins) and to allow the simulation of the future behavior of flows for the period 2020-2050 under RCPs 2.6, 4.5 and 8.5 scenarios of the CIMP5 model, is therefore developed. The conceptual model of RG, in monthly time step with two parameters (GR2M), was considered as adequate and retained in the exploitation of the data of the sub-basins studied.

The Ksob watershed (Igrounzar-Zelten-Ksob) contains three main Wadis in the Essaouira Basin: Igrounzar Wadi, Zelten Wadi in the upstream part, and Ksob Wadi which results from the confluence of the first two at the entrance to Tidzi diapir (Fig. 1). It covers an area of 1500 km^2. Located in the south-east of Essaouira city, the Ksob watershed is under semi-arid climate with rainfall not exceeding 300 mm/year and the average annual temperature is about of 20 °C (Ouhamdouch et al. 2018). The basin studied is represented by low hills with a generally rounded head, cut by a shallow hydrographic network (Fig. 1). This architecture subdivides the study area into three sub-basins: the Igrounzar sub-basin in the North, the Zelten sub-basin in the South and the Ksob sub-basin (total basin) in West (Fig. 1).

The studied basin is of sedimentary type containing formations ranging from Trias to Plio-Quaternary. The Triassic and Jurassic formations have only very small outcrops and are located in the heart of anticlines (Hadid anticline, Amsittene anticline, and Tidzi diaper), while tertiary and quaternary formations meet in the synclines (Fig. 1).

The Triassic formations consist of saliferous red clays and doleritic basalts. While the Jurassic, it is composed of alternating carbonate deposits (limestones and dolomites) and marls rich in evaporites (gypsum and anhydrite) (Peybernès et al. 1987). As claimed by Duffaud et al. (1966), the Lower Cretaceous is formed of

limestones and marls. The Middle Cretaceous begins with marly-sandstone deposits of the Aptian, followed by green marl of the Albian and terminated by dolomitic marls and limestones.

Figure 1

Location and geological map of study area

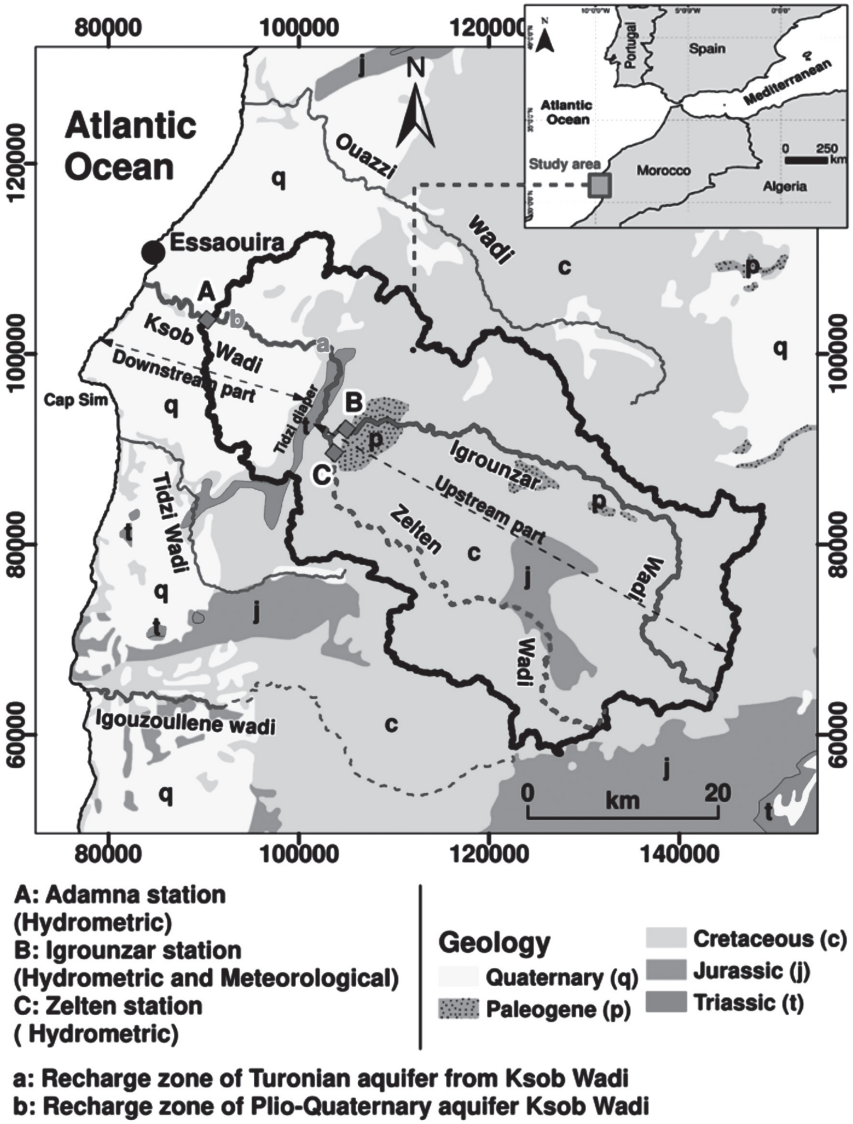

The studied area is a large synclinal zone open to the Atlantic Ocean. It has been the subject of several accidents allowing the appearance of many synclines such as (i) the synclinal basin of Bouabout representing the upstream part of the basin, crossed by the Oued Igrounzar, and (ii) the synclinal basin of Essaouira (downstream part); the two are separated by the diapir of Tidzi. The upstream part is characterized by an aquifer housed in limestone and dolomitic limestone of the Cenomano-Turonian.

In the downstream part, groundwater resources are contained in two main reservoirs: The Plio-Quaternary with marine calcareous sandstone or dune matrix contains a large shallow aquifer. The second reservoir is represented by the Turonian, and is very rapidly captive under the Senonian marls in the synclinal structure and probably in contact with the Plio-Quaternary on the borders of this structure, especially to the North towards Ksob Wadi, to the West on the approach the coastline, to the east and south in the vicinity of Tidzi diaper (Fig. 1).

Due to the limited availability of climatic and hydrometric data, only data from the three stations Igrounzar, Zelten and Adamna were used. The Igrounzar station is the only station for measuring rainfall, flow rates, temperature, humidity, and evaporation. While the Adamna station allows the measurement of rainfall and flow rates only, and the Zelten station allows the measurement of flows only. The observed data exploited in this work consist in rainfall, potential evapotranspiration, and flow-rate, extend over the period 1978 to 2005. It was provided by Tensift Basin Hydraulic Agency (ABHT). These data are based on the monthly values recorded on the three stations. For the series of precipitation, potential evapotranspiration, and flow rate, no missing data are marked for the available period of 28 years (1978-2005). The location of the three stations of observation is depicted in Figure 1.

The studied basin is located in a semi-arid zone, characterized by oceanic, continental and mountain influence (Ouhamdouch et al. 2018). The aridity is marked in the basin especially in summer; it is relatively increasing from the Atlantic ocean to the continent. This increase is the result of the remoteness of oceanic influences, where precipitation decreases and thermal differences increase (Ouhamdouch et al. 2018). Annual precipitation shows significant year-to-year fluctuations around an average of 300 mm. According to Ouhamdouch et al. 2018, the annual precipitation trends show a general downward trend of 12%. As for the temperatures, they show a very significant seasonal variation. In winter, minimum temperatures can reach -11 °C while maximums are around 40 °C. While the annual average is around 20 °C, and the average annual temperatures trends show an upward trend with warming of around 2 °C (Ouhamdouch et al. 2018).

2. Methodology

The assessment of the climate change impact on future flows in the Essaouira basin was made combining the GR2M model, the projection of climate parameters under RCP 2.6, 4.5 and 8.5 scenarios, and the Mann-Kendall and Pettitt tests.

The monthly time step GR2M model was developed by Makhlouf and Michel (1994) on different river basins located in France, and it showed better performance compared to many other hydrological models in this area. Since then, it has been successfully used in many arid and semi-arid areas (Mahé et al. 2005; Bouanani 2013; Sakaa et al. 2015; Mouelhi et al. 2017). For this reason, and following the availability of data, this model was chosen to evaluate the climate change impact on future flows within Essaouira basin. GR2M structure used in this investigation is the recent version developed by Mouelhi et al. (2006) who benefited from the experience gained during the development of the GR4J model, a model with the daily time step, (Perrin et al. 2003). The GR2M model considers that each basin has two reservoirs, a reservoir (soil reservoir) denoted by Si controlling the production function with a maximum capacity X_1 (mm) (first free parameter of the model) and a routing reservoir denoted Ri controlling the transfer function with a capacity of 60 mm (Fig. 2). It uses monthly rainfall (P) and ETP (E) as input and outputs the flows (Q) in mm. The particularity of this model version lies in the introduction of the second free parameter X_2 (without unit). In order to correct the water balance errors, the parameter X_2 makes it possible to correct the possible biases in the climate and flow time series. At each time step of the modeling, rainfall is channeled either by infiltration to the soil reservoir (1), or directly towards the routing reservoir in the form of surface flows (P_1) (2). The reservoir Si reaches the level S_1 (mm) then loses a part by evaporation (3) to reach a new level S2 (mm). Part of the soil moisture P_2 (mm) is then transferred to the routing reservoir by percolation (4). The sum of P_1 and P_2 (P_3, (5)) joins the routing reservoir to reach the level Ri (6). A quantity of the water will be gained or lost by the routing reservoir by exchanging lateral waters between the underground part of the basin and its external environment (7). If $X_2 > 1$, there is a water supply coming from outside the basin, on the other hand, if $X_2 < 1$ the routing tank supplies the flow Qi (8) (Fig. 2).

Calibration and validation of GR2M model were evaluated by the Nash criterion (Nash and Sutcliffe 1970) considered as the best-performing criterion. This criterion is founded on the comparison of estimated and observed flow rates based on follow equation (Eq. 1):

$$\text{Nash (Q)} = 100 \times \left[1 - \frac{\sum_i (Q_{i\,obs} - Q_{i\,cal})^2}{\sum_i (Q_{i\,obs} - \bar{Q}_{obs})}\right] \quad \text{(Eq. 1)}$$

With $Q_{i\ obs}$ represents observed flow; $Q_{i\ cal}$ represents calculated flow and $\bar{Q}_{obs}$ is the observed flow rates average.

Figure 2

Structure of GR2M model (modified from Mouelhi et al. 2006)

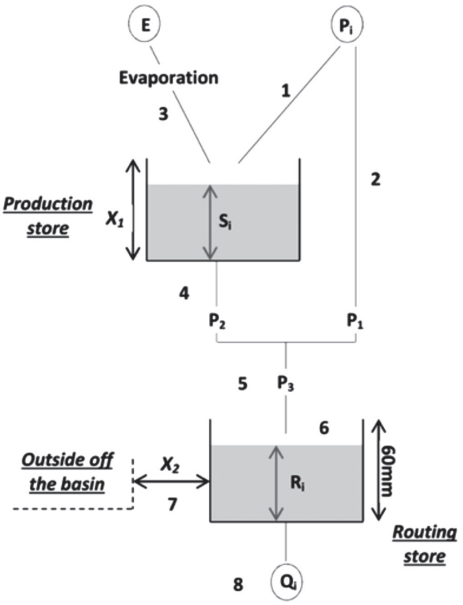

(1) $S_1 = \frac{S_i + X_1\varphi}{1!}$, with $\varphi = \tanh(\frac{P_i}{X_1})$

(2) $P_1 = P_i + S_i - S_1$

(3) $S_2 = \frac{S_1(1-\Psi)}{1+\Psi\left(1-\frac{S_1}{X_1}\right)}$, with $\Psi = \tanh(\frac{E}{X_1})$

(4) $S_i = \frac{S_2}{\left[1+\left(\frac{S_2}{X_1}\right)^3\right]^{1/3}}$, $P_2 = S_2 - S_1$

(5) $P_3 = P_1 + P_2$

(6) $R_1 = R_i + P_3$

(7) $R_2 = X_2 \times R_1$

(8) $Q_i = \frac{R_2^2}{R_2+60}$, $R_i = R_2 - Q_i$

The GR2M model is considered efficient when the estimated flows are close to the observed flow rates, i.e. when the Nash criterion is close to 100%. According to Perrin et al. (2003), a performance ≥ 70% is satisfactory.

The potential monthly evapotranspiration (ETP) was calculated using Thornthwaite formula (Eq. 2) (Thornthwaite 1948). The choice of the Thornthwaite method lies in the fact that the other methods (e.g. Pennman, Turc) use unavailable climatic parameters (e.g. insolation duration, hygrometric degree, wind speed...).

$$\mathrm{ETP} = 16 \times \left(\frac{10 \times t}{I}\right)^{a} \times F\,(m, \lambda) \qquad \text{(Eq.2)}$$

With

ETP: potential monthly evapotranspiration (mm)

t: Average monthly temperature in °C

I: Annual thermal index is calculated using the equation (Eq. 3)

$\mathrm{I} = \sum i$ (Eq. 3), with $\mathrm{i} = \left(\frac{t}{5}\right)^{1.514}$

F: Correlation coefficient that is based on month (m) and latitude (λ)

a: Complex function of the thermal index calculated via the formula (Eq. 4)

$$a = 0.49239 + (1792 \times 10^{-5} \times I) + (771 \times 10^{-7} \times I^2) + (675 \times 10^{-9} \times I^3) \quad \text{(Eq. 4)}$$

For the climate projection, the results of the study realized by Ouhamdouch and Bahir in 2017 were used. By the same approach, future rainfall from the Adamna station was calculated. The GR2M model, with parameters X_1 and X_2 obtained during calibration and validation phase, by using historical values of rainfall and potential monthly evapotranspiration, has been applied again to estimate future flows under new climatic conditions determined under the RCPs 2.6, 4.5 and 8.5 scenarios. In order to determine the trend direction of the flow series as well as the break dates of these series, the Pettitt test (break detection), and the Mann-Kendall test were applied using the XLSTAT® software (trial version).

Pettitt test

The Pettitt (1979) test allows to examine the existence of a break in a time series from a formulation derived from that of the Mann-Whitney test. This test is based on the calculation of the variable $U_{t,T}$ defined by equation (Eq. 5):

$$U_{tT} = \sum_{I=1}^{T} \sum_{J=I+1}^{T} D_{IJ} \quad \text{(Eq. 5)}$$

Where, Dij = -1 if (xi-xj)>0, Dij = 0 if (xi-xj) = 0, Dij = 1 if (xi-xj) > 0.

Mann-Kendall's test

The Mann-Kendall test (Mann, 1945, Kendall, 1975) is a test used to detect the presence or the absence of a linear trend within a time series. With the ai series (a_1, a_2,...a_n), this method sets the standard U_{MK} multi-variable standard as follows (Eq. 6):

$$U_{MK} = \frac{S}{\sqrt{Var\,(s)}} \quad \text{(Eq. 6)}$$

With $S = \sum_{i=1}^{n-1} \sum_{j=i+1}^{n} sgn(a_j - a_i)$, $Var\,(s) = \frac{n(n-1)(2n+5)}{18}$, and n the number of data in the series.

The trend sense is defined by the statistical coefficient "U_{MK}". If U>0, the trend is upward and if U<0 the trend is downward.

3. Historical evapotranspiration and flow

Going from north to south, the Essaouira basin contains six main Wadis named Ouazzi, Ksob, Igrounzar i, Zelten, Tidzi, and Igouzoullene. In this study, we are interested in Igrounzar, Zelten, and Ksob Wadis because only they are equipped by hydrometrical stations. With the exception of the Adamna station installed in Ksob Wadi, the other two stations (Igrounzar and Zelten) are named according to their own names.

Regarding flow rates, the obtained results for the three stations are grouped in Figure 3. For Zelten and Igrounzar stations, observed flows are showing an upward trend. The application of Mann-Kendall test (alpha = 5%) shows an upward trend in the series studied with a standard multi-variable U_{MK} equal to +0.04 and +0.23 for Igrounzar and Zelten stations, respectively (Table 1). This trend is corroborated by the Pettitt test, which shows a break in the average monthly flow series of Zelten and Igrounzar stations. For Igrounzar station, the break is observed in October 1995 and the mean before and after this break is 0.28 and 0.55 mm/month, respectively (Fig. 3a). As for Zelten station, the break is observed in September 1995. The mean before and after the break is 0.36 and 0.75 mm/month, respectively (Fig. 3b). This upward trend could be explained by the return of rainfall during the last decades in the form of a storm characterizing the semi-arid, arid, and Saharan environments. This return of rainfall in the form of a storm is very marked by spades presented by the series of rainfall (Fig. 4).

Figure 3

Historical flows at (a) Igrounzar station, (b) Zelten station and (c) Adamna station within Essaouira basin for the period of 1978-2005. A1 = mean before break and A2 = mean after break

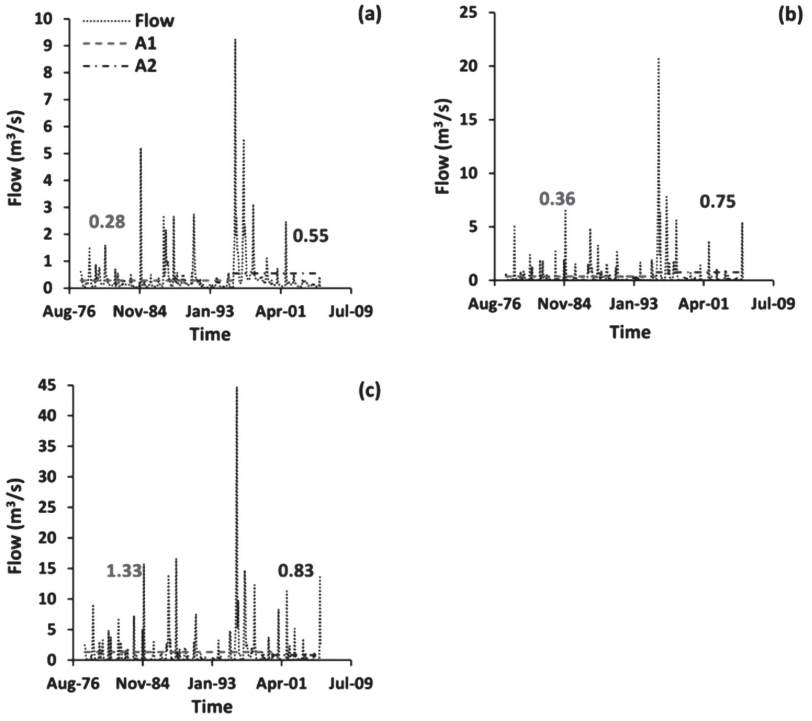

On the other hand, the flows observed at Adamna station show a downward trend during the 1978-2005 period. Indeed, the application of Pettitt test on this serie raises the presence of a break in February 2000 with a deficit of 37.6% (Fig. 3c). The mean of flow before and after the break is 1.33 and 0.83 mm/month, respectively. This trend is corroborated by the Mann-Kendall test with a negative U_{MK} (U_{MK} = -0.64) (Table 1). However, the downward trend of flows recorded at Adamna station could be explained by the infiltration of a quantity of run-off water by recharging the Plio-Quaternary and Turonian aquifer before arriving at the gauging station of Adamna, especially in zone a and b located in Figure 1 (Fekri 1993).

In order to evaluate the rainfall effect on flows, the rainfall-flow relationship was developed (Fig. 4). At first glance, it is clear that the rainfall peaks coincide perfectly with the flow peaks. This coincidence is very clearly observed during periods a, b, and c for the Igrounzar station, during d, e, f, and g for the Zelten station and during h, i, j, k, l, and m for the Adamna station (Fig. 4). Outside the rainy periods, the flows are reduced to their lowest levels, or even cancel each other out. The highest flow observed during the study period at the three stations was January 1996, 9.23 m^3/s, 20.8 m^3/s and 44.7 m^3/s for the Igrounzar, Zelten and Adamna stations, respectively. However, there is a cause-and-effect relationship between rainfall and flow, and this rule holds for any arid to semi-arid zone.

As Igrounzar station has the peculiarity of having a thermometer for measuring atmospheric temperature, the ETP used in this paper is the one calculated at this station. The calculation of evapotranspiration over a period of 336 months (1978-2005) was done using the equation 2 (Eq. 2). The results obtained are shown in Figure 5. During the observation period (1978-2005), potential monthly evapotranspiration values vary between 95.44 and 186.84 mm/month (Fig. 5).

The results of the statistical tests applied to the potential monthly evapotranspiration series are presented in Table 1. The Mann-Kendall test (with alpha=5%) show an upward trend in potential monthly evapotranspiration series (U_{MK} = +1.56). The Pettitt test (significance level = 5%) confirms this result by highlighting the presence of a significant break in the monthly mean in March 1994. Sub-series average before and after this break is 122.99 and 128.18 mm/month, respectively, with a slight increase of 4.2% from 1978 to 2005 (Fig. 5).

4. GR2M Model performance during Calibration and Validation phase

GR2M model evaluation is based on the examination of the performance of the Nash criterion and the determination coefficient R^2.

For model calibration, we proceeded to change the values of the parameters X1 and X2 until obtaining the optimum values of determination coefficient and Nash criterion (≥ 70%). The limit values proposed by the model for X1 are between 140 and 2640 and between 0.21 and 1.31 for X2. For the validation phase, we used the series of precipitation and evapotranspiration for the period January 1997 to December 2001, not already used to develop the model. The calculation is initiated by taking parameters X1 and X2 optimized in the calibration phase. The results obtained are grouped in Table 2. The reason for choosing this period is that this period gave a Nash crest of over 70% for both phases. GR2M model evaluation is based on the examination of the performance parameters (Nash and R^2) and the hydrographs of observed and simulated flows during the calibration and validation phases (Kouamé et al., 2013).

Figure 4

Relationship between rainfall and flow for (a) Igrounzar station, (b) Zelten station, and (c) Adamna station from Essaouira basin

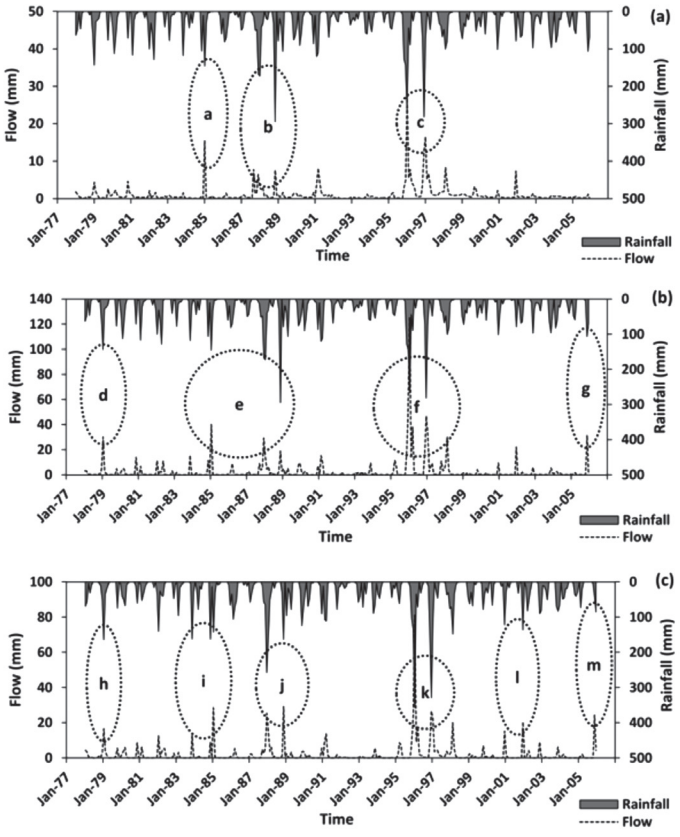

Figure 5

Historical ETP at Igrounzar station from Essaouira basin for the period of 1978-2005. A1 = mean before break and A2 = mean after break

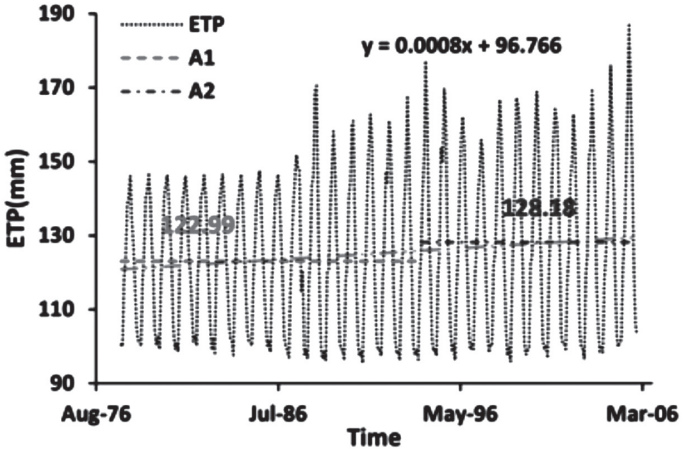

For Igrounzar station, the obtained Nash criterion values, in calibration (83%), as in validation (78%), are higher than 70%. This allows us to say that the GR2M used is powerful for modeling the data collected on the Igrounzar station. The calculated difference between the Nash value obtained during the calibration and validation time is of 5%. This gap defines the robustness criterion of the model used. Indeed, the degradation thus recorded by the Nash criterion (5%), is considered quite acceptable, since its absolute value is less than 10% (Kouamé et al., 2013). Figures 6a and 6b show that the hydrographs obtained during calibration and validation phase are of good quality. The simulated flow versus observed flow rates resulting from calibration and validation (Fig. 6a and b) give very significant R^2 values (R^2 = 0.88 for both phases). Indeed, the rain-flow modelling, using the GR2M model, gives satisfactory and very encouraging results at the Igrounzar station.

As for Zelten station, the value of the Nash criterion obtained through the calibration and validation phase is equal to 72%. Hence, GR2M model is still powerful for modeling the data collected on the Zelten station. For this station, the difference between the Nash value obtained at calibration phase and the validation phase is null. This demonstrates the efficiency of the model used. The hydrographs of Figure 7a and 7b show a significant coincidence between the curve of observed and simulated flows. The correlation coefficient obtained from the observed flow rate-simulated flows diagram is 0.81 for the calibration and validation phase. This corroborates again the robustness of the GR2M model used for the Zelten station.

Figure 6

Calibration (a) and validation (b) of GR2M model obtained at Igrounzar station. Rainfall-flow observed and simulated (left). Correlation diagram between observed and simulated flow (right)

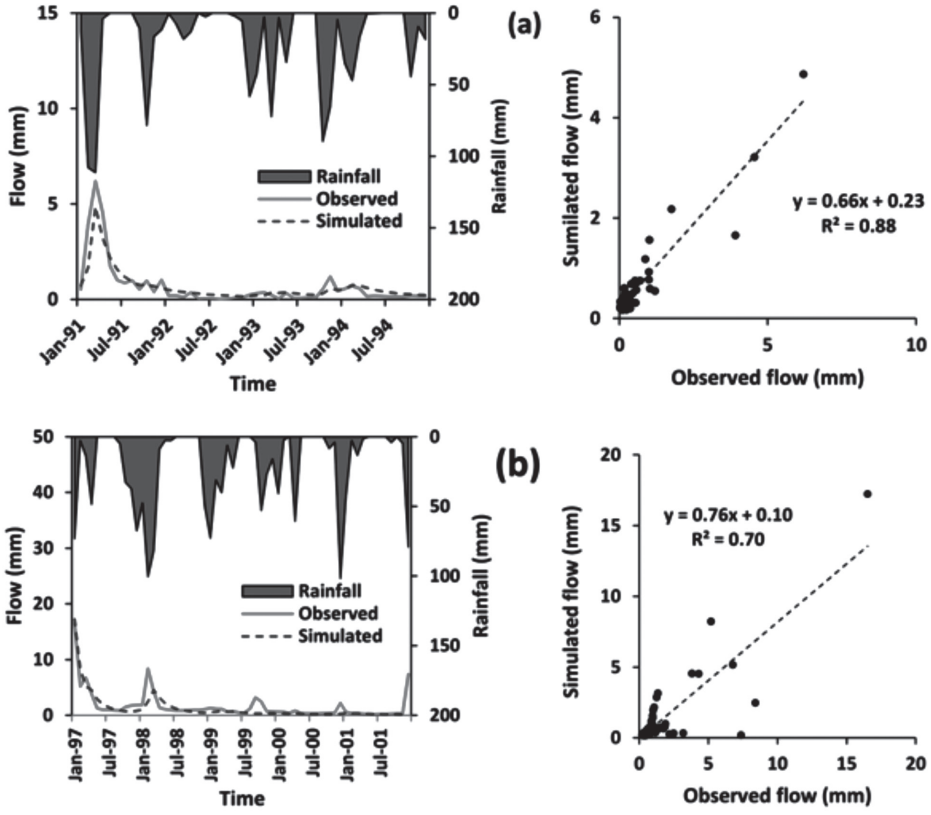

Concerning Adamna station, the obtained results for the Nash criterion and the R^2 coefficient of determination for the Adamna station are shown in Table 2. Since the value of the Nash criterion in the calibration phase (74%) is greater than 70%, the calibration of GR2M model appears correct for the Adamna station. This calibration is validated with a Nash criterion equal to 76% during the validation phase. The good superposition of the observed and simulated flows curves and the important values of R^2 (Fig 8a, 8b) confirm the good performance of the GR2M model at the Adamna station.

Figure 7

Calibration (a) and validation (b) of GR2M model obtained at Zelten station. Rainfall-flow observed and simulated (left). Correlation diagram between observed and simulated flow (right)

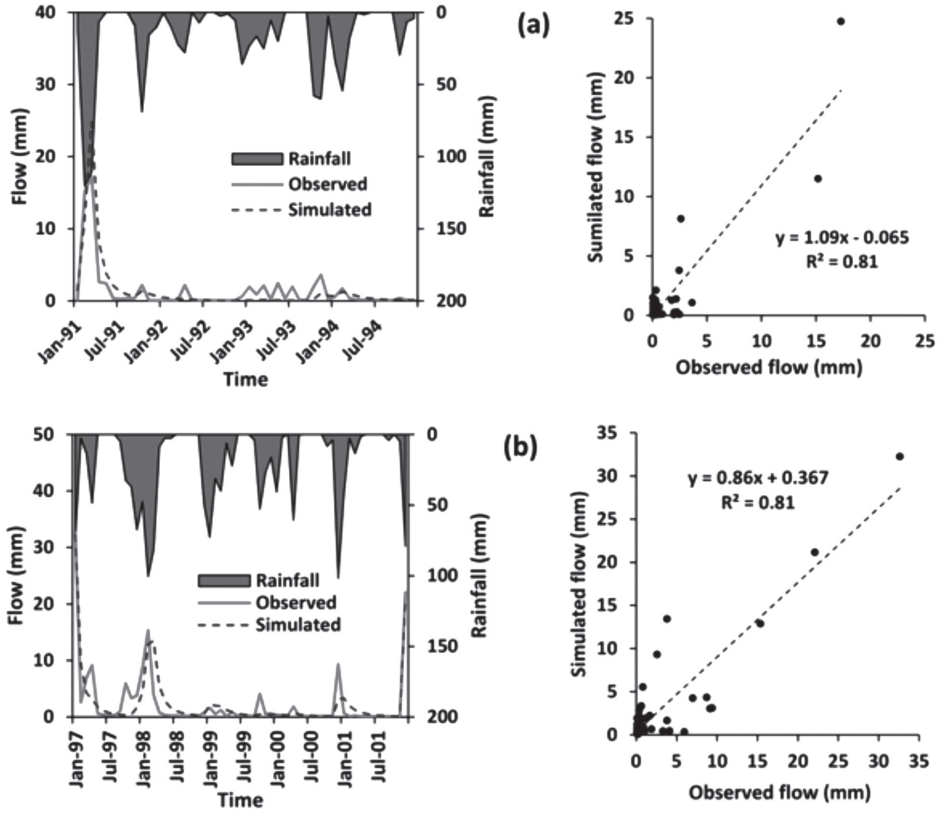

Figure 8

Calibration (a) and validation (b) of GR2M model obtained at Adamna station. Rainfall-flow observed and simulated (left). Correlation diagram between observed and simulated flow (right)

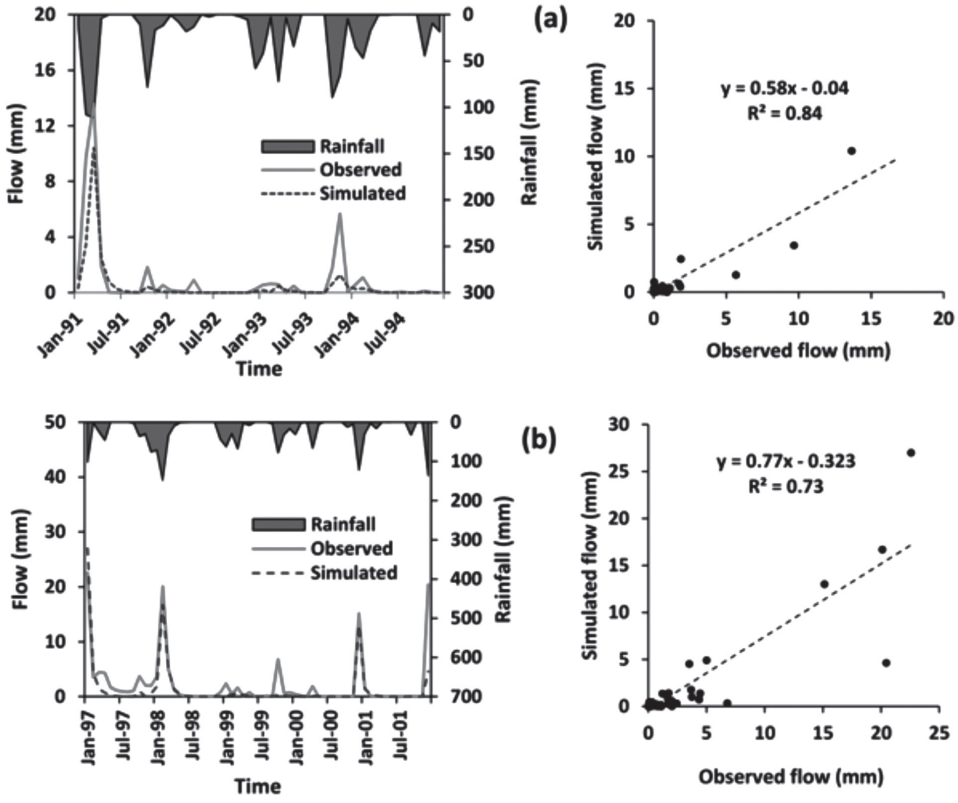

5. Future evapotranspiration and flows

According to Ouhamdouch and Bahir (2017), the model used to predict future temperature and rainfall within Essaouira basin is CanESM2, one of the participating models in CMIP5. The combined use of this model and the statistical tests of Pettitt and of Mann-Kendall showed an increase in mean temperature of 0.72 °C under the RCP 2.6 scenario, 0.57 °C and 0.69 °C under the RCP 4.5 and RCP 8.5 scenarios by 2050 (Ouhamdouch and Bahir 2017). For the precipitation, they showed an increase under scenarios RCP 2.6 and 8.5 with an excess of 12.50% and 21.33%, respectively. Under RCP 4.5 scenario a decline in mean annual precipitation during the study period of the order of 17.29% is predicted by 2050.

Since flow simulation under the GR2M model uses rainfall and evapotranspiration data, simulation of future flows requires the use of future rainfall and future evapotranspiration. Future temperatures were used to calculate future evapotranspiration using the Thornthwaite formula (Eq. 2).

The results of the statistical tests applied to the future potential monthly evapotranspiration time series at the Igrounzar station are mentioned in Table 3. Under RCPs 2.6, 4.5, and 8.5 scenarios, the application of the Mann-Kendall test on the future potential monthly evapotranspiration series shows an upward trend with UMK equal to +0.59, +0.78and +0.68, respectively. This trend is affirmed by the Pettitt test (Fig. 9), which shows a break in the series in April 2029, March 2036, and March 2034 for RCP 2.6, 4.5 and 8.5, respectively. For the studied period (2020-2050), the mean potential monthly evapotranspiration before and after the break under RCP2.6 is 127.17 and 129.59 mm/month, respectively; with an excess of 1.9%. For RCP 4.5, the mean before and after the break is 125.75 and 127.63 mm/month, respectively; with an excess of 1.5%. As for RCP 8.5, the mean before and after the break equal to 128.21 and 130.33 mm/month, respectively; with an excess of 1.6% (Fig. 9). Since potential monthly evapotranspiration is related to air temperature, upward trend of potential monthly evapotranspiration is due to the upward trend in future temperatures as demonstrated by Ouhamdouch and Bahir in 2017.

The results of the future flow simulation under the RCPs 2.6, 4.5 and 8.5 scenarios for the period 2020-2050 are displayed in Figure 10. Under the RCP 2.6 scenario, the application of Mann-Kendall test on the future flow series shows an upward trend for the three Igrounzar, Zelten and Adamna stations (Table 3). This trend is confirmed by the Pettitt test (Fig. 10a), which shows a break in the series in January 2043, December 2042, December 2042 for the Igrounzar, Zelten and Adamna stations, respectively. For the Igrounzar station, the mean before and after the break is 0.45 m^3/s and 0.54 m^3/s respectively; with an estimated excess of 20% for the 2020-2050 period. For the Zelten station, the mean before and after the break is 0.59 m^3/s and 0.76 m^3/s, respectively, with an increase of 28.80% for the study period (Fig 10a). For the same period, the Adamna station series has an average before and after the break equal to 0.76 m^3/s and 0.91 m^3/s, respectively with an estimated excess of 19.70% (Fig 10a).

Figure 9

Monthly variation of future ETP at Igrounzar station under RCP 2.6, 4.5 and 8.5 scenarios for the period 2020-2050. A1 = mean before break and A2 = mean after break

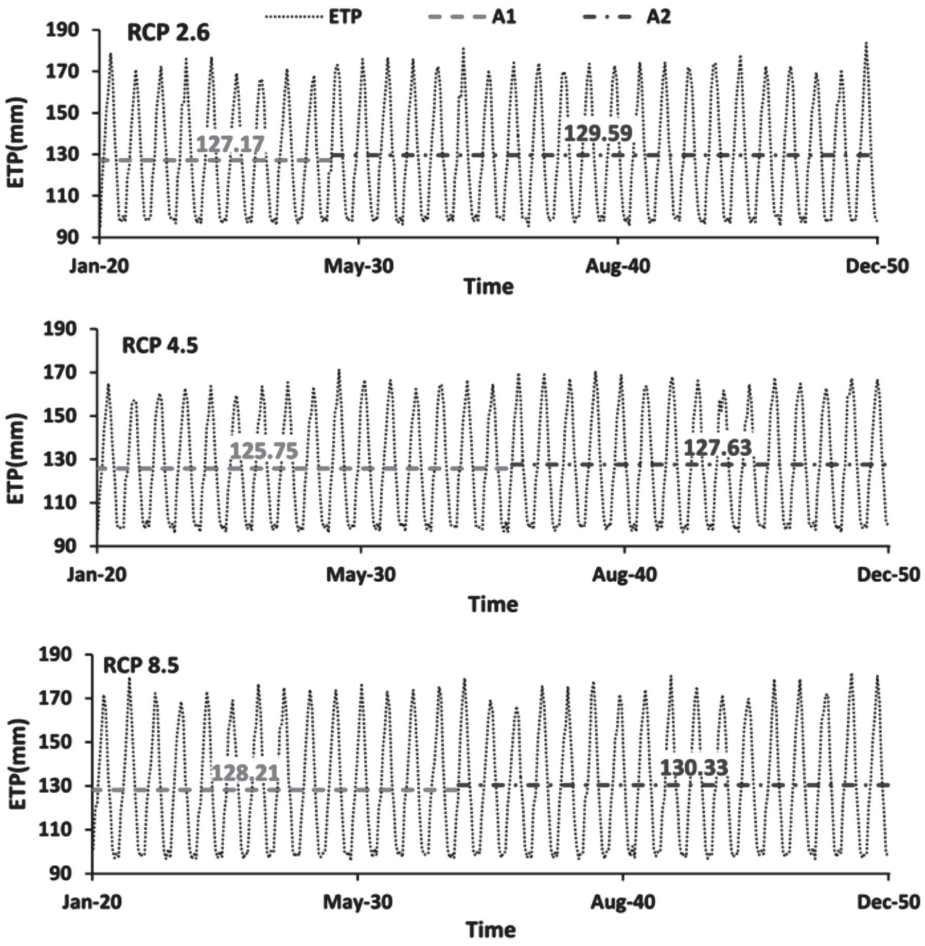

Under the RCP 4.5 scenario, the application of the Mann-Kendall and Pettitt test on the future flow series for the three stations shows a downward trend with a 42.5%, 42.1% and 40.6% deficit for Igrounzar; Zelten; and Adamna stations, respectively (Fig. 10b). The break dates of the future flow series for the Igrounzar, Zelten and Adamna stations are June 2040, May 2039 and May 2040, respectively.

Under the RCP 8.5 scenario, the behavior is like that observed under scenario 2.6. The use of Mann-Kendall test results (Table 3) and Pettitt test results with a confidence

interval of 5% (Fig. 10c), future flows show an upward trend. This upward trend is of 44.4%, 53.8% and 43.7% for the Igrounzar, Zelten and Adamna series respectively by 2050.

Figure 10

Monthly variation of future flow at Igrounzar, Zelten and Adamna station under (a) RCP 2.6, (b) RCP 4.5 and (c) RCP 8.5 scenarios for the period 2020-2050. A1 = mean before break and A2 = mean after break

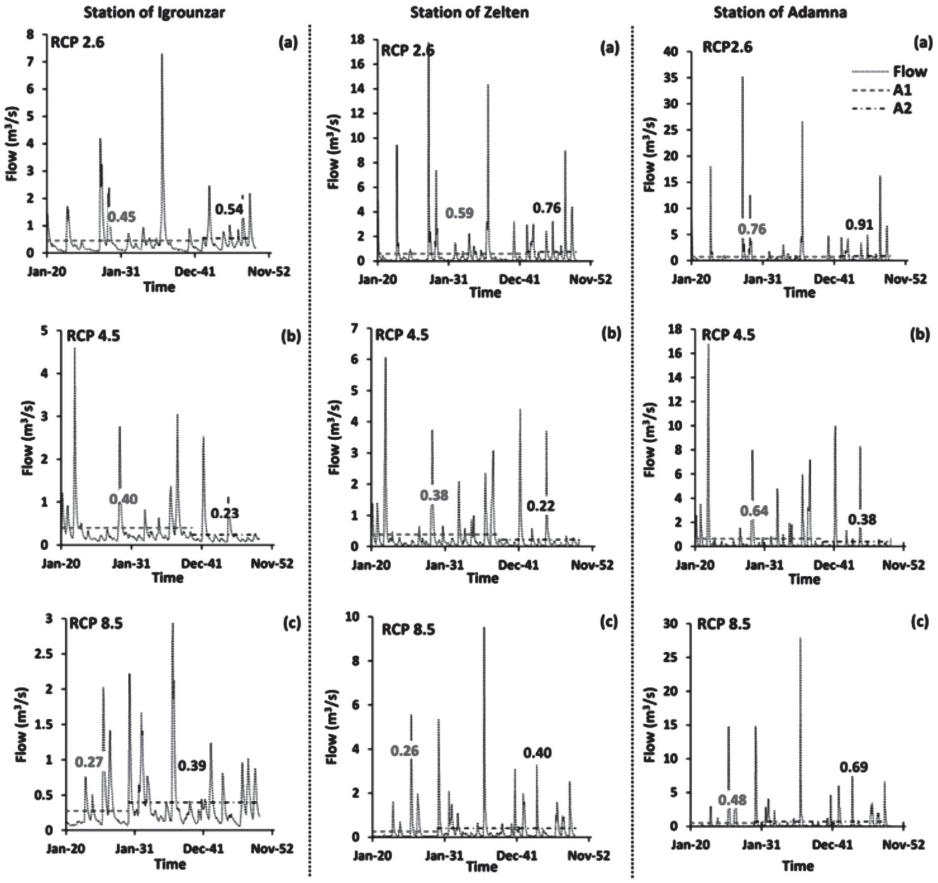

Figure 11 shows comparison of observed and future flows. It is to be noticed that the flows observed at the Adamna station are twice as much as those observed at the Igrounzar and Zelten stations. This is due to the fact that Wadi Ksob (where the Adamna station is installed) is the result of the confluence of Igrounzar (where the Igrounzar station is installed) and Zelten Wadi (where the Zelten station is located).

Average discharges observed during the period 1978-2001 is equal to 0.38, 0.5, and 1.23 m3/s for Igrounzar, Zelten and Adamna stations, respectively. While this average during the period 1991-2001 is equal to 0.55, 0.72, and 1.59 m3/s for the Igrounzar, Zelten, and Adamna stations, respectively. This slight increase could be explained by the slight return of precipitation, which is manifested by floods, notably that of January 1996. The comparison of future flows with those observed, whether during the period of 1978-2001 or the period 1991-2001, shows a decrease.

Figure 11

Comparison of observed and future flows at Igrounzar, Zelten, and Adamna within Essaouira basin

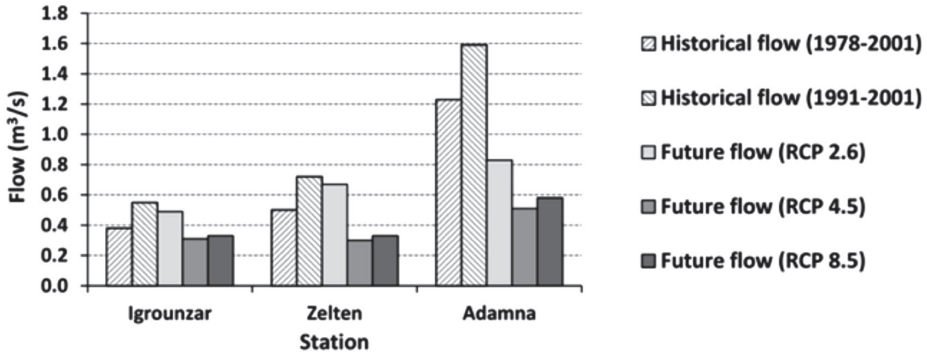

Under the RCP2.6 scenario, an increase in future flows is observed for Zelten and Igrounzar stations, while a decrease is observed for the Adamna station. Under RCP 4.5 and 8.5 scenarios, a downward trend in mean flow rates compared to historical flows is observed during the period of 1978-2001. For RCP4.5 scenario, a difference of 0.07 (Igrounzar), 0.2 (Zelten), and 0.72 m^3/s (Adamna) was estimated. While under the RCP8.5 scenario, the difference is estimated at 0.05 for Igrounzar station, 0.17 for Zelten station, and 0.65 m^3/s for Adamna station. For Adamna station where the total flow of the basin is measured, the percentage of decrease in flows is equal to 33% under the RCP 2.6 scenario, 59% under the RCP 4.5 scenario, and 37% under the RCP 8.5 scenario.

The obtained results are close to the results of previous studies for flows in semi-arid zones, based on the old AR4 scenarios, though this study predicts the trend in the 21st century and builds on new AR5 scenarios. By 2050, the study of Driouech et al. (2010) showed that future flows in Moulouya watershed (Morocco) show a downward trend compared to the 1958-2000 period. This decline is of 20 to 30% for the winter, and of 7 to 10% for the other seasons. As for the study of Zeroual et al. (2013)

has been made on the Hodna basin (Algeria) and for the 2050 horizon, it shows a downward trend in the future flow's series compared to the period of 1961-1990, with a decrease of 26% in winter and of 17% in autumn. In addition, the downward trend of future flows compared to those observed in our study confirms the results obtained by IPCC (GIEC 2007).

6. Conclusion

Like all semi-arid basins, the Essaouira Basin is experiencing a decrease in precipitation as a result of climate change. Seeing that the flows and rainfall within these basins are causally related, this investigation aimed to evaluate the climate change impact on the hydrological regime within the Essaouira basin for the period 2020-2050.

To achieve this objective, the Rural Genius GR2M model was used to simulate flows based on rainfall and evapotranspiration. The Mann-Kendall and Pettitt tests were used to study the homogeneity and trend sense of the time series studied. The series of potential monthly evapotranspiration (ETP), for the period 1978 to 2005, shows an upward trend with an increase of 4.2%. Under 2.6, 4.5, and 8.5 RCPs of CIMP5, the trend rate is 1.9%, 1.5%, and 1.6%, respectively. The relationship study between rainfall and flows for the period 1978 to 2005 in the Essaouira basin shows the existence of a cause-and-effect relationship between these two parameters, and this rule remains valid for all zones under arid and semi-arid climate.

The future flows at the Igrounzar station using the GR2M model under the RCP 2.6 and 8.5 scenarios show an upward trend of 20% and 44.4% respectively by 2050. For the same period but under the RCP 4.5 scenario, the future flow series shows a downward trend of 42.5%. Concerning Zelten station, the future flows show an upward trend of 28.8% under RCP 2.6 scenario and 53.8% under RCP 8.5 scenario and a downward trend of 42.1% under the RCP 4.5 scenario. For the future flows at Adamna station by 2050, they show an upward trend of 19.70% and 43.7% under the RCPs 2.6 and 8.5 scenarios, respectively, and a downward trend of 40.6 % under the RCP 4.5 scenario. However, these results can serve as a basis for water resource protection and management in the Essaouira watershed by constructing hill reservoirs along the Igrounzar, Zelten and Ksob Wadi. These hydraulic structures can attenuate the flow of water during floods periods and therefore supply the aquifers. This technique of hill dams remains relevant for watersheds under arid, semi-arid and saharan climate.

Table 1

Mann-Kendall test results on Evapotranspiration and flow in the Essaouira basin from 1978 to 2005

Station			Mann-Kendall test	
	Evapotranspiration			
	p-value (%)	Alpha (%)	UMK	Trend
Igrounzar	3	5	+1.56	Upward
	Flow			
Igrounzar	4	5	+0.04	Upward
Zelten	2.5	5	+0.23	Upward
Adamna	3.2	5	-0.64	Downward

Table 2

Results of GR2M Calibration and validation for the Igrounzar, Zelten and Adamna stations: parameter values, Nash criterion and determination coefficient

Parameter	Units	Calibration (01/1991 to 12/1994)	Validation (01/1997 to 12/2001)
Igrounzar station			
X1	mm	665.14	665.14
X2	-	1.01	1.01
Nash	%	83	78
R^2	-	0.88	0.88
Zelten station			
X1	mm	148.41	148.41
X2	-	0.93	0.93
Nash	%	72	72
R^2	-	0.81	0.81
Adamna station			
X1	mm	148.41	148.41
X2	-	0.65	0.65
Nash	%	74	76
R^2	-	0.84	0.73

Table 3

Results of the Mann-Kendall test applied to future flows within Essaouira basin for the period 2020–2050 according to RCPs 2.6, 4.5 and 8.5 scenarios

Variable	p-value (%)	Alpha (%)	H0: no trend	UMK	Trend sense
Igrounzar station					
Flow					
RCP 2.6	0.1	5	no	+3.22	Upward
RCP 4.5	<0.01	5	no	-6.43	Downward
RCP 8.5	0.02	5	no	+3.70	Upward
Zelten station					
Flow					
RCP 2.6	1.1	5	no	+2.52	Upward
RCP 4.5	<0.01	5	no	-4.87	Downward
RCP 8.5	0.06	5	no	+3.45	Upward
Adamna station					
Flow					
RCP 2.6	4	5	no	+2.05	Upward
RCP 4.5	<0.01	5	no	-4.07	Downward
RCP 8.5	4.6	5	no	+1.68	Upward

Groundwater level evolution

1. Introduction

Over time, the hydrodynamic functioning of the aquifers within the Essaouira basin has experienced variations that are manifested by fluctuations in the piezometric level. This evolution of the piezometric level results mainly from the precipitation variability, the volumes of exploitation, as well as the contributions of surface waters which have been largely disturbed in recent decades following global warming. In this chapter, we try to study the evolution of the piezometric level of different aquifers of Essaouira basin, to assess the climate change impact on this vital resource. The Essaouira basin is subdivided into two parts; upstream part located on the east of the Tidzi diapir and the downstream part located on the other side of the diapir. Depending on the availability and distribution of the water points catching each aquifer in the study area, the piezometric maps were drawn up for the downstream part including the Plio-Quaternary, Barremian-Aptian and Hauterivien aquifers and the upstream part containing the Cenomano-Turonian aquifer. The points capturing the Turonian are too few to map their piezometric maps. As part of this study, thirteen campaigns were carried out over 43 years (1976 to 2019), as well as data from piezometric monitoring carried out by the ABHT (Annex II).

2. Upstream part

2.1. Cenomano-Turonian aquifer

2.1.1. Piezometric maps

The piezometric level measurement campaigns carried out in April 2016, April 2017, May 2018, and March 2019 concerned the Cenomano-Turonian aquifer system of the Meskala and Kourimat region. Examination of the maps (Fig.1) reveals that: (i) The general direction of groundwater flow appears to be controlled by the direction of the synclines and the direction of fracturing. The existence of a groundwater dividing line with a SE-NW direction influences the direction of flow. The general direction of flow takes place from the Southeast to the Northwest in the northern

part (Ouazzi-Kourimat) and from the Northeast to the Southwest in the southern part (Meskala). (ii) The mean hydraulic gradient shows variations that can be induced by the quantitative and qualitative variations of the fracturing and/or by the lithological nature of the reservoir. However, it is relatively strong in the upstream part reaching 2.5%. In the center, it decreases to 0.9%. This central part with a low hydraulic gradient corresponds to the Kourimat and Et Tleta Hanchane area where the pumping tests carried out show better

Figure 1

Piezometric maps of Cenomano-Turonian aquifer

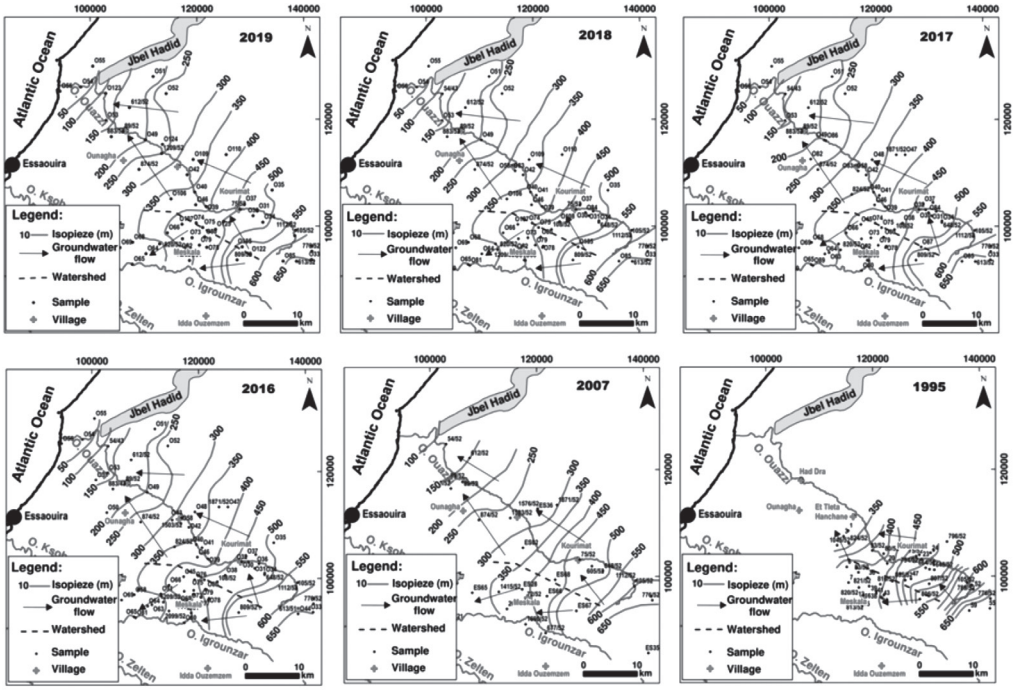

hydrodynamic characteristics of the study area. This area is a recharge zone of the aquifer, and therefore is the most favorable place to install water points. Towards downstream, the hydraulic gradient increases again to reach an average value of 2%.

For the observation period spread over 24 years, the groundwater keeps the same direction of flow with however a decent piezometric level. This situation is materialized comfortably, for example, by the shift of the isopiezes with altitudes 450 and 600 m more and more upstream, for the six piezometric maps.

2.1.2. Piezometric evolution

A comparison of the piezometric level evolution of the wells having experienced measurements of their water body during the four campaigns 2007, 2016, 2018, and 2019 was made (Fig. 2) and their location is shown in Figure 3. This comparison reveals a decrease in piezometric levels at all wells. This decline varies from one well to another, and this probably follows the nature of the geological formations crossed, demand intensity to meet the drinking water needs, and the scarcity of precipitation caused by climate change. It reached 9.8 m at well 89/52 and 12.3 m at well 75/52, between 2007 and 2019, i.e. an average annual drop of 0.82 m at well 89/52 and 1 m at well 75/52.

Figure 2

Evolution of the piezometric level of some wells capturing the Cenomano-Turonian aquifer

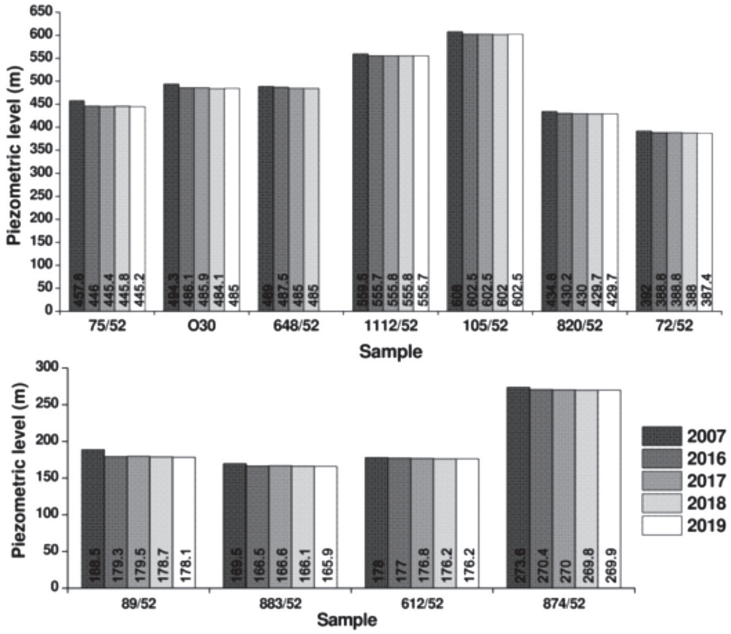

To monitor the piezometric level of the Cenomano-Turonian aquifer system, the ABHT installed a network of piezometers and its geographical distribution is presented in Figure 3. Unfortunately, it is to be noticed that there is a poor distribution of these piezometers. The majority of control wells are found in the Ouazzi-Kourimat syncline. Likewise, the majority of piezometers present limited series of data which make it impossible to follow the piezometric evolution of this aquifer system over a long period.

Figure 3

Location of the wells capturing the Cenomano-Turonian aquifer and piezometers for monitoring the piezometric level

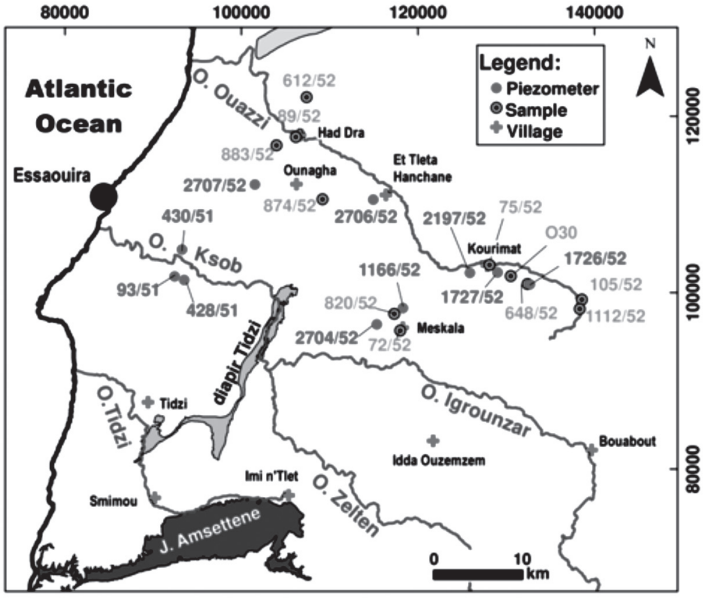

The piezometric level of groundwater within the Essaouira basin presents significant fluctuations between the periods of high water and low water (Bahir et al. 2002).

Piezometric monitoring data from seven piezometers with a monthly observation period spread over 11 years for 1726/52 and 1727/52, over 9 years for 2197/52 and 1166/52 and over 4 years for 2704/52, 2706/52, and 2707/52 were used to monitor the piezometric level of the Cenomano-Turonian carbonate aquifer system (Fig. 4).

Piezometer N° IRE 1166/52

This well is located on the Meskala basin north of the Meskala village. It shows amplitude of variation of the piezometric level of 4 m. The shape of its fluctuation curve is characterized by annual variations as a function of rainfall inputs. From 2008 to 2010, the water level experienced a slight stabilization with an altitude of 432 m. The deficit period 2010-2015 was marked by a very clear drop in the groundwater level with a decline of 4 m. Thereafter, the water level gradually increases to reach a piezometric level of 430 m. However, the groundwater level history shows a decrease between 2013 and 2016 of 5.4 m, i.e., an average annual decrease of 1.35 m.

Figure 4

Monitoring piezometric of the Cenomano-Turonian aquifer

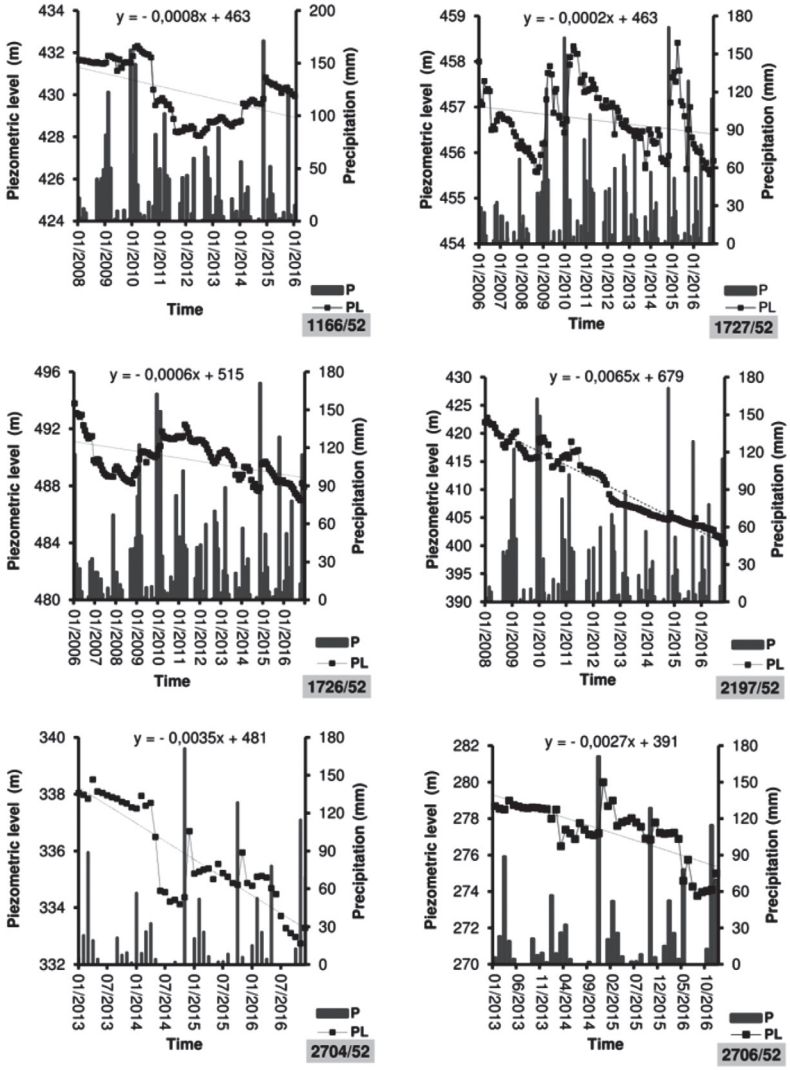

Piezometer N° IRE 2704/52

This well presents fluctuations and amplitude variation of the groundwater level of 6 m, for an observation period of 4 years. From January 2013 to May 2014, the groundwater level at this well experienced stability around a piezometric altitude of

338 m. Thereafter, it suffered a remarkable decline (≈ 4 m) before stabilizing at a level of 334 m. The precipitation at the end of 2014 raised the water level to reach a piezometric level of 337 m. After two months, the groundwater altitude will enter a phase of continuous lowering until the end of the study period. The average annual decline between 2013 and 2016 is around 0.98 m.

Piezometer N ° IRE 1727/52

This piezometer is located east of the Kourimat village. The piezometric level control chronicle is limited to 11 years. At first glance, the peaks of precipitation are accompanied by a rapid recovery of the groundwater level, in particular, the peaks at the end of 2009 and mid-2010, and early 2015 where the groundwater level reaches a piezometric altitude equal to 456.6, 458.3, and 458.4 m, respectively. Between these peaks, the groundwater altitude shows declining trends.

Piezometer N ° IRE 1726/52

This well is located further east of the piezometer 1727/52. Its groundwater altitude has the same appearance as that of 1727/52 with a lower rise during the rainy phase. This could probably be due to the low degree of fissuring at this well. The average annual downward is 0.39 m.

Piezometer N ° IRE 2197/52

This well located west of the Kourimat village experienced a monthly observation period spread over 9 years going from January 2008 to December 2016. Its groundwater altitude has a continuous downward trend with slight increases during the rainy periods, with an average of 1.98 m/year.

Piezometers N ° IRE 2706/52 and 2707/52

To downstream where wells 2706/52 (Et Tleta Hanchane) and 2707/52 (Ounagha) are installed, the groundwater level shows a downward trend with remarkable increases during excess phases during a 4 years chronic. Indeed, the rains of December 2014, where the rainfall reached 171 mm, caused the water level in well 2706/52 to rise from a piezometric level of 277.2 m to a 280 m, i.e a rise of 2.8 m for a month. At the 2707/52 piezometer, this rise is very significant, it is around 8.85 m. This reflects that the infiltration at Ounagha region is more important than at Et Tleta Hanchane region.

3. Downstream part

3.1. Plio-Quaternary aquifer

3.1.1. Piezometric maps

The Plio-Quaternary forms a large free water table in the northern part of the downstream part of the Essaouira basin. The relatively large number of wells capturing this aquifer made it possible to define its piezometry and its variations. The piezometric maps were drawn from data collected from the campaigns carried out in June 2015, April 2017, May 2018 and March 2019. These maps are depicted in Figure 5. Examination of these maps reveals that:

The general direction of the groundwater flow of the Plio-Quaternary aquifer is generally from south-east to north-west, imposed by the inclination of its substratum. Towards the downstream, the existence of a groundwater dividing line with the same orientation influences the flow direction. Indeed, in the north the streamlines are oriented in a similar way to that of the global flow; in the south, the streamlines are rather oriented from east to west. This groundwater dividing line originates from the hidden Essaouira diapir detected by geophysics in the western part of the aquifer.

The hydraulic gradient is strong in the upstream part, as a result of the strong inclination of the substratum caused by the outcrop of the Tidzi diapir. It is around 2.3% on average. In the center, it decreases to 0.4% on average. Then, it tries to increase towards the downstream, to reach an average value of 1% vertical to the hidden diapir of Essaouira.

For the observation period spread over 29 years, the groundwater keeps the same flow direction, this is quite logical since the main flow follows substantially the geometry of the aquifer, with however a decent piezometric level. This situation is materialized comfortably, for example, by shifting the isopiezes with altitude 40 and 180 m more and more upstream, on the nine piezometric maps.

3.1.2. Piezometric evolution

A comparison of the piezometric level evolution of the wells capturing this aquifer. Measurements of water levels during the 1990, 1995, 2000, 2004, 2009, 2015, 2017, 2018, and 2019 campaigns was made (Table 1). The wells location is shown in Figure 6. This comparison reveals a decrease in the piezometric level at these wells. It varies from one well to another, and this probably follows the intensity of the solicitation by the population to meet their drinking water needs, the nature of the aquifer matrix, and the decrease in precipitation in recent years as a result of climate change.

Figure 5

Piezometric evolution within the Plio-Quaternary aquifer

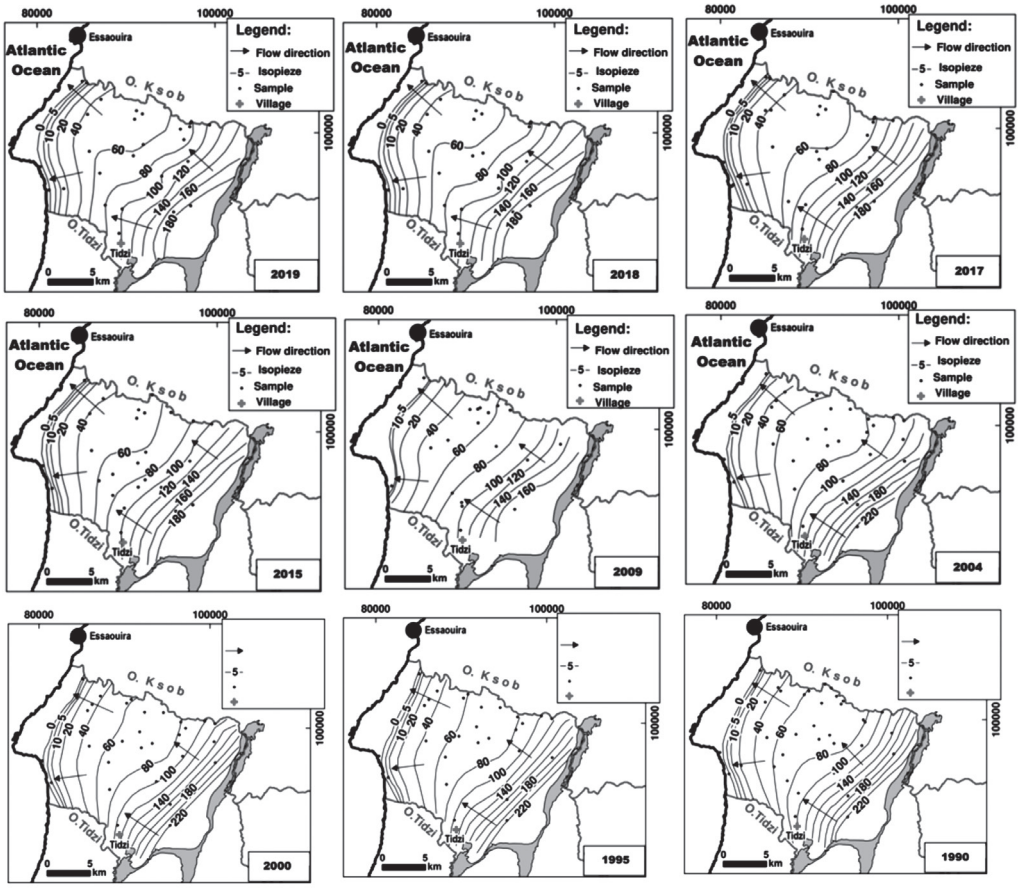

Figure 6

Location of wells capturing the Plio-Quaternary, Barremian-Aptian and Hauterivian aquifers

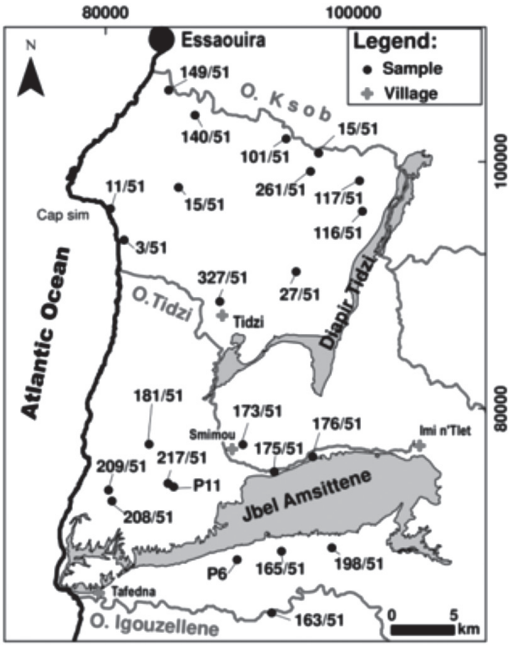

It reached 17.45 m at well 261/51 and 6.66 m at well 140/51, between 1990 and 2019, an average annual downward of 0.72 m at well 261/51 and 0.23 m at well 140/51, respectively. The 1995 drought, the driest year in Morocco during the twentieth century, led to a general decline in the groundwater level, the effects of which still persist, since the rise in groundwater level during the campaigns beyond this year has not returned to its initial level in 1990 at some wells, such as 15/51 and 140/51, and this despite several rainy hydrological cycles (notably those of 1996/97, 2003/04, 2009/10, and 2010/11).

Other wells have become dry, such as wells 116/51 and 117/51 (since 2004) and 101/51 (since 2009). The piezometric control of the Plio-Quaternary aquifer is ensured by two piezometers: 93/51 and 428/51 whose survey of the groundwater level is carried out at monthly time intervals over 8 years (January 2007-December 2014) and 11 years (January 2006-December 2016), respectively (Figure 7). These two piezometers 93/51 and 428/51 monthly monitored for piezometric levels over an observation period spread over 8 and 11 years are located on the left bank of the Ksob wadi near Sidi

Yassine. The groundwater level monitoring at these piezometers shows an identical evolution. Before the precipitation at the end of 2009, the groundwater level showed a decline of 0.5 m at well 93/51 and 1 m at well 428/51. Beyond this date, the piezometer level begins to rise again to reach a piezometric level equal to 62.3 and 67.9 m at the well 93/51 and 428/51, respectively. Thereafter, it shows a decline until the end of the study period. The average annual downward equal to 0.08 and 0.16 m at wells 93/51 and 428/51, respectively. However, the evolution shape of the groundwater level at these two wells is identical. This is because they are located in an identical geological context and that the Plio-Quaternary aquifer regime follows that of precipitation.

Figure 7

Monitoring piezometric of the Plio-Quaternary aquifer

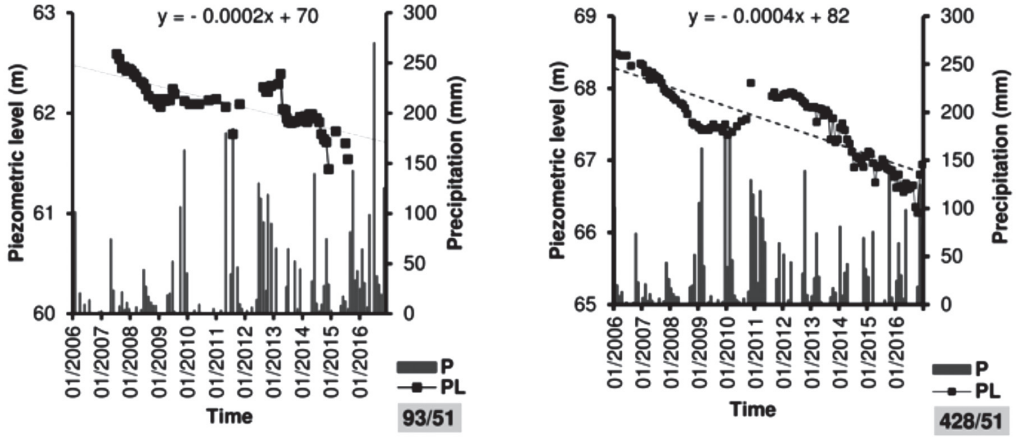

3.2. Barremian-Aptian and Hauterivian aquifers

3.2.1. Piezometric maps

The Barremian-Aptian aquifer is bounded to the North by Tidzi wadi, to the South by Amssittene anticline, to the East by formations of the Lower Cretaceous and to the West by the Atlantic Ocean. For the Hauterivian aquifer, it is bounded to the North by the Amssittene anticline, to the South by Igouzoullene Wadi, to the East by the Atlantic Ocean, and to the West by formations of the Lower Cretaceous. The relatively large number of wells capturing these two aquifers made it possible to define its piezometry and its variations. The piezometric maps were drawn up based on data from the campaigns carried out in June 2015, April 2017, May 2018, and March 2019. The maps obtained are shown in Figure 8.

The general direction of the groundwater flow of the Barremian-Aptian aquifer is generally from south-east to north-west, it is imposed by the northern flank of the Amssittene anticline and the uplift of the lower Cretaceous formation's substratum. While that of the Hauterivian aquifer, it is from the northeast to the southwest, this flow is imposed by the southern flank of the Amssittene anticline. According to these maps, the Igouzoullene wadi seems drains the Hauterivian aquifer and this is manifested by sources with low flows along this wadi.

3.2.2. Piezometric evolution

With a total of 12 wells, eight wells capture the Barremian-Aptian aquifer and four wells capture the Hauterivian aquifer. Measurements of the groundwater altitude during 1976, 1997, 2015, 2017, 2018, and 2019 campaigns, have permitted a study of groundwater level evolution of the aforementioned aquifers (Table 2). The geographic location of these wells is shown in Figure 6. This comparison shows a decrease in piezometric levels at the majority of wells. It varies from one well to another, and this probably follows the intense solicitation to meet the drinking water needs and the nature of the lithological facies of the aquifer added to the decrease in precipitation. Within the Barremian-Aptian aquifer, it reached 9.1 m at well 176/51 and 8.8 m at well 173/51, between 1976 and 2019, with an average annual drop of 0.2 m. For the groundwater level of the Hauterivian aquifer, this decrease reached 3.85 m at the well P6 and 3 m at the well 193/51, representing an average annual decrease of 0.17 and 0.14 m, respectively. We note, as well for the Barremian-Aptian aquifer as for the Hauterivian, a rise in the piezometric level within the wells having experienced measurements of their groundwater level in 1997. This rise is linked to climatic variations where the rainfall reached 680 mm in 1996/97. Beyond this date, the piezometric level shows a downward trend and this for all wells.

Figure 8

Piezometric evolution within the Barremian-Aptian and Hauterivian aquifers

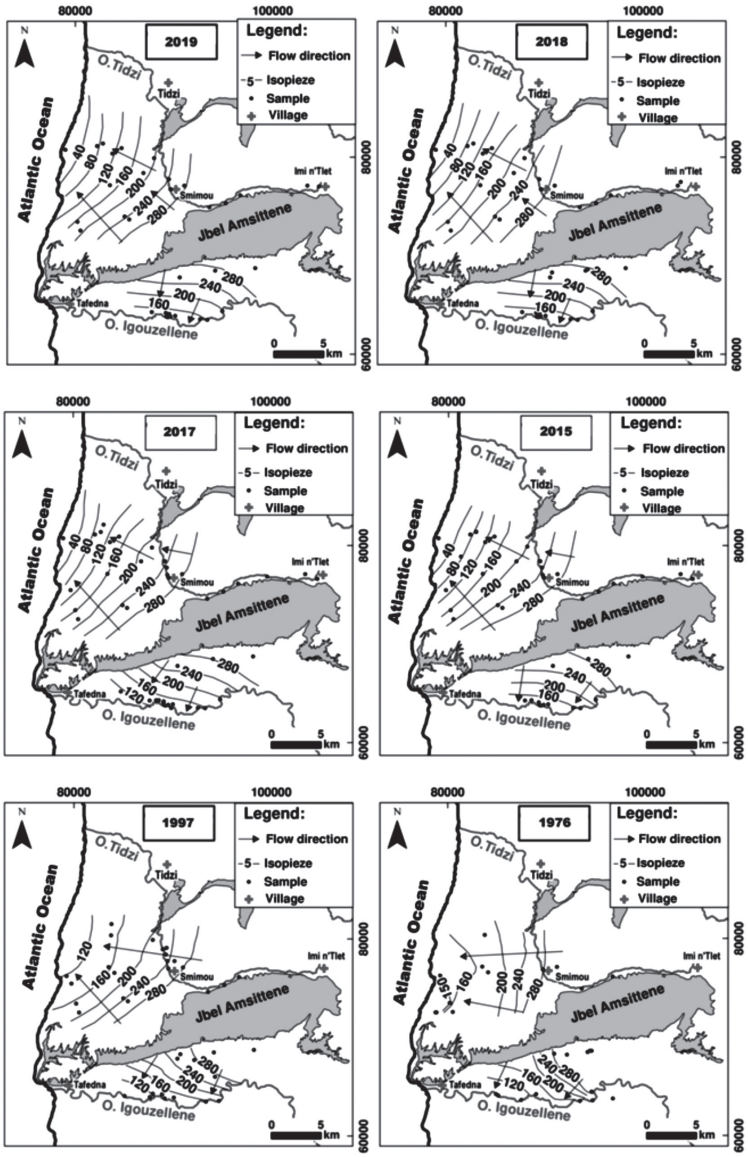

Since the study area is characterized by the total absence of industrial activity and the agricultural activity practiced is of the "food type", the decline in the piezometric level could only be explained by the downward trend precipitation during the last decades as

a result of climate change and over-exploitation to meet drinking water needs. The rise in the piezometric level for some wells is induced by the effect of intense precipitation which is often grouped in the form of floods in the wadis of this region.

4. Conclusion

The piezometric study has shown that the general direction of the groundwater flow of the Cenomano-Turonian aquifer is from south-east to north-west in its northern part (Ouazzi-Kourimat) and from north-east towards the southwest in its southern part (Meskala). For the Plio-Quaternary and Barremian-Aptian aquifers, the major flow axes are oriented from south-east to north-west. As for the Hauterivian aquifer, the direction of flow is from the northeast to the southwest. The main outlet for groundwater in the Essaouira basin is the Atlantic Ocean. Monitoring of piezometry over 24 years (1995-2019) for the Cenomano-Turonian aquifer, 29 years (1990-2019) for the Plio-Quaternary aquifer and 43 years (1976-2019) for the Barremian-Aptian and Hauterivian aquifers show a continuous drawdown of the aquifers which exceeds 12 m for the Cenomano-Turonian aquifer, 17 m for the Plio-Quaternary aquifer, around 8 m for the Barremian-Aptian aquifer, and 5 m for the Hauterivian. The general decline in the piezometric altitude could be explained by the decrease in precipitation during the last decades as a result of climate change and by over-exploitation to meet the drinking water needs. In turn, this drawdown would undoubtedly cause degradation in groundwater quality.

Table 1

Piezometric variation at the wells capturing the Plio-Quaternary

Wells	H1990	H1995	H2000	H2004	H2009	H2015	H2017	H2018	H2019	H2019-H1990
3/51	2.4	3.8	4.2	4.5	3.0	0.7	–	–	-2.9	-5.3
11/51	-1.0	-1.8	-0.5	0.0	-	-0.9	-1.0	-1.1	-1.2	-0.17
15/51	60.2	47.6	49.0	60.0	58.0	53.0	57.4	56.9	56.8	-3.35
27/51	169.5	156.9	164.0	173.0	–	171.8	170.3	–	170.3	0.78
140/51	50.2	50.3	50.5	51.5	–	43.6	43.8	43.5	43.6	-6.66
149/51	-2.7	-2.3	-2.5	0.0	-1.2	-1.6	-1.6	-1.7	-1.7	1.00
261/51	-	89.9	86.2	87.5	–	–	72.3	-	72.5	-17.45
272/51	76.4	79.3	81.1	69.5	–	–	76.4	76.9	76.0	-0.4
101/51	72.0	70.0	71.0	72.0	dry	dry	dry	dry	dry	–
116/51	178.6	178.0	178.2	dry	dry	dry	dry	dry	dry	–
117/51	136.4	-	136.7	dry	dry	dry	dry	dry	dry	–

Table 2

Piezometric variation at the wells capturing the Barremian-Aptian and Hauterivian aquifers

Wells	H1976	H1997	H2015	H2017	H2018	H2019	H2019-H1976
Barremian-Aptian							
P11	-	256	253.5	253.48	253.5	252.84	-3.16
173/51	272.21	277.8	263.8	263.75	263.3	263.4	-8.81
176/51	423	420	414.23	414.45	414.07	413.9	-9.1
181/51	159.6	160	159.7	159.5	159.3	159.5	-0.1
209/51	137.18	140.4	137.75	137.6	137.4	137.5	0.32
208/51	215.8	217.5	216.45	216.5	216.5	216.6	0.8
217/51	-	244.55	240.64	240.1	239.4	238.7	-5.85
Hauterivian							
198/51	-	328.69	326	326.5	326.83	325.7	-2.99
165/51	278.55	277.8	278.1	278.45	278.78	277.2	-1.35
P6	-	261.3	258.9	259.3	259.8	257.45	-3.85

Quantitative and qualitative assessment of groundwater in semi-arid zones in the context of climate change, example of Essaouira region, Morocco

1. Introduction

Climate change is a global problem, involving the long term complex interactions between environmental factors and economic, social, technological and political conditions which cause significant effects at regional level (Lebel and Vischel 2005; Alpert et al. 2008; Misra 2014), including the Maghreb region (Bahir et al. 2016; El Kharraz 2012; Ouhamdouch et al. 2018, 2020a; Ragab and Prudhomme 2002).

In arid and semi-arid regions, rainfall is one of the determining factors of climatic characterization. The study of recent evolution in climate is an essential tool to determine optimal general solutions to the problems resulting from the relationship between water requirement and their availability, and therefore better management of water resources (Bahir et al. 2018a, 2019, 2020b; Carreira et al. 2018; Ragab and Prudhomme 2002).

Studies on climate change show that global warming in the Maghreb country is significant than the global average. Indeed, on a global scale, the increase estimated at 0.74 ° C in the 20th century, while it was oscillating between 1 and 2 ° C on the Mediterranean scale and the region of North Africa (GIEC 2007; Green et al. 2011; Ouhamdouch et al. 2018, Ragab and Prudhomme 2002). As for precipitation, it has decreased in the Mediterranean region, in the Sahel, in southern Africa and in certain parts of South Asia at different temporal and spatial scales (Alpert et al. 2008; IPCC 2013).

Morocco, like the Mediterranean countries (Vicente-Serrano 2006), have suffered from several periods of drought (Bahir et al. 2002; Driouech 2010; Babqiqi 2014). Its water resources are limited; they are estimated to 20 billion cubic meters, or an average of 700 m^3/year/inhabitant, which corresponds to a situation of fairly high water stress. The number of years in rainfall deficit is greater than the number of wet years (Driouech 2010; Stour and Agoumi 2009; Sinan et al. 2009), especially the cycles of 1980-1985, 1990-1995 and 2007-2010. According to Babqiqi (2014), the comparison of the average annual temperatures over the two periods 1971-1980 and 1998-2007

shows an increasing trend (from 0.3 to 2.5 ° C depending on the region). This decrease in precipitation and the increase in temperatures linked to the climate change are likely to have a negative impact on water resources, especially in arid and semi-arid areas.

In these regions, few studies have been done to assess the climate change impact on water resources, but they are generally focused on surface water (Abutaleb et al. 2018; Hallouz et al. 2019; Xu et al. 2004). Some other studies studies have evaluated the global warming effect on groundwater by limiting ourselves to the piezometric and/or hydrochemical approach (Al-Maktoumi et al. 2018; Berhail 2019; Lachaal et al. 2018). For a complete study, we assessed the impact of climate change on the water resource of the Essaouira basin (Morocco) by combining several approaches such as hydroclimatology, piezometry, hyrochemistry and isotopy.

The study area, called the Essaouira syncline basin, covers an area of 6000 km². It is part of the Atlantic Atlas, which is the westernmost part of the southwestern Moroccan basin (Dresh 1962; Duffaud 1960). This basin is bounded to the north by Hadid anticline, to the south by Tidzi wadi, to the east by the Bouabout region, and to the west by the Atlantic Ocean. It is subdivided into two parts, the first known as the "Bouabout unit" (upstream part) and the second known as the "coastal zone" (downstream part) (Fig. 1).

Figure 1

Location of study area

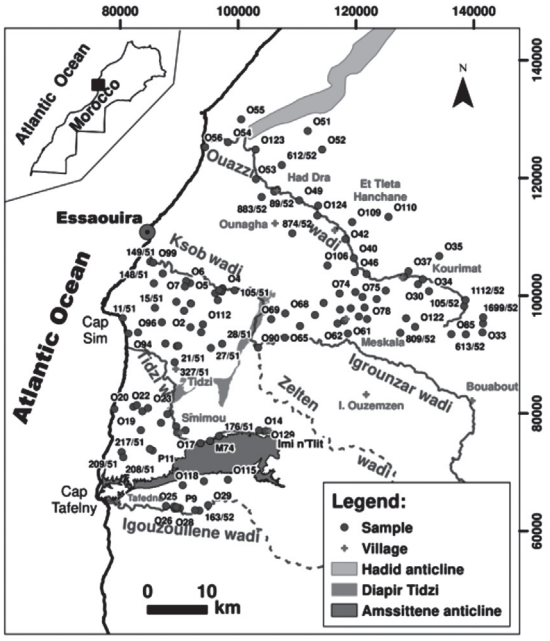

From a morphological point of view, the study area is made up of a set of synclinal basins filled with formations ranging from the Triassic to the Quaternary (Fig. 2). The elevations vary between 400 and 1600 m for the upstream part and less than 400 m for the downstream part. Hydrographically, the study area is characterized by a less-developed network. This is mainly represented by Ouazzi wadi in the North and Igouzoullene wadi in the South, passing through Ksob wadi resulting from the confluence of Igrounzar and Zelten wadi and through Tidzi wadi. All of these wadis flow into the Atlantic Ocean (Fig. 2).

Figure 2

Geological map of study area and cross sections location

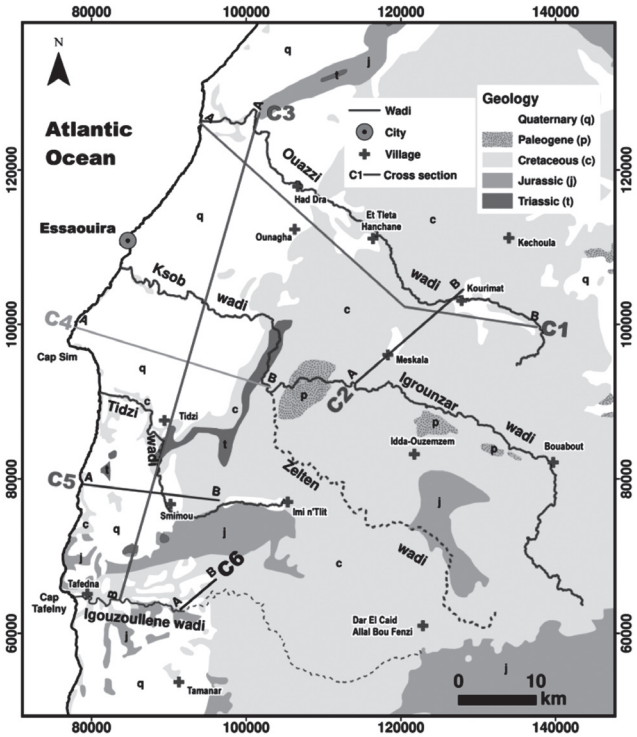

Geologically and hydrogeologically, the upstream part of the study area is marked by the outcrop of formations of Middle and Upper Cretaceous age, in particular, Albian-Vraconian, Cenomanian and Turonian (Duffaud 1960; Amghar 1989) (Fig. 3). These formations are composed of limestone and dolomitic benches interspersed with marl and sandstone. The Albian-Vraconian formations contain sandstone and limestone dolomites alternating with sandstone banks and sandy clays.

Figure 3
Cross sections (cf Figure 2)

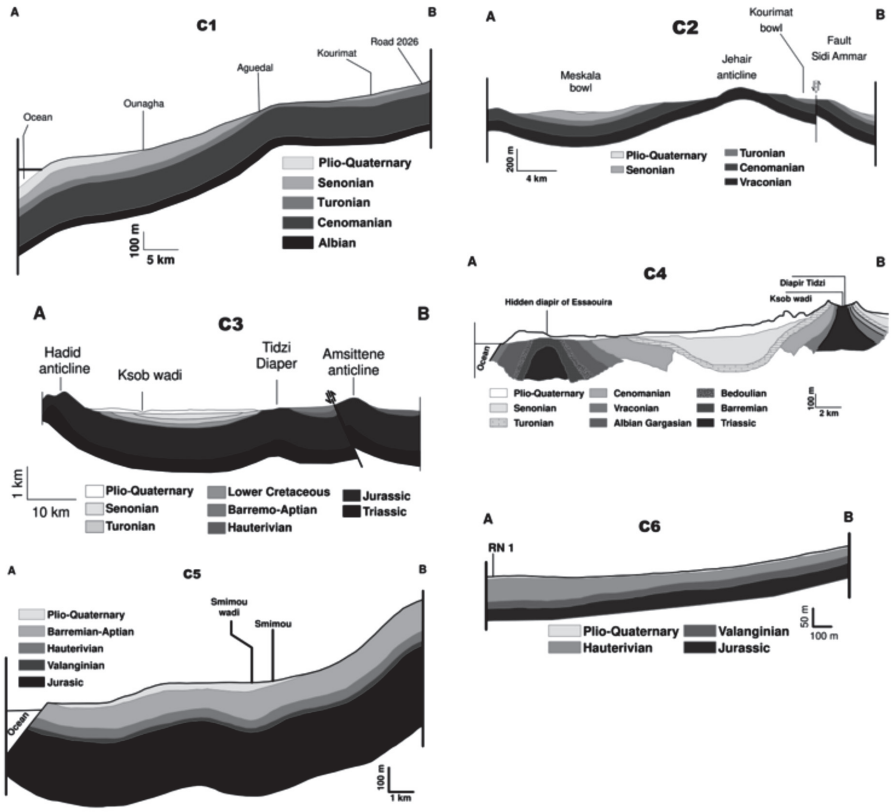

The Cenomanian (about 200 m thickness) is represented by alternating marls with anhydrite, lumachellic and dolomitic limestones. As for the Turonian, it is composed of limestones with an abundance of silica. These synclines contain important water reservoirs, notably the Cenomanian-Turonian aquifer which remains the most important in the region. According to Jalal et al. (2001), this aquifer has transmissivities varying between 2.2*10-4 and 2.7*10-1 m^2/s.

The downstream part contains two aquifers: (i) the Plio-quaternary and the (ii) Turonian in the northern part, between Ksob wadi and Tidzi wadi, (iii) the Barremian-Aptian located between Tidzi wadi and Amssittene anticline and (iv) the Hauterivian, southern limit of the study area, is interposed between the Amssittene anticline and Igouzoullene wadi (Fig. 2). The Plio-quaternary is characterized by a matrix of limestone sandstone. It contains an important water table, the wall of which is formed

in the synclinal structure by the marls of Senonian (Fig. 3). According to Mennani (2001), this water table has transmissivities varying between $6.1*10^{-2}$ and $4.5*10^{-5}m^2/s$. As for the Turonian, represented by limestones, it contains a captive aquifer under the Senonian marls in the synclinal structure and probably in direct contact with the Plio-Quaternary at the confines of this structure (Fig. 3). It has a transmissivity ranging between $0.8*10^{-4}$ and $2.7*10^{-2}$ m^2/s (Mennani 2001). The Barremo-Aptian aquifer contains Barremian formations (about 70 m thickness) represented by an alternation of gray marl (with traces of gypsum), fractured fossiliferous limestones and sandstone and Aptian formations (about 100 m thickness) composed of red clays and sandstone with intercalations of dolomitic sandstones or bioclastic limestones (Duffaud 1960; Duffaud et al. 1966) (Fig. 3). The transmissivity is of the order of $1.5*10^{-3}$ m^2/s (Mennani 2001). The Hauterivian aquifer, whose thickness is about 200 m, is composed of marly clays and fractured siliceous limestones, marly and dolomitic limestones more or less fractured (Fig. 3) (Duffaud 1960; Duffaud et al. 1966). According to Mennani (2001), this aquifer has transmissivities varying between $1.6*10^{-5}$ and $6.7*10^{-5}$ m^2/s.

2. Materials and methods

In this investigation, the results of nine campaigns 1990, 1995, 1997, 2009, 2015, 2016, 2017, 2018 and 2019 were used to assess the quality of groundwater in the Essaouira region in the context of climate change. Electrical conductivities, temperatures, pH and nitrates were measured in situ with a portable conductivity meter (HI-9829 multiparametric instrument), and the depth of the water level was measured using a 200 m piezometric probe.

The analyses of the chemical elements were carried out at the Laboratory of Hydrogeology at the Faculty of Sciences Semlalia of Marrakech (Morocco) for the campaigns 1990 to 2009. As for that of 2015 to 2019, the analyses were carried out at the Laboratory of Geosciences and Environment- ENS at the Ecole Normale Superieure of Marrakech (Morocco). The SO_4^{2-} anion contents were determined by the nephelometric method (Rodier et al. 2009). Concentrations of Ca^{2+} and Mg^{2+} cations were measured by the complexometry method (EDTA) and those of Cl^- by the Mohr method (Rodier et al. 2009). The Na^+ and K^+ contents were determined by flame photometry (Rodier et al. 2009). As for HCO_3- contents, they were determined by titration using a sulfuric acid solution. All the samples display an ion balance of less than 10%, which allowed us to validate the obtained results. The obtained results are grouped in Appendix 1.

A Geographic Information System (GIS) was used to map the spatial distribution maps of the electrical conductivity and the physicochemical elements.

The PHREEQC program (Parkhurst and Appelo 1999) was used to calculate the saturation indices (SI) using the following formula: $SI = \log\left(\frac{K_{IAP}}{K_{SP}}\right)$.

With: K_{IAP} is the product of the ionic activity of ions. KSP is the mineral solubility product. The saturation index corresponds to the deviation from the equilibrium of the water from the mineral phase. If SI = 0, the water is in equilibrium; if SI is negative, the water is undersaturated with respect to the mineral; if SI is positive, the water is supersaturated with respect to this mineral.

4. Results and discussion

A hydrogeochemical approach is a valuable tool for characterizing groundwater chemistry. The latter is largely influenced by the characteristics of the host rock, the hydrodynamics of the aquifers and also by the climatic and exploitation conditions.

4.1. Electrical conductivity

Electrical conductivity is mainly governed by the concentration of dissolved ions. It is closely linked to the lithological nature of the soil, the speed and direction of groundwater flow as well as the groundwater residence time. This parameter is proportional to the temperature. The results obtained are shown in Figure 4.

The electrical conductivity of Cenomano-Turonian waters (upstream part) analyzed in 1995 does not exceed 3 mS/cm, with more than 80% falling into classes below 1.5 mS/cm. In 2007, the values of the EC knew an increase where some samples present values higher than 2.5 mS/cm. Thereafter, the EC values are increasing to reach values of 5 mS/cm in certain places, and this since 2016.

This increase may be the result of the decrease in precipitation experienced by the study area in recent decades. As for the Plio-Quaternary aquifer, the EC values vary between 1 and 6 mS/cm for 1990, 1995, 2004, and 2009 campaigns. The values become higher and higher towards the West and the South. This can be explained in the South by the influence of the Triassic terrains rich in halite and the West by the combined action of the hidden diapir of Essaouira as well as that of aerosols and sea spray near the ocean. While the low values are observed in the north-east and east (aquifer recharge zone).

From 2015, we see the appearance of outliers reaching 12 mS/cm in 2019, and this towards the West. EC values measured for the Plio-Quaternary aquifer are greater than those obtained for the Cenomano-Turonian aquifer. This could be due to the effect of the Triassic formations (Tidzi diapir) rich in halite and the leaching of sea spray and

aerosols by the rains feeding the aquifer. The outliers measured since 2015 and which increase to reach 12 mS/cm in 2019 are due to the intrusion of seawater.

The Turonian aquifer has known the EC measurement from 2004 to 2019. The obtained results show an oscillation of the values of this parameter around 2 mS/cm with a slight increase exceeding 2.5 mS/cm in 2018 and 2019. This stability of the EC within this aquifer can be explained by its captive nature and by the homogeneity of their facies consisting of limestones and dolomitic limestones. For the Barremian-Aptian aquifer, the majority of the samples have EC values that range over the class 1-2 mS/cm, while the rest fall within the class 2-4 mS/cm. The highest values are observed towards the North-west and West, under the influence of the Triassic salt formations as well as the effect of sea spray and aerosols leached by the rain infiltrating towards the aquifer. Towards the East, the influence of these factors decreases and the EC values decrease, this is the aquifer recharge zone. Except the samples from the 1997 campaign, the waters of the Hauterivien aquifer show EC values between 1 and 2 mS/cm. Outliers observed in 1997 can be explained by the fact that some water points sampled in 1997 were not sampled during the other campaigns. Generally, the evolution of the mean of EC values observed within the Barremian-Aptian and Hauterivian aquifers are stable and this could be explained by their captive nature.

4.2. Chemical facies

To clarify the groundwater chemical facies in the study area, the composition of major elements has been plotted on the Piper diagram (Piper 1944). This uses the major elements expressed in meq/l to represent the different groundwater facies. Also, it makes it possible to follow the evolution of water, passing from one facies to another. The practice is to plot the percentage of each major element on two equilateral triangles, one for cations and the other for anions. The projection of the representative points on the rhombus allows us to determine the chemical facies of water (Figure 5).

Figure 4

Temporal evolution of the electrical conductivity of groundwater

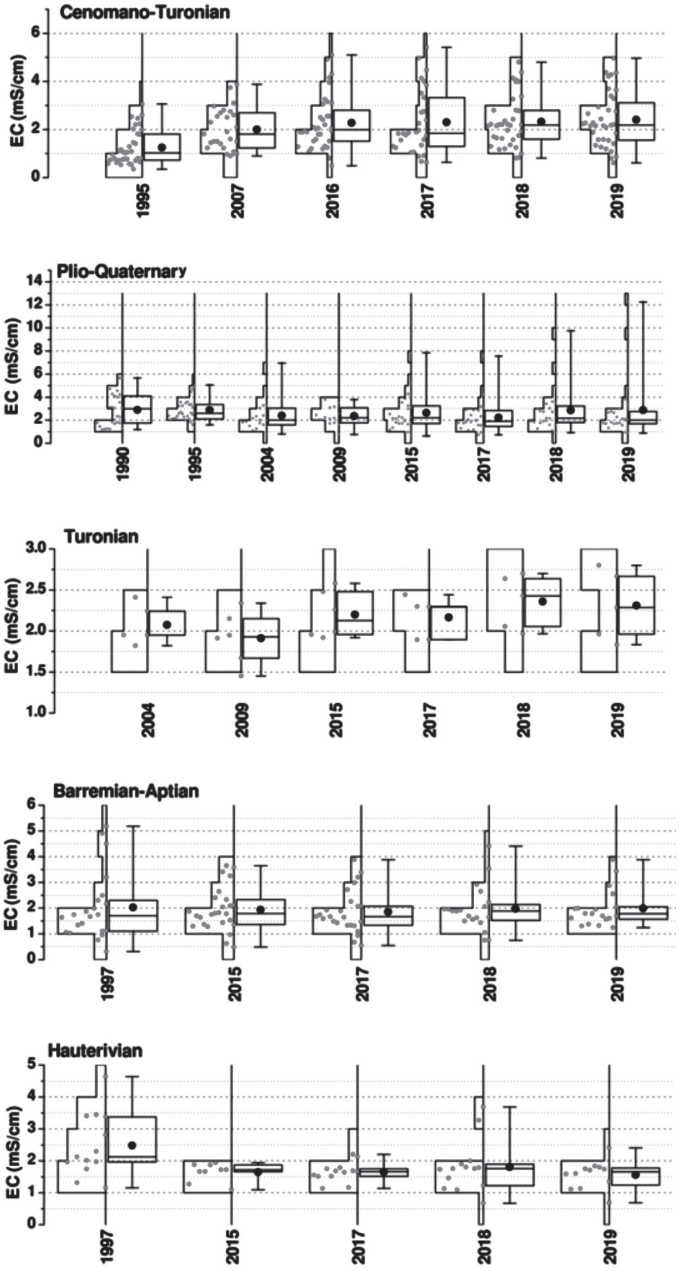

Figure 5

Graphical representation of the Piper diagram

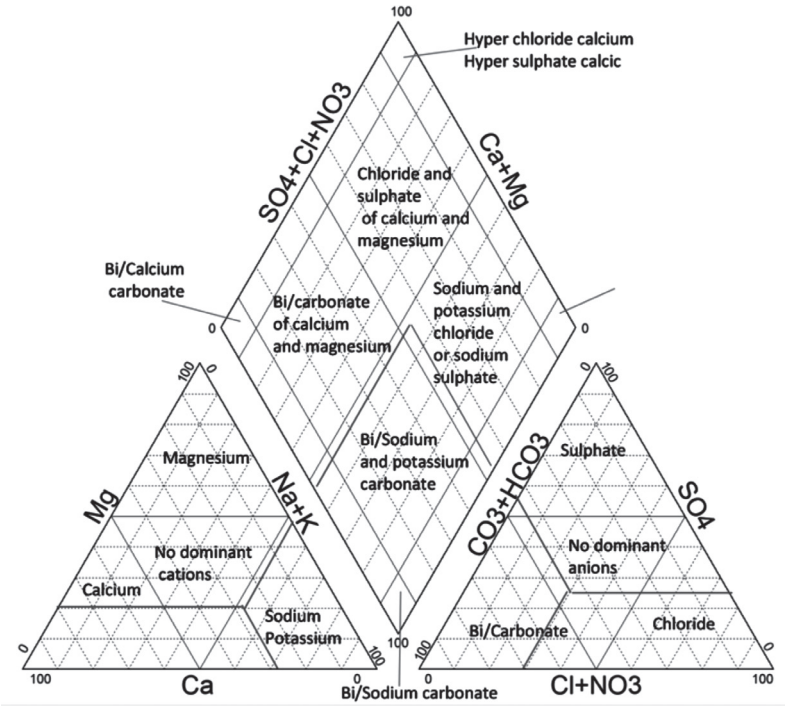

To specify the groundwater chemical facies in the study area, the major element composition has been plotted on the Piper diagram (Piper 1944).

– For the Cenomanian-Turonian aquifer, representing the upstream part of the basin studied, the projection of the analysed samples on the Piper diagram (Fig. 6a) shows that the waters have mixed facies between Cl-Na, Cl-Ca-Mg, SO_4-Ca-Mg, and HCO_3-Ca-Mg. In 1995, the majority of the samples presented Cl-Ca-Mg facies. For the samples of the 2007 campaign, the chemical facies of the waters are of Cl-Ca-Mg, SO_4-Ca-Mg and HCO_3-Ca-Mg type with the dominance of the Cl-Ca-Mg type. As for the samples analysed in 2016, they have facies of Cl-Na type and of the Cl-Ca-Mg and SO_4-Ca-Mg type. For the 2017, 2018 and 2019 campaigns, we note that the analysed waters present three types of facies: Cl-Na, Cl-Ca-Mg, SO_4-Ca-Mg, and HCO_3-Ca-Mg with the dominance of the Cl-Ca-Mg type. A comparison of the results of the 1995 campaign and those of 2019 (Fig. 6b) shows that the groundwater facies of the Cenomanian-Turonian aquifer have not experienced any remarkable change.

Figure 6

Piper Diagram of analysed samples of (a) Cenomanian-Turonian aquifer from 1995 to 2019 and (b) comparison between samples of 1995 and 2019

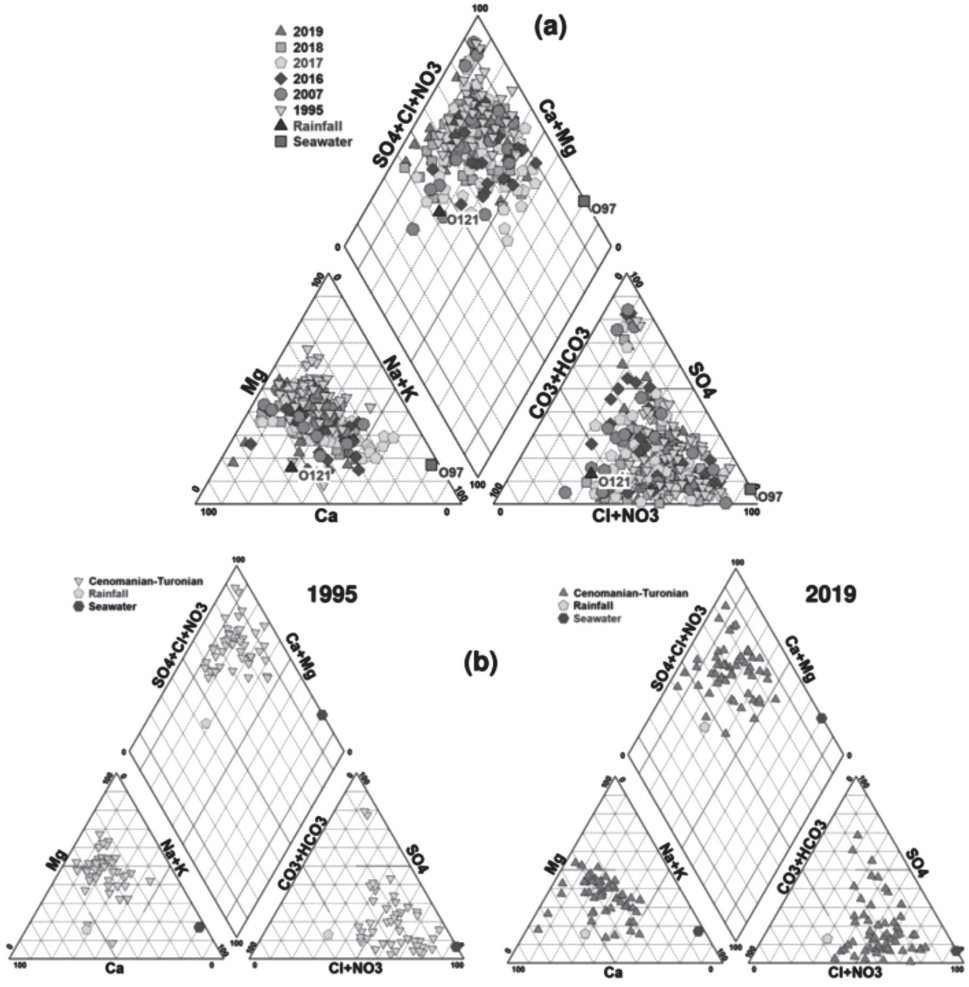

– For groundwater of the downstream part, the analysis of the Piper diagrams for the Plio-Quaternary and Turonian aquifers (Fig. 7a, b) shows that they are classified under mixed facies between Cl-Na and Cl-Ca-Mg. The regrouping of the points of the Plio-Quaternary aquifer near the Turonian aquifer suggests an interconnection between these two aquifers.

Figure 7

Piper Diagram of analysed samples of (a) Plio-Quaternary from 1990 to 2019 and of (b) Turonian from 2009 to 2019, and (c) comparison between samples of 1990 and 2019 for the Plio-Quaternary aquifer

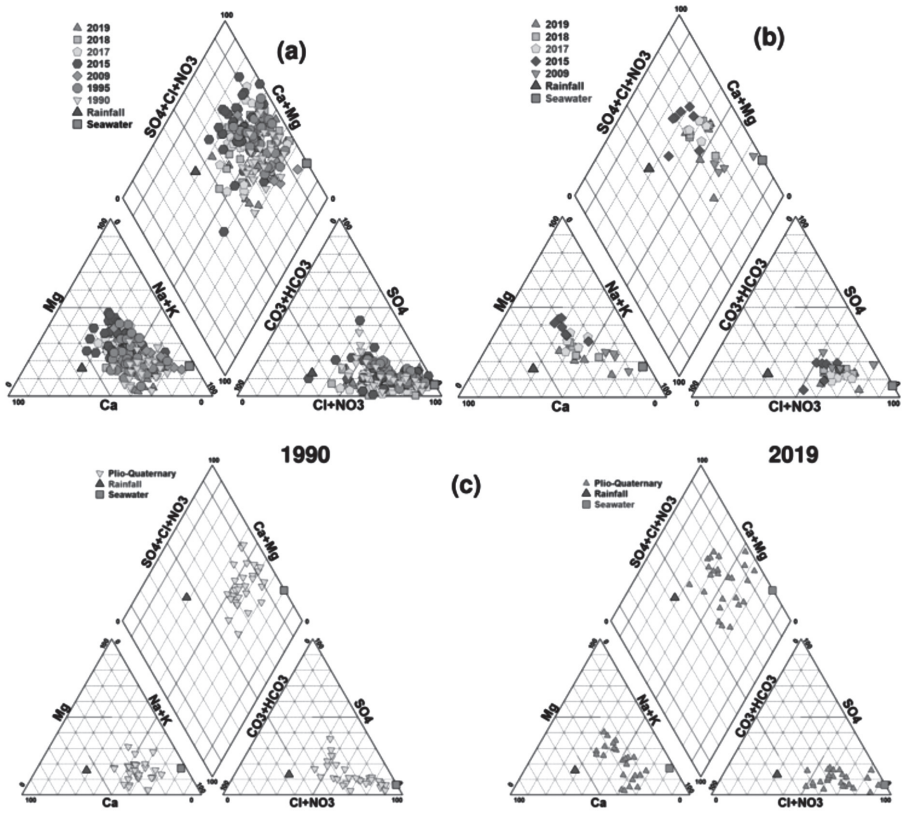

The comparison between the results of 1990 and 2019 is presented in Figure 7c. This shows that there is a slight evolution in the chemical facies of the Plio-Quaternary groundwater. Indeed, on the cation's triangle concerning the 1990 campaign, the majority of the points have a percentage higher than 50% in Na^+ with a tendency towards the Na pole. However, in 2019, the majority of the points do not exceed 50% in Na^+ with a tendency towards the center of the sorting "no dominant cations". For the anion triangle, a clear dominance of $C1^-$ is noted, whether in 1990 or in 2019. The position of certain samples relative to the sample representing seawater on the Piper diagram suggests that the Plio-Quaternary aquifer is probably affected by the marine intrusion.

The groundwater of the Barremian-Aptian and those of the Hauterivian generally present three types of chemical facies: Cl-Na, Cl-Ca-Mg, and HCO_3-Ca-Mg with the dominance of the second facies (Fig. 8a, b). The dominance of Cl over HCO_3 could be explained by the influence of Triassic saliferous formations. The comparison between the water points sampled in 1997 and 2019 (Fig. 8c) shows a remarkable evolution in the groundwater chemistry of the Barremian-Aptian and Hauterivian aquifers from the mixed facies Cl-Na and Cl-Ca-Mg to the facets Cl-Ca-Mg.

Figure 8

Piper Diagram of analysed samples of (a) Barremian-Aptian and (b) Hauterivian aquifers from 1997 to 2019, and (c) comparison between samples of 1997 and 2019 for the two aquifers

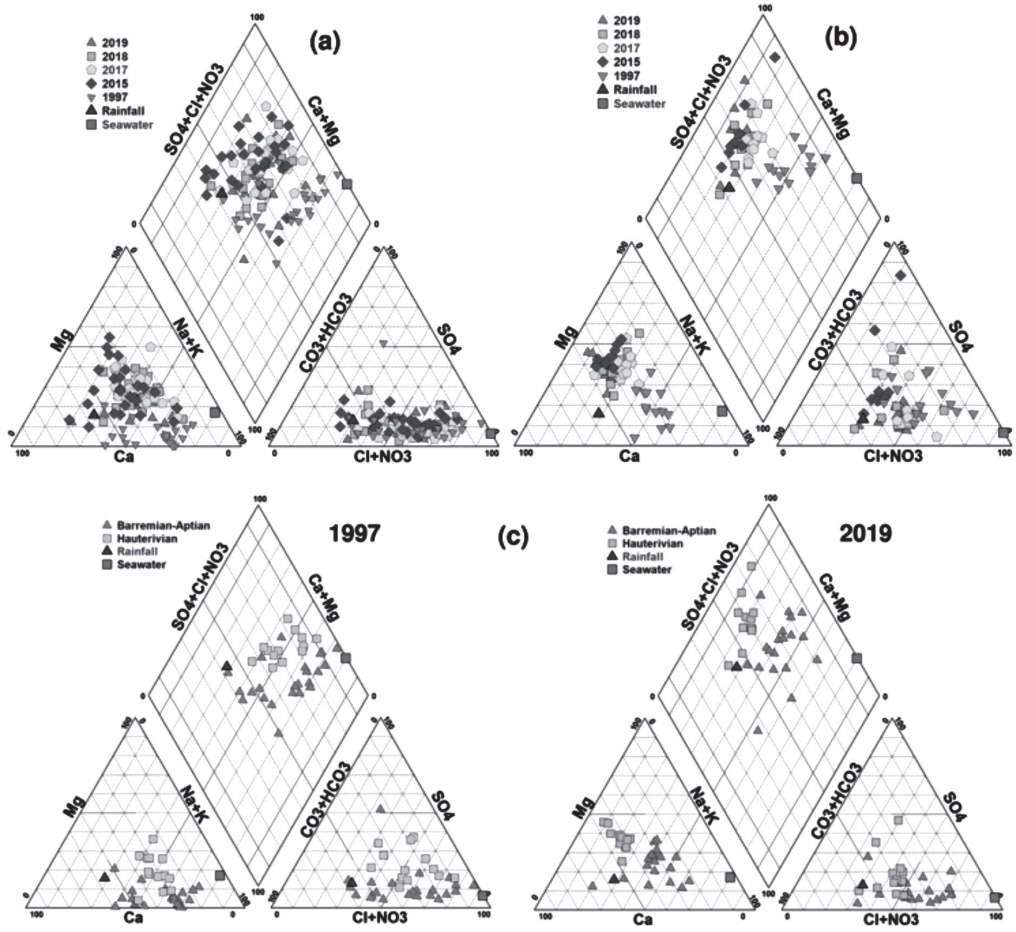

4.3. Groundwater mineralization

To determine the origin and the main processes responsible for the groundwater mineralization of the study area, the correlations between the main major elements have been studied.

Chloride is a conservative ion that is always found in natural waters at very variable contents (Fetter 1993) and sodium is generally associated with chlorides. Chlorides concentrations in groundwater of the upstream part vary widely from 113 to 1818 mg/l with an average of 574 mg/l. As for those of sodium, they vary between 12 and 541 mg/l with an average of 167 mg/l. According to the Piper diagram (Fig. 6), it can be seen that the Cl^- ions are the most dominant in the waters. For the downstream part, the Cl^- contents vary between 120 and 4800 mg/l with an average of 620 mg/l and the Na^+ concentrations vary between 28 and 1950 mg/l with an average of 261 mg/l. The highest Na^+ and Cl^- contents are observed at the Plio-Quaternary aquifer.

The Na^+ vs Cl^- correlation diagram (Fig. 9a) shows a significant positive correlation between these two ions. This reflects that these two elements probably have the same origin. Some points are scattered around the halite dissolution line (line 1:1), reflecting the contribution of this mineral in the groundwater mineralization of the study area. This hypothesis is confirmed by negative values of the saturation indices with respect to this mineral (Fig. 10). The rest of the samples are located below the line 1:1 and parallel to it, reflecting a Na^+ deficit. This suggests the contribution of a phenomenon other than the halite dissolution in the groundwater mineralization.

The Na^+ deficit compared to Cl^- could be linked to the basic exchange reactions, as shown in the Figure 9f, with the aquifer matrix where the Na^+ ions are released from the complex and are replaced by Ca^{2+} ions according to equation (1) (Capaccioni et al. 2005):

$$Na^+ + \tfrac{1}{2}Ca - X_2 \rightarrow Na - X + \tfrac{1}{2}Ca^{2+} \quad (1)$$

With X being the natural exchanger

Also, an excess of Na+ could be explained by the second type of cations exchange where the Ca^{2+} and/or Mg^{2+} ions will be released in water and the Na ions will be fixed by the matrix according to equation (2):

$$\tfrac{1}{2}Ca^{2+} + Na - X \rightarrow \tfrac{1}{2}Ca - X_2 + Na^+ \quad (2)$$

The Ca^{2+} contents of the groundwater from the upstream part vary between 82 to 770 mg/l with an average of 214 mg/l. As for those of SO_4^{2-}, they vary between 13 and 1942 mg/l with an average of 339 mg/l. As for the downstream part, the Ca^{2+} concentrations oscillate between 64 and 850 mg/l with an average of 158 mg/l and those of SO_4^{2-} vary between 30 and 830 with an average of 147 mg/l.

Figure 9

Correlation diagram
(a) Na^+ vs Cl^-, (b) Ca^{2+} vs SO_4^{2-}, (c) Ca^{2+} vs Mg^{2+}, (d) Ca^{2+} vs HCO_3^-, (e) NO_3^- vs Cl^-, and (f) (Ca^{2+}+Mg^{2+}-HCO_3^--SO_4^{2-}) vs (Na^++K^+-Cl^-)

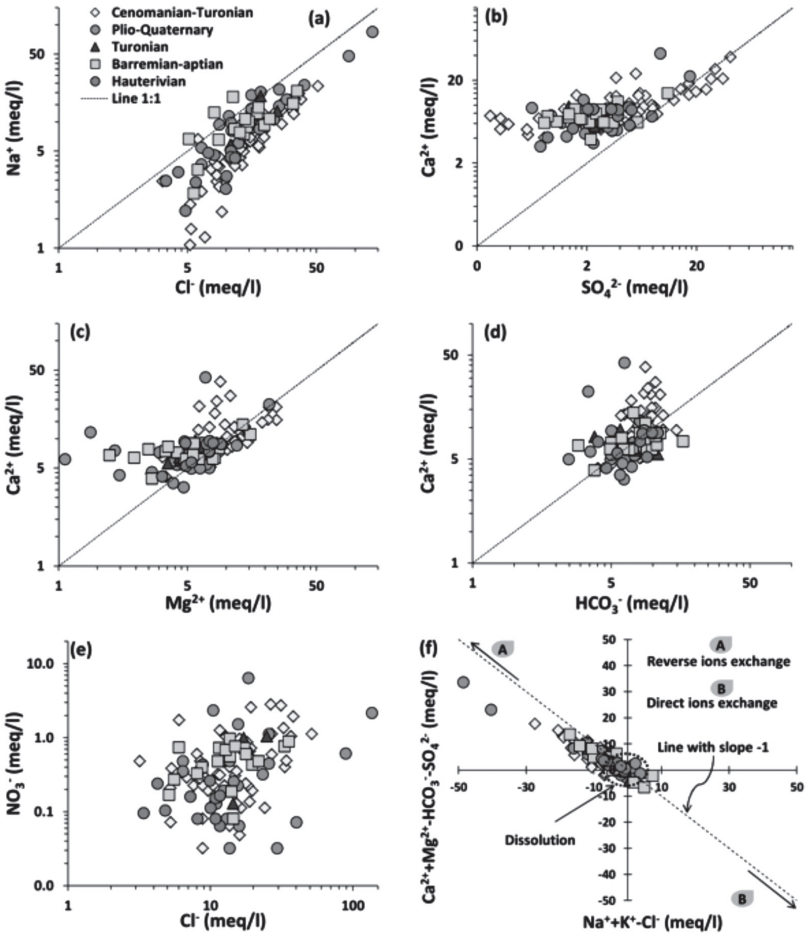

Figure 9b shows the existence of a significant correlation between the Ca^{2+} and SO_4^{2-} ions. Indeed, the points whose Ca^{2+}/SO_4^{2-} molar ratio is close to or equal to 1, reflect the same origin of these two ions which could be the dissolution of gypsum and/or anhydrite. This is confirmed by negative values of the indices of saturation with respect to gypsum and/or anhydrite (Fig. 10). However, the excess of Ca^{2+} compared to SO_4^{2-} observed for the majority of the points could be linked to the phenomenon of reverse bases exchange. Also, the saturation indices calculated for these points with

respect to carbonate minerals are close to or greater than zero, corroborating that the enrichment of Ca^{2+} is mainly due to the bases exchange (Fig. 12f).

Figure 10

Saturation indices of analysed samples of (a) Cenomanian-Turonian, (b) Plio-Quaternary, (c) Turonian, (d) Barremian-Aptian, and (e) Hauterivian aquifers

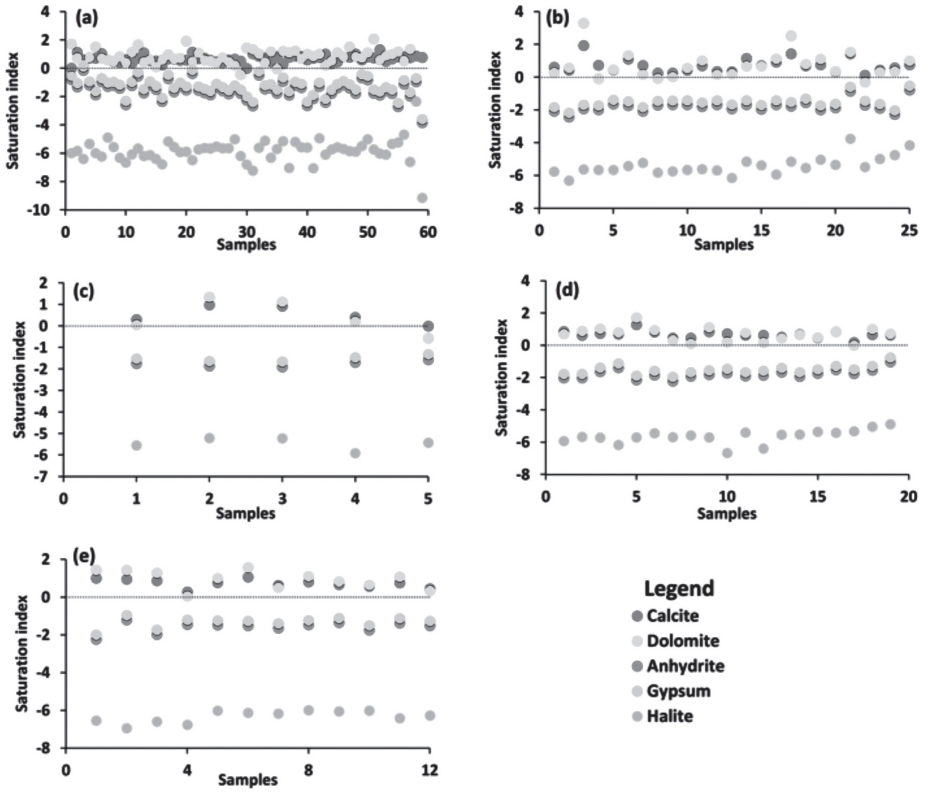

The Ca^{2+} vs Mg^{2+} diagram (Fig. 9c) shows a positive correlation between these two ions, this reflects that these two elements come from the same origin. The majority of the points are scattered around the dolomite dissolution line (line 1:1), thus suggesting the contribution of the dissolution of this mineral to the groundwater mineralization. Other points are located above the line 1:1, confirming the contribution of the bases exchange process in the groundwater mineralization of the aquifers studied.

The Ca^{2+} vs HCO_3^- correlation (Fig. 9d) shows that these two elements do not have a significant correlation and that the majority of the analyzed samples show a

Ca^{2+}/ HCO_3^- molar ratio greater than 1. This excess of Ca^{2+} compared to HCO_3^- ions translates the existence of other sources of calcium which could be the phenomenon of ion exchange and that of dedolomitization (incongruent dissolution of dolomite) (Marfia et al. 2004) accompanied by simultaneous precipitation of calcite.

4.4. Nitrates contamination

The main source of nitrate in water is the leaching of nitrogenous products in the soil following the decomposition of organic matter or synthetic and/or natural fertilizers. The nitrate content of unpolluted natural waters is highly variable, varying from 1 to 15 mg/l depending on the season and the origin (Chenaker et al. 2017). The NO_3^- contents in groundwater of the Cenomanian-Turonian aquifer (upstream part) measured in March 2019 vary from 0 to 175 mg/l with a punctual spatial distribution (Fig. 11a). Generally, levels are high in the Meskala region and exceed the threshold (50 mg/l) set by the World Health Organization (WHO 2011). Also, high values have been noted in some other wells such as 613/52 upstream O37 and 75/52 west of the Kourimat and O56 downstream.

For the Plio-Quaternary and Turonian aquifers, the NO_3^- contents vary, respectively between 0 and 400 mg/l and between 0 and 65 mg/l (Fig. 11b). As for the Barremian-Aptian aquifer, it has NO_3^- contents varying between 5 and 60 mg/l. While the Hauterivian, has concentrations varying between 3 and 16 mg/l (Fig. 11c).

The very weak correlation between $C1^-$ and NO_3^- (Fig. 9e) makes it possible to say that the levels of NO_3^- assayed in the samples analyzed are not of agricultural origin since the chlorides are due to the dissolution of the evaporate minerals.

The highest concentrations within the Plio-Quaternary aquifer are recorded in the southwest part, near Cap Sim (wells 11/51, O94 and O95) and in the northwest; tourist area of the Diabate (well 149/51). These high levels could be explained by the intense concentration of septic tanks constructed by the guest houses in the tourist area of Sidi Kaouki because of the absence of a sanitation network. As for the Turonian and Barremian-Aptian aquifers, only two points for each aquifer have levels exceeding the limit set by WHO (2011). The high grades at well P5 (Barremian-Aptian aquifer) are caused by the public waste dump of the Smimou center because this dump is located a few meters from this water point. Regarding the Hauterivian aquifer, all the samples have NO_3^- concentrations of less than 50 mg/l. The low NO_3^- concentrations in Hauterivian aquifer compared with the other aquifers could be explained by a low concentration of the population in this zone.

The contamination (<50 mg/l) of the other wells at the level of the aquifers studied could be explained by traditional methods of drawing. These result in a significant

amount of water flowing around the catchment wells, constituting quasi-permanent pools that are enriched in NO_3^- by livestock waste during watering. Note also that the number of contaminated wells in the Plio-Quaternary and Turonian aquifer (northern part of the downstream part) is greater than that of the Barremian-Aptian and Hautarivian aquifers (southern part of the downstream part). This is mainly due to the concentration of inhabitants in the northern part, where the water points are located in the middle of the agglomerations, while in the southern part and because of highly uneven geology, most wells are far from the place's habitat.

Figure 11

Spatial distribution of NO_3^- content in groundwater of (a) Cenomanian-Turonian, (b) Plio-Quaternary and Turonian, and (c) Barremian-Aptian and Hauterivian aquifers

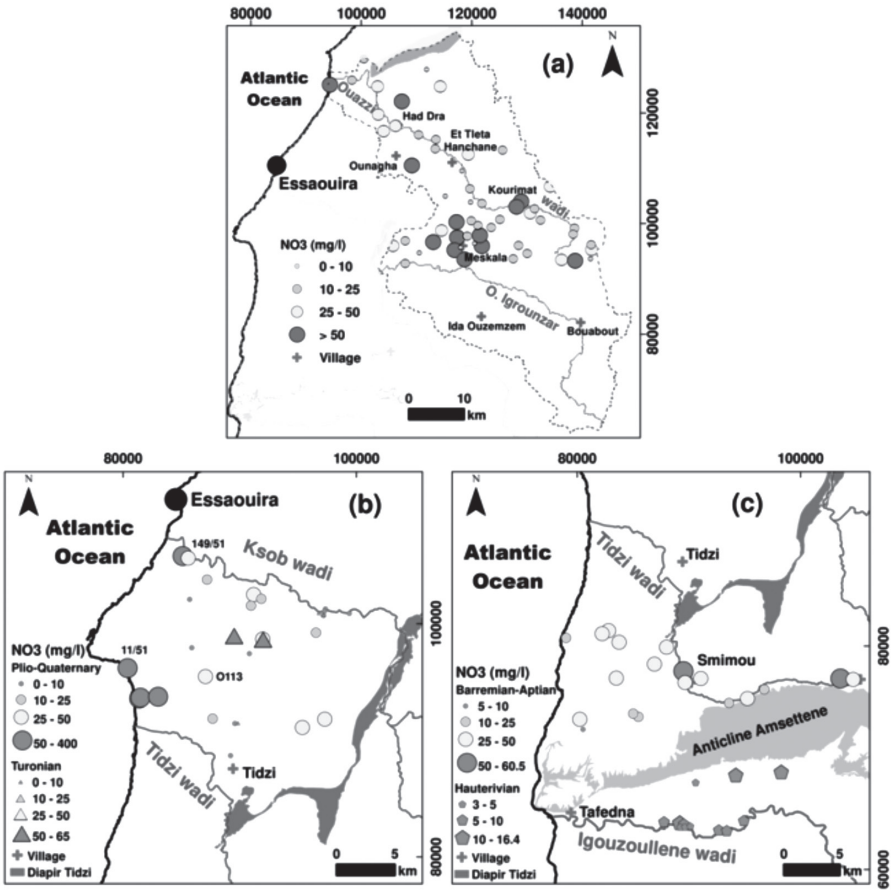

4.5. Evolution of groundwater salinity

The groundwater salinization is a very marked phenomenon in areas of water scarcity, especially the Saharan, arid and semi-arid zones. The scarcity or even the absence of surface water and the increasing demand for water as well as the decrease in precipitation have created enormous pressures on groundwater which have thus resulted in the degradation of their quality.

The spatio-temporal distribution of salinity was studied to assess the impact of climate change on the groundwater quality by using the results of the campaigns of 1995, 2007, 2016, 2017, 2018, and 2019. For the upstream part, the 1995 campaign shows that the salinity values vary between 0.2 and 1.9 g/l with an average of 0.7 g/l. In 2007, the salinity values fluctuated between 0.5 and 2.4 g/l with an average of 1.1 g/l. As for the 2016 campaign, its values vary between 0.3 and 4.6 g/l with an average of 1.37 g/l. For the 2017 campaign, the salinity fluctuates between 0.3 and 4 g/l with an average of 1.29 g/l. In 2018, the salinity values vary between 0.4 and 4.3 g/l with an average of 1.4 g/l and between 0.35 and 4.4 g/l with an average of 1.4 for samples from the 2019 campaign (Fig. 12).

From the analysis of the maps in Figure 12, it can be seen that the salinity values become more important by advancing in time and going from east to west during the six campaigns. Taking, for example, the region of Sebt Kourimat, recharge area of the Cenomanian-Turonian aquifer, the salinity values fluctuate around 0.46 g/l in 1995 to reach 2.9 g/l in 2019. However, the general spatio-temporal evolution of salinity shows an increasing trend.

For the downstream part, the groundwater from the Plio-Quaternary aquifer has salinity values varying between 0.6 and 3.4 g/l with an average of 1.7 g/l in 1990, between 0.9 and 3 g/l with an average of 1.6 g/l in 1995, from 0.4 to 4.1 g/l with an average of 1.3 g/l in 2004, between 0.9 to 2.2 g/l with an average of 1.4 g/l in 2009, from 0.3 to 4.7 with an average of 1.5 g/l in 2015, between 0.4 and 4.8 g/l with an average of 1.53 g/l in 2017, between 0.5 and 6.5 g/l with an average of 1.6 g/l in 2018 and between 0.46 and 8.4 g/l with an average of 1.7 g/l in 2019 (Fig. 13). From the maps of Figure 13, the highest values are observed in the southern and western part and this further to the remoteness to the recharge zones, to the residence time, to the influence of the Triassic terrains, and to the influence from the sea (marine intrusion (well 11/51)). While the low values of salinity are recorded in the north (along the Ksob wadi) and in the east of the Plio-Quaternary aquifer which represent the recharge zones. These low values are due to the fact that these places represent the recharge zones of this aquifer. The temporal evolution of groundwater salinity of the Plio-Quaternary aquifer shows an upward trend going from year to year and consequently deterioration in the groundwater quality. As for the Turonian aquifer, the minimum

values of salinity are around 0.8 g/l and the maximum values are around 1.3 g/l with an average of 1.1 g/l for 2004, 2009, 2015, 2017, 2018 and 2019 campaigns (Fig.13). The temporal evolution of the groundwater salinity of this aquifer does not show a significant trend, this could be explained by its significant depth and its captive nature.

Concerning the Barremian-Aptian aquifer, the salinity values vary between 0.2 and 3.2 g/l with an average of 1.1 g/l for the points of the 1997 campaign, from 0.3 to 2.1 g/l with an average of 1.1 g/l for the samples collected in 2015 and 2017, between 0.4 to 2.8 g/l with an average of 1.1 g/l for the points of 2018 campaign waters and between 0.7 and 2.4 g/l with an average of 1.2 g/l for 2019 campaign (Fig. 14).

The spatio-temporal distribution of the groundwater salinity of the Barremian-Aptian aquifer (Fig. 14) shows a slight upward trend in the minimum values of the salinity while the maximum values have experienced slight stability. For the Hauterivian aquifer, the salinity values vary between 0.6 to 2.6 g/l with an average for waters representing the 1997 campaign, between 0.5 and 1.1 g/l with an average of 0.8 g/l for the 2015 samples, between 0.6 to 1.2 g/l with an average of 0.9 g/l for the points of the 2017 campaign, between 0.4 and 1.1 g/l with an average of 0.8 g/l for the 2018 campaign and between 0.4 to 1.3 g/l with an average of 0.8 g/l for the 2019 samples. The spatio-temporal distribution of the salinity of the Hauterivian aquifer shows a slight dilution of the waters analyzed in 2015, 2017, 2018 and 2019 compared to those representing the 1997 campaign. This could be explained by the installation of the Igouzoullene dam (in 2004) upstream favoring the recharge of this aquifer.

As the study area is under a semi-arid climate, with a tendency towards an arid climate in recent years accompanied by a decrease in precipitation and an increase in the temperature, which frequently causes intense periods of drought resulting in evaporation that affects surface and groundwater, especially the shallow waters, the degradation of the groundwater quality is mainly due to this situation and the decrease in the piezometric level caused by climate change.

Figure 12

Spatial distribution of salinity in Cenomanian-Turonian aquifer

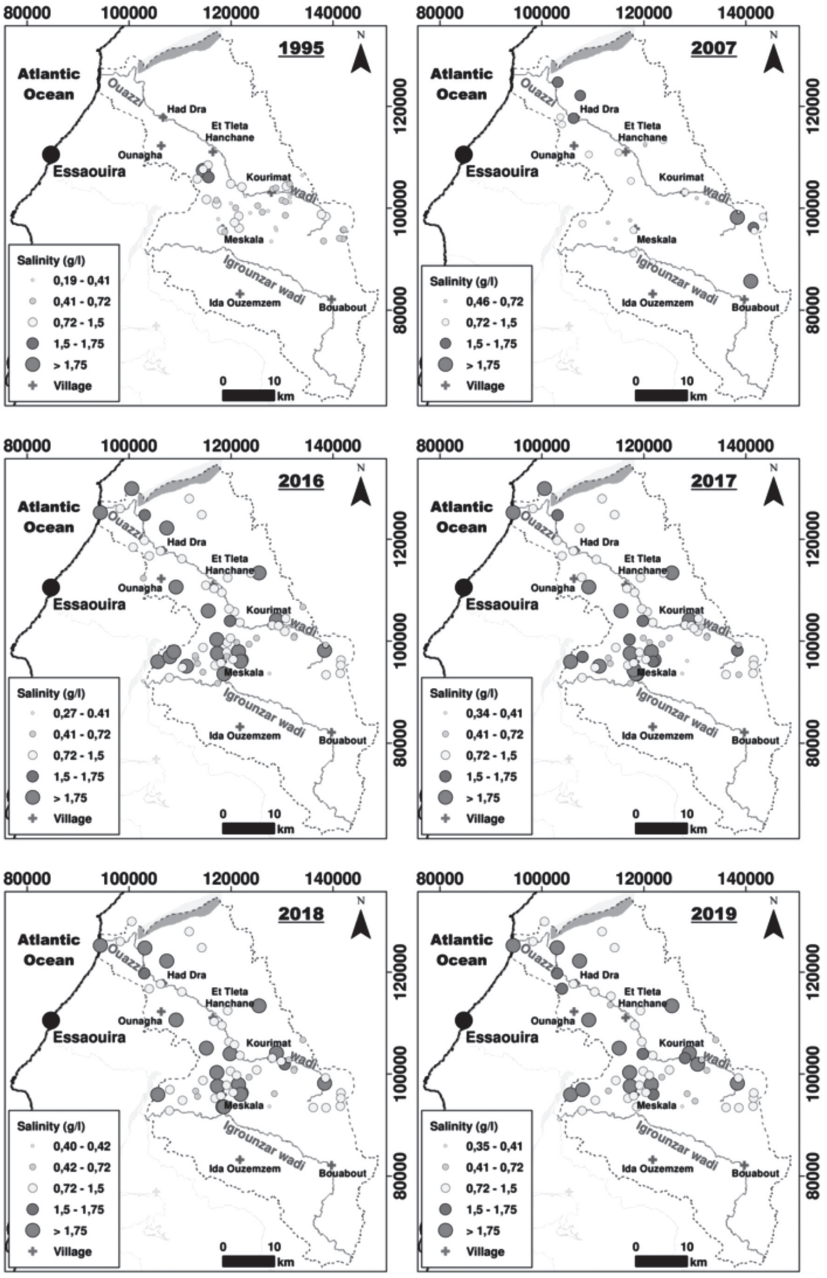

Figure 13

Spatial distribution of salinity in Plio-Quaternary and Turonian aquifers

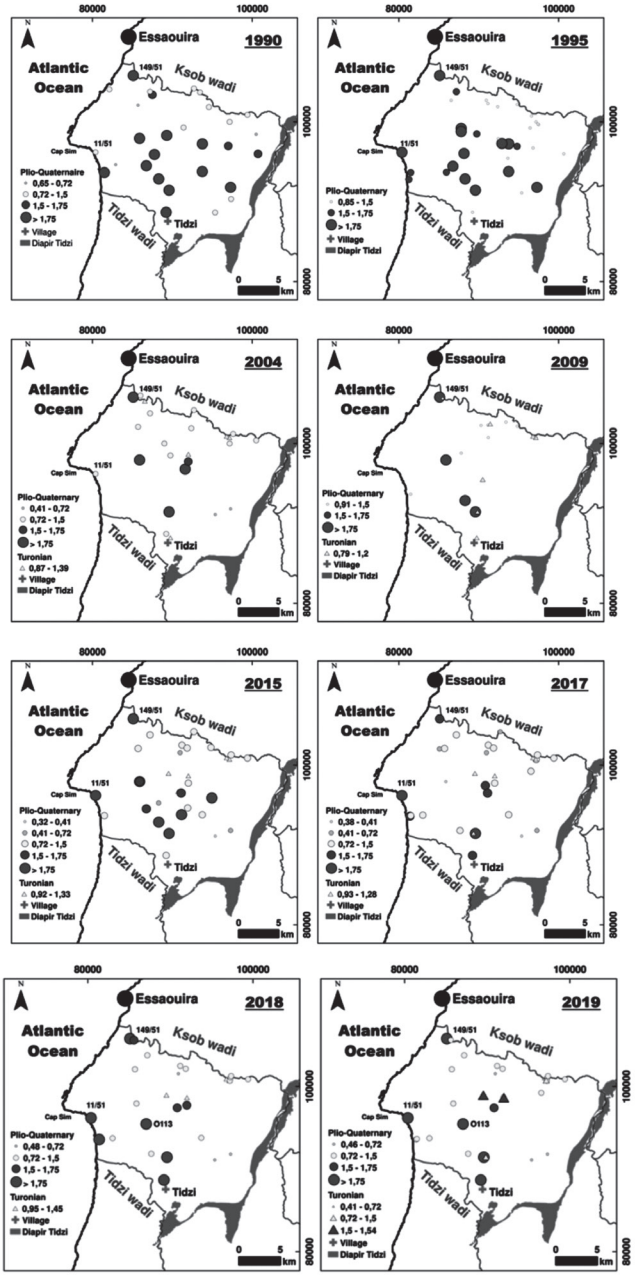

5. Conclusion

The water resource within the Essaouira basin is limited and unevenly distributed in space and time. This problem could limit water supply, which will be aggravated by the depletion of this resource due to the climate change impact which has become an ambiguous reality and whose effects on the environment are already visible. The hydrogeochemical study showed that the groundwater of the Cenomanian-Turonian aquifer presents the Cl-Ca-Mg, Cl-Ca, Cl-Na, and HCO_3-Ca mix facies with the dominance of the Cl-Ca-Mg mix facies, and Cl-Ca. The study of the temporal evolution of these facies shows that there has been no remarkable change. The groundwater of the Plio-Quaternary and Turonian aquifers are of mixed type between Cl-Na and Cl-Ca-Mg. The chemical facies experienced a slight evolution from the Cl-Na facies to the Cl-Na and Cl-Ca-Mg facies for the Plio-Quaternary aquifer and from the Cl-Na facies to the Cl-Ca-Mg facies for the Turonian aquifer. As for the Barremian-Aptian and Hauterivian aquifers, they generally have three types of chemical facies: Cl-Na, Cl-Ca-Mg, and HCO_3-Ca-Mg, with the dominance of the Cl-Ca-Mg facies. For the study period, a remarkable evolution of the facies was observed; from the Cl-Na facies to the Cl-Ca-Mg facies. Examination of the correlations established between the concentrations of major elements has shown that the mineralization of groundwater is controlled by the phenomenon of the dissolution of the evaporitic minerals (halite, gypsum and/or anhydrites) and carbonates (dolomite), by the reverse ion exchange phenomenon and by the marine intrusion, especially at the Plio-Quaternary aquifer. The study of the spatio-temporal evolution of the groundwater quality in the study area shows a gradual deterioration in time and space. However, the Essaouira basin is more vulnerable to climate change because its recharge is entirely dependent on meteoric waters.

Figure 14

Spatial distribution of salinity in Barremian-Aptian and Hauterivian aquifers

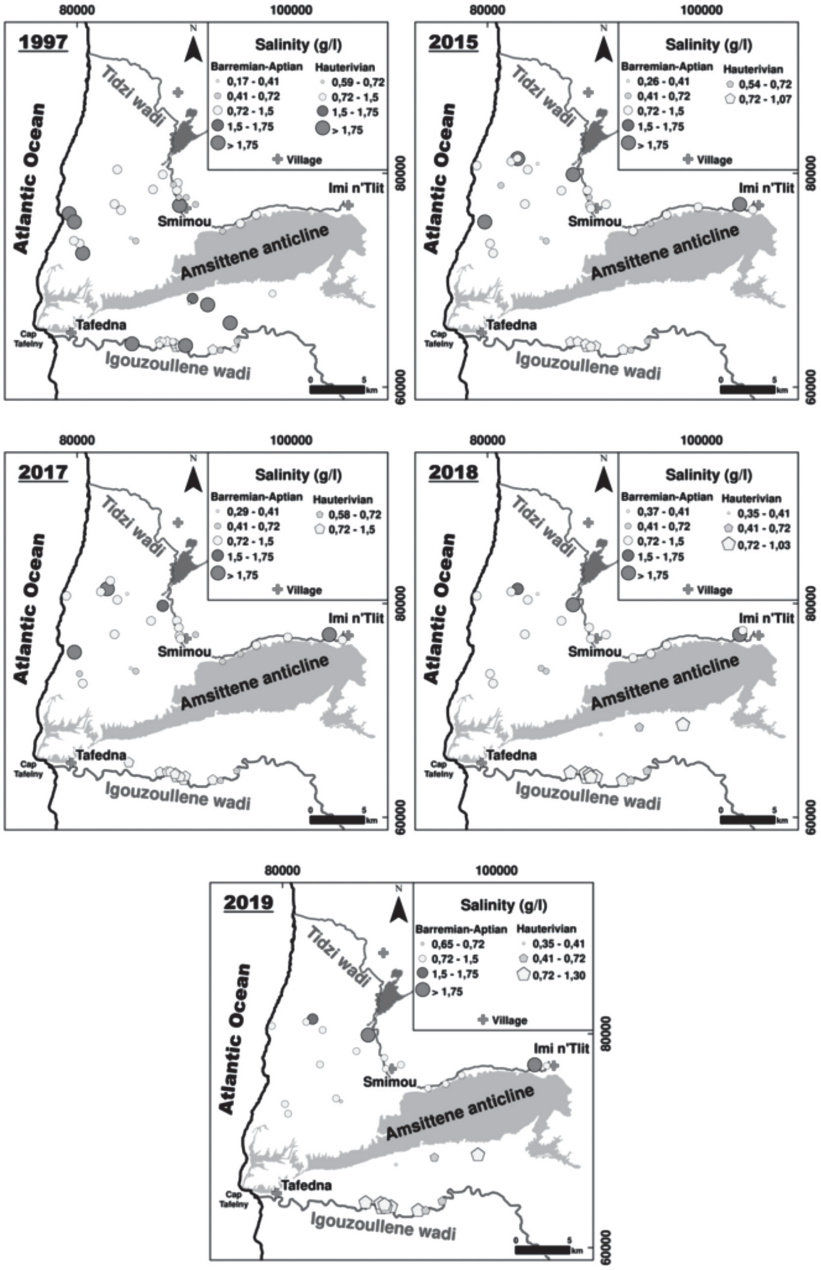

Appendix 1

Results of physico-chemical analyzes

Campaign 2019

Parameter	pH	T	EC	Ca^{2+}	Mg^{2+}	Na^{+}	K^{+}	HCO_3^{-}	Cl^{-}	SO_4^{2-}	NO_3^{-}
		°C	µs/cm	meq/l							
Cenomanian-Turonian aquifer											
	N = 57										
Minimum	7.0	14.9	615	4.1	2.6	0.5	0.0	4.0	3.2	0.3	0.0
Maximum	8.4	24.0	5738	38.4	24.5	23.5	4.3	14.7	51.3	40.4	2.8
Median	7.5	20.8	2203	9.0	8.3	6.3	0.2	8.0	13.6	3.9	0.4
Mean	7.5	20.5	2428	10.7	9.7	7.3	0.4	8.2	16.2	7.1	0.6
Standard deviation	0.3	1.8	1182	6.4	4.8	5.1	0.7	1.9	9.7	8.8	0.6
Plio-Quaternary aquifer											
	N = 29										
Minimum	7.1	17.3	880	3.2	0.6	3.7	0.0	2.5	6.4	0.6	0.0
Maximum	9.2	25.0	12250	42.4	21.4	84.8	1.9	9.8	135.4	17.3	6.5
Median	7.6	21.4	2041	5.7	5.0	10.3	0.2	6.2	15.4	2.3	0.3
Mean	7.7	21.4	2855	8.2	5.6	15.6	0.3	6.2	23.6	3.1	0.7
Standard deviation	0.5	1.8	2564	7.9	4.1	16.7	0.5	1.8	27.9	3.3	1.3
Turonian											
	N = 5										
Minimum	7.1	20.0	1833	5.6	3.5	5.9	0.1	3.8	10.8	1.4	0.0
Maximum	7.8	26.5	2800	9.7	6.2	18.6	0.3	10.8	24.8	3.3	1.0
Median	7.3	24.8	2287	6.5	4.4	11.7	0.1	5.8	17.1	2.5	0.2
Mean	7.4	23.9	2310	7.2	4.8	11.9	0.2	6.7	17.1	2.4	0.5
Standard deviation	0.3	2.6	423	1.7	1.1	4.6	0.1	2.6	5.2	0.7	0.5
Barremian-Aptian aquifer											
	N = 20										
Minimum	7.1	16.9	1240	3.9	1.2	1.8	0.1	2.9	5.1	0.8	0.1
Maximum	8.1	23.8	3880	14.0	15.3	20.9	1.7	16.4	35.2	10.9	1.0
Median	7.5	20.9	1783	6.9	5.4	9.3	0.2	8.0	13.7	2.1	0.6
Mean	7.5	20.9	1984	7.5	5.9	10.2	0.3	8.0	14.9	2.7	0.5
Standard deviation	0.3	2.0	721	2.2	3.7	4.7	0.4	3.1	8.2	2.3	0.3

Parameter	pH	T	EC	Ca^{2+}	Mg^{2+}	Na^{+}	K^{+}	HCO_3^{-}	Cl^{-}	SO_4^{2-}	NO_3^{-}
		°C	µs/cm	meq/l							
Hauterivian aquifer											
	N = 12										
Minimum	7.1	18.0	687	4.1	3.2	1.2	0.1	4.0	3.4	0.9	0.0
Maximum	8.2	24.8	2405	9.5	9.0	5.0	0.4	10.8	11.6	7.8	0.3
Median	7.4	22.4	1655	8.8	7.3	3.7	0.2	8.8	9.0	3.8	0.1
Mean	7.5	22.5	1559	7.8	6.6	3.5	0.2	8.2	8.2	3.7	0.1
Standard deviation	0.4	1.8	440	1.8	1.7	1.3	0.1	2.3	3.0	1.9	0.1

Campaign 2018

Parameter	pH	T	EC	Ca^{2+}	Mg^{2+}	Na^{+}	K^{+}	HCO_3^{-}	Cl^{-}	SO_4^{2-}	NO_3^{-}
		°C	µs/cm	meq/l							
Cenomano-Turonian aquifer											
	N = 62										
Minimum	7.2	16.2	601	3.3	2.5	0.5	0.0	3.1	2.4	0.1	0.1
Maximum	9.6	24.6	6845	29.1	27.1	24.4	0.9	11.3	48.1	46.2	2.7
Median	7.8	20.9	2195	7.4	8.0	5.9	0.1	6.1	10.8	4.3	0.4
Mean	8.0	20.9	2482	8.8	9.5	6.6	0.1	6.3	14.0	5.9	0.6
Standard deviation	0.6	1.6	1309	4.9	5.3	4.5	0.2	1.5	10.0	7.4	0.6
Plio-Quaternary aquifer											
	N = 24										
Minimum	7.2	17.6	916	2.9	1.2	3.3	0.0	2.3	2.8	0.1	0.0
Maximum	8.4	26.3	9744	18.2	19.6	63.7	1.7	9.0	89.1	8.5	6.4
Median	7.6	22.0	2176	5.6	5.8	7.8	0.2	4.4	12.4	2.4	0.3
Mean	7.7	22.0	2850	7.2	5.9	12.9	0.3	4.6	19.5	2.5	0.7
Standard deviation	0.3	1.8	1987	4.4	3.6	13.4	0.4	1.5	19.1	2.0	1.4
Turonian aquifer											
	N = 6										
Minimum	6.0	21.5	48	0.1	0.2	0.0	0.1	0.2	0.1	0.0	0.0
Maximum	7.9	27.1	2699	7.9	6.9	12.0	0.4	6.3	16.3	3.8	1.0
Median	7.3	23.5	2241	5.9	5.5	8.7	0.1	4.4	13.5	3.0	0.2
Mean	7.3	24.1	1972	5.3	4.8	7.9	0.2	4.1	11.4	2.6	0.4
Standard deviation	0.7	2.3	989	2.8	2.4	4.3	0.1	2.1	6.0	1.3	0.4
Barremian-Aptian aquifer											
	N = 20										
Minimum	7.2	17.0	744	2.9	1.1	2.3	0.0	2.5	2.0	0.3	0.0

Parameter	pH	T	EC	Ca^{2+}	Mg^{2+}	Na^{+}	K^{+}	HCO_3^{-}	Cl^{-}	SO_4^{2-}	NO_3^{-}
		°C	µs/cm	meq/l							
Maximum	8.3	23.5	4409	13.1	13.4	15.6	1.6	8.4	28.0	9.5	0.9
Median	7.5	20.3	1892	5.5	5.4	8.6	0.1	5.8	8.5	1.5	0.5
Mean	7.5	20.5	1969	5.8	5.6	8.3	0.2	5.8	10.5	2.1	0.5
Standard deviation	0.3	2.0	878	2.3	3.2	4.1	0.3	1.7	7.2	2.1	0.3
Hauterivian aquifer											
	N = 14										
Minimum	7.1	18.1	668	2.6	1.7	2.0	0.1	3.4	3.2	0.8	0.0
Maximum	8.3	24.3	3688	12.3	15.4	8.6	0.2	9.0	25.2	7.1	0.2
Median	7.6	22.1	1754	6.0	6.7	4.2	0.1	7.7	9.2	2.9	0.1
Mean	7.6	21.9	1804	6.3	6.8	4.0	0.1	7.0	8.5	3.2	0.1
Standard deviation	0.4	1.9	807	2.4	3.0	1.7	0.0	1.8	5.8	1.7	0.1

Campaign 2017

Parameter	pH	T	EC	Ca^{2+}	Mg^{2+}	Na^{+}	K^{+}	HCO_3^{-}	Cl^{-}	SO_4^{2-}	NO_3^{-}
		°C	µs/cm	meq/l							
Cenomanian-Turonian aquifer											
	N = 67										
Minimum	6.9	17.9	635	0.0	0.0	0.0	0.0	0.0	0.0	0.0	0.0
Maximum	8.1	29.3	6776	26.7	25.2	33.1	2.1	11.2	69.7	30.0	3.1
Median	7.4	21.3	1936	7.3	7.8	5.4	0.1	6.3	10.8	3.6	0.5
Mean	7.4	21.4	2318	8.3	8.7	8.1	0.1	6.3	15.0	5.5	0.7
Standard deviation	0.3	1.8	1234	5.1	5.1	6.9	0.3	1.9	13.1	6.0	0.7
Plio-Quaternary aquifer											
	N = 27										
Minimum	7.1	18.9	724	2.2	2.6	3.7	0.1	3.1	4.8	0.2	0.1
Maximum	8.0	25.4	7555	18.4	16.9	62.2	1.9	9.3	88.5	5.4	2.0
Median	7.6	22.2	1859	5.7	6.2	8.1	0.3	5.2	14.4	1.8	0.3
Mean	7.6	22.1	2203	6.7	6.6	11.4	0.4	5.5	19.2	1.9	0.6
Standard deviation	0.2	1.6	1349	3.8	3.3	11.0	0.4	1.4	16.4	1.1	0.5
Turonian aquifer											
	N = 5										
Minimum	7.2	23.9	1892	4.8	5.8	6.6	0.2	4.7	13.2	2.0	0.1
Maximum	7.8	27.4	2442	8.7	7.7	10.4	0.5	6.2	19.2	3.4	0.6
Median	7.5	25.4	2293	6.0	6.6	9.3	0.2	6.0	16.0	2.7	0.2
Mean	7.5	25.4	2164	6.4	6.7	8.7	0.3	5.7	16.1	2.7	0.3
Standard deviation	0.2	1.5	254	1.5	0.7	1.8	0.1	0.6	2.7	0.5	0.2

Barremian-Aptian aquifer											
	N = 25										
Minimum	7.0	17.8	549	3.2	2.1	2.6	0.1	3.5	3.6	0.4	0.1
Maximum	8.1	23.9	3884	13.0	15.3	18.6	1.6	10.3	28.0	8.5	1.2
Median	7.4	21.9	1670	5.6	5.9	7.4	0.2	6.9	12.4	1.6	0.5
Mean	7.4	21.5	1851	6.0	6.3	8.3	0.2	6.9	14.2	2.2	0.5
Standard deviation	0.3	1.7	832	2.2	3.2	4.2	0.3	1.9	7.5	1.7	0.3
Hauterivian aquifer											
	N = 13										
Minimum	6.9	19.4	1134	5.3	4.9	2.2	0.1	4.0	3.6	1.2	0.1
Maximum	8.4	24.8	2203	7.9	14.7	9.4	0.3	8.5	18.0	10.7	0.3
Median	7.2	23.0	1661	6.2	7.4	4.9	0.2	7.7	10.0	3.1	0.2
Mean	7.3	22.9	1648	6.3	7.4	5.0	0.2	7.3	9.8	3.9	0.2
Standard deviation	0.4	1.5	305	0.7	2.5	1.6	0.0	1.3	3.5	2.5	0.1

Campaign 2016

Parameter	**pH**	**T**	**EC**	**Ca^{2+}**	**Mg^{2+}**	**Na^{+}**	**K^{+}**	**HCO_3^-**	**Cl^-**	**SO_4^{2-}**	**NO_3^-**
		°C	***µs*/cm**	**meq/l**							
Cenomanian-Turonian aquifer											
	74										
Minimum	6.9	16.4	493	3.8	1.1	1.6	0.0	3.6	2.2	0.4	0.0
Maximum	8.2	24.3	7600	28.5	22.2	22.2	2.6	7.7	29.3	46.2	6.3
Median	7.4	20.9	2000	7.4	6.9	5.2	0.1	4.9	8.0	5.0	1.0
Mean	7.4	21.0	2384	9.4	7.8	7.3	0.2	5.1	10.5	7.7	1.2
Standard deviation	0.2	1.6	1418	5.9	4.1	5.4	0.5	1.1	8.3	9.6	1.2

Campaign 2015

Parameter	**pH**	**T**	**EC**	**Ca^{2+}**	**Mg^{2+}**	**Na^{+}**	**K^{+}**	**HCO_3^-**	**Cl^-**	**SO_4^{2-}**	**NO_3^-**
		°C	***µs*/cm**	**meq/l**							
Plio-Quaternary aquifer											
	N = 27										
Minimum	7.5	20.6	626	2.2	1.1	1.2	0.3	0.2	1.3	0.1	0.0
Maximum	8.2	25.0	7840	19.5	18.1	20.1	5.8	9.2	54.0	9.7	3.8
Median	7.8	22.3	2210	6.0	7.0	4.8	2.5	4.6	9.6	2.6	0.5
Mean	7.8	22.5	2637	6.9	7.1	5.8	2.6	4.7	14.1	2.8	0.9
Standard deviation	0.2	1.3	1497	4.1	4.1	3.9	1.4	2.2	11.3	2.0	1.1

Parameter	pH	T	EC	Ca^{2+}	Mg^{2+}	Na^{+}	K^{+}	HCO_3^{-}	Cl^{-}	SO_4^{2-}	NO_3^{-}
		°C	µs/cm	meq/l							
Turonian aquifer											
	N = 7										
Minimum	7.4	23.6	1920	4.0	5.7	3.1	1.4	4.2	8.6	1.6	0.0
Maximum	7.9	27.8	4190	10.0	11.3	5.7	5.3	16.8	18.3	3.9	1.2
Median	7.5	24.8	2260	6.0	8.1	4.2	2.7	5.2	10.2	3.3	0.3
Mean	7.6	25.7	2483	6.4	8.1	4.4	2.6	6.5	11.5	2.9	0.5
Standard deviation	0.2	1.8	797	1.9	1.7	1.1	1.4	4.5	3.4	0.9	0.5
Barremian-Aptian aquifer											
	N = 26										
Minimum	7.2	18.8	490	1.9	0.5	0.7	0.3	1.5	1.0	0.4	0.0
Maximum	8.2	25.2	3650	11.1	16.5	8.4	2.8	15.4	21.3	9.5	2.5
Median	7.7	22.2	1788	6.0	4.1	3.7	1.4	4.7	6.4	1.6	0.7
Mean	7.7	22.2	1930	5.8	5.2	3.9	1.6	5.4	7.7	2.2	0.8
Standard deviation	0.3	1.5	834	2.3	4.0	2.3	0.8	3.2	5.6	1.9	0.5
Hauterivian aquifer											
	N = 9										
Minimum	7.4	21.2	1090	5.5	5.5	1.1	0.7	0.7	1.5	3.5	0.0
Maximum	8.1	25.1	1940	7.6	10.9	2.8	1.6	12.1	7.2	11.3	0.1
Median	7.7	24.6	1720	7.1	8.2	2.3	1.4	8.3	5.6	4.7	0.1
Mean	7.6	24.2	1646	6.8	8.1	2.1	1.3	7.4	5.1	5.5	0.1
Standard deviation	0.2	1.3	286	0.8	1.8	0.6	0.3	3.4	2.1	2.3	0.0

Campaign 2009

Parameter	pH	T	EC	Ca^{2+}	Mg^{2+}	Na^{+}	K^{+}	HCO_3^{-}	Cl^{-}	SO_4^{2-}	NO_3^{-}
		°C	µs/cm	meq/l							
Plio-Quaternary aquifer											
	N = 14										
Minimum	6.7	15.5	770	1.5	2.0	1.6	0.1	1.1	2.1	0.6	0.0
Maximum	7.5	23.0	3780	2.3	3.8	19.1	0.3	3.6	21.6	2.7	3.2
Median	7.3	20.0	2215	2.0	3.2	9.3	0.1	2.9	9.8	2.3	0.5
Mean	7.3	20.1	2382	2.0	3.0	9.0	0.2	2.7	10.0	2.1	0.8
Standard deviation	0.2	1.8	833	0.2	0.5	4.5	0.1	0.7	5.0	0.7	0.9

Parameter	pH	T	EC	Ca^{2+}	Mg^{2+}	Na^{+}	K^{+}	HCO_3^{-}	Cl^{-}	SO_4^{2-}	NO_3^{-}
		°C	µs/cm	meq/l							
Turonian aquifer											
	N = 6										
Minimum	7.1	21.0	1450	1.7	2.5	6.5	0.1	0.5	7.5	2.2	0.0
Maximum	7.7	27.0	2340	1.9	3.1	12.5	0.6	3.6	11.9	3.7	0.1
Median	7.3	23.8	1929	1.8	2.9	7.6	0.3	3.1	8.3	2.6	0.1
Mean	7.4	23.9	1911	1.8	2.8	8.6	0.3	2.6	9.0	2.7	0.1
Standard deviation	0.2	2.0	320	0.1	0.2	2.7	0.3	1.4	2.0	0.7	0.1

Campaign 2007

Parameter	pH	T	EC	Ca^{2+}	Mg^{2+}	Na^{+}	K^{+}	HCO_3^{-}	Cl^{-}	SO_4^{2-}	NO_3^{-}
		°C	µs/cm	meq/l							
Cenomanian-Turonian aquifer											
	N = 27										
Minimum	6.7	17.4	900	0.0	0.0	0.0	0.0	0.0	0.0	0.0	0.0
Maximum	7.8	29.5	3880	34.0	27.8	13.4	1.7	7.5	33.9	49.9	3.5
Median	7.2	22.8	1810	7.2	8.5	4.7	0.1	5.5	6.9	4.5	0.6
Mean	7.2	23.0	2000	9.0	9.7	5.3	0.2	5.0	9.7	8.6	0.6
Standard deviation	0.3	2.8	864	7.9	6.8	3.6	0.3	2.2	8.1	13.1	0.7

Campaign 1997

Parameter	pH	T	EC	Ca^{2+}	Mg^{2+}	Na^{+}	K^{+}	HCO_3^{-}	Cl^{-}	SO_4^{2-}	NO_3^{-}
		°C	µs/cm	meq/l							
Barremian-Aptian aquifer											
		N = 23									
Minimum	–	18.0	316	2.2	0.1	1.3	0.0	2.6	1.9	0.4	–
Maximum	–	26.0	13249	25.4	17.9	119.7	0.9	10.2	116.9	15.9	–
Median	–	21.3	1743	6.7	1.0	13.3	0.1	5.6	11.0	1.8	–
Mean	–	21.4	2510	8.3	1.9	19.7	0.2	5.9	18.8	3.1	–
Standard deviation	–	2.0	2673	5.2	3.7	24.8	0.2	1.9	24.6	3.5	–
Hauterivian aquifer											
	N = 13										
Minimum	–	17.0	1154	4.6	0.7	4.9	0.1	2.6	5.3	2.4	–
Maximum	–	24.0	4636	17.2	10.2	35.9	0.6	9.2	37.9	14.8	–
Median	–	21.5	2121	8.3	4.3	11.1	0.2	7.6	13.7	5.4	–

Parameter	pH	T	EC	Ca^{2+}	Mg^{2+}	Na^{+}	K^{+}	HCO_3^{-}	Cl^{-}	SO_4^{2-}	NO_3^{-}
		°C	µs/cm	meq/l							
Mean	–	21.6	2480	9.1	5.3	14.8	0.3	6.7	15.8	6.9	–
Standard deviation	–	1.8	996	3.8	2.8	8.5	0.1	1.9	8.7	4.1	–

Campaign 1995

Parameter	pH	T	EC	Ca^{2+}	Mg^{2+}	Na^{+}	K^{+}	HCO_3^{-}	Cl^{-}	SO_4^{2-}	NO_3^{-}
		°C	µs/cm	meq/l							
Cenomanian-Turonian aquifer											
	N = 45										
Minimum	–	15.00	352	0.13	0.10	0.07	0.00	0.05	0.08	0.01	0.00
Maximum	–	23.00	3060	1.41	1.90	1.00	0.01	0.14	1.40	1.00	0.08
Median	–	19.00	1020	0.35	0.54	0.22	0.00	0.10	0.21	0.08	0.01
Mean	–	19.13	1214	0.44	0.66	0.30	0.00	0.10	0.32	0.15	0.02
Standard deviation	–	1.61	697	0.30	0.42	0.25	0.00	0.02	0.27	0.21	0.02
Plio-Quaternary aquifer											
	N = 34										
Minimum	–	15.5	1590	4.6	1.6	7.2	0.0	1.7	11.9	0.9	0.0
Maximum	–	24.5	5040	18.8	12.3	32.0	0.9	6.8	48.8	8.7	4.4
Median	–	21.0	2595	8.1	6.1	14.3	0.1	4.7	21.4	3.4	1.2
Mean	–	21.1	2876	9.2	6.6	15.9	0.1	4.6	25.1	3.8	1.5
Standard deviation	–	1.8	921	4.1	2.4	6.8	0.1	1.2	11.7	1.6	1.2

Campaign 1990

Parameter	pH	T	EC	Ca^{2+}	Mg^{2+}	Na^{+}	K^{+}	HCO_3^{-}	Cl^{-}	SO_4^{2-}	NO_3^{-}
		°C	µs/cm	meq/l							
Plio-Quaternary aquifer											
	N = 29										
Minimum	7.7	15.0	1197	2.8	0.6	7.5	0.1	6.1	3.0	0.6	–
Maximum	8.6	25.0	5654	17.0	16.4	35.0	0.5	44.0	7.7	6.6	–
Median	8.1	21.0	2993	7.2	4.0	15.0	0.1	16.8	5.1	2.8	–
Mean	8.1	20.7	2881	8.4	4.8	17.1	0.2	19.3	4.9	3.0	–
Standard deviation	0.2	2.0	1392	3.9	3.3	8.2	0.1	11.3	1.3	1.3	–

Behavior of the isotopic signature of groundwater facing climate change within a semi-arid environment

1. Introduction

Water resources in Saharan, arid and semi-arid zones are limited and come mainly from groundwater. In recent years, this resource has experienced quantitative and qualitative degradation due to the natural (drought, variability and climate change) and anthropogenic (agricultural, industrial, etc.) effects (Babqiqi 2014; Bahir et al. 2002, 2016, 2020a; Boughariou et al. 2014; Carreira et al. 2018; El Gayar and Hamed 2018; Pazand et al. 2018; Singhal et al. 2020; Trabelsi and Zouari 2019).

The main recharge source of various aquifers in Saharan, arid and semi-arid environments is represented by the precipitations (Edmunds et al. 2004; Zouari et al. 2011). As a result of climate change, precipitation has decreased, causing deteriorate in groundwater quality (Bahir et al. 2016; Hamed et al. 2018; Ouhamdouch et al. 2016, 2018, 2019; Taheri 2019). However, the study of this vital resource has become essential, especially in Saharan, arid and semi-arid environments. Among the studies adopted to assess groundwater are hydrogeology, geophysics, hydrogeochemistry, and isotopic hydrology. These last two approaches are widely used and give very satisfactory results (Bahir et al. 2007, 2018a,b, 2019; Farid et al. 2013; Lopo Mendonça et al. 2004; Mokadem et al. 2015).

The water molecule is composed of two elements (Oxygen and Hydrogen) which each have three stable or radioactive isotopes. The relative abundance of an isotope depends on several factors, such as altitude, latitude, distance from the ocean, evaporation, and condensation (Clark and Fritz 1997). The stable isotope contents are measured by a mass spectrometer, in terms of difference compared to a standard in part per thousand (‰). This difference is expressed by the notation δ:

$$\delta(‰) = \left[\frac{R_{sample} - R_{standard}}{R_{standard}}\right] \times 1000$$

The reference standard used in is the SMOW (Standard Mean Ocean Water) representative of the mean isotopic composition of the oceans (Craig 1961) or that

distributed by the International Atomic Energy Agency (IAEA) in Vienna: V-SMOW (Vienna Standard Mean Ocean Water). By definition: δ SMOW = 0 ‰ (for ^{2}H and ^{18}O). On a world average, the general relationship between $^{18}O/^{16}O$ and $^{2}H/^{1}H$ for natural water from precipitation at a particular site over time is linear and expressed by the world meteoric water line (Craig 1961): $\delta^{2}H = \delta^{18}O+10$.

Increasing global temperatures and climate change are having major consequences for the natural resources of semi-arid environments, such as water resources. However, the consequences of climate change are said to have significant direct and indirect effects and, although arid and semi-arid areas have contributed little to the magnitude of the global phenomenon, they are expected to bear some of the serious consequences. In this context, the Essaouira basin located on the Atlantic coast of Morocco was used as an example, based on the isotopic signature of groundwater.

The study area covers an area of 6000 km^2. It is limited to the North by Hadid anticline, to the South by Tidzi wadi, to the Eeast by the Bouabout region, and by the Atlantic Ocean to the West. This basin is subdivided into two parts, the first known as the "Bouabout unit" (upstream part) with altitudes vary between 400 and 1600 masl and the second called the "coastal zone" (downstream part) with altitudes less than 400 masl (Fig.1).

The study area is characterized by a semi-arid climate with an average annual rainfall of 300 mm and an average annual temperature of 20 °C (Ouhamdouch and Bahir 2017).

From a Geological and hydrogeological point of view, the upstream part is characterized by the outcrop of Middle and Upper Cretaceous formations, in particular, Albian-Vraconian, Cenomanian and Turonian (Duffaud 1960; Amghar 1989) (Fig.1). These formations are composed of limestone and dolomitic interspersed with marl and sandstone. The Albian-Vraconian formations are composed of sandstone and limestone dolomites alternating with sandstone banks and sandy clays. The Cenomanian, with a thickness of about 200 m, is composed by alternating marls with anhydrite, lumachellic and dolomitic limestones. As for the Turonian, it is represented by limestones with an abundance of silica. This part contains important aquifers, noting the Cenomanian-Turonian aquifer which remains the most important in the region. According to Jalal et al. (2001), this aquifer presents transmissivities ranging between $2.2*10^{-4}$ and $2.7*10^{-1}$ m^2/s.

The downstream part contains 2 important aquifers: (i) the Plio-quaternary and the (ii) Turonian, located between Ksob wadi and Tidzi wadi (Fig.1). The Plio-quaternary is composed by a matrix of limestone sandstone. It contains an important aquifer (Fig.1). According to Mennani (2001), this water table has transmissivities varying between

$6.1*10^{-2}$ and $4.5*10^{-5}$ m²/s. As for the Turonian, represented by limestones, it contains a captive aquifer under the Senonian marls in the synclinal structure and probably in direct contact with the Plio-Quaternary at the confines of this structure (Fig.1). It has a transmissivity varying between $0.8*10^{-4}$ and $2.7*10^{-2}$ m²/s (Mennani 2001).

Figure 1

Location and geological map of study area

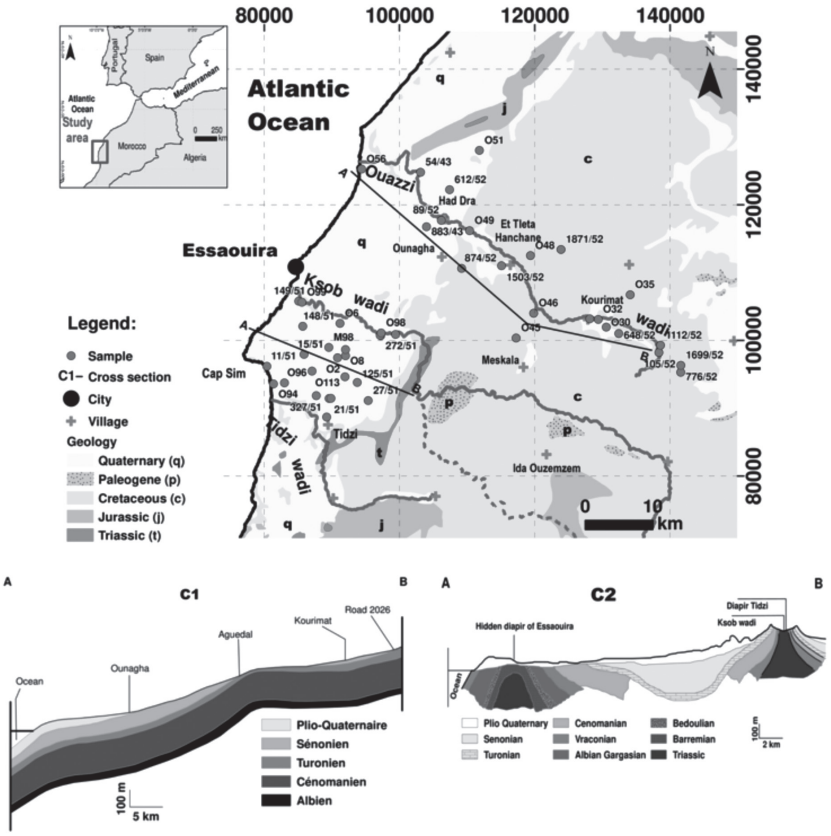

2. Material and methods

A total of 142 samples were collected in 1996 (16), 2004 (26), 2006 (18), 2007 (35), 2016 (22), and in 2018 (25). The samples taken in 1996 were analyzed at the laboratory of Avignon (France) using the mass spectrometry method. Those taken in 2004, 2006, 2007, and 2016 were analyzed in the Center "Centro de Ciências e Tecnologias Nucleares (C2TN), Campus Tecnológico e Nuclear" in Lisbon (Portugal), adopting the

mass spectrometry method for stable isotopes (^{18}O and ^{2}H), electrolytic enrichment followed by a counting method by liquid scintillation for radioactive isotopes (^{3}H).

For ^{13}C and ^{14}C, we based on total dissolved inorganic carbon (TDIC) of groundwater, precipitated in the field as $BaCO_3$. The ^{14}C (benzene) count rates were determined using a liquid scintillation counter. The 25 water points taken in 2018 have been the subject of stable isotope analyzes. The analyses were carried out at the Radio-Analysis and Environment Laboratory at the National School of Engineers of Sfax (ENIS, Tunisia) using a laser spectrometer. The results obtained are collated in Table 1.

4. Results and discussion

4.1. Cenomanian-Turonian Aquifer

4.1.1. Oxygen-18/deuterium diagram

The samples analysed in April 2016 show oxygen-18 contents varying between a minimum of -6.0‰ vs SMOW (O45) and a maximum of -3.3‰ vs SMOW (O46), with an average of -4.9‰ vs SMOW. For deuterium, the maximum value is -20.2‰ vs SMOW (O56), the minimum value equal to -34.5‰ vs SMOW (648/52), and the average value is -28.4‰ vs SMOW (Table 1, Fig. 2).

Figure 2

Spatial distribution of the ^{18}O and ^{2}H content of the groundwater within the Cenomanian-Turonian aquifer (Campaign of 2016)

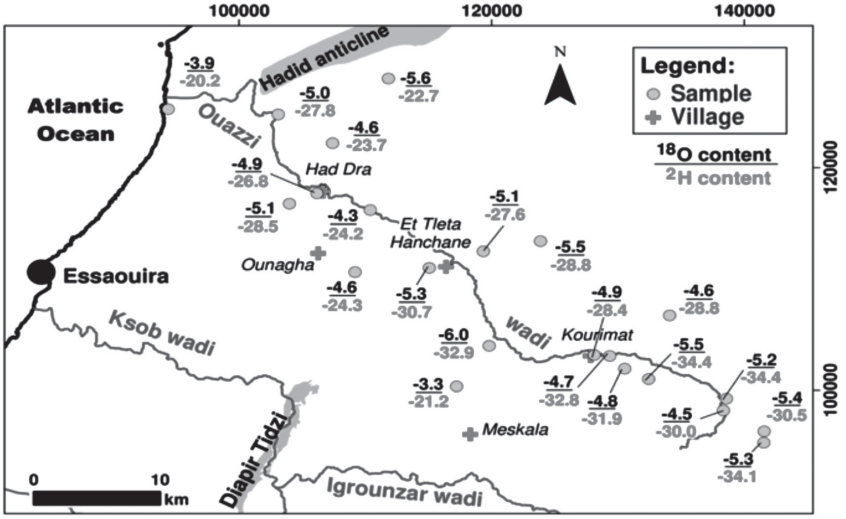

As for the samples taken in October 2007, they have oxygen-18 contents oscillate between a minimum of -6.2‰ vs SMOW (883/52) and a maximum of -3.8‰ vs SMOW (874/52), with an average of -5.2‰ vs SMOW. Regarding the deuterium contents, they vary between -38.4 (883/52) and -20.7 (874/52)‰ vs SMOW with an average of 30.6‰ vs SMOW (Table 1, Fig. 3).

Figure 3

Spatial distribution of the ^{18}O and ^{2}H content of the groundwater within the Cenomanian-Turonian aquifer (Campaign of 2007)

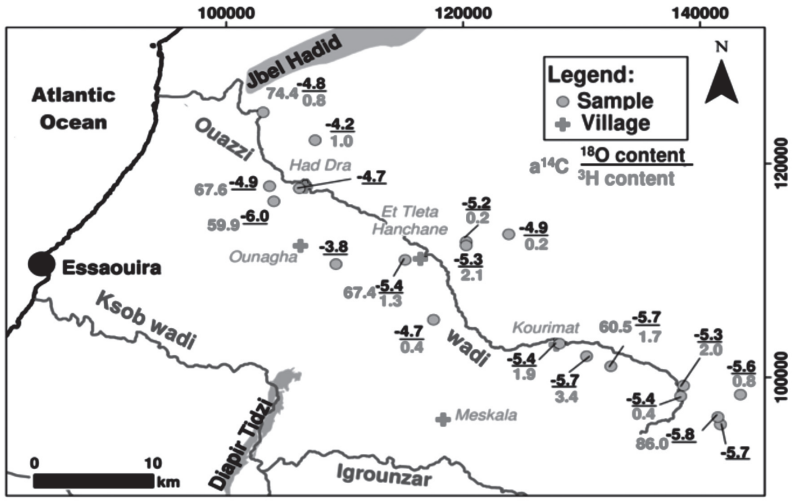

For the June 1996 campaign, the water points analyzed show oxygen-18 contents varying between a minimum of -6 ‰ vs SMOW and a maximum of -4.6 ‰ vs SMOW, with an average of -5.6 ‰ vs SMOW. As for those of deuterium, they balance between -35.9 and -28.3 ‰ vs SMOW with an average of 32.8 ‰ vs SMOW (Table 1).

Based on the frequency histograms (Fig. 4) 45% of the samples analyzed in 2016 are characterized by oxygen-18 contents between -4 and -5‰ vs SMOW, 41% have contents vary between - 5 and -6‰ vs SMOW, 9% have contents between -6 and -7‰ vs SMOW, while the range of values between -3 and -4‰ vs SMOW is represented by 5% of the total samples.

Concerning the 2007 campaign, more than 50% of the waters are characterized by oxygen-18 contents between -5 and -6‰ vs SMOW (60%), while 30% of the samples, present ^{18}O contents vary between -4 and -5‰ vs SMOW. The content ranges between -3 and -4‰ vs SMOW and between -6 and -7‰ vs SMOW are each represented by 5% of the total water points analyzed.

For the 1996 campaign, if except for a single sample with oxygen-18 contents vary between -4 and -5 ‰ vs SMOW, the rest of the water points analyzed are characterized by oxygen-18 contents oscillates between - 5 and -6‰ vs SMOW. These are pointing that flow along the bed of the Igrounzar wadi, constituting the outlet of the Cenomano-Turonian aquifers, in its southern part.

As for deuterium, the frequency of samples collected in 2016 with contents between -30 and -35‰ vs SMOW is in first place with a percentage of 41%, the second, with a percentage of 32%, is represented by the contents varies between -25 and -30 ‰ vs SMOW, while the samples with ^{2}H contents between -20 and 25‰ vs SMOW are dedicated to the third place with the lowest frequency, i.e 27% of the total of the analyzed samples. However, the waters of the Cenomano-Turonian aquifer are characterized by ^{18}O contents ranging from -4 to -6‰ vs SMOW and ^{2}H contents ranging from -25 to 35‰ vs SMOW.

Figure 4

Frequency distribution of oxygen-18 and deuterium contents in the waters of the Cenomanian-Turonian aquifer: (a) campaign of 1996, (b) campaign of 2007 and (c) campaign of 2016

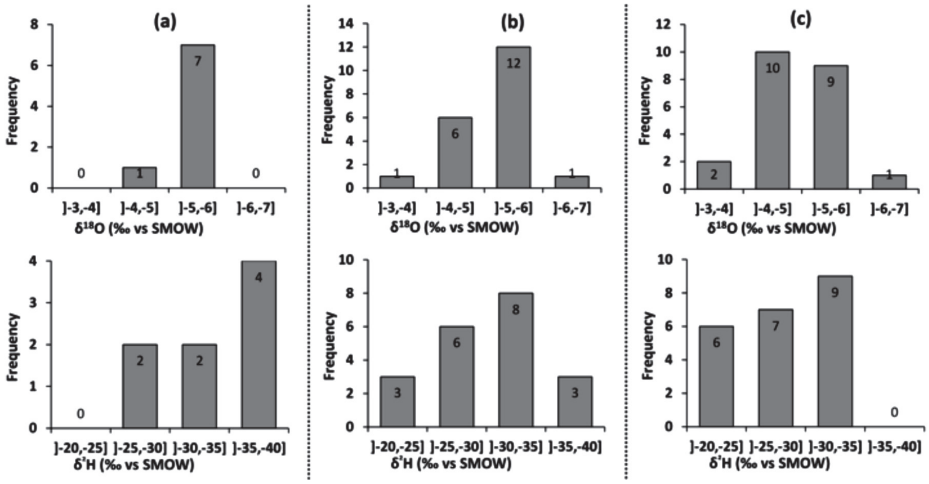

For the 2007 campaign, 40% of water points have ^{2}H contents vary between -30 and -35 ‰ vs SMOW, 30% have contents vary between -25 and -30‰ vs SMOW, while the ranges of contents between -20 and -25‰ vs SMOW and between -35 and -40‰ vs SMOW are each represented by 15% of the total of the analyzed samples.

As for the samples taken in 1996, 50% of the samples have ^{2}H contents oscillate between -35 and -40‰ vs SMOW, while the two ranges of contents between -25 and

-30‰ vs SMOW and between -30 and -35‰ vs SMOW represents each 25% of the total samples analyzed.

The distribution of representative groundwater points on the oxygen-18/deuterium diagram in relation to the global (GMWL) and local (LMWL) meteoric lines, makes it possible to define the main phenomena involved in the hydrodynamic and hydrogeochemical functioning of the aquifer. Figure 5 representing the variation δ^2H vs $\delta 18O$ of groundwater in the study area, shows that the groundwater samples representing the two campaigns 1996 and 2007 (Fig. 5a, b) are located above the meteoric line world (GMWL) and around the local meteoric line (LMWL: $\delta^2H = 7.95 \times \delta 18O + 11.3$) established by Mennani (2001). This reflects that the aquifer recharge is ensured by the infiltration of precipitation of Atlantic origin without significant evaporation. As for the 2016 campaign samples (Fig. 5c), some points are located below GMWL suggesting that these points underwent evaporation before being infiltrated into the aquifer. Other points are located above GMWL reflecting a direct recharge of the aquifer by precipitation of Atlantic origin without significant evaporation. Concerning the precipitation sample, it is an annual average of the analysed samples of rainfall in 2004, 2006, 2016, and 2018 (Fig. 6). The very clear variation in isotopic contents between 2016 and 2007 is due to a paleorecharge and the low recharge rate following the decrease in precipitation in recent decades (Ouhamdouch et al. 2020b).

Figure 5

Correlation diagram δ^2H vs $\delta^{18}O$ of the groundwater of the Cenomanian-Turonian aquifer: (a) campaign of 1996, (b) campaign of 2007 and (c) campaign of 2016

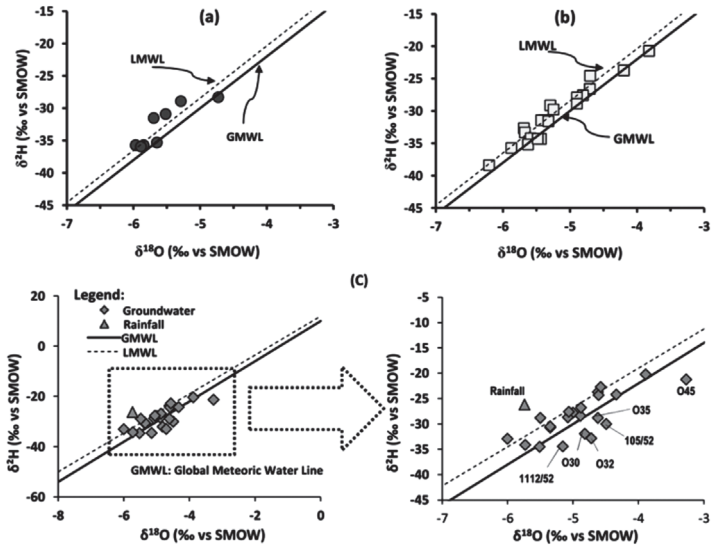

Figure 6

Isotopic content of precipitations within Essaouira basin

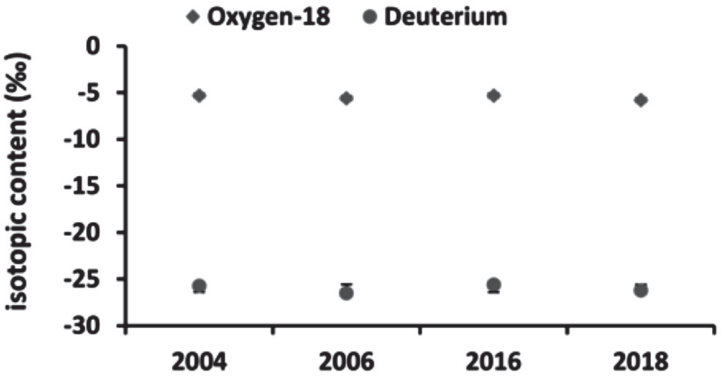

4.1.2. Tracking of groundwater with Tritium and Carbon-14

For the 2016 campaign, the tritium contents range between 0 and 2.1 TU. The highest values were recorded the Et Tleta Hanchane region and in the Kourimat region. This confirms that the recharge of the aquifer through rainwater is low and limited to a few places (Fig.7).

Figure 7

Spatial distribution of the 3H content of the groundwater within the Cenomanian-Turonian aquifer (Campaign of 2016)

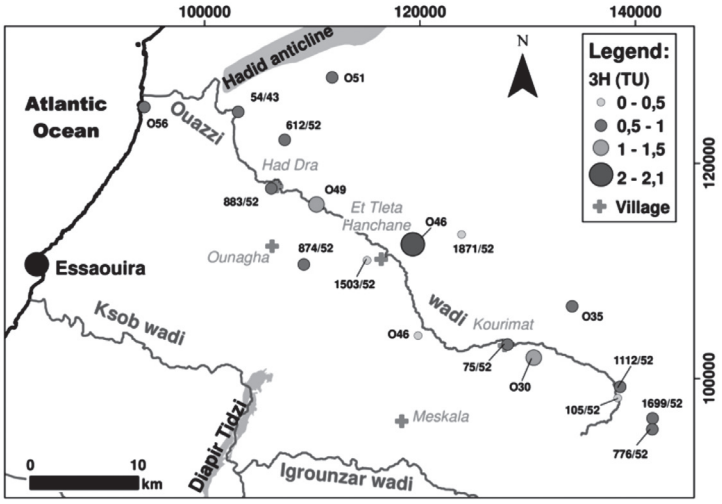

According to Mazor (1991), a tritium content greater than 1 TU indicates a post-nuclear recharge of groundwater and content less than 1 TU represents a pre-nuclear recharge or a mixture between recent and old waters. Indeed, the high tritium contents have been observed in the Kourimat and Et Tleta Hanchane region (recharge area), and they can be attributed to the recent infiltration of precipitation.

The projection of the samples from the two campaigns 2016 and 2007 (Fig. 8) shows that some points are located above the line representing 1 TU reflecting a recent recharge of the Cenomanian-Turonian aquifer, while the other points are located below the line of 1 TU confirming a pre-nuclear recharge or a mixture of recent and old waters. A comparison of the ^{3}H content of the same water point analysed in 2007 and 2016 shows a decrease in the ^{3}H content. At certain points such as O30, the decrease in the ^{3}H content is accompanied by an increase in ^{18}O, this could be explained by a mixing phenomenon between a source (coming from the well O30) and the well O30 well. However, the general decrease in ^{3}H levels could be explained by the low recharge rate following the decrease in the precipitation rate as a result of climate change.

Figure 8

Relation oxygen-18 and tritium content of water points sampled

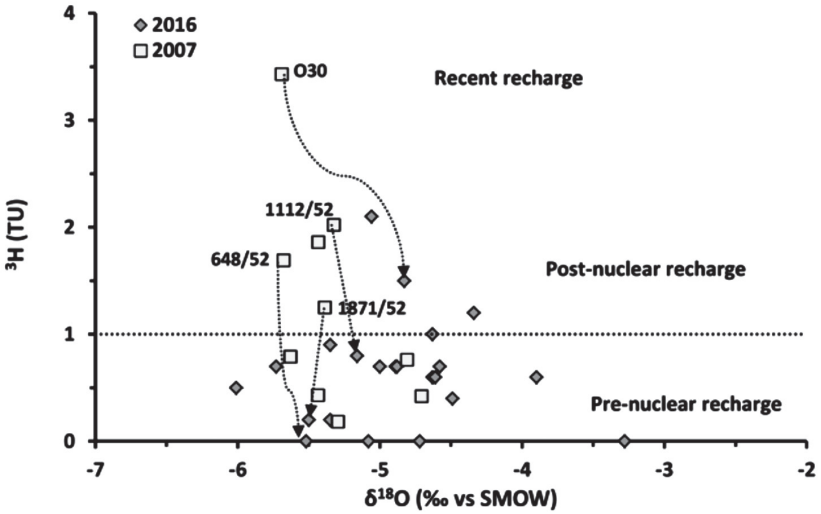

Nine samples capturing the Cenomanian-Turonian aquifer were analysed for carbon-14 and carbon-13. The $\delta^{13}C$ of analysed samples range from -10.82 (605/52) to -5.12‰ (1699/52) with an average of -8.70‰ vs PDB (Table 1). The majority of the samples have more homogeneous ^{13}C contents which vary between -7.41 and

-10.82‰. This small variation in $\delta^{13}C$ contents suggests that the carbon sources are very limited. Represented on the diagram $\delta^{13}C$/Carbon-14 activities (Fig. 9), the waters of the Cenomanian-Turonian aquifer show a depletion in $\delta^{13}C$ as the time of the residence of the waters increases. This depletion can be attributed to the phenomenon of carbonate mineral precipitation leading to a decrease in the proportion of the heavy isotope of carbon in water.

Dating groundwater at ^{14}C is not an easy procedure, especially in carbonate aquifers or even when carbonate layers are present in geological strata, as it occurs in the Essaouira sedimentary basin.

Figure 9

Correlation $\delta^{13}C$ vs carbon-14 activity of the samples capturing the Cenomanian-Turonian aquifer

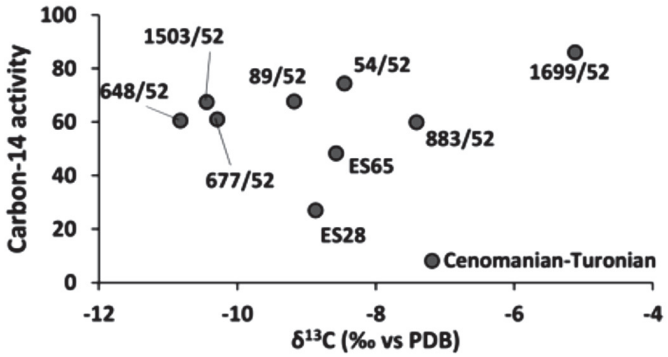

A common and simple way to estimate the initial activity of ^{14}C is to relate the $\delta^{13}C$ content of TDIC in groundwater to the mixed carbon of carbonate rocks, using carbon from soil CO_2 and a fractionation factor between the different carbonate phases as a function of temperature (Salem et al. 1980; Gonfiantini and Zuppi, 2003). The equation proposed by these authors was used to estimate the apparent radiocarbon age of the groundwater samples from the Cenomanian-Turonian aquifer:

$$t_s = 8267 \times Ln\left(\frac{A_0}{A_t}\right)$$

With $A_0 = [100\ (\delta_{CITD} - \delta_R)\ (1+2.3\varepsilon_{13}\ /1000)]\ /\ (\delta_S - \delta_R + \varepsilon_{13})$

The apparent radiocarbon age of groundwater was estimated using the value $\delta^{13}C$ as a correction factor. A_0 is the initial ^{14}C activity in TDIC during the recharge of the aquifer and At the residual ^{14}C activity in TDIC measured in a sample capturing this aquifer (expressed in pmc).

It has been assumed that the ^{14}C activity of soil CO_2 is 100 pmc (Fontes 1976).

δ_{CITD} = the measured ^{13}C content of soil CO_2

δR = the ^{13}C content of $CaCO_3$ in the soil and in the rock matrix

δS = represents the ^{13}C content of soil CO_2

ε_{13} = represents the ^{13}C enrichment factor during the CO_2 dissolution from the soil in water infiltration.

To estimate the apparent radiocarbon age, the value of δ_S = -23‰ was adopted to calculate the initial ^{14}C activity and 0‰ was adopted as representative of δ_R (Carreira et al. 2014). To take into account the fractionation during the dissolution of CO2 from the soil in the infiltration water, we adopted ε_{13} = 9.0‰ (Mook et al. 1974). This simple model was considered appropriate because in all the water samples analyzed, the saturation index with respect to calcite is not significant (Bahir et al. 2018c; Bahir and Ouhamdouch 2020b), and the $\delta^{13}C$ measured in the TDIC of samples is about -10‰, indicating a small contribution of the dissolved carbonate. However, the estimated radiocarbon ages vary from the actual (samples 54/52, 89/52, 883/52, and 1699/52) to 7212 years BP (BP = before present) (samples ES28) (Table 2).

However, the presence of ancient waters in the study area suggests a low rate renewal of the groundwater within the Cenomanian-Turonian aquifer. This must be taken into account in the context of the exploitation and management of this resource. Uncontrolled exploitation can cause a decline in the water level and consequently hydrochemical imbalances causing an irreversible degradation of the groundwater quality as well as a depletion of the resource.

4.1.3. Temporal evolution of ^{18}O contents as a function of electrical conductivity

Following the availability of data, a comparison of the ^{18}O contents of the same water points having known the dosage of this element in 2007 and 2016 was made in order to assess the behavior of the isotopic signature when facing of climate change. The obtained results are grouped in Figure 10.

From this, we note that the evolution of the oxygen-18 content, which is accompanied by an increase in the electrical conductivity (salinity) from 2007 to 2016, presents a slight increase in ^{18}O. This slight enrichment in ^{18}O, on the order of 1‰, is probably due to the phenomenon of evaporation following the increase in the air temperature caused by climate change. However, it can be concluded that the groundwater isotopic signature of the Cenomanian-Turonian aquifer has not been spared by the effect of climate change.

Figure 10

Interannual variation in $\delta^{18}O$ contents vs electrical conductivity of samples taken in 2007 and 2016

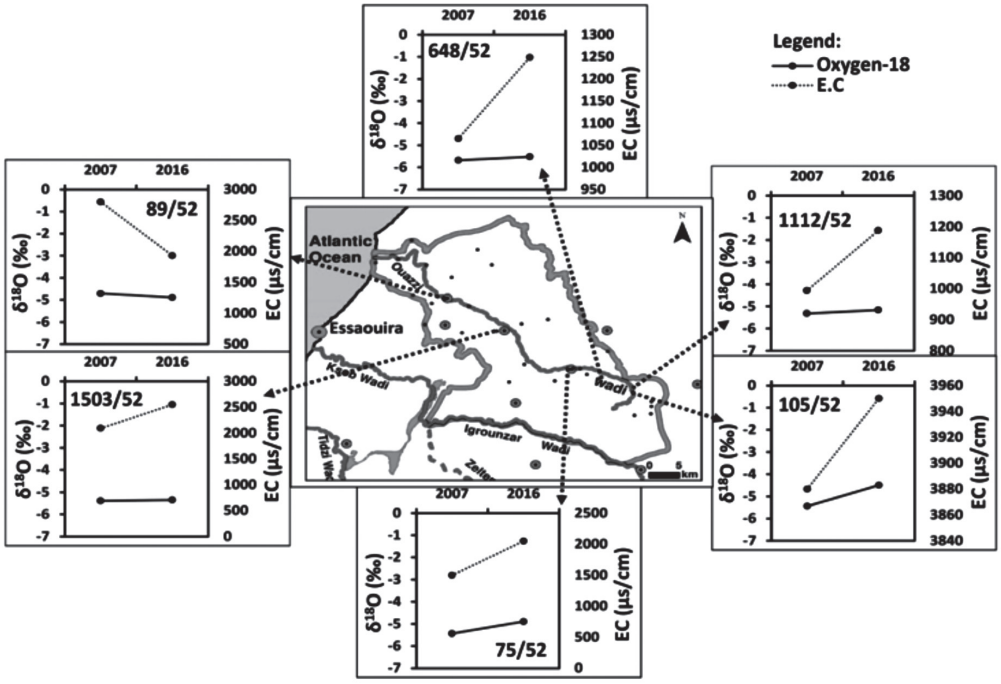

4.2. Plio-Quaternary and Turonian Aquifers

4.2.1. Oxygen-18/deuterium diagram

Oxygen-18 contents vary between a minimum of -5.0‰ vs SMOW (27/51) and a maximum of -1.8‰ vs SMOW (11/51), with an average of -3.9‰ vs SMOW for the Plio-Quaternary aquifer and between a minimum of -5.0‰ vs SMOW (380/51) and a maximum of -4.4‰ vs SMOW (346/51), with an average of -4.7‰ vs SMOW for the Turonian aquifer. As for deuterium contents, the maximum value is -8.9‰ vs SMOW (11/51) and the minimum value equal to -29.7‰ vs SMOW (O8) with an average value of -22.6‰ vs SMOW for the Plio-Quaternary aquifer. As for the Turonian aquifer, the maximum value is -27.3‰ vs SMOW (386/51) and the minimum value equal to -28.5‰ vs SMOW (380/51) with an average value of -27.9‰ vs SMOW (Table 1, Fig. 11).

Figure 11

Spatial distribution of the ^{18}O and ^{2}H content of the groundwater within the Plio-Quaternary and Turonian aquifers (Campaign of 2018)

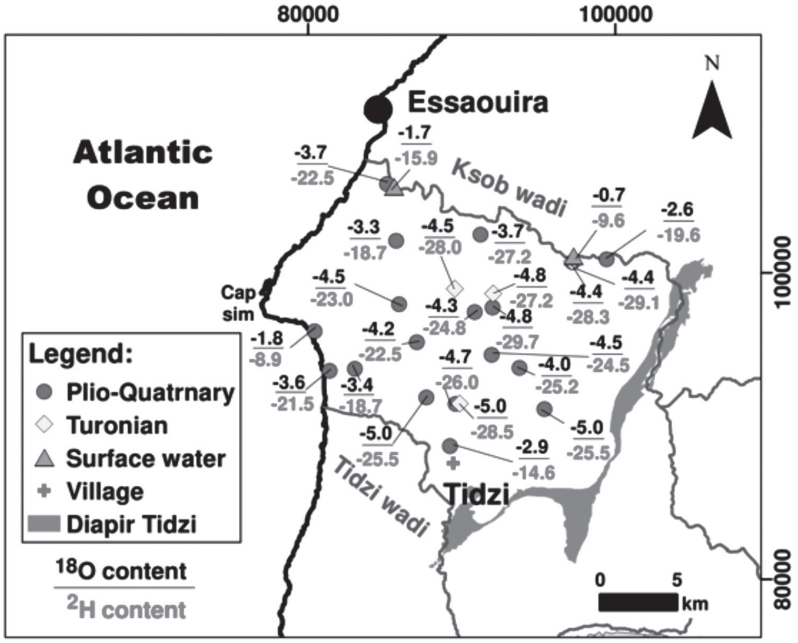

The frequency histograms representing the Plio-Quaternary aquifer (Fig. 12a) show that half of the analyzed samples are characterized by oxygen-18 contents between -4 and -5‰ vs SMOW, 27% have contents vary between -3 and -4‰ vs SMOW, 11% have contents between -6 and -7‰ vs SMOW, while the ranges of values between -5 and -6‰ vs SMOW and between -1 and -2‰ vs SMOW are represented by 5% each one of the total samples. As for those representing the Turonian aquifer (Fig. 12a), they show that the 18O contents of the groundwaters vary between -4 and -6‰ vs SMOW with the dominance of waters with contents vary between -4 and -5‰ vs SMOW (75%). As for deuterium, the frequency histograms (Fig. 12b) show that the range of the most frequent values are in the ranges of]-20, -25] and] -25, -30] for the Plio-Quaternary aquifer with a percentage of 39 and 33%, respectively. Concerning the Turonian, the ^{2}H contents of all the samples analyzed are between -25 and -30‰ vs SMOW. However, the waters of the Plio-Quaternary and Turonian aquifers are characterized by ^{18}O contents varying from -4 to -5‰ vs SMOW and ^{2}H contents ranging from -25 to -30‰ vs SMOW.

Figure 12

Frequency distribution of oxygen-18 (a) and deuterium (b) contents in the waters of the Plio-Quaternaty and Turonian aquifer (Campaign of 2018)

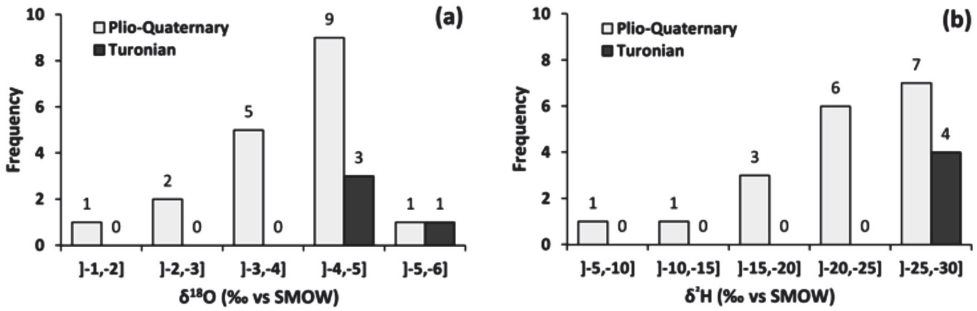

The distribution of representative samples of the Plio-Quaternary and Turonian aquifers (campaign of 2018) on the correlation diagram δ^2H vs $\delta^{18}O$ (Fig. 13), makes it possible to define the main phenomena involved in the hydrodynamic and geochemical functioning of aquifers.

The majority of the points are scattered around the GMWL and LMWL lines reflecting a recharge by infiltration of rainwater of Atlantic origin (Group 1). This recharge results in the decrease in the salinity in these wells (in particular well 27/51 which has a low electrical conductivity (salinity)). This well is the closest to the freshwater pole (rainwater). Other local recharge points for rainwater have been identified (for example O6, 15/51). This recharge is probably favored by the lithological nature and the small thickness of the unsaturated zone. This group contains both the majority of the samples representing the shallow Plio-Quaternary aquifer and all the water points representing the deep Turonian aquifer. However, the water in Group 1 wells is free of all evaporation traces, which indicates rapid infiltration of rainwater. Other water points are distinguished by their position below the GMWL (Group 2), they line up in 8 characteristics of the evaporation phenomenon. This last process mainly concerns surface water (O98 and O99) and wells 105/51 and 327/51 located respectively in the northeast and south part of the aquifer. Evaporation can probably take place before water infiltration, in the unsaturated zone or during sampling. The Freshwater-Seawater line is drawn up taking the isotopic signature of rainwater and that of seawater from the Atlantic Ocean (Carreira et al. 2014).

In the same diagram, well 11/51 is aligned on the line freshwater-seawater mixture. This point located on the coastal fringe near Cap Sim is characterized by high salinities which are accompanied by a decrease in the piezometric level, and this since 2015.

This confirms that the increase in mineralization in this well is mainly caused by the marine intrusion phenomenon.

Figure 13

Deuterium vs oxygen-18 diagram of the groundwaters sampled in 2018 of the Plio-Quaternary and Turonian aquifers

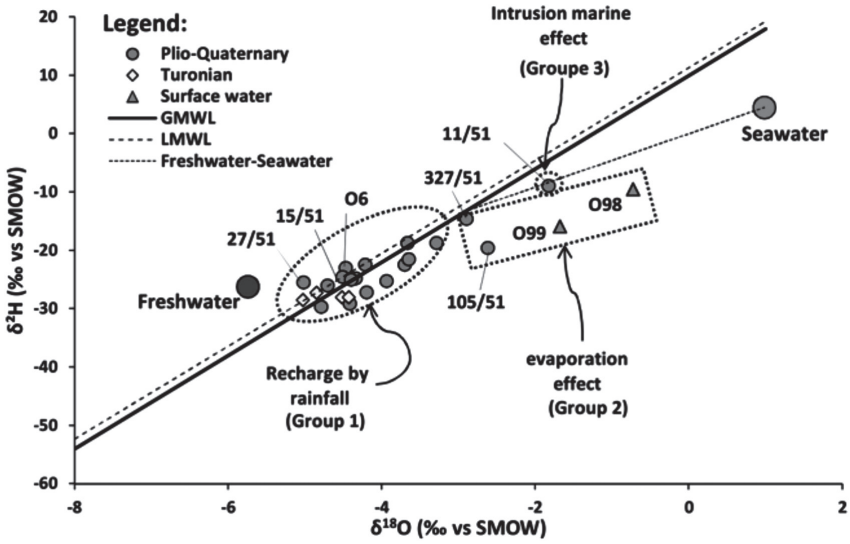

4.2.2. Tracing the groundwater of the Plio-Quaternary and Turonian aquifer with Tritium and ^{14}C

For the campaign of May 2004 (Table 1, Fig. 14a), the tritium contents of the groundwater from the Plio-Quaternary aquifer vary between 0.2 and 4.2 TU with an average of 1.7 TU. As for the groundwater of the Turonian, the contents vary between 0.9 and 2.5 TU with an average of 1.6 TU. Concerning the campaign of June 2006 (Table 1, Fig. 14b), the ^{3}H contents of the samples catching the Plio-Quaternary aquifer oscillate between 2 and 4.4 TU with an average of 3.2 TU. Those of the samples representing the Turonian vary between 2 and 3.8 TU with an average of 2.5 TU. The ^{3}H enrichment between 2004 and 2006 could be explained by the increase in precipitation in 2006 (514 mm/year) compared to 2004 (393 mm /year). The highest values were marked in the North, near the Ksob wadi, and in the East, aquifer recharge zones. The highest values were marked in the North, near Ksob Wadi and in the East; these are the aquifer recharge zones. This confirms that the recharge of the aquifer through rainwater is low and limited to a few places. The presence of water with very

low ^{3}H contents, reflects the low recharge rate and requires the use of ^{14}C in order to estimate the age of this vital resource.

Figure 14

Spatial distribution of the ^{18}O and ^{3}H content of the groundwater within the Plio-Quaternary and Turonian aquifers: (a) Campaign of 2004, (b) Campaign of 2006

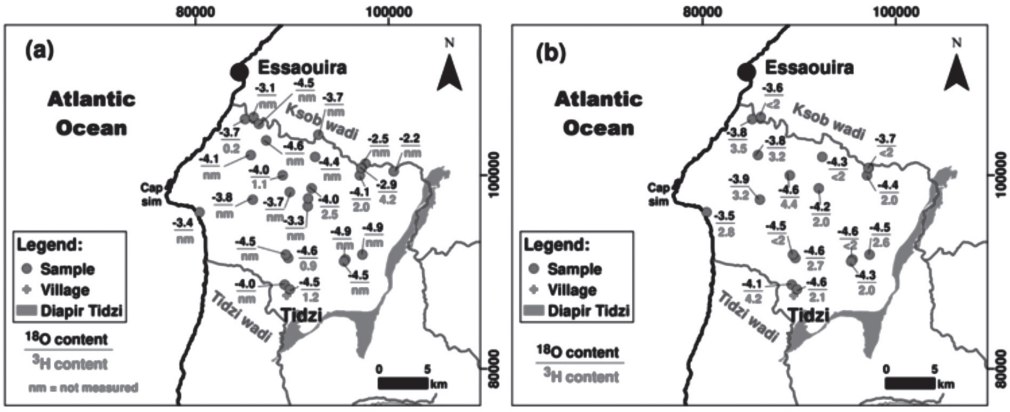

Seven water points, three of which capture the Plio-Quaternary aquifer and four captures the Turonian (Table 1) were analysed for carbon-14 and carbon-13. Carbon-13 contents measured in the waters of the Plio-Quaternary aquifer vary between -8.4‰ (128/51) and -6.3‰ (389/51) with an average of -7.5‰. As for the Turonian aquifer, the 13C contents oscillate between -10.3 (386/51) and 9.4‰ (390/51) with an average of 9.8‰. The samples show more homogeneous ^{13}C contents which vary between -6.3 and -10‰. This reflects that the origin of carbon is probably from a single source. The plotting of the Plio-Quaternary and Turonian aquifers on the diagram δ13C/Carbon-14 activities (Fig. 15) shows that the waters of the Turonian aquifer are slightly depleted in ^{13}C compared to those of the Plio-Quaternary. This could be explained by the significant depth of the Turonian aquifer. For the two aquifers, certain points have a carbon-14 activity greater than 70 pmc suggesting the presence of interconnection between them, particulary in upstream and downstream of the basin. Some samples show a ^{13}C depletion which can be attributed to the phenomenon of carbonate mineral precipitation causing a reduction in the proportion of the heavy isotope of carbon in water.

Figure 15

Correlation $\delta^{13}C$ vs carbon-14 activity of the samples capturing the Plio-Quaternary and Turonian aquifers

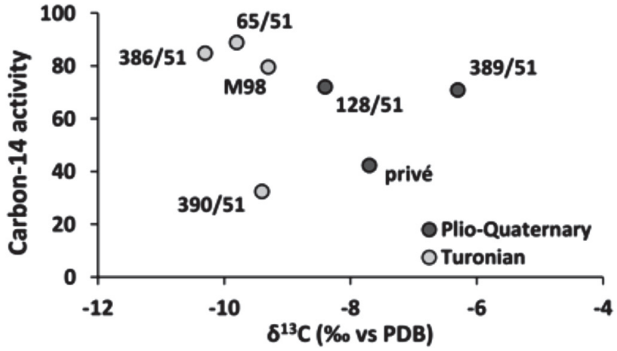

After estimating the initial carbon-14 (A0) activity, the radiocarbon age of the waters representing the Plio-Quaternary and Turonian aquifers was estimated based on the equation established by Salem et al. 1980 and validated by Gonfiantini and Zuppi 2003, and Carreira et al. 2014. The waters of the Plio-Quaternary aquifer show radiocarbon ages ranging from the actual to 2326 years BP and those of the Turonian aquifer show ages varying from the actual to more than 6000 years BP (Table 2). The difference in water ages between the two aquifers results in the fact that the Plio-Quaternary aquifer is superficial while the Turonian is a deep aquifer.

However, as in the case of the Cenomano-Turonian aquifer, the presence of old waters within the Plio-Quaternary and Turonian aquifers suggests a low rate of renewal of groundwater. This must be taken into account in the context of the exploitation and management of this resource.

4.2.3. Temporal evolution of ^{18}O contents of the groundwater of the Plio-Quaternary and Turonian aquifers

Evolution of the oxygen-18 content in some wells capturing the Plio-Quaternary and Turonian aquifers is grouped in Figure 16 and Figure 17. The ^{18}O vs ^{2}H correlation diagram for each point during 25 years shows that the recharge of the Plio-Quaternary and Turonian aquifers is ensured by precipitation of Atlantic origin without notable evaporation. Only two points are located below the GMWL, it is point 272/51 (in 2004) and point 11/51 (in 2018). This situation could be explained by the fact that point 272/51 underwent evaporation before infiltration, while point 11/51 underwent marine contamination as shown in Figure 17 where the electrical conductivity is around 10 mS/cm.

Figure 17 represents the evolution of the oxygen-18 content and the electrical conductivity of the points capturing the Plio-Quaternary and Turonian aquifers. From this Figure we see that the increase in electrical conductivity (salinity) is accompanied by a slight increase in oxygen-18 contents. This slight enrichment in ^{18}O, from 1 to 1.5‰, may be due to the effect of evaporation caused by the increase in atmospheric temperature under the effect of global warming (Fig. 18). This suggests that the isotopic signature of the study area is influenced by climatic variations and therefore it can be concluded that climate change has an effect on the isotopic content of groundwater within the Essaouira basin.

Figure 16

Isotopic contents evolution of the groundwater of the Plio-Quaternary and Turonian aquifers

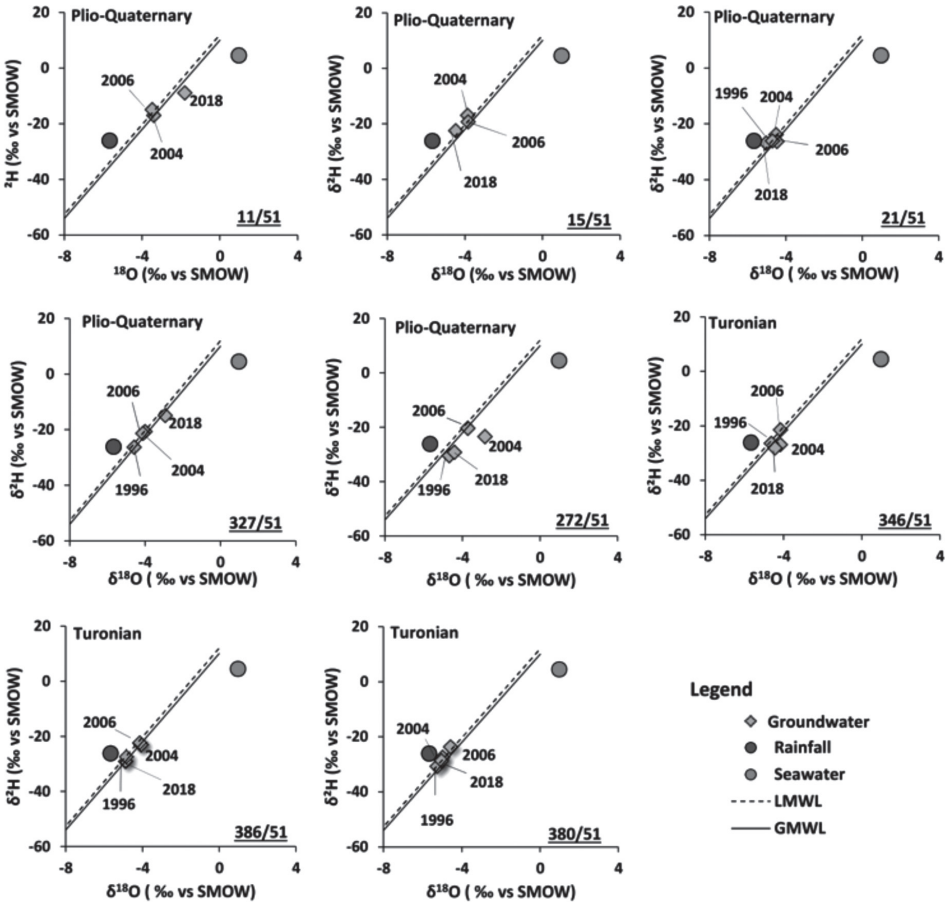

Figure 17

Interannual variations in $\delta^{18}O$ contents vs electrical conductivity of the samples taken in 1996, 2004, 2006 and 2018 from Plio-Quaternary and Turonian aquifers

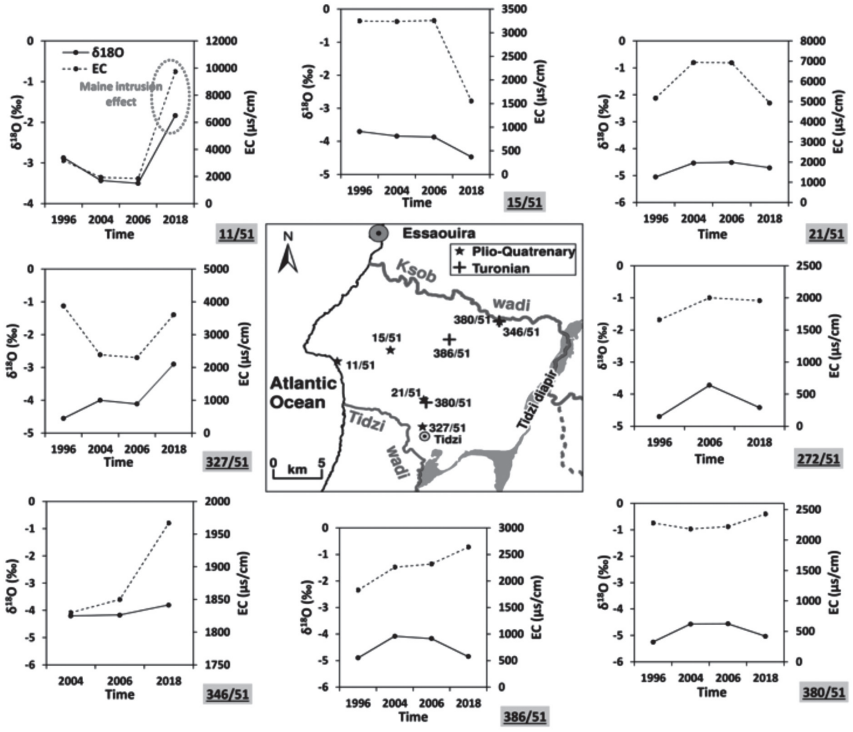

Figure 18

Temperature evolution within the Essaouira basin

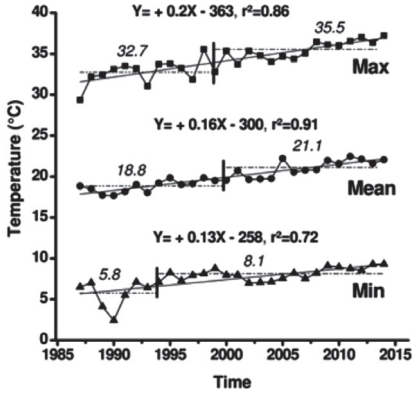

5. Conclusion

Tracing the groundwater of the Essaouira basin with stable and radioactive isotopes of the water molecule has permitted to determine the origin, mode, and recharge areas of these waters.

The correlation between the deuterium and oxygen-18 contents of the groundwater of the Cenomanian-Turonian aquifer highlighted that the recharge of these waters is ensured by precipitation of Atlantic origin without significant evaporation. For the Plio-Quaternary and Turonian, this correlation has shown that groundwater recharge is also ensured by precipitation of Atlantic origin without significant evaporation and that these waters have been subjected to contamination by seawater.

This approach has shown that the recharge areas of the Cenomanian-Turonian aquifer are represented by the Et Tleta Hanchane region (altitude ≈ 300 m asl), the Krimat region (altitude ≈ 500 to 620 m asl) and the far East of the study area.

Tritium tracing based on the same wells sampled in 2007 and 2016 shows a significant decrease that reaches 2 TU in some wells. This trend could be explained by the low recharge rate following the decrease in precipitation experienced by the study area in recent years. The presence of old or fossil water in the study area suggests a low rate of renewal of the groundwater in this basin. This must be taken into account in the context of the exploitation and management of these waters.

The temporal evolution of the 18O contents generally shows an enrichment character, of the order of 1 to 1.5‰. This may be due probably to the phenomenon of evaporation generated by the increase in air temperature caused by climate change. The latter also seems to affect the isotopic signature of groundwater in the Essaouira basin.

Table 1

Isotopic results of analysed samples

Sample	Depth/soil	T	pH	EC	$\delta^{18}O$	$\delta^{2}H$	^{3}H	$\delta^{13}C$	^{14}C
	m	°C		µs/cm	‰ vs SMOW		TU	‰	pmc
Cenomanian-Turonian Aquifer									
Campaign of 1996									
610/52	-	21.0	-	771	-5.81	-35.70	-	-	-
O.Tagmout	-	26.5	-	596	-5.71	-	-	-	-
A.bouSetta	-	21.0	-	625	-4.73	-28.30	-	-	-
1319/52	-	19.5	-	815	-5.97	-35.70	-	-	-
1317/52	-	21.0	-	952	-5.65	-35.30	-	-	-
141/52	-	20.5	-	920	-5.52	-30.90	-	-	-
681/52	-	21.0	-	528	-5.29	-28.90	-	-	-
Campaign of 2007									
1503/52	20	20.8	6.9	2092	-5.39	-31.39	1.3	-10.4	67.4
ES02	75.0	22.0	7.28	2600	-4.71	-26.57	0.4	-	-
75/52	6.2	20.0	7.24	1500	-5.43	-31.42	1.9	-	-
605/52	1.7	17.4	7.5	998	-5.69	-32.67	3.4	-	-
648/52	32.0	21.9	7.39	1065	-5.68	-33.32	1.7	-10.8	60.5
1112/52	34.5	21.3	7.69	994	-5.32	-31.57	2.0	-	-
105/52	-	17.4	7.64	3880	-5.43	-34.32	0.4	-	-
776/52	5.2	18.3	7.6	1600	-5.59	-34.23	-	-	-
1699/52	-	21.5	7.11	2750	-5.88	-35.71	-	-5.1	86.0
883/52	24.5	26.6	6.9	2500	-6.21	-38.37	-	-7.4	59.9
89/52	7.5	22.8	6.9	2800	-4.70	-24.54	-	-	-
54/52	-	22.2	6.75	3100	-4.81	-27.57	0.8	-8.5	74.4
89./52	-	24.8	6.65	2700	-4.90	-27.89	-	-9.2	67.7
874/52	8.4	24.4	7.35	2540	-3.82	-20.69	-	-	-
612/52	25.0	22.2	7.35	2970	-4.20	-23.69	-	-	-
1576/52	-	23.2	7.8	900	-5.29	-29.13	0.2	-	-
ES34	7.0	22.1	7.1	1900	-5.63	-35.14	0.8	-	-
ES35	-	26.4	7.65	3740	-5.48	-34.26	-	-	-
ES36	88.0	25.0	7.4	1220	-5.25	-29.76	-	-	-
1871/52	-	26.2	7	2300	-4.90	-28.87	-	-	-

Sample	Depth/soil	T	pH	EC	$\delta^{18}O$	$\delta^{2}H$	^{3}H	$\delta^{13}C$	^{14}C
	m	°C		µs/cm	‰ vs SMOW		TU	‰	pmc
1415/52	29.6	24.4	7.15	966	-5.23	-28.59	0.9	-	-
ES28	95.0	25.8	7.1	1400	-4.52	-22.32	-	-8.9	27.0
72/52	6.0	23.5	7.35	1500	-4.31	-27.39	-	-	-
677/52	2.7	22.8	7.1	1500	-5.10	-30.91	1.8	-10.3	61.0
1690/52	90.0	24.4	6.9	1450	-5.18	-31.13	3.2	-	-
2099/52	9.5	24.6	7.15	1232	-5.54	-30.59	-	-9.5	60.7
ES65	3.3	29.5	6.85	1810	-5.38	-31.81	1.6	-8.6	48.3
Campaign of 2016									
54/43	-	23.2	7.1	3100	-27.8	-5	0.7	-	-
75/52	15.0	18.5	7.7	2050	-28.40	-4.89	0.7	-	-
89/52	10.7	21.2	7.4	1933	-26.80	-4.88	0.7	-	-
105/52	1.5	20.2	7.6	3950	-30.00	-4.49	0.4	-	-
612/52	27.0	20.8	7.3	3150	-23.70	-4.63	1.0	-	-
648/52	36.5	22.1	7.3	1249	-34.50	-5.52	0.0	-	-
776/52	15.1	19.2	7.4	1300	-34.10	-5.73	0.7	-	-
874/52	12.6	23.0	7.3	4150	-24.30	-4.61	0.6	-	-
883/43	33.5	24.0	7.2	2550	-28.70	-5.08	0.0	-	-
1112/52	35.0	21.0	7.8	1188	-34.40	-5.16	0.8	-	-
1503/52	20.0	23.4	7.1	2550	-30.70	-5.35	0.2	-	-
1699/52	25.7	20.7	7.7	1800	-30.50	-5.35	0.9	-	-
1871/52	-	23.7	7.1	1800	-28.80	-5.50	0.2	-	-
O30	13.9	19.5	7.2	2190	-31.90	-4.83	1.5	-	-
O32	15.6	20.4	7.2	1590	-32.80	-4.72	0.0	-	-
O35	23.8	19.8	7.5	803	-28.80	-4.63	0.6	-	-
O45	6.0	18.0	7.5	3250	-21.20	-3.28	0.0	-	-
O46	8.4	22.1	6.9	3050	-32.90	-6.01	0.5	-	-
O48	31.6	20.9	7.5	1883	-27.60	-5.06	2.1	-	-
O49	25.3	23.3	7.4	1894	-24.20	-4.34	1.2	-	-
O51	50.1	22.1	7.2	2020	-22.70	-4.58	0.7	-	-
O56	9.0	20.5	7.4	4450	-20.20	-3.90	0.6	-	-

Sample	Depth/soil	T	pH	EC	$\delta^{18}O$	$\delta^{2}H$	^{3}H	$\delta^{13}C$	^{14}C
	m	°C		µs/cm	‰ vs SMOW		TU	‰	pmc
Plio-Quaternary Aquifer									
Campaign of 1996									
11/51	-	-	-	-	-2.87	-	-	-	-
15/51	-	-	-	-	-3.70	-	-	-	-
20/51	-	-	-	-	-4.21	-	-	-	-
21/51	-	21.7	7.1	5170	-5.05	-26.80	-	-	-
272/51	-	20.6	7.7	1660	-4.70	-30.30	-	-	-
327/51	-	22.2	7.2	1110	-4.55	-26.20	-	-	-
Wadi	-	-	-	-	-3.35	-22.10	-	-	-
Campaign of 2004									
149/51	36	23	7.3	3280	-3.70	-22.00	0.2	-	-
132/51	26.2	19	8.5	1260	-3.70	-18.00	-	-	-
M98	84	22	7.3	2330	-4.00	-24.00	1.1	-	-
15/51	5	19	7.5	3240	-3.80	-17.00	-	-	-
11/51	3	22	7.3	1940	-3.40	-17.00	-	-	-
21/51	62.6	22	7.1	6940	-4.50	-24.00	-	-	-
380/51	75	22	8.1	2180	-4.60	-27.00	0.9	-	-
327/51	21.1	23	7.6	2390	-4.00	-21.00	-	-	-
27/51	28	23	7.5	798	-4.90	-28.00	-	-	-
M24	174	28	7.5	4660	-4.50	-25.00	-	-	-
28/51	177	23	8	1080	-4.90	-24.00	-	-	-
140/51	8.5	24	6.8	2010	-4.60	-29.00	-	-	-
148/51	14	20	7.4	1590	-4.10	-24.00	-	-	-
389/51	64	24	7.4	4600	-3.30	-22.00	-	-	-
134/51	37	23	7.5	3040	-4.30	-24.00	-	-	-
53/51	61	22	7.3	1490	-3.70	-28.00	-	-	-
93/51	70	23	7.4	1750	-4.40	-26.00	-	-	-
puits particul	87.5	21	7.2	1890	-2.50	-24.00	-	-	-
272/51	36	21	7.4	2000	-2.90	-23.00	4.2	-	-
Wadi upstream	-	26	8.8	1840	-2.20	-24.00	-	-	-
Wadi downstream	-	21	8	2160	-3.10	-12.00	-	-	-

Sample	Depth/soil	T	pH	EC	$\delta^{18}O$	$\delta^{2}H$	^{3}H	$\delta^{13}C$	^{14}C
	m	°C		µs/cm	‰ vs SMOW		TU	‰	pmc
Campaign of 2006									
149/51	-	-	-	-	-3.79	-19.20	3.5	-	-
M98	-	-	-	-	-4.56	-24.20	4.4	-	-
15/51	-	-	-	-	-3.87	-19.30	3.2	-	-
nov-51	-	-	-	-	-3.50	-14.90	2.8	-	-
21/51	-	-	-	-	-4.51	-26.20	<2	-	-
327/51	-	-	-	-	-4.11	-21.30	4.2	-	-
27/51	-	-	-	-	-4.55	-22.90	<2	-	-
28/51	-	-	-	-	-4.50	-22.70	2.6	-	-
M24	-	-	-	-	-4.34	-23.50	2	-	-
148/51	-	-	-	-	-3.82	-20.70	3.2	-	-
272/51	-	-	-	-	-3.72	-20.30	<2	-	-
380/51	-	-	-	-	-4.56	-23.60	2.7	-	-
93/51	-	-	-	-	-4.33	-22.30	<2	-	-
Wadi downstream	-	-	-	-	-3.57	-19.00	-	-	-
Campaign of 2007									
457/51	-	27.0	7.7	1930	-4.79	-28.12			
829/51	-	20.0	7.5	547	-5.46	-27.83	3.4	-	-
327/51	-	24.0	7.1	2270	-4.78	-24.69	-	-	-
128/51	-	22.0	7.2	1700	-4.53	-27.02	2.0	72.1	-8.4
Privé	-	24.0	6.9	2430	-5.59	-32.79	1.7	42.4	-7.7
389/51	-	24.9	7.2	4670	-3.77	-21.27	-	70.9	-6.3
Campaign of 2018									
11/51	4.1	17.6	8.4	9744	-1.80	-8.90	-	-	-
15/51	8.1	19.8	7.8	1557	-4.50	-23.00	-	-	-
21/51	28.06	23.3	7.4	4933	-4.70	-26.10	-	-	-
27/51	30.75	22.2	7.8	916	-5.00	-25.50	-	-	-
105/51	11.4	22.7	7.5	2187	-2.60	-19.60	-	-	-
125/51	57.03	26.3	8	2716	-3.90	-25.20	-	-	-
148/51	14.5	21.2	7.5	1602	-3.30	-18.70	-	-	-
149/51	37.7	23.1	7.4	3482	-3.70	-22.50	-	-	-

Sample	Depth/soil	T	pH	EC	$\delta^{18}O$	$\delta^{2}H$	^{3}H	$\delta^{13}C$	^{14}C
	m	°C		µs/cm	‰ vs SMOW		TU	‰	pmc
272/51	28.6	22	7.5	1957	-4.40	-29.10	-	-	-
327/51	27.4	21.9	7.7	3608	-2.90	-14.60	-	-	-
O2	84.3	25.2	7.9	1960	-4.50	-24.50	-	-	-
O6	15.9	21.7	7.3	2176	-4.20	-27.20	-	-	-
O8	-	20.5	7.9	2731	-4.80	-29.70	-	-	-
O91	40	23.2	7.6	3034	-4.30	-24.80	-	-	-
O94	4.5	20.7	7.4	3408	-3.70	-21.50	-	-	-
O96	6.7	20.7	8.1	1842	-3.70	-18.70	-	-	-
O111	32.2	23.6	7.2	2794	-4.40	-25.10	-	-	-
O113	16.4	21.3	8.1	6716	-4.20	-22.50	-	-	-
O98	-	20.7	8.2	1896	-0.70	-9.60	-	-	-
O99	-	25.8	8.7	2965	-1.70	-15.90	-	-	-
Turonian Aquifer									
Campaign of 1996									
65/51	-	22.5	7.5	2870	-4.05	-24.70	-	-	-
380/51	-	26.1	7.5	2280	-5.25	-30.60	-	-	-
386/51	-	23.2	7.6	1828	-4.90	-28.90	-	-	-
390/51	-	26.7	7.4	1995	-5.10	-29.00	-	-	-
M98	-	22.0	7.6	2380	-5.00	-28.80	-	-	-
Wadi	-	-	-	-	-3.35	-22.10	-	-	-
Campaign of 2004									
386/51	30	17	7.7	2240	-4.00	-	2.5	-	-
363/51	60	20	7.7	2410	-4.50	-	1.2	-	-
157/51	-	24	7.4	1950	-4.50	-	-	-	-
390/51	26.2	28	7.2	1820	-4.10	-	2	-	-
346/51	26	27	7.2	1950	-4.20	-	1.5	-	-
Campaign of 2006									
386/51	-	-	-	-	-4.17	-22.20	2.0	-	-
363/51	-	-	-	-	-4.55	-26.80	2.1	-	-
390/51	-	-	-	-	-4.37	-25.80	2.0	-	-
346/51	-	-	-	-	-4.17	-21.40	3.8	-	-

Sample	Depth/soil	T	pH	EC	$\delta^{18}O$	$\delta^{2}H$	^{3}H	$\delta^{13}C$	^{14}C
	m	°C		µs/cm	‰ vs SMOW		TU	‰	pmc
Campaign of 2007									
380/51	-	26.0	7.6	2530	-5.02	-27.34	0.0	-	-
346/51	-	27.0	6.8	1920	-4.60	-26.33	1.0	-	-
Campaign of 2018									
M98	-	23.2	7.2	2699	-4.50	-28.00	-	-	-
346/51	-	27.1	7.3	1967	-4.40	-28.00	-	-	-
380/51	-	21.5	7.9	2428	-5.00	-28.60	-	-	-
386/51	-	22.3	7.8	2638	-4.90	-27.30	-	-	-

Table 2

Initial activity of carbon-14 (A_0) and radiocarbon age of groundwater of the Cenomanian-Turonian, the Plio-Quaternary and the Turonian aquifers within Essaouira basin

Sample	$\delta^{13}C$	^{14}C	A_0	Age
	‰	pcm		year
Cenomanian-Turonien Aquifer				
1503/52	-10.44	67.43	76.1	1001
648/52	-10.82	60.5	78.9	2193.7
1699/52	-5.12	86	37.3	actual
883/52	-7.41	59.85	54	actual
54/52	-8.45	74.36	61.6	actual
89/52	-9.18	67.65	66.9	actual
677/52	-10.29	60.97	75	1714.5
ES28	-8.87	27.03	64.7	7211.5
ES65	-8.57	48.26	62.5	2135.09
Plio-Quaternary Aquifer				
128/51	-8.4	72.07	61.24	actual
privé	-7.7	42.37	56.13	2326
389/51	-6.3	70.93	45.93	actual
Turonian Aquifer				
65/51	-9.8	88.9	71.45	actual
390/51	-9.4	32.5	68.53	6168
386/51	-10.3	84.8	75.1	actual
M98	-9.3	79.6	67.8	actual

Seawater intrusion into coastal aquifers in semi-arid environments, Case study of the alluvial aquifer of Essaouira basin

1. Introduction

The populations density in coastal zones, almost 70% of the world population lives in coastal zones (Bear et al. 1999). The groundwater overexploitation, the proximity to seawater and climate change cause qualitative and quantitative degradation of groundwater in these areas (Bahir et al. 2016, 2018a; Carreira et al. 2018; Hamed et al. 2018; Ouhamdouch et al. 2018, 2020; Farid et al. 2013). The marine intrusion phenomenon is closely linked to the geographical context (i.e. sea proximity). It remains one of the major problems impacting groundwater in several coastal aquifers around the world (Custodio 1997). It is defined as the temporary or permanent migration of saltwater into the freshwater of the aquifer following a decline in the piezometric level and/or a rise in sea level.

Generally, two main factors can cause a seawater advance in coastal aquifers; a natural factor and an anthropogenic factor. The natural factor corresponds to the rise in sea level since the Holocene (Edmunds and Milne 2001; Vella et al. 2005). The aquifers set up before the sea level rose (quaternary glaciation period) have been invaded by the sea; marine waters have entered aquifers. After the sea level stabilized, aquifers with strong hydraulic gradients were able to push marine waters, on the other hand, aquifers which have a weak hydraulic gradient, could not repel marine intrusion (Edmunds and Milne 2001; Custodio 2002; Post 2004).

The anthropogenic factor is caused by intensive pumping into aquifers. Overexploitation occurs when groundwater withdrawals are greater than recharge, which causes a lowering in the piezometric level and therefore in the hydraulic gradient. According to Custodio (2002), the marine intrusion degree depends on the hydrogeological parameters of the aquifer (such as geometry, permeability, hydraulic gradient...). However, the importance of marine intrusion varies widely from place to place. Good hydrogeological knowledge will enhance the understanding of aquifers

and a rational and good management of the aquifer will allow wise exploitation avoiding or limiting saline intrusion.

In North Africa, this phenomenon has been studied in several aquifers and has reached 60 km inland (Sherif et al. 1999), according to studies based on the piezometric approach, hydraulic, geometric and transport parameters of the aquifer, numerical models, and taking into account climate variability. According to Paniconi et al. (2001), and by examination of the interplay between pumping regimes and recharge scenarios and their effect on the saline water distribution, the coastal aquifer of Korba (Tunisia) has experienced saltwater intrusion since 1970. In Libya, the intrusion increased steadily from 1960 to 2005 (El hassadi 2008) and this extends up to 10 km from the coast of Gefara plain in Tripoli by adopting the hydrogeochemistry approach and applying a two-stage finite element simulation algorithm (Sadeg and Karahanoglu 2001). On the Algerian coast, the work of Morsli et al. (2007) and Belkhiri et al. (2012) highlighted the presence of a marine intrusion in this sector by using multivariable statistical and geochemical modeling techniques.

Moroccan coastal aquifers are also submitted to saltwater intrusion phenomenon. The Saïdia sandy aquifer located in the extreme northeast of the country is experiencing a marine intrusion demonstrated by electrical and logging soundings (El Halimi et al. 1999). In the Temara-Rabat region enclosing an aquifer system that contains marine deposits, a marine intrusion was identified by Pulidoschoch et al. (1999). Further south of the country, the Sahel of Doukkala Abda experienced deterioration in the groundwater quality attributed to marine intrusion (Fadili et al. 2012; Kaid Rassou et al. 2005).

To continue the study of marine intrusion along the Moroccan Atlantic coast, we took the shallow Pli-Quaternary aquifer of Essaouira basin as an example. To achieve the objective of this study, we adopted hydrogeochemical and isotopic approaches.

Geographically, the aquifer studied is located on the Moroccan Atlantic coast between latitude 31° 24’ and 31° 49’ N, longitude 9° 52’ and 9° 85’ W. Its eastern limit is represented by the Triassic outcrops (Tidzi diapir) while its western limit is represented by the Atlantic Ocean (Fig. 1). The study area is characterized by a semi-arid climate with an average annual rainfall of 300 mm and an average annual temperature of 20 °C (Ouhamdouch and Bahir 2017). According to Ouhamdouch et al. 2020, the annual precipitation within the study area presents a decrease of 12 to 16% accompanied by an increase in temperatures with significant warming from 1.2 °C to 2.3 °C. This decline in precipitation and an increase in temperature caused a decline in the piezometric level and deterioration in the groundwater quality of the study area. Geologically, the shallow aquifer is hosted in sandstones and conglomerates, with some sandy marl, limestone, and dolomite (Fig. 1). This aquifer whose thickness

varies between 5 and 60 m, rests on the impermeable gypsiferous and siliceous marls of the Senonian (200 m) (Bahir et al. 2000). According to Mennani (2001) this shallow aquifer presents permeability varying between 0.27 to 132 m/d and transmissivity variying between 4.5 x 10^{-5} to 6.02 x 10^{-2} m^2/s. The highest values are presented near the Ksob wadi (recharge area). The piezometric map shows a flow direction from the South East towards North West with a hydraulic gradient varying between 1.2% (downstream part) and 2.5% (upstream part). The groundwater flow direction is conditioned by the substratum geometry of the aquifer.

Figure 1

Location and geological map of study area

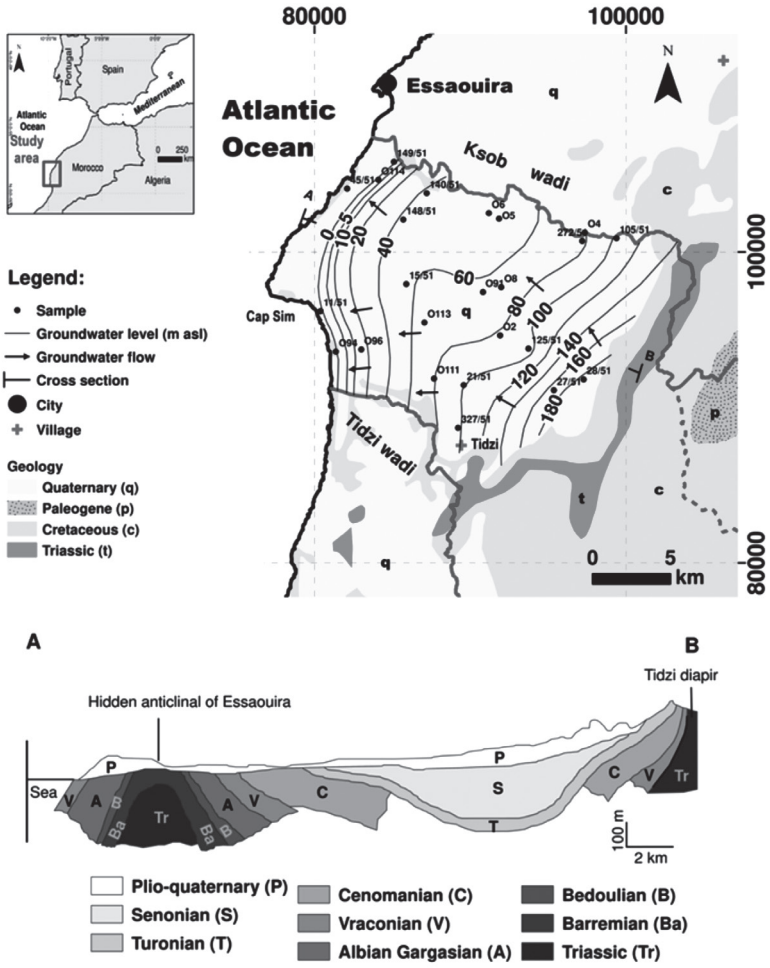

2. Material and methods

A total of 26 samples reprinting the groundwater of the shallow aquifer of Essaouira basin were analysed for chemical and isotopic content. 24 samples are reserved for groundwater, 1 for rainfall, and 1 for seawater. The measurements of electrical conductivity (EC), pH and temperature (T) were performed on-field using HI-9829 Multiparametric Instrument. A 200 m probe was used to measure the depth of the water table. The water samples were taken after pumping for 15-20 min to obtain representative values under ambient aquifer conditions. Samples are collected in clean polyethylene bottle of 500 mL and then stored at a temperature below 6 °C before analysis in the laboratory.

Chemical element analysis was done at Laboratory of Geosciences and Environment-ENS of the Ecole Normale Superieure of Marrakech (Morocco). The contents of Chloride (Cl) and sulfate (SO_4) anions were determined to adopt the Mohr technique and the nephelometric technique, respectively. Ca and Mg concentrations were determined using the EDTA titrimetric method. Na and K were measured by flame spectrometry. HCO_3 and CO_3 contents were analysed by titration using 0.1 M HCl acid. As for Bromide concentration, it was measured using Mettler Toledo SevenCompact meter. The ionic balance for all samples was within ± 10%.

Stable isotope composition of the groundwater samples was determined at the Laboratory of Radio Analyses and Environment in the National School of Engineers of Sfax (Tunisia), using the laser absorption spectrometer LGR DLT 100 (Penna et al. 2010) with a measurement uncertainty of ± 0.1‰ for $\delta^{18}O$ and ± 1‰ for $\delta^{2}H$. The results are reported in delta value expressed in‰ versus SMOW.

The obtained results are grouped in Table 1.

3. Results and discussion

3.1. Chemical Facies

The Piper diagram (Piper 1944) is a diagram for determining the water chemical facies. It corresponds to a rhombic representation based on the percentages of the major elements of water whose concentrations expressed in meq/l. According to Freeze and Cherry (1979), the process consists of raising the percentage of each element to two equilateral triangles, the first for the anions and the second for the cations. The projection of the samples analyzed on the Piper diagram (Fig. 2) shows that the groundwater of the shallow aquifer of the Essaouira basin is of two types; Cl-Ca-Mg (64%) and Cl-Na type (36%). This transition from one facies to other

highlights the complexity of the hydrogeochemical processes contributing to the groundwater mineralization of this aquifer.

3.2. Ionics ratio

To highlight the contribution of marine intrusion in groundwater salinization of the Plio-Quaternary of Essaouira basin, we integrated some ionic relationships, the trace element "bromide" and the stable isotopes of the analysed samples.

Figure 2

Piper Diagram of analysed samples

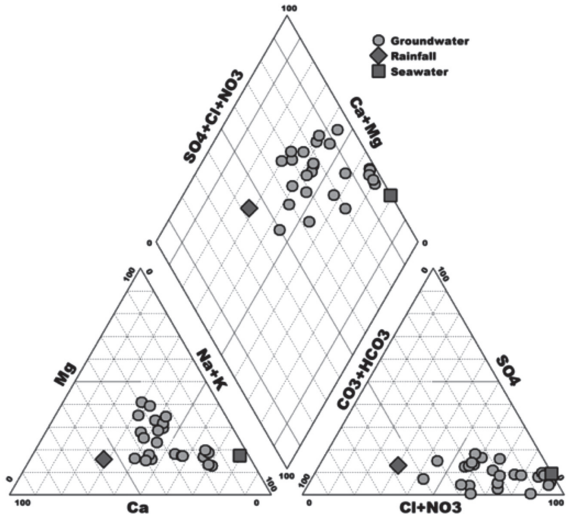

3.2.1. Na/Cl couple

The Na/Cl ratio is an indicator of marine influence. In the case of a marine intrusion or during the early stages of salinization, this ratio is usually lower than the marine values (0.86, molar ratio) (Bouderbala 2015; Jones et al. 1999; Pulido-Lebouef et al. 2003; Telahigue et al. 2018, 2020). The low Na/Cl ratio under seawater intrusion conditions can be distinguished from a Na/Cl ratio greater than 1, which generally characterizes anthropogenic sources such as domestic wastewater (Bear and Cheng 2010).

Table 2 shows that the EC has a significant positive correlation with Cl, Na, Ca, Mg, K, Br, and SO_4 ions reflecting the contribution of these elements in the

groundwater mineralization. With the exception of HCO_3, the Cl are very positively correlated with Na, Ca, Mg, K, Br, and SO_4. This reflects that the groundwater mineralization is controlled by evaporates dissolution, evaporation phenomenon, and seawater contamination. This hypothesis is corroborated by negative values of the saturation indices with respect to halite, anhydrite and gypsum (Table 1) and by the Gibbs diagrams (Gibbs 1970) where the predominant samples fall in the rock-water interaction field and evaporation dominance field (Fig. 3). The positive correlation close to 1 is marked between Na and Cl and between Cl and Br, this suggests that some samples are contaminated by seawater.

Figure 3

Gibbs' diagrams

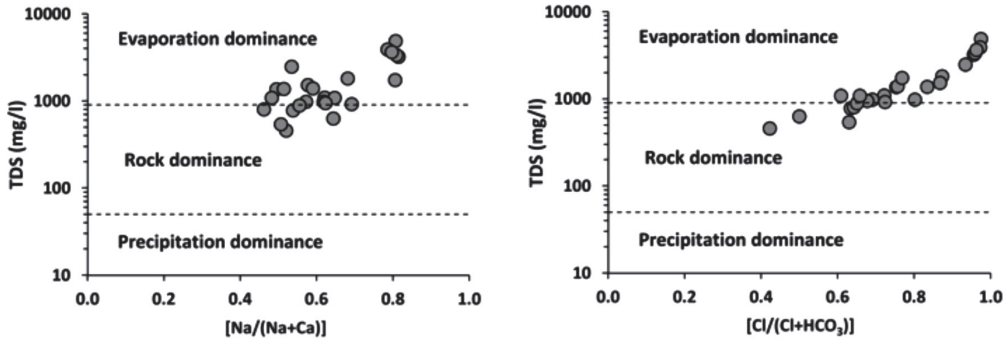

Chloride considered as a conservative element is strongly correlated with sodium for water samples of the shallow aquifer of the Essaouira basin ($r^2 = 0.99$) (Fig. 4, Table 2). Even for samples far from the sea, the Na/Cl molar ratio does not differ significantly from that of seawater (example of well 15/51), and therefore remains insufficient for a real distinction of the origin of the waters nor between the dissolution of the evaporitic formations, which cause high concentrations of Na and Cl. However, for this coastal aquifer, the presence of the sea near permeable sandy formations can defend in favor of a possible advance of the salt bevel in certain places of the aquifer and can explain the origin of the high concentrations of these elements. Also, the increase in Cl contents can be caused by the dissolution of marine aerosols carried by the wind.

Herein, the average Na/Cl molar ratio is 0.7 with a minimum of 0.4 and a maximum of 1.2. This average is close to that of seawater (0.86) (Jones et al. 1999), which suggests that the Plio-Quaternary aquifer is contaminated in certain places by

seawater, especially at the point where the Cl contents exceed 70 meq/l with a molar ratio equal to 0.7, in particular, the samples 11/51, 45/51, 149/51, O94, and O114.

Figure 4

Correlation diagram (a) Na/Cl vs Cl and (b) Na vs Cl of analysed samples

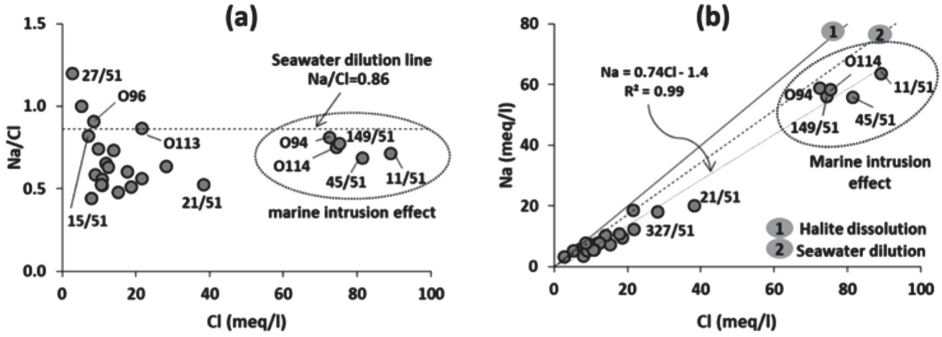

3.2.2. Ca/Mg couple

One of the most visible features of seawater intrusion is the enrichment of Calcium concerning its concentration in seawater. The Mg/Ca ratio can be used as one of the natural tracers of marine intrusion phenomenon into coastal aquifers (Bouderbala 2015; Pulido-Lebouef et al. 2003; Telahigue et al. 2018, 2020). This ratio increases as a function of the proportion of the marine water in the mixture which the salinity is represented by the chloride concentrations (Pulido-Lebouef et al. 2003) because seawater is characterized by a Ca/Mg ratio of 0.2 and freshwater by a ratio greater than 1. However, it should be noted, that this saline water with a high calcium concentration can be caused by a different mechanism, not necessarily related to the cation exchange phenomenon (Jones et al. 1999). The Ca/Mg ratio decreases as a function of the seawater proportion introduced into the mixture.

In this case study, the ratio also decreases depending on the chloride content. by comparing, for example, point 27/51 (the least mineralized sample) and point 11/51 (the most mineralized sample); there is a very clear decrease in the Ca/Mg ratio accompanied by an increase in the Cl contents (Fig. 5a). This could, once again, show a marine origin of the mineralization, in particular at the well 11/51 45/51, 149/51, O94 and O114 whose ratio is close to that of seawater with grades high in Cl. For the samples having the Ca/Mg greater than 1, seawater intrusion cannot be implicated in the mineralization, so another hydrochemical process, probably related to water–rock interaction must be involved such as bases exchange phenomenon, with the release of Ca present in the aquifer matrix and adsorption of Na from the solution (Gimenez et al. 2010).

3.2.3. SO_4/Cl couple

According to Pulido-Lebouef et al. (2003), the SO_4/Cl ratio can be used as natural tracers of marine intrusion phenomenon in coastal aquifers. This ratio decreases when the seawater proportion in the mixture increases (Bouderbala 2015; Pulido-Lebouef et al. 2003; Pulido-Lebouef et al. 2003; Telahigue et al. 2018, 2020;Tellam and Lloyd 1986).

For the shallow aquifer of the Essaouira basin, all the samples have a SO4/Cl ratio of less than 1, suggesting the dominance of chlorides over sulfates (Fig. 5b). The SO_4/Cl ratio for the analysed samples varies from 0.02 to 0.37 and the majority of the samples have SO_4/Cl ratio greater than that of the seawater sample (0.1) (Fig. 4b). This indicates the mixing between seawater and freshwater. The enrichment of these samples with SO4 suggests other sources, such as the gypsum and Anhydrite dissolution (Table 1). The samples 11/51 45/51, 149/51, O94 and O114 show a weak SO_4/Cl ratio accompanied by high Cl contents, indicating that the increase in salinity in these wells is mainly caused by the intrusion of seawater and confirms the results obtained by the Na/Cl and Ca/Mg ratios.

Figure 5

Correlation diagram (a) Ca/Mg vs Cl and (b) SO_4/Cl vs Cl of analysed samples

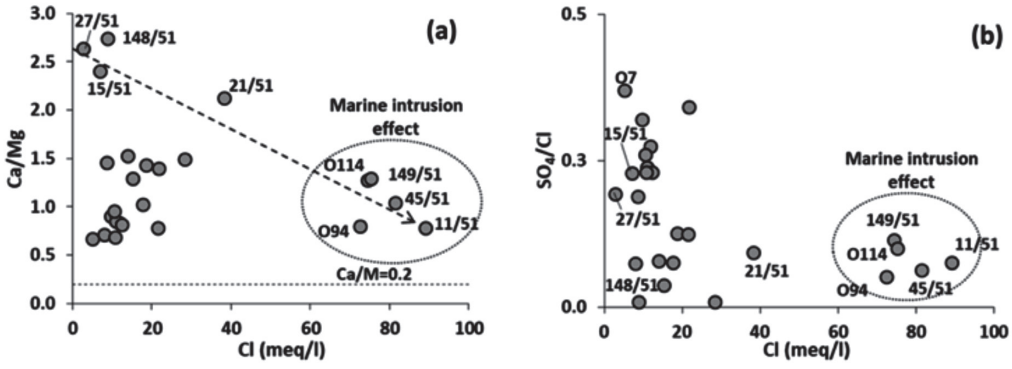

3.2.4. Br/Cl couple

Bromide is considered a reliable indicator of the marine intrusion phenomenon (Kim et al. 2003; De Montety et al. 2008; Telahigue et al. 2018, 2020). Like chloride, bromide is a conservative element and does not react with the aquifer matrix except in the case where there is a significant presence of organic matter (Davis et al. 1998). Indeed, these two conservative elements make it possible to obtain ideas on the

origin of the solutions and/or the identification of possible contributions of marine water, because their concentrations are neither influenced by the redox processes nor controlled by the low solubility minerals (Fedrigoni et al. 2001). Following an extremely long residence time of bromides and chlorides in oceanic masses, the Br/Cl ratio of current seawater is relatively constant (between 1.5 and 1.7x10-3) (Kim et al. 2003; De Montety et al. 2008). This relationship also remains constant if these two elements have a common origin. However, seawater is distinguished from relics of evaporated seawater or hypersaline waters (Starinsky et al. 1983), products of evaporite formations dissolution and anthropogenic sources, such as wastewater effluents (Vengosh et al. 1998) or the return of irrigation water.

During the evaporation of seawater, the Br/Cl ratio remains fixed until the start of the halite precipitation.

When the halite precipitates, the solution becomes richer in bromide, which leads to an increase in the Br/Cl ratio (Ben Hamouda et al. 2011). However, the Br/Cl ratio of residual brine continues to increase as the amount of precipitated halite increases. This means that a solution resulting from a simple concentration of seawater before halite saturation will have a Br/Cl ratio equal to that of seawater. On the other hand, more concentrated brine having passed the halite precipitation phase will have a higher Br/Cl ratio than that of seawater. So, freshwater dissolving halite until saturation will display a Br/Cl ratio lower than that of seawater knowing that primary halite is the only chlorinated salt to have a Br/Cl ratio lower than that of seawater. While a mixture of freshwater and brine that has passed the halite precipitation phase will have a higher Br/Cl ratio than that of the marine ratio.

The Br vs Cl correlation diagram (Fig. 6a) shows a strong positive correlation ($r^2 = 0.99$) between these two ions. This suggests that bromides and chlorides have the same origin. On the Br/Cl diagram as a function of Cl (Fig. 6b) the samples 11/51, 45/51, 149/51, O94, and O114 is in the field of dilution of seawater with a Br/Cl ratio of between 1.5 and 1.7, reflecting a marine origin of salinity. The increase in bromide contents in some wells with a Br/Cl molar ratio greater than that of seawater can be explained by the fact that these wells were abandoned more than a decade ago and that they are very far from the recharge zone and this favors the formation of brines that have passed the halite precipitation phase. The rest of the points have lower molar ratios than that of seawater, indicating that these points are outside the phenomenon of marine intrusion and therefore the existence of another source of salinization (such as salts dissolution).

Figure 6

Correlation diagram (a) Br vs Cl and (b) Br/Cl vs Cl of analysed samples

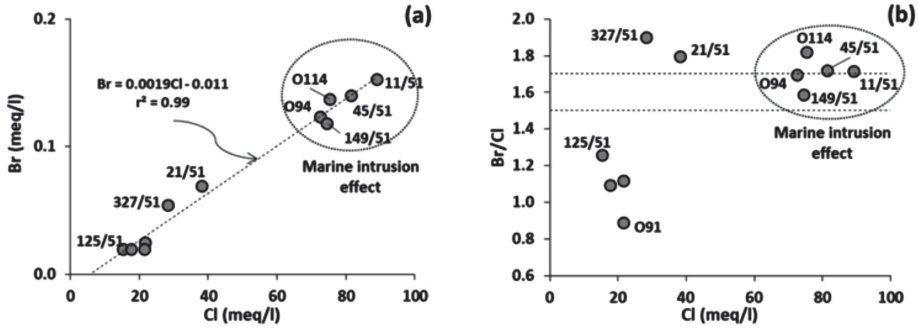

3.2.5. $\delta^{18}O$, $\delta^{2}H$ and $\delta^{18}O$, Cl couple

The isotopic tool is a complement to determine the groundwater origin, the area, and the recharge mode of aquifers. Also, it highlights the processes that can affect a water molecule (Geyh 2000). For the study area, the oxygen-18 contents vary between -1.83 and -5.02‰ vs SMOW with an average of -3.66‰ vs SMOW, while the deuterium contents oscillate between -8.92 and 29.71‰ vs SMOW with an average of -20.60‰ vs SMOW (Fig. 7, Table 1).

Figure 7

Correlation diagram $\delta^{2}H$ vs $\delta^{18}O$ of analysed samples

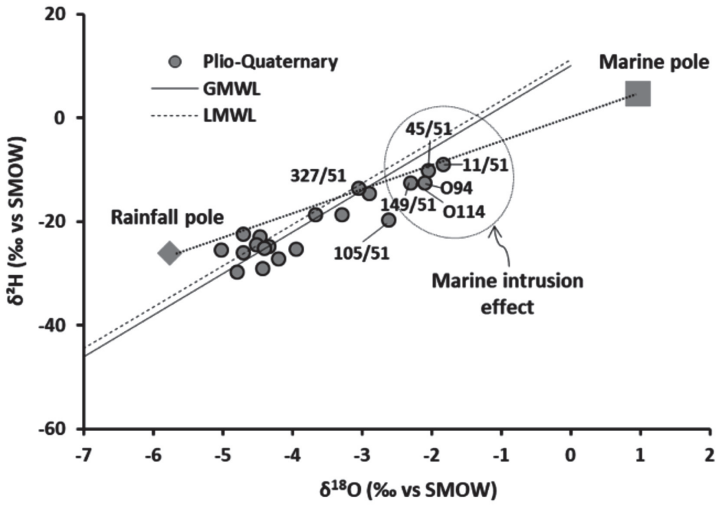

The frequency histograms of the Figure 8a show that 45% of the analyzed samples are characterized by oxygen-18 contents between -5 and -4‰ vs SMOW, 25% have contents between -3 and -2‰ vs SMOW, 20% have contents vary between -4 and -3‰ vs SMOW, while the ranges of values between -6 and -5‰ vs SMOW and between -2 and -1‰ vs SMOW are represented by 5% each one of the total samples. As for deuterium, the frequency histograms (Fig. 8b) show that 35% of the analyzed samples have contents vary between -25 et -30‰ vs SMOW, 25% have the values vary between -15 and -10‰ vs SMOW, 20% have the contents oscillate between -25 and -20‰ vs SMO. The range of contents between -20 et -15‰ vs SMOW is represented by 15% of the samples analyzed, while the range of values between -10 and -5‰ vs SMOW is represented by 5% of the total of the analyzed samples. From these frequencies, we see that the study area contains two types of water; waters depleted in stable isotopes and waters rich in these elements. This reflects that the groundwater has probably been subjected to phenomena leading to enrichment in stable isotopes such as evaporation and/or marine intrusion.

Figure 8

Frequency distribution of oxygen-18 and deuterium contents in the waters of analysed samples

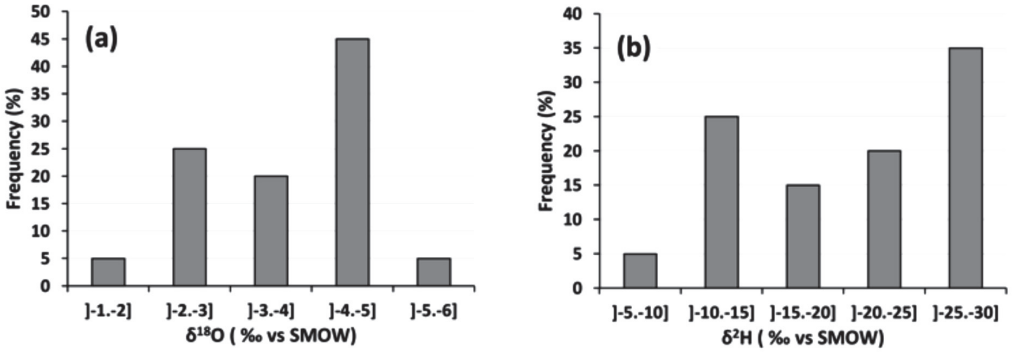

The distribution of representative samples of the Plio-Quaternary and Turonian aquifers (campaign of 2018) on the correlation diagram δ^2H vs $\delta^{18}O$ (Fig. 7), makes it possible to define the main phenomena involved in the hydrodynamic and geochemical functioning of aquifers. This diagram shows that the majority of the points are scattered around the GMWL (Craig 1961) and LMWL (Mennani et al. 2001), which means that the current recharge of the Plio-Quaternary aquifer is ensured by direct infiltration of rainfall of oceanic origin, in particular for the points located near the Ksob wadi.

The majority of the points are scattered around the GMWL and LMWL lines reflecting a recharge by infiltration of rainwater of Atlantic origin. This recharge results in the decrease in the salinity in these wells (in particular well 27/51 which has a low electrical conductivity. This well is the closest to the freshwater pole (rainwater).

Other water points are distinguished by their position below the GMWL, they line up along a line with a slope less than 8 characteristics of the evaporation phenomenon. This last process mainly concerns the wells O6, 105/51, 125/51, 272/51, and 327/51 located respectively in the northeast and south part of the aquifer. Evaporation can probably take place before water infiltration, in the unsaturated zone or during sampling. The Freshwater-Seawater line is drawn up taking the isotopic signature of rainwater and that of seawater from the Atlantic Ocean (Carreira et al. 2014).

Some other points are located below the LMWL with more enriched isotopic compositions, notably 11/51, 45/51, 149/51, O94, and O114 reflecting the intervention of another phenomenon in the groundwater mineralization, such as evaporation and marine effect. These samples are located between the "rainfall" and "marine" poles; this suggests the advancement of seawater in the aquifer studied at these places.

The combined use of the chloride and oxygen-18 content makes it possible to support the results obtained previously. Indeed, the Cl versus $\delta^{18}O$ diagram (Fig. 9) shows that the groundwater in the study area is dominated by the processes of evaporitic formations dissolution and by the marine intrusion by location.

Figure 9

Correlation diagram Cl vs δ18O of analysed samples

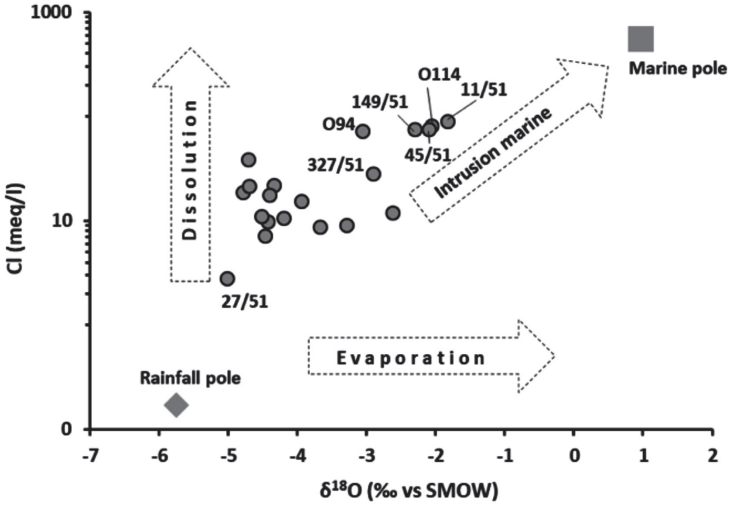

3.3. Estimate of mixture with seawater

The highest Cl contents are observed at sample 11/51 (89.1 meq/l) at Cap Sim and at point 45/51 (81.5 meq/l) towards the North. Other Cl contents vary between 70 and 80 meq/l characterize the samples O114 (75.3 meq/l), 149/51 (74.4 meq/l), O94 (72.5 meq/l). The rest of the samples have Cl concentrations varying between 2.8 and 38.3 meq/l. Considering the average content of this element for the Plio-Quaternary aquifer (average of samples with EC <1000 μs/cm) and the seawater content, respectively 2.8 and 545.9 meq/l, a mass balance of chlorides allows the calculation of the mixing rate (F) with seawater, for each sample affected by the intrusion.

This mixing rate can be estimated based on the equation (1) (Abou Zakhem and Hafez 2007):

$$F(\%) = \frac{[Cl_{sample}]-[Cl_{freash}]}{[Cl_{sea}]-[Cl_{freash}]} \times 100 \quad (1)$$

With:

F corresponds to the seawater fraction.

Cl_{sample} corresponds to the concentration of chlorides in the water sampled.

Cl_{freash} corresponds to the concentration of chlorides in fresh groundwater. For our case, the average chloride concentrations of wells with electrical conductivity values less than 1000 μs/cm were used as Cl concentrations. Cl_{sea} corresponds to the concentration of chlorides in seawater.

The mixing rates calculated vary from 0 to 15.9% (Fig. 10). The highest values are estimated for the samples 11/51 (15.9 %), 45/51 (14.5%), 149/51 (13.2%), O114 (13.3%) and O94 (12.8%). while the rest of the samples present mixing rates vary between 0 and 6.5%. The high values are scattered along the coast (Fig. 10) reflecting an advancement of the seawater frond in the aquifer. The average width of this advancement is of the order of 2 km. This contamination is probably due to the decline in the piezometric level following the decrease in precipitation over the past decades in the study area (Ouhamdouch et al. 2018) and the rise in sea level caused by global warming (GIEC 2013).

Figure 10

Seawater fraction of analysed samples

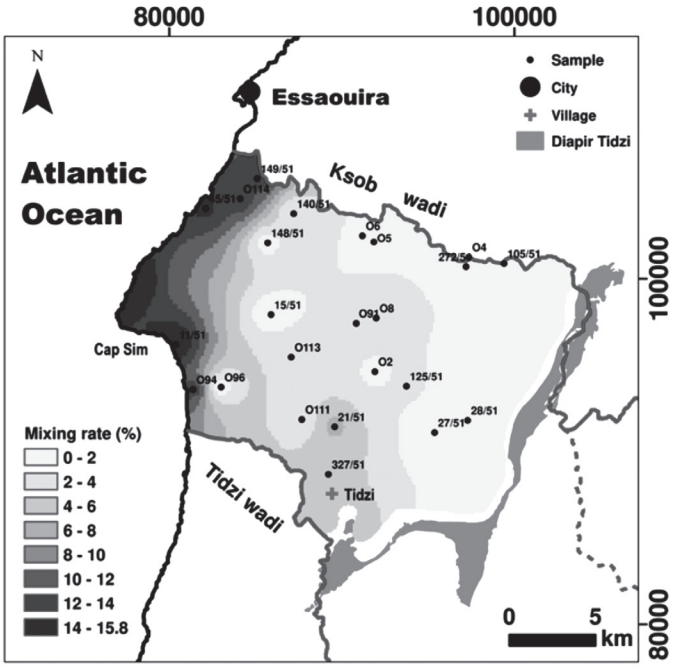

4. Conclusion

The crossing of the different results obtained by the hydrogeochemical and isotopic approaches such as the couples (Na, Cl), (Ca, Mg), (Br, Cl), (δ^2H, $\delta^{18}O$), ($\delta^{18}O$, Cl) provide clearer information on the origin of the groundwater salinization in the study area.

The ionic ratios Br/Cl ≈ 1.5 to 1.7‰, Na/Cl close to 0.86, Mg/Ca and SO_4/Cl weak showed that the seawater begins to invade the freshwater of the Plio-quaternary aquifer of Essaouira basin. This intrusion demonstrated by ionic ratios and corroborated by stable isotopes and the combined use of oxygen-18 contents and chlorides has a mixing rate of 15.9% at the well 11/51, 14.5% at the sample 45/51, 13.2% at the well 149/51, 13.3% at point O114 and 12.8% at the well O94. These high rates are dispersed along the coast with the advancement of the saline frond on the order of 2 km. However, this intrusion is probably caused by the decline in the piezometric level following the decrease in precipitation over the last decades in the study area and by the rise in sea level due to the climate change.

Table 1

Physicochemical and isotopic results of analysed samples

Sample	pH	T	EC	Ca	Mg	Na	K	HCO_3	Cl	SO_4	NO_3	Br	$\delta^{18}O$	$\delta^{2}H$	SIG	SIA	SIH	SIC	SID	IB
		°C	mS/cm	meq/l									‰							%
11/51	8.4	17.6	9.74	15.2	19.6	63.7	1.7	2.3	89.1	6.7	2.1	0.2	-1.8	-8.9	-1.1	-1.3	-4.0	1.0	2.2	0
15/51	7.8	19.8	1.55	5.0	2.1	5.8	0.3	4.1	7.1	1.6	0.1	-	-4.5	-23.0	-1.7	-1.9	-6.0	0.5	0.8	1
21/51	7.4	23.3	4.93	17.4	8.2	20.1	0.6	2.7	38.3	3.6	0.2	0.1	-4.7	-26.1	-1.1	-1.4	-4.9	0.4	0.6	2
27/51	7.8	22.2	0.92	3.1	1.2	3.3	0.1	3.8	2.8	0.5	0.5	-	-5.0	-25.5	-2.3	-2.5	-6.7	0.4	0.6	0
28/51	7.6	23.3	1.08	3.4	4.9	3.5	0.0	4.7	8.0	0.6	0.5	-	-	-	-2.3	-2.5	-6.2	0.3	0.9	-7
45/51	8.1	21.5	7.74	15.2	14.6	55.8	1.3	2.3	81.5	5.2	1.9	0.1	-2.1	-10.2	-1.5	-1.7	-2.7	0.3	0.7	-2
105/51	7.5	22.7	2.19	4.8	5.7	7.8	0.1	4.6	12.0	3.3	0.0	-	-2.6	-19.6	-2.1	-2.3	-5.7	1.0	2.1	-4
125/51	8.0	26.3	2.72	7.5	5.8	7.3	0.3	5.0	15.3	0.6	0.0	0.0	-3.9	-25.2	-1.9	-2.1	-5.5	0.8	1.5	0
140/51	7.7	20.3	2.16	5.6	3.7	10.3	0.6	9.0	14.0	1.1	0.2	-	-	-	-3.0	-3.2	-6.0	0.4	0.5	-9
148/51	7.5	21.2	1.60	6.1	2.2	5.2	0.2	5.0	9.0	0.1	0.0	-	-3.3	-18.7	-1.5	-1.7	-5.8	0.2	0.6	-1
149/51	8.1	21.3	6.72	13.2	10.4	56.1	1.1	3.1	74.4	8.5	0.6	0.1	-2.3	-12.5	-2.5	-2.7	-5.0	0.7	1.2	-4
272/51	7.5	22.0	1.96	4.5	5.0	7.3	0.1	4.4	9.9	3.2	0.1	-	-4.4	-29.1	-1.6	-1.8	-5.9	0.4	1.1	-2
327/51	7.7	21.9	3.61	8.4	5.7	18.0	0.7	4.1	28.3	0.2	0.1	0.1	-2.9	-14.6	-1.6	-1.8	-5.7	0.3	0.8	0
O2	7.9	25.2	1.96	4.6	5.4	6.1	0.3	2.7	11.0	2.6	0.0	-	-4.5	-24.5	-1.6	-1.9	-5.9	0.4	1.0	0
O4	7.5	21.3	1.90	4.7	5.8	7.8	0.1	5.9	12.4	2.8	0.1	-	-	-	-1.5	-1.7	-5.9	0.2	0.5	-7
O5	7.5	22.1	1.77	4.5	6.6	5.6	0.0	5.8	10.8	2.5	0.3	-	-	-	-1.9	-2.1	-6.2	0.4	1.1	-7
O6	7.3	21.7	2.18	6.0	6.3	5.6	0.1	5.5	10.6	2.8	0.6	-	-4.2	-27.2	-1.4	-1.7	-5.5	0.8	1.6	-4
O7	7.8	22.1	1.26	2.9	4.3	5.2	0.1	5.2	5.2	1.9	0.4	-	-	-	-1.0	-1.2	-5.3	0.5	0.9	-1
O8	7.9	20.5	2.73	9.0	6.3	9.6	0.1	3.7	18.7	2.4	1.1	-	-4.8	-29.7	-1.4	-1.6	-4.2	0.2	0.7	-2
O91	7.6	23.2	3.03	8.9	6.4	12.2	0.1	3.3	21.7	7.4	0.0	0.0	-4.3	-24.8	-1.8	-2.1	-5.8	0.6	1.1	-8
O94	7.4	20.7	6.41	13.4	16.9	58.8	1.5	3.3	72.5	3.7	6.4	0.1	-3.1	-13.5	-1.8	-2.0	-5.4	0.3	0.6	3
O96	8.1	20.7	1.84	3.5	2.4	7.9	0.2	3.3	8.7	1.6	1.5	-	-3.7	-18.7	-1.7	-1.9	-5.1	0.3	0.8	-4
O111	7.2	23.6	2.79	7.4	7.2	10.7	0.2	5.7	17.7	1.3	0.3	0.0	-4.4	-25.1	-1.0	-1.2	-4.2	0.9	1.8	1
O113	7.4	23.1	3.48	4.5	5.8	18.7	0.2	6.5	21.6	2.7	1.1	0.0	-4.7	-22.5	-1.2	-1.4	-4.1	0.8	1.8	-4
O114	8.0	20.5	7.25	14.8	11.5	58.3	1.0	2.9	75.3	7.5	0.9	0.1	-2.1	-12.5	-1.0	-1.2	-4.1	0.8	1.6	-1
Rainfall	6.0	23.8	0.05	0.4	0.1	0.2	0.0	0.4	0.2	0.1	0.0	-	-5.8	-26.2	-	-	-	-	-	-1
Seawater	-	-	-	20.6	105.6	469.1	10.2	1.8	545.9	56.5	-	-	1.0	4.5	-	-	-	-	-	0

SI= Saturation Index. SIG=SIGypsum, SIA=SIAnhydrite, SIH=SIHalite, SIC=SICalcite, SID=SIDolomite.

Table 2

Correlation matrix for the analyzed parameters

	EC	Ca	Mg	Na	K	HCO_3	Cl	SO_4	NO_3	Br
EC	1									
Ca	0.90	1								
Mg	0.92	0.80	1							
Na	0.96	0.83	0.90	1						
K	0.92	0.81	0.87	0.94	1					
HCO_3	-0.54	-0.58	-0.48	-0.52	-0.45	1				
Cl	0.98	0.88	0.92	0.99	0.94	-0.55	1			
SO_4	0.74	0.66	0.66	0.73	0.56	-0.51	0.74	1		
NO_3	0.52	0.42	0.67	0.63	0.64	-0.29	0.58	0.23	1	
Br	0.97	0.82	0.88	0.97	0.95	-0.80	0.99	0.61	0.51	1

Conclusions and perspectives

The combination of climatic, hydrological, hydrogeological, hydrochemical, and isotopic tools to study the groundwater resource in the Essaouira basin has enabled a better understanding of the behavior of the water resource of the Essaouira basin facing climate change.

The analysis of annual precipitation, using Nicholson rainfall index graphical method and statistical tests, shows a decrease in precipitation of 12 to 16%. This decrease is accompanied by an increase in temperatures and evapotranspiration with very significant warming of 1.2 °C in the downstream part and 2.3 ° C in the upstream part of the basin.

The study of the flow evolution shows also trends similar to those of precipitation and this deficit becomes larger after the famous wet year of 1995/96. The projection of the climate and hydrometry within the Essaouira basin by the middle of the 21st century shows an upward trend in temperatures under the two scenarios RCP4.5 and 8.5 with a warming of 0,5 °C. As for precipitation, it shows a downward and upward trend under the RCPs4.5 and 8.5 scenarios with a deficit of 17.3 and an excess of 21%, respectively. Future flows also show a trend similar to that of precipitation. However, climate change in the study area has a negative impact on the precipitation cycle, including on the entire water resource.

The piezometric study showed that the Cenomano-Turonian, Plio-Quaternary, Barremian-Aptian and Hauterivian aquifers kept the direction of flow of their groundwater, and this during the study period. Monitoring of piezometry, over 24 years (1995-2019) for the Cenomano-Turonian aquifer, 29 years (1990-2019) for the Plio-Quaternary aquifer, and 43 years (1976-2019) for the Barremian-Aptien and Hauterivian aquifers shows a continuous drop in the piezometric altitude which exceeds 12 m for the Cenomano-Turonian aquifer, 17 m in certain areas for the Plio-Quaternary aquifer, around 8 m for the aquifer Barremian-Aptian, and 5 m for the Hauterivian.

The general decline in the piezometric altitude could be explained by the decrease in precipitation due to the effect of climate change. This drawdown would undoubtedly lead to the groundwater qualitative degradation.

The hydrogeochemical study showed that the groundwater of the Cenomanian-Turonian aquifer presents the Cl-Ca-Mg, Cl-Ca, Cl-Na, and HCO_3-Ca mix facies with the dominance of the Cl-Ca-Mg mix facies, and Cl-Ca. The study of the temporal evolution of these facies shows that there has been no remarkable change. The groundwater of the Plio-Quaternary and Turonian aquifers are of mixed type between Cl-Na and Cl-Ca-Mg. The chemical facies experienced a slight evolution from the Cl-Na facies to the Cl-Na and Cl-Ca-Mg facies for the Plio-Quaternary aquifer and from the Cl-Na facies to the Cl-Ca-Mg facies for the Turonian aquifer. As for the Barremian-Aptian and Hauterivian aquifers, they generally have three types of chemical facies: Cl-Na, Cl-Ca-Mg, and HCO_3-Ca-Mg, with the dominance of the Cl-Ca-Mg facies. For the study period, a remarkable evolution of the facies was observed; from the Cl-Na facies to the Cl-Ca-Mg facies.

The correlations established between the concentrations of major elements have shown that the mineralization of groundwater is controlled by the phenomenon of the dissolution of the evaporitic minerals (halite, gypsum and/or anhydrites) and carbonates (dolomite), by the reverse ion exchange phenomenon and by the marine intrusion, especially at the Plio-Quaternary aquifer. The study of the spatio-temporal evolution of the groundwater quality in the study area shows a gradual deterioration in time and space.

Stable isotopes approach highlights that the recharge of Cenomanian-Turonian aquifer is ensured by precipitation of Atlantic origin without significant evaporation. For the Plio-Quaternary and Turonian, the recharge is also ensured by precipitation of Atlantic origin without significant evaporation and that these waters have been subjected to contamination by seawater. This approach has shown that the recharge areas of the Cenomanian-Turonian aquifer are represented by the Et Tleta Hanchane region (altitude ≈ 300 m), the Krimat region (altitude ≈ 500 to 620 m) and the far East of the study area. Tritium tracing based on the same wells sampled in 2007 and 2016 shows a significant decrease that reaches 2 TU in some wells. This trend could be explained by the low recharge rate following the decrease in precipitation experienced by the study area in recent years. The presence of old or fossil water in the study area suggests a low rate of renewal of the groundwater in this basin. This must be taken into account in the context of the exploitation and management of these waters. The temporal evolution of the $\delta^{18}O$ contents generally shows an enrichment character, of the order of 1 to 1.5‰. This may be due probably to the phenomenon of evaporation generated by the increase in air temperature caused by climate change. The latter also seems to affect the isotopic signature of groundwater in the Essaouira basin.

The crossing of the different results obtained by the hydrogeochemical and isotopic approach such as the couples (Na, Cl), (Ca, Mg), (Br, Cl), (δ^2H, $\delta^{18}O$), ($\delta^{18}O$, Cl)

provide clearer information on the origin of the groundwater salinization in the study area.

The ionic ratios Br/Cl ≈ 1.5 to 1.7‰, Na/Cl close to 0.86, Mg/Ca and SO_4/Cl weak showed that the seawater begins to invade the freshwater of the Plio-quaternary aquifer of Essaouira basin. This intrusion demonstrated by ionic ratios and corroborated by stable isotopes and the combined use of oxygen-18 contents and chlorides has a mixing rate vary between 12.8 an seawater d 15.9%. These high rates are dispersed along the coast with the advancement of the saline frond on the order of 2 km. However, this intrusion is probably caused by the decline in the piezometric level following the decrease in precipitation over the last decades in the study area and by the rise in sea level due to the climate change phenomenon.

However, the country's future should rest on rational planning and integrated management based on water savings and quality protections to make the most of available water resources. For sustainable development and to mitigate the climate change impact, we recommend a strategy based on the following elements:

- recourse to unconventional water.
- maintenance of the existing hydraulic infrastructures and construction of new ones.
- economy of water in all sectors that consume large quantities (i.e agriculture).
- leak detection programs.
- Artificial recharge programs.
- sensitization programs for the value of water.

The Essaouira region, on the Atlantic coast of Morocco, illustrates the multiple problems encountered in semi-arid zones. Beyond its regional interest in water control, the approach adopted can be easily transposed and adapted to other regions suffering from the same climatic and anthropogenic constraints:

- Construction of hill dams to reduce erosion of the wadis bed, to fight siltation by increasing the lifespan and the mobilization of the resource by the dams.
- Ensure an artificial recharge in deficit, vulnerable areas, especially those subject to marine intrusion.
- The mixture of desalinated seawater, with the available resource, to improve its quality.
- Reuse of purified wastewater for watering golf courses, green spaces, and for agriculture when conditions allow.
- Substitution of withdrawals from overexploited aquifers by withdrawals from surface waters.

References

Abou Zakhem B, Hafez R (2007) Environmental isotope study of seawater intrusion in the coastal aquifer (Syria). Environ Geol, 51:1329-1339.

Abutaleb KAA, Mohammed AHE, Ahmed MHM (2018) Climate change impacts, vulnerabilities and adaption measures for Egypt's Nile Delta. Earth Syst Environ 2:183-192.

Agoumi A, (1999) Introduction à la problématique des changement climatiques. Projet Magrébin sur les changements climatiques RAB/94/G31: SOMIGRAF mai 1999; 43 p.

Agoumi A, Senoussi S, Yacoubi M, Fakhredine A, Sayouti EH, Mokssit A, Chikri N (1999) Changements climatiques et ressources en eau. Hydrogeol appl 12:163-182.

Ait Brahim Y, El Mehdi Saidi M, Kouraiss K, Sifeddine A, Bouchaoua L (2017) Analysis of observed climate trends and high resolution scenarios for the 21st century in Morocco. JMES 8:1375-1384

Al-Maktoumi A, Zekri S, El-Rawy M, Abdalla O, Al-Wardy M, Al-Rawas R, Charabi Y (2018) Assessment of the impact of climate change on coastal aquifers in Oman. Arab J Geosci 11: 501. DOI:10.1007/s12517-018-3858-y.

Amghar M (1989) Apports des méthodes d'analyses de la tectonique cassante à la connaissance de l'histoire alpine du Haute Atlas Occidental. L'exemple du versant nord du bloc ancien et de l'Atlas d'Agadir (Haut Atlas, Maroc). Thèse 3ème cycle, Université Cadi Ayyad, Maroc.

Alpert P, Krichak SO, Shafir H, Haim D, Osetinsky I (2008) Climatic trends to extremes employing regional modeling and statistical interpretation over the E. Mediterranean. Glob Planet Change 63:163-170.

Assani AA (1999) Analyse de la variabilité temporelle des précipitations (1916-1996) à Lubumbashi (Congo-Kinshasa) en relation avec certains indicateurs de la circulation atmosphérique (oscillation australe) et océanique (El Niño/La Niña). Sécheresse 10(4):245-252.

Babqiqi A (2014) Changements Climatiques au Maroc: Etude du cas de la Région de Marrakech Tensift Al Haouz et implications sur l'agriculture à l'horizon 2030. Thèse de doctorat, Université cadi Ayyad.

Bahir M, Mennani A, Jalal M, Youbi N (2000) Contribution à l'étude des ressources hydriques du bassin synclinal d'Essaouira (Maroc). Estud Geol 56:185-195.

Bahir M, Jalal M, Blavoux (2001) Apport de l'hydrochimie isotopique à la connaissance des zones de recharge en zones aride et semi-arides : Cas du bassin de Meskala-Kourimat, Journal of Environmental Hydrology.

Bahir M, Mennani A (2002) Problematique de la gestion des eaux souterraines au Maroc. Estudios Geol 58:103-108.

Bahir M, Mennani A, Jalal M, Fakir Y (2002) Impact de la sécheresse sur les potentialités hydriques de la nappe alimentant en eau potable la ville d'Essaouira (Mogador, Maroc). Sécheresse 13:13-9.

Bahir M, Silva MO, Carreira P (2007) Ressources en eau en zones semi-aride, état des lieux: cas du bassin d'Essaouira (Maroc atlantique). In Pulido Bosch, A., López Geta J.A., Ramos González G., (Eds.), Los acuíferos costeros: retos y soluciones. Coastal aquifers: challenges and solutions. Instituto Geológico y Minero de España, Madrid. 529-540 pp.

Bahir M, Ouhamdouch S, Carreira PM (2016) La ressource en eau au Maroc face aux changements climatiques; cas de la nappe Plio-Quaternaire du bassin synclinale d'Essaouira. Comun Geol (2016) 103(1):35-44.

Bahir M, Ouhamdouch S, Carreira PM (2018a) Geochemical and isotopic approach to decrypt the groundwater salinization origin of coastal aquifers from semi-arid areas (Essaouira basin, Western Morocco). Environ. Earth. Sci. 77:485. https://doi.org/10.1007/s12665-018-7663-4.

Bahir M, Ouhamdouch S, Carreira PM (2018b) Isotopic and geochemical methods for studying water–rock interaction and recharge mode: application to the Cenomanian-Turonian and Plio-Quaternary aquifers of Essaouira Basin, Morocco. Mar. Freshwater Res. 69:1290-1300.

Bahir M, Ouazar D, Ouhamdouch S (2018c) Characterization of mechanisms and processes controlling groundwater salinization in coastal semi-arid area using hydrochemical and isotopic investigations (Essaouira basin, Morocco). Environ Sci Pollut Res 25:24992-25004.

Bahir M, Ouazar D, Ouhamdouch S (2019) Hydrogeochemical investigation and groundwater quality in Essaouira region, Morocco. Mar Freshwater Res 70:1317-1332.

Bahir M, Ouhamdouch S, Ouazar D, El Moçayd N (2020a) Climate change effect on groundwater characteristics within semi-arid zones from western Morocco. Groundw Sustain Dev 11:1-14. https://doi.org/10.1016/j.gsd.2020.100380.

Bahir M, Ouhamdouch S (2020b) Groundwater quality in semi-arid environments (Essaouira Basin, Morocco) Carbonates Evaporites 35:1-16. https://doi.org/10.1007/s13146-020-00576-7

Bagnouls F, Gaussen H (1953) Saison sèche et indice xérothermique. Bull Soc Hist Nat Toulouse. 88(3-4):193-239.

Bear JJ, Cheng HDA (2010) Modeling Groundwater Flow and Contaminant Transport. In Hassanizadeh SM (Ed), Theory and Applications of Transport in Porous Media, Springer Nature Switzerland pp 593-636.

Bear J, Cheng AHD, Sorek S, Ouazar D, Herrera I (1999) Seawater Intrusion in Coastal Aquifers-Concepts, Methods, and Practices. In Bear J, Cheng AHD, Sorek S, Ouazar D, Herrera I (Eds), Theory and Applications of Transport in Porous Media. Kluwer Academic Publishers, Dordrecht/ Boston/London, pp 51-71.

Belarbi H, Touaibia B, Boumechra N, Amiar S, Baghli N (2015) Sécheresse et modification de la relation pluiedébit: Cas du bassin versant de l'Oued Sebdou (Algérie Occidentale). Hydrolog Sci J 62:124-136.

Belkhiri L, Mouni L, Boudoukha A (2012) Geochemical evolution of groundwater in an alluvial aquifer: Case of El Eulma aquifer, East Algeria. J Afr Earth Sci 66:46-55.

Ben Hamouda MF, Tarhouni J, Leduc C, Zouari K (2010) Understanding the origin of salinization of the Plio-quaternary eastern coastal aquifer of Cap Bon (Tunisia) using geochemical and isotope investigations. Environ Earth Sci 63:889-901Berhail S (2019) The impact of climate change on groundwater resources in northwestern Algeria. Arab J Geosci 12:770. DOI:10.1007/s12517-019-4776-3.

Bouanani R, Baba-HamedK, Bouanani A (2013) Utilisation d'un modèle global pour la modélisation pluie-débit: cas du bassin d'Oued Sikkak (NW algérien). Nature & Technologie 9:61-66.

Bouderbala A (2015) Groundwater salinization in semi-arid zones: an example from Nador plain (Tipaza, Algeria). Environ Earth Sci 73:5479-5496.

Boughariou E, Bouri S, Khanfir H, Zarhloule Y (2014) Impacts of climate change on water resources in arid and semi-arid regions: Chaffar Sector, Eastern Tunisia. Desalin. Water Treat 52:2082-2093.

Capaccioni B, Didero M, Paletta C, Didero L (2005) Saline intrusion and refreshening in a multilayer coastal aquifer in the Catania Plain (Sicily, Southern Italy): dynamics of degradation processes according to hydrochemical characteristics of groundwaters. J Hydrol 307:1-16.

Carreira PM, Marques JM, Nunes D (2014) Source of groundwater salinity in coastline aquifers based on environmental isotopes (Portugal): Natural vs. human interference. A review and reinterpretation. Appl Geochem 41:163-175.

Carreira PM, Bahir M, Ouhamdouch S, Fernandes PG, Nunes D (2018) Tracing salinization processes in coastal aquifers using an isotopic and geochemical approach: comparative studies in western Morocco and southwest Portugal. Hydrogeol J 26:2595-2615.

Castany G, (1982) Principes et méthodes de l'hydrogéologie. Edition Dunod, Paris 236p

Chen H, Xu CY, Guo S (2012) Comparison and evaluation of multiple GCMs, statistical downscaling and hydrological models in the study of climate change impacts on runoff. J Hydrol 434-435:36-45.

Chenaker H, Houha B, Valles V (2017) Isotope studies and chemical investigations of hot springs from North-Eastern Algeria. J Mater Environ Sci 8:4253-4263.

Clark ID, Fritz P (1997) Environmental isotopes in Hydrogeology, Editions Lewis publisher, 290 p.

Craig, H., 1961. Isotopic variations in meteoric waters. Science, 133,1702-1703.

Custodio E (1997) Seawater Intrusion in Coastal Aquifers. Guidelines for Study, Monitoring andControl, Water report N°11. Food and Agriculture Organization of the United Nation, Rome, Italie, 152 pp.

Custodio E (2002) Coastal aquifers as important natural hydrogeological structures. In Bocanegra M, Massone H (Eds), Groundwater and human development, pp 1905-1918.

Daget P (1977) Le bioclimat méditerranéen: Caractères généraux, modes de caractérisation. Vegetatio 34(1):1-20.

Davis SN, Whittemore DO, Fabryka Martin J (1998) Uses of chloride/bromide ratios in studies of potable water. Groundwater 36:338-350.

De Montety V, Radakovitch O, Vallet-Coulomb C, Blavoux B, Hermitte D, Vallès V (2008) Origin of groundwater salinity and hydrogeochemical processes in a

confined coastal aquifer:Case of the Rhône delta (Southern France). Appl Geochem 23:2337-2349.

Dezetter A, Girard S, Paturel JE, Mahé G, Ardoin-Bardin S, Servat E (2008) Simulation of runoff in West Africa: Is there a single data-model combination that produces the best simulation results?. J Hydrol 354:203-212.

Direction de la Météorologie Nationale (DMN) (2007) Les changements climatiques au Maroc:Observations et projections, Maroc-Météo, Casablanca. 2007.

Dorji S, Herath S, Mishra BK (2017) Future climate of Colombo downscaled with SDSM-Neural Network. Climate 5(1) 24:1-11. doi: 10.3390/cli5010024.

Dresh J (1962) Le Haut Atlas Occidental. Dans «Aspect de la géomorphologie du Maroc». Notes et Mémoire du Service Géologique-Maroc 96:107-121.

Driouech F (2010) Distribution des précipitations hivernales sur le Maroc dans le cadre d'un changement climatique: descente d'échelle et incertitudes. Thèse de doctorat, Université. Toulouse, France.

Driouech F, Mahé G, Déqué M, Dieulin C, El Heirech T, Milano M, Benabdelfadel A, Rouche N (2010) Evaluation d'impacts potentiels de changements climatiques sur l'hydrologie du bassin versant de la Moulouya au Maroc. In: Global Change: Facing Risks and Threats to Water Resources (Proc. VIth FRIEND World Conf., Fes, Morocco, October 2010), 561–567. IAHS Publ. 340. IAHS Press.

Duffaud F (1960) Contribution à l'étude stratigraphique du bassin secondaire du Haut Atlas Occidental (Sud-Ouest du Maroc). Bull Soc Géol Fr 7:728-734.

Duffaud F, Brun L, Planchot B (1966) Bassin du Sud-Ouest Marocain (SW Morocco Basin). In: Reyre (ed.) Bassin Sédimentaire du Littoral Africain, partie I, Paris, pp 5-12.

Edmunds WM, Milne CJE (2001) Palaeowaters in coastal Europe: Evolution of groundwater since the late Pleistocene. Geological society, Special Publications, London, 189:289-311.

Edmunds WM, Dodo A, Djoret D, Gasse F, Gaye CB, Goni IB, Travi Y, Zouari K, Zuppi GM (2004) Groundwater as an archive of climatic and environmental change: Europe to Africa. In Battarbee, R.W., Gasse, F., Stickley, C.E., (eds.) Past Climate Variability through Europe and Africa. pp 279-292 Netherlands, Springer.

El Gayar A, Hamed Y (2018) Climate Change and Water Resources Management in Arab Countries. In: Kallel A, Ksibi M, Ben Dhia H, Khélifi N. (eds) Recent Advances in Environmental Science from the Euro-Mediterranean and Surrounding

Regions. EMCEI. 2017. Advances in Science, Technology & Innovation (IEREK Interdisciplinary Series for Sustainable Development). Springer, Cham

El Halimi N, Alia AC, Lebbe L, Beeuwsaert E, Walraevens K (1999) The fresh-/salt-water flow and distribution in a cross-section through the dunes of Saidia Plain (Northeastern Morocco). In 15th Salt Water Intrusion meeting, Ghent 1998. Proceedings,pp 205-211.

El Hassadi A (2008) Seawater intrusion in Derna located in the Green Mountain region, Libya: a threatening recurrent phenomenon calling for desalination. Desalination 220:189-193.

El Hebil A, (1995) Gestion des Eaux Souterraines au Maroc, Séminaire sur «Gestion des Ressources en eaux», Institut Agronomique Méditerranéen de Saragosse, 12p.

El Kharraz J, El-Sadekb A, Ghaffourc N, Mino E (2012).Water scarcity and drought in WANA countries. Procedia Eng 33:14-29.

Elouissi A, Habi M, Benaricha B, Boualem SA (2017) Climate change impact on rainfall spatio-temporal variability (Macta watershed case, Algeria). Arab J Geosci 10:496.

Epstein S, Mayeda T (1953) Variation of 18O content of waters from natural sources. Geochim Cosmochim Acta 4:213-224.

Fadili A, Mehdi K, Malaurent P, Riss J, Boutayeb K, Guessir H (2012) Influence de la marée océanique sur la variation du niveau piézométrique de l'aquifère karstique côtier de Oualidia (Maroc), Africa Geoscience Review 19:135-150.

Farid I, Trabelsi R, Zouari K, Beji R (2013) Geochemical and isotopic study of surface and groundwaters in Ain Bou Mourra basin, central Tunisia. Quatern Int 303:210-227.

Fedrigoni L, Krimissa M, Zouari K, Maliki A, Zuppi GM (2001) Origine de la minéralisation et comportement hydrogeochimique d'une nappe phréatique soumise à des contraintes naturelles et anthropiques sévères: exemple de la nappe de Djebeniana (Tunisie). C R Acad Sci 332:665-671.

Fekri A (1993) Contribution à l'étude hydrogéologique et hydrogéochimique de la zone synclinale d'Essaouira (Bassin synclinal d'Essaouira). Thèse de 3ème cycle, Université Cadi Ayyad, Maroc. 172p.

Feng S, Hu Q, Huang W, Ho CH, Li R, Tang Z (2014) Projected climate regime shift under future global warming from multi-model, multi-scenario CMIP5 simulations. Glob Planet Chang 112:41-52.Fetter CW (1993) Contaminant Hydrogeology. Macmillan Publishing Company, New York.

Filho WL (2012) Climate Change and the Sustainable Use of Water Resources, Climate Change Management, Springer, 801 p. ISBN 978-3-642-22265-8.

Fiseha BM, Melesse AM, Romano E, Volpi E, Fiori A (2012) Statistical downscaling of precipitation and temperature for the Upper Tiber Basin in Central Italy. Int J Water Sci 1(3):1-14.

Fontes JC (1976) Isotopes du milieu et cycle des eaux naturelles: quelques aspects. Thèse Doctorat d'Etat. Université de Paris VI, France Friedman I (1953) Deuterium content of natural waters and other substances. Geochim Cosmochim Acta 4:89-103.

Fowler HJ, Blenkinsop S, Tebaldi C (2007) Linking climate change modelling to impacts studies: recent advances in downscaling techniques for hydrological modelling. Int. J. Climatol. 27 (12):1547-1578. doi: 10.1002/Joc.1556.

Freeze RA, Cherry JA (1979) Groundwater, Prentice-Hall, Englewood Cliffs, NJ, 604 p.

Gagnon S, Singh B, Rousselle J, Roy L (2005) An application of the statistical downscaling model (SDSM) to simulate climatic data for streamflow modelling in Québec. Can Water Resour J 30:297-314

Gebremeskel S, Liu YB, Smedt F, Hoffmann L, Pfister L (2005) Analysing the effect of climate changes on streamflow using statistically downscaled GCM scenarios. Int J River Basin Manag 2:271-280. doi: 10.1080/15715124.2004.9635237.

Geyh MA (2000) An overview of 14C analysis in the study of the groundwater. Radiocarbon 42:99-114.

Gibbs RJ (1970) Mechanisms controlling world water chemistry. Science 170:1081-1090

Gibelin AL, Déqué M (2003) Anthropogenic climate change over the Mediterranean region simulated by a global variable resolution model. Clim Dyn 20:327-339.

Gimenez E, Bencini A, Pranzini G (2010) Hydrogeochemical considerations about the origin of groundwater salinization in some coastal plains of Elba Island (Tuscany,Italy). Environ Geochem Health 32:243-257.

GIEC (2007) Résumé à l'intention des décideurs. In: Bilan 2007 des changements climatiques: Les bases scientifiques physiques. Contribution du Groupe de travail I au quatrième Rapport d'évaluation du Groupe d'experts intergouvernemental sur l'évolution du climat. (Solomon, S, Qin D, Manning M, Chen Z, Marquis M, Averyt KB, Tignor M and Miller HL (eds)). Cambridge University Press, Cambridge, United Kingdom and New York, NY, USA.

GIEC (2013) Climate Change 2013: The Physical Science Basis. Contribution of Working Group I to the Fifth Assessment Report of the Intergovernmental Panel on Climate Change (Stocker TF, Qin D, Plattner GK, Tignor M, Allen SK, Boschung J, Nauels A, Xia Y,Bex V and Midgley PM (eds)) Cambridge University Press, Cambridge, United Kingdom and New York, NY, USA.

Gonfiantini R, Zuppi GM (2003) Carbon exchange rate of DIC in karst groundwater. Chem Geol 197:319-336.

Green TR, Makoto T, Henk K, Gurdak JJ, Allen DM, Hiscock KM, Holger T, Alice A (2011) Beneath the surface of global change: Impacts of climate change on groundwater. J Hydrol 405:532-560.

Hallouz F, Meddi M, Mahe G, Karahacane H, Rahmani SEA (2019) Tendance des précipitations et évolution des écoulements dans un cadre de changement climatique : bassin versant de l'oued Mina en Algérie. RSE 32:83-114.

Hamed Y, Hadji R, Redhaounia B, Zighmi K, Bâali F, El Gayar A (2018) Climate impact on surface and groundwater in North Africa: a global synthesis of findings and recommendations. Euro-Mediterr J Environ Integr 3:25. https://doi.org/10.1007/s41207-018-0067-8.

Hannachi A, Fenni M (2013) Etude floristique et écologique des mauvaises herbes des cultures de la région de Batna (Algérie). Revue Agriculture 5:24-36.

Haut-Commissariat au Plan (2013) Séminaire sur: «La comptabilité des actifs naturels pour une croissance verte dans la région MENA» 26 et 27 mars 2013, Marseille, France. https://www.hcp.ma.

Hassani My D, Mokssit A, Henia L, (1998) Changements climatiques et ressources en eau dans les pays du Maghreb. Juin 1998, 55p.

Hay LE, Wilby RL, Leavesley GH (2000) A comparison of delta change and downscaled GCM scenarios for three mountainous basins in the United States. J Am Water Resour Assoc 36:387-397. doi:10.1111/j.1752-1688.2000.tb04276.x.

Herrera E, Ouarda TBMJ, Bobée B (2006) Méthodes de désagrégation appliquées aux Modèles du Climat Global Atmosphère Océan (MCGAO). Rev Des Sci De L'Eau 19:297-312.doi: 10.7202/014417ar.

Huang J, Zhang J, Zhang Z, Xu C,Wang B, Yao J (2011) Estimation of future precipitation change in the Yangtze River basin by using statistical downscaling method. Stoch Env Res Risk A 25:781-792. doi: 10.1007/s00477-010-0441-9.

Hughes JP, Guttorp P, Charles SP (1999) A non-homogenous hidden Markov model for precipitation occurrence. Appl Statist 48:15-30.doi:10.1111/1467-9876.00136.

IPCC (2007a) Climate Change 2007: The Physical Science Basis. Contribution of Working Group I to the Fourth Assessment Report of the Intergovernmental Panel on Climate Change (ed. by S. Solomon, D. Qin, M. Manning, Z. Chen, M. Marquis, K. B. Averyt, M.Tignor& H. L. Miller). Cambridge University

IPCC (2007b) Climate Change 2007: Impacts, Adaptation and Vulnerability. Contribution of Working Group II to the Fourth Assessment Report of the Intergovernmental Panel on Climate Change (ed. by M. L. Parry, O. F. Canziani, J. P. Palutikof, C. E. Hanson & P. J. van der Linden). Cambridge University Press, Cambridge.

IPCC (2013) Climate Change 2013: The Physical Science Basis. Contribution of Working Group I to the Fifth Assessment Report of the Intergovernmental Panel on Climate Change [Stocker, T.F., D. Qin, G.-K. Plattner, M. Tignor, S.K. Allen, J. Boschung, A. Nauels, Y. Xia, V. Bex and P.M. Midgley (eds.)]. Cambridge University.

IPCC (2014) Changements climatiques 2014:Rapport de synthèse. Contribution des Groupes de travail I, II et III au cinquième Rapport d'évaluation du Groupe d'experts intergouvernemental sur l'évolution du climat [Sous la direction de l'équipe de rédaction principale, R.K. Pachauri et L.A. Meyer]. GIEC, Genève, Suisse, 161 p.

Jalal M, Blavoux B, Bahir M, Bellion Y, Laftouhi N, Puig JM, Mennani A, Daniel M (2001) Etude du fonctionnement du système aquifère karstique Cenomano-Turonian de l'oued Igrounzar (Bassin d'Essaouira, Maroc). J Afr Earth Sci 32:803-817.

Jones BF, Vengosh A, Rosenthal E, Yechieli Y (1999) Geochemical investigations. In Bear J et al. (eds), Seawater Intrusion in Coastal Aquifers, Kluwer Academic Publisher, pp 51-71.

Kaid Rassou K, Fakir Y, Bahir M, Zouari K, Marah M, Monteiro JP (2005) Apports des analyses isotopiques à la compréhension du fonctionnement des aquifères côtiers du bassin hydrologique de la lagune d'Oualidia. Comun Geol 92:129-142

Kannan S, Ghosh S (2011) Prediction of daily rainfall state in a river basin using statistical downscaling from GCM output. Stoch Env Res Risk A 25(4):457-474. doi: 10.1007/s00477-010-0415-y.

Kendall MG (1975) Multivariate nonparametric tests for trend in water quality. Water Resour Bull 24:505-512.

King LM, Irwin S, Sarwar R, McLeod AIA, Simonovic SP (2012) The effects of climate change on extreme precipitation events in the Upper Thames River Basin: a comparison of downscaling approaches. Can Water Resour J 37:253-274.

Kim Y, Lee K, Koh D, Lee D, Lee S, Park W, Koh G, Woo N (2003) Hydrogeochemical and isotopic evidence of groundwater salinization in a coastal aquifer:a case study in Jeju volcanic island, Korea. J Hydrol 270:282–294.

Knutson TR, Sirutis JJ, Vecchi GA, Garner S, Zhao M, H. Kim H, Bender M, Tuleya RE, Held IM, Villarini G (2013) Dynamical downscaling projections of twenty first century Atlantic hurricane activity: CMIP3 and CMIP5 model based scenarios. J Clim 26:6591-6617.

Kouamė KF, Kouassi AM, N'guessan BTM, Kouao JM, Lasm T, Saley MB (2013) Analyse de tendances dans la relation pluie-débit dans un contexte de changements climatiques: cas du bassin versant du N'zo-Sassandra (Ouest de la Côte d'Ivoire). IJIAS 2:92-103.

Kour R, Patel N, Krishna AP (2016) Climate and hydrological models to assess the impact of climate change on hydrological regime: a review Arab J Geosci 9:544. https://doi.org/10.1007/s12517-016-2561-0.

Lachaal F, Chargui S, Messaoud RB, Chekirbane A, Tsujimura M, Mlayah A, Massuel S, Leduc C (2018) Impacts of global changes on groundwater resources in north-east Tunisia: The case of the Grombalia phreatic aquifer. In Calvache ML et al. (eds.), Groundwater and Global Change in the Western Mediterranean Area, Environmental Earth Sciences. Springer International Publishing Switzerland, 179-188.

Lebel T, Vischel T (2005) Climat et cycle de l'eau en zone tropicale: un problème d'échelle. CR Geoscience, 337:29-38.

Leung LR, Mearns LO, Giorgi F, Wilby RL (2003) Regional climate research: needs and opportunities, Bull. Am Meteorol Soc 82:89-95.

Lopo Mendonça J, Oliveira da Silva M, Bahir M (2004) Considerations concerning the origin of the Estoril (Portugal) thermal water. Estudios Geol 60:153-159.

Lucas LL, Unterweger MP (2000) Comprehensive review and critical evaluation of the half-life of tritium. Journal of Research of NIST 105:541-549.

Mahé G, Paturel, JE, Servat E, Conway D, Dezetter A (2005) The impact of landuse change on the water holding capacity and river discharge modelling in the Nakambe River, Burkina Faso. J Hydrol 300:33-43.

Makhlouf Z, Michel C (1994) A two-parameter monthly water balance model for French watersheds. J Hydrol 162:299-318.

Mann HB (1945) Nonparametric tests against trend, Econometrical 13:245-259.

Mann HB, Whitney DR (1947) On a test of whether one of two random variables is stochastically larger than the other. Ann Math Stat 18:50-60.

Marfia AM, Krishnamurthy RV, Atekwana EA, Panton WF (2004) Isotopic and geochemical evolution of ground and surface waters in a karst dominated geological setting:a case study from Belize, Central America. Appl Geochem 19:937-946.

Mazor E (1991) Applied chemical and isotopic groundwater hydrology. Buckingham: Open University Press.

Meddi M, Talia M, Martin C (2009) Recent evolution of weather conditions and flows on the basin of Macta (Northwest of Algeria). PhysioGeo 23:61-84.

Mennani A (2001) Apport de l'hydrochimie et de l'isotopie à la connaissance du fonctionnement des aquifères de la zone côtière d'Essaouira (Maroc Occidental). Thèse de doctorat, Université Cadi Ayyad, Maroc.

Mennani A, Blavoux B, Bahir M, Bellion Y, Jalal M, Daniel M (2001) Apports des analyses chimiques et isotopiques à la connaissance du fonctionnement des aquifères plio-quaternaire et turonien de la zone synclinale d□Essaouira (Maroc occidental). J Afr Earth Sci 32:819-835.

Meddi H, Meddi M (2007) Variabilité spatiale et temporelle des précipitations du nord-ouest de l'Algérie. Geographia Technica 2:49-55.

Misra AK (2014) Climate change and challenges of water and food security. Int J Sustain Built Environ 3:153-165.

Mokadem N, Hamed Y, Hfaid M, Ben Dhia H (2015) Hydrogeochemical and isotope evidence of groundwater evolution in El Guettar Oasis area, Southwest Tunisia. Carbonates Evaporites 30:417-437.

Mokadem N, Redhaounia B, Besser H, Ayadi Y, Khelifi F, Hamad A, Hamed Y, Bouri S (2018) Impact of climate change on groundwater and the extinction of ancient "Foggara" and springs systems in arid lands in North Africa: a case study in Gafsa basin (Central of Tunisia). Euro-Mediterr J Environ Integr 3:28. https://doi.org/10.1007/s41207-018-0070-0.

Mook WG, Bommerson JC, Staverman WH (1974) Carbon isotope fractionation between dissolved bicarbonate and gaseous carbon dioxide. Earth Planet Sci Lett 22:169-176.

Morsli B, Habi M, Hamoudi A (2007) Contraintes et perspectives des aménagements hydroagricoles et antiérosifs en Algérie. Actes des JSIRAUF, Hanoi, 6-9 novembre 2007.

Mouelhi S, Michel C, Perrin C, Andréassian V (2006) Stepwise development of a two-parameter monthly water balance model. J Hydrol 318:200-214.

Mouelhi S, Nemri S, Jebari S, Slimani M (2017) Coupling between a rain-runoff model, GR2M, and a rain generator to evaluate the transfer between two dams the Tunisian Semi-arid Sidi Saad and El Houareb. IJIAS 19:944-959.

Myoung-Seok S, Seok-Geun O, Young-Suk L, Joong-Bae A, Dong-Hyun C, Dong-Kyou L, Song-You H, Seung-Ki M, Seong-Chan P, Hyun-Suk K (2016) Projections of high resolution climate changes for South Korea using multiple-regional climate models based on four RCP scenarios. Part 1: surface air temperature. Asia-Pac J Atmos Sci 52:151-169. doi: 10.1007/s13143-016-0017-9.

Nadifi K, (1998) Ressource en eau du Maroc, Séminaire « échelle et modèles de gestion de l'eau du bassin du Haouz au Bassin occidental de la Méditerranée, Faculté des sciences Semlalia de Marrakech.

Nash JE, Sutcliffe JV (1970) River discharge forecasting through conceptual models. Part I - a discussion of principles. J Hydrol 10:282-290.

Nassopoulos H (2012) Les impacts du changement climatique sur les ressources en eaux en Méditerranée. Thèse de doctorat, Université Paris-Est, France. 153 p.

Nicholson SE (1986) The spatial coherence of African rainfall anomalies: inter hemisphericteles connections. J Appl Meteor Climato 25:1365-1381.

Nigatu ZM (2013) Hydrological impacts of climate change on Lake Tana's water balance. Thesis, University of Twente.

Ouhamdouch S, Bahir M, Carreira P, Chkir N, Goumih A, Chamchati H (2016) Climate change impact on aquifer system of Essaouira basin during the past 4 decades (Morocco). OJMH 6: 19-33. doi: 10.4236/ojmh.2016.61003.

Ouhamdouch S, Bahir M, Souhel A, Carreira PM (2016) Vulnerability and Impact of Climate Change Processes on Water Resource in Semi-Arid Areas: In Essaouira Basin (Morocco). In Grammelis, P., (ed.), Energy, Transportation and Global Warming, Green Energy and Technology. Springer International Publishing Switzerland, pp 719-736. DOI 10.1007/978-3-319-30127-3_53.

Ouhamdouch S, Bahir, M (2017) Climate Change Impact on Future Rainfall and Temperature in Semi-arid Areas (Essaouira Basin, Morocco). Environ Process 4:975-990.

Ouhamdouch S, Bahir M, Carreira PM, Zouari Kamel (2018a) Groundwater Responses to Climate Change in a Coastal Semi-arid Area from Morocco; Case of Essaouira Basin. In Calvache ML et al. (eds.), Groundwater and Global Change in the Western Mediterranean Area. Environ Earth Sciences, pp 253-260. https://doi.org/10.1007/978-3-319-69356-9_29.

Ouhamdouch S, Bahir M, Carreira P (2018) Impact du changement climatique sur la ressource en eau en milieu semi-aride: exemple du bassin d'Essaouira (Maroc). Rev Des Sci De L'Eau 31:13-27.

Ouhamdouch S, Bahir M, Ouzar D, Carreira PM, Zouari K (2019) Evaluation of climate change impact on groundwater from semi-arid environment (Essaouira Basin, Morocco) using integrated approaches. Environ Earth Sci 78:449. https://doi.org/10.1007/s12665-019-8470-2.

Ouhamdouch S, Bahir M, Ouazar D, Goumih A, Zouari K (2020a) Assessment of the climate change impact on the future evapotranspiration and flows from a semi-arid environment. Arab J Geosci (2020) 13:82. DOI:10.1007/s12517-020-5065-x.

Ouhamdouch S, Bahir M, Ouazar D (2020b) Climate change impact assessment on a carbonate aquifer under semi-arid climate; example of the Cenomanian-Turonian aquifer within Meskala-Ouazzi region (Essaouira Basin, Morocco). Arab J Geosci (2020) 13: 173. https://doi.org/10.1007/s12517-020-5180-8.

Paniconi C, Khlaifi I, Lecca G, Giacomelli A, Tarhouniy J (2001) Modeling and analysis of seawater intrusion in the Coastal Aquifer of Eastern Cap-Bon, Tunisia, Transport Porous Med 43:3-28.

Penna D, Stenni B, Wrede S, Bogaard TA, Gobbi A, Borga M, Fischer BMC, Bonazza M, Charova Z (2010) On the reproducibility and repeatability of laser absorption spectroscopy measurements for [delta] 2H and [delta] 18O isotopic analysis. Hydrol Earth Syst Sc 14:1551-1566.

Parkhurst DL, Appelo CAJ 1(999) User's guide to PHREEQC (version 2) -A computer program for speciation, batch–reaction, one–dimensional transport, and inverse geochemical calculations. USGS Water–Resour. Invest. Rep. 99-4259, 312 pp.

Parvaze S, Parvaze S, Haroon S, Khurshid N, Khan JN, Ahmad L (2016) Projected Change in climate under A2 scenario in Dal Lake catchment area of Srinagar City in Jammu and Kashmir. Curr World Environ 11(2):429-438.

Pazand K, Khosravi D, RezaGhaderi M, Rezvanianzadeh MR (2018) Identification of the hydrogeochemical processes and assessment of groundwater in a semi-arid region using major ion chemistry: A case study of Ardestan basin in Central Iran. Groundw Sustain Dev 6:245-254.

Pettitt AN (1979) A non-parametric approach to the change-point problem. Appl Statist 28(2):126-135.

Perrin C, Michel C, Andréassian V (2003) Improvement of a parsimonious model for streamdischarge simulation. J Hydrol 279:275-289.

Peybernès B, Bouaouda MS, Almeras Y, Ruget CH, Cugny P (1987) Stratigraphy of the Lias-Dogger deposits from Essaouira coastal basin (Morocco) before and during the beginning of oceanic accretion in the central Atlantic; comparisons with the Agadir basin. CR Acad Sci 305: 1449-1555.

Piper AM (1944) A graphic procedure in the geochemical interpretation of water analyses. Trans Am Geophys Union 25:914-923.

PNUD-FEM (1998) Changements climatiques et ressources en forum régional sur les changements climatiques: Eau dans les pays du Maghreb, Algérie -Maroc-Tunisie, enjeux et perspectives. Projet RAB/94/G31.

Post VEA (2004) Groundwater salinization processes in the coastal area of the Netherlands due to transgressions during the Holocene. PhD thesis, Vrije University, Amsterdam, 138 p.

Pulido-Bosch A, Tahiri A, Vallejos A (1999) Hydrogeochemical characteristics of processes in the Temara Aquifer in Northwestern Morocco. Water Air Soil Pollut 114:323-337.

Pulido-Leboeuf P, Pulido-Bosch A, Calvache Ml, Vallejos A, Andreu JM (2003) Strontium, SO4/Cl and Mg /Ca ratios as tracers for the evolution of seawater into coastal aquifers: The example of Castell de Ferro-aquifer. CR Geosci 335:1039-1048.

Ragab R, Prudhomme C (2002) Climate change and water resources management in arid and semi-arid regions: Prospective and challenges for the 21st Century. Biosystems Eng 81:3-34.

Rashid M and Mukand SB (2012) Evaluation of SDSM developed by annual and monthly sub-models for downscaling temperature and precipitation in the Jhelum basin, Pakistan and India. Theor Appl Climatol 113:27-44. doi: 10.1007/s00704-012-0765-0.

Rashid MM, Beecham S, Chowdhury RK (2015) Statistical downscaling of CMIP5 outputs for projecting future changes in rainfall in the Onkaparinga catchment. Sci Total Environ 530-531:171-182.

Riahi K, Rao S, Krey V, Cho C, Chirkov V, Fischer G, Kindermann G, Nakicenovic N, Rafaj P (2011) RCP 8.5-A scenario of comparatively high greenhouse gas emissions. Clim Chang 109:33-57.

Rifai N, Khattabi A, Rhazi L (2014) Impact du changement climatique sur les températures journalières minimales et maximales et les précipitations de la région de Tanger (nord-ouest du Maroc) quantifié à partir d'une méthode de descente d'échelle statistique. Vertigo 14:1-16.

Rodier J, Legube B, Merlet N, Mialocq JC, Leroy P, Houssin M, Lavison G, Bechemin C, Vincent M, Rebouillon P, Moulin L, Chomodé P, Dujardin P, Gosselin S, Seux R, Al Mardini F (2009) L'Analyse de l'eau. 9e édition, Dunod, Paris.

Rwasoka DT, Madamombe CE, Gumindoga W, Kabobah AT (2014) Calibration, validation, parameter indentifiability and uncertainty analysis of a 2-parameter parsimonious monthly rainfall-runoff model in two catchments in Zimbabwe. Phys Chem Earth 67-69:36-46.

Sachindra D, Huang F, Barton A, Perera B (2014a) Statistical downscaling of general circulation model outputs to precipitation-part 2: bias□correction and future projections. Int J Climatol 34:3282-3303. doi: 10.1002/joc.3915.

Sadeg SA, Karahanoglu N (2001) Numerical assessment of seawater intrusion in the Tripoli region, Libya. Environ Geol 40:1151-1168.

Sakaa B, Boulghobra N, Chaffai H, Hani A, Djabri L (2015) Application of GR2M for Rainfall-Runoff Modeling in Kébir Rhumel Watershed, North East of Algeria. World Appl Sci J 33(10):1623-1630.

Salem O, Visser JM, Dray M, Gonfiantini R (1980) Groundwater flow patterns in the Western Libyan Arab Jamahiriya evaluated from isotopic data. Arid-zone Hydrology: Investigation With Isotope Techniques. IAEA, Vienna, 165-179 pp.

Sebbar A (2013) Etude de la variabilité et de l'évolution de la pluviométrie au Maroc (1935-2005): Réactualisation de la carte des précipitations. Thèse de doctorat, Université Hassan II. 155 p.

Sherif MM (1999) The Nile Delta aquifer in Egypt, chap 17. In Bear J, Cheng A, Sorek S, Ouazar D, Herrera A (Eds) Theory and application of transport in porous media, Kluwer Academic Publishers, Dordrecht/ Boston/London 559-590.

Sinan M, Boussetta M, El Rherari A (2009) Changements climatiques: causes et conséquences sur le climat et les ressources en eau. Revue HTE 142:21-30.

Singhal A, Gupta R, Singh AN, Shrinivas A (2020) Assessment and monitoring of groundwater quality in semi-arid region. Groundw Sustain Dev 11:100381. https://doi.org/10.1016/j.gsd.2020.10038.1.

Starinsky A, Bielski M, Lazar B, Steinitz G, Raab M (1983) Strontium isotope evidence on the history of oilfield brines, Mediterranean Coastal Plain, Israel. Geochim Cosmochim Acta 47:687-695.

Stour L and Agoumi A (2008) Sécheresse climatique au Maroc durant les dernières décennies. Hydroécol Appl 16:215-232.

Sunyer MA, Madsen H, Ang PH (2012) A comparison of different regional climate models and statistical downscaling methods for extreme rainfall estimation under climate change. Atmos Res 103:119-128. doi: 10.1016/j.atmosres.2011.06.011.

Taabni M, El Jihad MD (2012) Eau et changement climatique au Maghreb : quelles stratégies d'adaptation ?. Les Cahiers d'Outre-Mer 260:493-518.

Taheri Tizro A, Fryar AE, Khodamorad Pour M, Voudouris KS, Javad Mashhadian M (2019) Groundwater conditions related to climate change in the semi-arid area of western Iran. Groundw Sustain Dev 9: 100273. https://doi.org/10.1016/j.gsd.2019.100273.

Telahigue F, Agoubi B, Souid F, Kharroubi A (2018) Groundwater chemistry and radon-222 distribution in Jerba Island, Tunisia. J Environ Radioact 182:74-84.

Telahigue F, Mejri H, Mansouri B, Souid F, Agoubi B, Chahlaoui A, Kharroubi A (2020) Assessing seawater intrusion in arid and semi-arid Mediterranean coastal aquifers using geochemical approaches. Phys Chem Earth 115. https://doi.org/10.1016/j.pce.2019.102811

Tellam JH, Lloyd JW (1986) Problems in the recognition of seawater intrusion by chemical means:an example of apparent equivalence. Q J Eng Geol Hydroge 19:389-398.

Theodossiou N (2016) Assessing the Impacts of Climate Change on the Sustainability of Groundwater Aquifers. Application in Moudania Aquifer in N. Greece. Environ Process 3:1045-1061.

Thomson AM, Calvin KV, Smith SJ, Kyle GP, Volke A, Patel P, Delgado-Arias S, Bond-Lamberty B, Wise MA, Clarke LE, Edmonds JA (2011) RCP4.5: A pathway for stabilization of radiative forcing by 2100. Clim Chang 109:77-94.

Thornthwaite CW (1948) An approach toward a rational classification of climate. Geor Review 38:55-94.

Trabelsi R, Zouari K (2019) Coupled geochemical modeling and multivariate statistical analysis approach for the assessment of groundwater quality in irrigated areas: A study from North Eastern of Tunisia. Groundw Sustain Dev 8:413-427.

United Nations Economic and Social Commission for Western Asia (ESCWA) et al. (2017) Arab Climate Change Assessment Report - Main Report. Beirut, E/ESCWA/SDPD/2017/RICCAR/Report.

Vella C, Fleury TJ, Raccasi G, Provansal M, Sabatier F, Bourcier M (2005) Evolution of the Rhone delta plain in the Holocene. Mar Geol 222-223:235-265.

Vengosh A, Gert JD, Starinsky A (1998) Boron isotope and geochemical evidence for the origin of Urania and Bannock brines at the eastern Mediterranean:effect of water-rock interactions. Geochim Cosmochim Acta 62:3221-3228.

Vennetier M, Vila B, Liang EY, Guibal F, Ripert C, Chandioux O (2005) Impact du changement climatique sur la productivité forestière et le déplacement d'une limite bioclimatique en région méditerranéenne française. Ingénieries-EAT 49:49-61.

Vicente-Serrano SM (2006): Spatial and temporal analysis of droughts in the Iberian Peninsula (1910-2000). Hydrolog Sci J 51:83 -97.

Von Storch H (1999) On the use of 'inflation' in statistical downscaling. J Clim 12(12):3505-3506.

Wang Y, Leung LR, McGregor JL, Lee DK, Wang WC, Ding Y, Kimura F (2004) Regional climate modeling: progress, challenges and prospects, J Meteor Soc Japa 82:1599-1628.

Wang J, Zhang X (2008) Downscaling and projection of winter extreme daily precipitation over North America. J Clim 21(5):923-937. doi:10.1175/2007jcli1671.1.

Wayne GP (2013) The Beginner's Guide to Representative Concentration Pathways. Skeptical Science. https://skepticalscience.com/rcp.php. Accessed 25 August 2017

Wetterhall FA, Bárdossy D, Chen SH, Xu CY (2006) Daily precipitation-downscaling techniques in three Chinese regions. Water Resour Res 42:W11423. doi: 10.1029/2005WR004573.

Wetterhall FA, Bárdossy D, Chen SH, Halldin S, Xu CY (2009) Statistical downscaling of daily precipitation over Sweden using GCM output. Theor Appl Climatol. 96(1):95-103. doi: 10.1007/ s00704-008-0038-0.

White CJ, McInnes KL, Cechet RP, Stuart SP, Grose MR, Holz GK, Katzfey JJ, Bindoff NL (2013) On regional dynamical downscaling for the assessment and

projection of temperature and precipitation extremes across Tasmania, Australia. Clim.Dyn 14:3145-3165. doi: 10.1007/s0038201317188.

Wilby RL, Dawson CW (2013) The Statistical DownScaling Model: insights from one decade of application. Int J Climatol. 33:1707-1719. doi: 10.1002/joc.3544.

Wilby RL, Hay LE, Gutowski WJ, Arritt RW, Takle ES, Pan Z, Leavesley GH, Martyn PC (2000) Hydrological responses to dynamically and statistically downscaled climate model output. Geophys Res Lett 27(8):1199-1202. doi: 10.1029/1999GL006078.

WHO (2011) Guidelines for drinking water quality, fourth edition. Geneva.

Xu ZX, Chen YN, Li JY (2004) Impact of climate change on water resources in the Tarim River Basin. Water Resour Manag 18:439-458.

Zeroual A, Meddi M, Bensaad S (2013) The impact of climate change on river flow in arid and semi-arid rivers in Algeria. Proceedings of H01, IAHS-IAPSO-IASPEI Assembly, Gothenburg, Sweden, July 2013 (IAHS Publ. 359, 2013).

Zouari K, Trabelsi R, Chkir N (2011) Using geochemical indicators to investigate groundwater mixing and residence time in the aquifer system of Djeffara of Medenine (southeastern Tunisia). Hydrogeol J 19:209-219.

Zulkarnain H, Supiah S, Sobri H (2014) Application of SDSM and LARS-WG for simulating and downscaling of rainfall and temperature. Theor Appl Climatol 16:243-257.

Appendices

Annex I

Climatic and hydrometric data

Rainfall at Igrounzar station

Year	S	O	N	D	J	F	M	A	M	J	JL	A	Total
1977/78	9.8	120.0	63.1	114.1	63.5	49.6	3.5	46.5	4.7	0.0	0.0	0.0	474.8
1978/79	0.0	8.8	2.0	58.1	143.7	27.7	23.6	18.1	0.0	0.0	0.0	0.0	282.0
1979/80	0.0	77.1	0.0	2.6	42.8	112.6	67.9	15.3	0.5	0.0	0.0	0.0	318.8
1980/81	0.0	0.0	71.5	0.0	3.7	116.8	23.0	6.2	4.8	0.0	0.0	0.0	226.0
1981/82	0.0	16.8	0.8	27.1	100.2	30.9	59.7	128.4	4.0	0.0	0.0	0.0	367.9
1982/83	0.0	0.0	41.3	3.5	1.7	78.2	14.0	8.0	8.1	0.0	0.0	0.0	154.8
1983/84	0.0	5.4	117.9	17.9	0.0	9.4	44.2	5.9	31.4	0.0	0.0	0.0	232.1
1984/85	0.0	0.0	106.2	10.2	145.6	32.4	3.5	3.2	0.0	0.5	0.0	0.0	301.6
1985/86	0.0	0.0	10.7	60.1	18.4	81.6	70.6	37.2	0.0	3.9	0.0	0.0	282.5
1986/87	10.0	0.0	16.1	1.2	50.0	42.6	8.8	0.0	0.6	0.3	0.0	5.2	134.8
1987/88	13.6	50.8	48.5	167.4	172.5	41.5	31.8	0.0	15.9	21.9	0.0	0.0	563.9
1988/89	0.0	32.2	294.4	0.0	79.0	18.4	38.4	106.6	0.6	0.0	0.0	0.0	569.6
1989/90	0.0	8.7	76.2	64.7	39.9	0.0	90.8	57.9	14.3	3.1	0.0	0.0	355.6
1990/91	0.2	7.0	9.8	86.5	10.4	120.6	110.5	6.7	0.0	0.0	0.0	0.0	351.7
1991/92	9.2	69.0	15.6	10.6	0.3	9.5	22.1	28.1	0.0	7.4	0.0	0.0	171.8
1992/93	2.7	1.0	5.5	36.1	23.2	16.6	25.3	5.6	20.2	0.0	0.0	0.0	136.2
1993/94	0.0	57.9	60.1	2.7	34.2	54.5	18.1	0.2	1.6	0.0	0.0	0.0	229.3
1994/95	0.0	29.8	6.7	4.3	0.0	41.8	47.0	20.1	0.0	0.0	0.0	0.0	149.7
1995/96	0.1	7.4	127.4	142.9	266.9	43.8	89.3	2.4	25.8	1.6	0.0	0.0	707.6
1996/97	2.4	1.0	71.7	281.4	73.2	2.8	13.8	48.6	0.0	0.0	0.0	0.0	494.9
1997/98	4.9	32.7	37.2	67.6	47.7	100.5	81.7	9.0	2.6	2.8	0.0	0.0	386.7

Year	S	O	N	D	J	F	M	A	M	J	JL	A	Total
1998/99	0.0	0.0	0.0	49.4	72.8	31.2	40.2	6.2	22.4	0.0	0.0	0.0	222.2
1999/00	3.8	53.0	26.9	16.1	40.8	2.2	0.0	60.7	0.3	0.0	0.0	0.0	203.8
2000/01	0.0	8.5	4.0	101.8	42.7	2.7	13.6	1.6	0.0	0.0	0.0	0.0	174.9
2001/02	4.2	0.0	4.8	79.2	0.3	21.9	68.8	63.7	2.1	0.0	0.0	0.0	245.0
2002/03	0.0	8.3	97.2	28.4	10.2	10.0	15.1	34.1	0.0	0.0	0.0	0.0	203.3
2003/04	0.0	65.8	96.6	43.6	0.5	82.5	63.5	18.6	22.6	0.0	0.0	0.0	393.7
2004/05	0.0	17.8	41.2	17.0	0.0	47.2	59.2	0.0	0.0	0.0	0.0	0.0	182.4
2005/06	0.0	5.1	106.4	67.6	260.0	28.5	15.4	24.7	6.5	0.0	0.0	0.0	514.2
2006/07	2.4	30.3	32.7	1.7	21.9	21.0	1.5	15.5	4.3	0.0	0.0	9.2	140.5
2007/08	0.0	2.2	67.0	15.4	21.9	11.8	11.9	8.0	0.0	0.0	0.0	0.0	138.2
2008/09	40.1	71.8	49.0	0.0	91.4	122.2	58.9	0.0	1.8	9.7	0.0	0.0	444.9
2009/10	10.4	0.0	1.5	162.6	62.8	148.9	34.6	7.1	2.9	5.3	0.0	18.1	454.2
2010/11	0.9	14.1	82.4	48.7	49.8	7.8	102.0	43.2	40.1	0.0	0.0	0.0	389.0
2011/12	2.1	17.0	46.7	0.0	27.8	3.9	7.0	59.7	0.0	0.0	0.0	0.8	165.0
2012/13	70.1	60.9	40.4	4.9	5.6	31.7	84.0	23.3	4.3	0.0	0.0	0.0	325.2
2013/14	21.2	7.5	9.4	1.4	56.6	8.9	26.1	32.5	4.2	0.0	0.0	0.0	167.8
2014/15	0.0	2.0	191.3	0.0	20.6	51.9	25.8	6.4	0.0	2.1	2.3	8.3	310.7
2015/16	1.7	120.0	5.0	0.0	-	-	-	-	-	-	-	-	126.7
Average	5.4	25.9	53.5	46.1	55.3	43.8	39.9	25.2	6.5	1.5	0.1	1.1	299.8

Rainfall at Adamna station

Year	S	O	N	D	J	F	M	A	M	J	JL	A	Total
1977/78	7.5	125.1	57.3	111.2	69.6	56.2	4.2	31.5	8.7	0.0	0.0	0.0	471.3
1978/79	0.0	3.6	11.0	51.5	163.8	34.1	18.6	6.2	0.0	0.0	0.0	0.0	288.8
1979/80	0.0	74.6	0.0	5.3	40.3	49.8	68.0	9.3	3.0	0.0	0.0	0.0	250.3
1980/81	0.5	10.5	60.8	0.0	5.6	53.4	34.4	16.2	5.4	0.0	0.0	0.0	186.8
1981/82	0.0	16.2	0.0	36.9	140.1	26.3	38.7	40.6	4.3	0.0	0.0	0.0	303.1
1982/83	0.0	0.0	47.1	5.9	2.8	96.0	15.8	8.4	3.7	0.0	0.0	0.0	179.7
1983/84	0.0	4.6	161.9	28.3	0.0	20.2	78.6	12.5	20.6	0.0	0.0	0.0	326.7
1984/85	0.3	0.0	162.5	13.3	143.0	30.9	1.2	8.4	5.5	0.0	0.0	0.0	365.1
1985/86	0.0	0.0	7.6	66.4	34.5	106.1	71.1	53.5	0.0	1.2	0.0	0.0	340.4
1986/87	9.2	0.4	12.0	1.1	58.1	33.3	12.4	3.9	1.2	0.0	0.0	0.0	131.6
1987/88	9.1	57.6	65.3	257.2	161.1	51.3	27.3	0.0	17.8	1.7	0.0	0.0	648.4

Year	S	O	N	D	J	F	M	A	M	J	JL	A	Total
1988/89	0.0	30.6	163.1	0.0	96.1	17.3	32.8	78.8	1.2	0.0	0.0	0.0	419.9
1989/90	0.0	23.4	124.6	76.2	35.6	0.0	69.7	47.9	0.5	4.3	0.0	0.0	382.2
1990/91	0.0	2.8	11.0	91.0	11.5	107.9	111.4	4.0	0.0	0.0	0.0	0.0	339.6
1991/92	10.5	78.5	16.4	11.8	0.5	7.7	18.3	13.3	0.0	2.6	0.0	0.0	159.6
1992/93	0.0	2.1	5.5	58.3	42.6	2.8	72.3	3.3	34.5	0.0	0.0	0.0	221.4
1993/94	0.0	89.6	65.7	4.6	35.2	47.1	17.1	0.6	0.4	0.0	0.0	0.0	260.3
1994/95	0.0	44.6	9.5	18.6	0.0	33.0	62.1	6.8	0.0	0.0	0.0	0.0	174.6
1995/96	1.1	13.5	103.4	133.4	355.9	34.3	71.3	1.7	32.0	11.0	0.0	0.0	757.6
1996/97	1.6	12.3	161.9	329.2	102.2	1.7	24.4	46.2	0.0	0.0	0.0	0.0	679.5
1997/98	2.9	36.3	30.4	76.0	71.5	148.6	35.3	9.3	1.5	0.8	0.0	0.0	412.6
1998/99	0.0	0.0	0.0	44.2	63.0	29.5	68.3	2.2	8.0	0.0	0.0	0.0	215.2
1999/00	4.0	78.6	32.4	16.9	31.5	2.0	0.8	66.7	5.5	0.0	0.0	0.0	238.4
2000/01	0.0	12.4	5.5	122.4	29.3	3.0	16.5	0.0	0.7	0.0	0.0	0.0	189.8
2001/02	32.7	0.0	1.6	136.3	0.0	14.9	82.8	49.3	22.0	0.0	0.0	0.0	339.6
2002/03	0.0	4.6	90.1	81.7	10.3	12.2	23.5	51.0	0.0	0.0	0.0	0.0	273.4
2003/04	0.0	70.0	83.4	67.1	0.0	48.7	45.8	18.5	18.3	0.0	0.0	0.0	351.8
2004/05	3.2	35.6	40.5	27.5	0.5	73.5	19.4	0.0	0.0	0.0	0.0	0.0	200.2
2005/06	0.0	4.0	39.1	85.7	101.4	20.7	9.4	13.9	1.8	2.8	0.0	0.0	278.8
2006/07	2.5	74.4	23.5	0.6	7.7	21.9	4.3	11.4	4.7	0.0	0.0	6.7	157.7
2007/08	0.0	4.2	44.1	25.8	17.4	6.5	8.2	8.3	0.9	0.0	0.0	0.0	115.4
2008/09	18.6	60.2	52.4	0.0	106.9	163.2	40.6	0.0	3.3	9.5	0.0	0.0	454.7
2009/10	5.2	0.0	3.3	216.1	39.8	184.5	46.7	10.0	5.1	3.1	0.0	6.6	520.4
2010/11	0.4	14.2	130.2	85.1	91.4	23.0	18.9	90.2	65.4	0.0	0.0	0.0	518.8
2011/12	0.4	27.1	65.1	0.0	0.0	53.2	0.0	44.6	0.0	0.0	0.0	0.0	190.4
2012/13	50.3	139.6	0.0	2.9	9.5	35.6	74.6	29.5	3.1	0.0	0.0	0.0	345.1
2013/14	8.3	17.7	12.9	1.0	81.7	9.6	33.6	43.0	1.0	0.0	2.0	0.0	210.8
2014/15	0.5	0.0	170.0	37.2	29.2	2.1	76.1	0.0	0.5	1.0	0.0	0.0	316.6
2015/16	0.0	142.6	7.9	0.0	-	-	-	-	-	-	-	-	150.5
Average	4.3	33.6	53.3	59.7	57.6	43.7	38.3	22.1	7.4	1.0	0.1	0.4	317.1

Rainfall at Essaouira station

Year	S	O	N	D	J	F	M	A	M	J	JL	A	Total
1977/78	2.1	91.1	29.1	87.9	73.8	20.8	1.7	40.6	5.7	1.6	0.0	0.0	354.4
1978/79	0.0	2.7	10.0	51.4	94.9	16.3	15.1	12.3	0.0	0.4	0.0	0.0	203.1
1979/80	0.0	25.0	0.0	6.8	16.7	32.6	24.4	6.7	3.5	0.0	0.0	0.0	115.7
1980/81	11.2	20.4	40.3	11.1	5.3	50.6	15.3	16.6	1.3	0.0	0.0	0.0	172.1
1981/82	0.3	23.9	0.0	17.5	128.7	13.8	28.5	22.3	0.2	0.0	0.0	0.0	235.2
1982/83	2.7	0.2	27.2	4.4	4.2	62.7	17.9	8.5	2.1	0.0	0.0	2.8	132.7
1983/84	0.0	2.3	132.1	25.0	0.4	11.4	60.9	19.4	12.5	0.0	0.0	0.0	264.0
1984/85	0.0	0.5	189.9	16.4	118.5	30.9	2.3	12.7	4.2	0.0	0.0	0.0	375.4
1985/86	0.0	0.0	5.9	62.8	18.3	71.5	43.8	18.4	0.0	1.5	0.0	0.0	222.2
1986/87	5.4	0.0	17.3	2.2	47.8	20.2	16.5	4.0	6.0	0.1	0.0	0.2	119.7
1987/88	1.6	59.4	61.3	158.5	175.2	38.9	44.8	1.0	13.2	7.1	0.0	0.0	561.0
1988/89	0.0	17.2	158.6	0.0	60.5	21.0	13.4	59.0	1.4	0.0	0.0	0.0	331.1
1989/90	0.5	107.0	108.1	72.1	25.4	0.0	37.6	8.8	0.7	2.8	0.0	0.0	363.0
1990/91	0.0	17.7	5.8	121.7	7.4	43.7	46.5	2.8	0.0	0.2	0.0	0.0	245.8
1991/92	4.9	25.8	25.4	4.9	1.0	15.1	15.7	11.0	0.0	0.0	0.0	0.0	103.8
1992/93	0.0	0.0	1.3	9.0	57.5	27.1	7.4	36.4	5.0	11.1	0.0	0.0	154.8
1993/94	0.6	83.0	178.8	5.8	31.3	34.1	24.9	0.0	1.6	0.0	0.0	0.0	360.1
1994/95	0.0	0.0	58.0	12.8	15.5	0.0	24.2	38.8	14.2	0.0	0.0	0.0	163.5
1995/96	0.0	0.0	1.0	63.0	109.6	21.0	34.3	69.4	2.7	23.4	0.8	0.0	325.2
1996/97	5.6	2.5	117.1	250.1	92.3	5.1	15.4	49.3	1.8	0.0	0.0	0.0	539.2
1997/98	3.2	35.4	42.8	77.1	54.7	98.9	19.1	18.6	2.0	0.5	0.0	0.0	352.3
1998/99	0.5	1.0	0.0	45.1	45.1	24.4	63.1	4.2	3.7	0.0	0.0	0.1	187.2
1999/00	7.7	58.1	44.9	22.8	35.0	7.5	0.5	81.0	10.1	0.0	0.0	0.0	267.6
2000/01	0.0	12.6	6.4	138.7	23.1	5.3	17.1	5.3	0.4	0.0	0.0	0.0	208.9
2001/02	12.0	6.6	4.9	96.8	0.4	20.5	80.0	51.1	14.5	0.0	0.0	0.5	287.3
2002/03	0.0	13.9	67.4	55.0	13.1	18.9	50.6	26.7	0.8	0.0	0.0	0.0	246.4
2003/04	0.0	71.7	65.9	53.3	0.4	36.2	55.7	25.5	25.5	0.0	0.0	0.0	334.2
2004/05	0.0	33.5	34.3	21.7	1.1	68.9	13.9	0.0	0.0	0.0	0.0	0.0	173.4
2005/06	0.0	0.0	61.1	108.3	91.0	13.0	7.2	8.5	0.0	0.0	0.0	0.0	289.1
2006/07	0.0	100.5	18.6	0.3	4.4	11.2	4.3	11.0	0.0	0.0	0.0	0.0	150.3
2007/08	0.0	60.0	12.0	0.5	10.5	2.0	5.5	7.2	0.4	0.0	0.0	0.0	98.1
2008/09	14.9	52.5	33.9	26.6	60.3	79.7	38.1	38.4	2.8	9.5	0.2	0.0	356.9

Year	S	O	N	D	J	F	M	A	M	J	JL	A	Total
2009/10	8.2	1.2	3.4	272.6	8.1	38.9	0.0	1.0	3.0	0.0	0.0	9.1	345.6
2010/11	72.4	0.0	0.0	0.0	53.1	2.0	78.0	1.0	27.7	0.0	0.0	0.0	234.2
2011/12	0.0	7.1	0.0	40.9	74.9	0.0	0.0	27.2	0.0	0.0	1.0	0.0	151.1
2012/13	0.0	6.1	4.1	0.0	7.1	13.0	177.5	19.8	4.1	0.0	0.0	0.0	231.6
2013/14	23.1	84.1	18.3	6.1	91.7	9.1	24.1	52.1	0.3	0.0	0.3	0.0	309.1
2014/15	0.0	18.3	18.5	4.3	20.1	8.9	59.2	0.5	0.0	0.0	-	-	129.8
2014/15	0.0	0.0	202.4	56.9	-	-	-	-	-	-	-	-	259.3
Average	4.5	26.7	46.3	51.5	44.2	26..2	31.2	21.5	4.5	1.5	0.1	0.3	255.2

Maximum temperature at Igrounzar station

Year	J	F	M	A	M	J	JL	A	S	O	N	D	Average
1987	22.5	24.3	24.0	31.5	30.0	28.2	30.0	35.2	42.2	31.0	28.0	25.4	29.4
1988	23.2	25.2	25.2	33.0	29.4	35.0	44.4	45.0	41.0	34.4	26.2	24.4	32.2
1989	21.8	24.8	24.8	30.0	34.0	39.6	40.4	41.0	37.6	38.0	29.8	27.6	32.5
1990	20.4	29.4	29.4	30.2	36.0	36.0	41.8	44.8	37.2	33.0	29.8	29.2	33.1
1991	23.6	25.6	25.6	31.4	38.0	40.8	44.0	42.0	41.0	31.0	33.2	25.8	33.5
1992	26.2	28.4	28.4	39.8	37.8	32.2	40.0	42.4	39.2	30.0	29.2	24.8	33.2
1993	23.0	26.8	26.8	29.6	28.8	35.0	45.2	44.0	34.4	30.0	23.0	26.0	31.1
1994	24.2	27.4	27.4	33.8	35.4	40.8	45.2	44.6	39.0	31.2	28.7	27.0	33.7
1995	24.4	30.8	30.8	30.4	40.0	37.0	42.6	44.0	34.0	36.2	31.8	23.6	33.8
1996	25.2	27.0	27.0	30.4	37.6	37.2	38.4	40.0	37.0	34.0	34.2	31.0	33.3
1997	28.0	30.0	30.0	33.8	29.6	30.8	37.4	38.0	34.2	34.2	31.0	25.2	31.9
1998	27.6	35.4	35.4	34.0	29.4	42.4	44.6	45.2	38.8	34.0	34.0	25.8	35.6
1999	24.8	28.2	28.2	32.2	34.6	37.6	43.2	39.2	34.0	32.0	33.2	26.2	32.8
2000	26.0	35.0	35.0	28.6	37.4	41.8	45.2	41.2	38.8	35.8	30.2	28.8	35.3
2001	25.6	24.6	24.6	34.6	37.4	38.6	41.2	46.2	34.0	37.0	32.6	28.2	33.7
2002	26.6	35.0	35.0	33.0	35.6	43.6	41.4	37.0	38.6	37.4	32.4	28.2	35.3
2003	25.2	35.0	35.0	31.0	40.0	40.0	41.0	39.6	39.6	34.0	29.8	27.4	34.8
2004	25.8	29.4	29.4	32.4	34.8	38.2	45.0	44.8	40.0	31.5	29.4	27.5	34
2005	26.3	31.3	30.8	31.6	36.3	39.6	45.0	45.0	41.0	31.2	30.0	28.2	34.7
2006	24.5	28.9	29.6	32.6	34.0	41.6	44.0	46.5	39.0	32.5	31.5	27.8	34.4
2007	27.6	30.6	31.5	33.4	37.5	43.6	44.0	43.0	38.5	31.5	30.2	29.4	35.1

Year	J	F	M	A	M	J	JL	A	S	O	N	D	Average
2008	26.2	35.6	33.6	36.4	40.6	42.0	46.0	44.5	39.5	33.5	29.6	30.0	36.5
2009	25.4	29.4	29.6	35.0	39.5	44.0	44.6	46.8	40.5	35.5	32.5	30.5	36.1
2010	27.6	32.5	33.0	33.5	40.5	39.5	45.0	47.0	36.8	34.6	31.2	31.0	36
2011	32.3	33.5	33.6	36.0	42.1	41.0	43.0	45.0	35.0	36.0	31.0	30.0	36.5
2012	27.2	36.0	35.5	38.0	38.6	43.0	44.0	46.0	38.5	35.5	32.6	29.5	37
2013	28.5	32.9	33.2	34.6	36.7	41.0	45.9	47.5	36.5	36.0	32.3	31.3	36.4
2014	29.6	34.5	34.0	37.0	39.0	44.0	46.5	47.8	35.5	34.0	33.6	31.0	37.2
Average	25.7	30.3	30.2	33.1	36.1	39.1	42.8	43.3	37.9	33.8	30.8	27.9	34.2

Minimum temperature at Igrounzar station

Year	J	F	M	A	M	J	JL	A	S	O	N	D	Average
1987	1.5	3.5	3.5	4.5	7.6	2.6	14.4	11.5	10.6	4.4	2.8	1.0	5.7
1988	2.0	4.0	4.0	5.5	7.6	10.0	20.6	22.4	9.5	1.0	2.2	-4.4	7
1989	-6.0	0.1	5.0	2.0	4.8	9.0	8.4	9.0	7.4	3.4	2.0	4.0	4.1
1990	-11.0	-7.6	3.4	4.6	5.0	3.0	13.0	8.6	10.0	3.0	-1.0	-2.0	2.4
1991	-6.0	-6.0	5.2	3.4	8.0	12.6	14.6	11.6	11.0	9.6	1.0	1.0	5.5
1992	0.0	3.0	2.8	5.0	9.8	10.2	14.6	14.0	11.4	8.0	3.6	3.0	7.1
1993	0.2	2.2	3.8	4.6	8.2	10.0	13.4	9.8	12.0	8.4	4.6	0.0	6.4
1994	0.0	1.4	6.0	2.8	8.0	12.8	15.4	10.0	11.0	10.6	4.6	2.6	7.1
1995	0.0	2.2	4.2	7.2	13.0	12.0	12.6	15.0	12.6	10.2	5.0	5.0	8.3
1996	0.0	4.0	3.6	5.4	7.8	11.4	14.0	14.0	10.2	7.6	5.4	3.8	7.3
1997	4.0	5.6	2.8	7.2	5.4	11.4	14.0	14.2	11.4	8.4	7.2	3.6	7.9
1998	1.2	4.0	3.0	8.2	7.4	14.0	14.6	16.0	13.0	10.0	3.6	2.6	8.1
1999	2.8	1.4	6.4	7.0	9.0	20.4	15.2	15.6	13.4	10.6	3.4	0.0	8.8
2000	0.0	3.0	5.0	5.6	9.2	11.6	15.8	16.4	12.8	8.6	4.6	3.0	8
2001	4.6	2.0	3.0	6.6	7.2	14.2	14.6	12.6	13.0	10.0	1.6	6.4	8
2002	2.0	4.8	5.4	4.4	8.0	9.4	14.0	13.4	11.8	6.4	2.2	2.0	7
2003	0.0	0.4	3.4	7.6	10.0	11.4	15.4	13.0	10.4	4.6	6.2	2.4	7.1
2004	0.0	1.4	2.4	2.4	8.0	12.2	15.6	14.8	12.5	8.5	4.2	3.7	7.1
2005	1.0	0.0	2.0	3.5	8.5	13.0	16.2	15.8	13.8	9.0	4.0	3.8	7.6
2006	0.5	0.0	2.5	4.8	9.0	12.5	17.2	18.6	14.0	10.0	5.3	4.0	8.2

Year	J	F	M	A	M	J	JL	A	S	O	N	D	Average
2007	-5.0	-1.0	2.0	4.3	8.0	14.0	17.7	17.5	13.8	9.5	4.9	4.8	7.5
2008	-4.0	-1.3	2.0	4.8	8.5	15.6	16.2	20.0	14.6	11.0	5.1	6.0	8.2
2009	-1.0	1.3	4.0	6.3	10.0	14.8	16.8	19.5	15.0	11.3	5.3	5.6	9.1
2010	-1.5	2.0	6.0	6.2	9.0	14.0	17.3	19.0	14.8	10.6	4.8	5.0	8.9
2011	-1.0	1.5	3.5	7.0	10.5	15.3	16.8	19.6	14.0	9.6	4.0	4.3	8.8
2012	0.0	-0.5	5.0	3.5	9.5	16.0	16.5	18.0	13.5	10.4	5.6	5.0	8.5
2013	0.0	1.0	3.5	5.0	10.0	18.0	17.5	18.6	15.0	11.2	6.0	5.6	9.3
2014	0.0	0.0	3.0	3.5	11.0	17.5	18.0	18.9	15.5	12.0	6.4	6.0	9.3
Average	-0.6	1.2	3.8	5.1	8.5	12.5	15.4	15.3	12.4	8.5	4.1	3.1	7.4

Mean temperature at Igrounzar station

Year	J	F	M	A	M	J	JL	A	S	O	N	D	Average
1987	12	13.9	13.8	18	17.9	20.4	22	23.3	28.2	17.5	25.7	13.5	18.8
1988	12.1	13.5	15.6	16.3	19.7	20.9	27.2	29.8	25.2	16.1	14.2	11.4	18.5
1989	9.2	12.7	17.1	13.8	16.6	21.7	24.1	23.6	22.2	20.6	15.9	15	17.7
1990	8.7	12.8	15.6	15.7	18.5	20.3	24.7	27.3	22.4	18.1	15.1	12.7	17.7
1991	10.2	10.9	14.1	16.1	19.1	23.3	25.5	25.7	23.2	18.5	16.4	14.7	18.1
1992	11.7	14.5	15.5	19.3	21.3	19.9	25	26.4	25.1	18.8	16.3	14.3	19
1993	10.9	12.8	16	17.1	17.7	20.8	26.9	25.1	22.7	18.9	14.2	13.2	18
1994	12.2	13.2	15.7	17	18.7	23	29.3	26.8	23.7	19.7	16.8	14.5	19.2
1995	12.2	14.4	16.2	17.4	23.5	22.1	27.4	27.1	22.9	21.7	18.2	14.9	19.8
1996	13.8	12.9	13.7	16.8	19.6	24.6	25.3	25.5	22.5	21.1	17.5	14.9	19
1997	14.2	16.1	16.1	18.3	18.8	21.3	23.4	24.6	23.4	21.3	17.8	14.1	19.1
1998	13.8	16.8	18.1	17.1	17.9	23.9	26.6	26.6	24.6	21.6	17.9	13.1	19.8
1999	12.7	12.2	15	19.3	20.8	27.5	26	26.8	23.8	20.7	15.8	13.4	19.5
2000	11.5	16	18.5	16.2	20	24.3	27.2	26.6	23.5	19.6	16.3	14.9	19.6
2001	14	13.7	17.9	19.9	20.1	24.5	25.9	27.4	29	22.4	17.1	16.5	20.7
2002	14.5	15.6	16.1	17.2	20.5	22.3	25.5	24.8	23.5	22.5	17.6	15.4	19.6
2003	12.3	13.3	16.6	16.8	22.6	23.6	27.4	26.6	26	18.9	17.9	14.4	19.7
2004	13	15.4	15.6	16.8	17.6	23.8	29	27.1	26.2	20	16.8	15.6	19.7
2005	15	17.9	18.1	19.3	20.1	26.3	31.5	29.6	28.7	22.5	19.3	18.1	22.2

Year	J	F	M	A	M	J	JL	A	S	O	N	D	Average
2006	14	14.3	19.2	18	19.3	26.7	26.9	26.7	21.9	21.6	20.7	17.2	20.5
2007	15	16.6	17.6	18.9	20	24.9	24	25.4	24.3	22.4	22.5	17.7	20.8
2008	16.5	17.5	18	18.8	21.7	24.7	25.2	23.7	23.3	21.5	20.2	18.9	20.8
2009	18	19.9	19.5	23.6	20.9	25.7	27.9	27.5	23.7	22	18.3	16.5	22
2010	15.5	18.2	21.2	19.1	20	24	26.7	25.3	24.7	23.1	20.4	20.6	21.6
2011	19.6	19.9	21	21.2	21.2	25.5	26.5	26.5	24	23.1	19.6	21.2	22.4
2012	19.7	18.9	19.5	21	23.8	24.9	26.2	26.5	22.4	22.6	21.1	18.7	22.1
2013	16.9	16.5	19.9	19	21.4	25.5	26.8	26.4	23.8	23.1	21.3	18.7	21.6
2014	17.8	18	19.6	20.1	22.2	23.7	26.2	30.5	24.7	22.7	20.3	18.8	22.1
Average	13.8	15.3	17.2	18.1	20.1	23.6	26.3	26.4	24.3	20.8	18.3	15.8	20

Maximum temperature at Essaouira station

Year	J	F	M	A	M	J	JL	A	S	O	N	D	Average
1987	18.8	18.2	20.1	20.2	20.3	21.3	22.1	22.8	24.6	21.6	20.8	19.9	20.9
1988	17.9	18.4	19.8	18.5	20.1	21.3	22	23.1	24.5	22.1	20.1	18.7	20.5
1989	16.7	18.2	18.6	17.8	20	20.5	21.5	23.2	22.5	23	21.2	21.7	20.4
1990	19.6	20.6	19.2	18.2	19.5	20.2	21.5	20.1	23.7	22.9	21	19.3	20.5
1991	18.4	16.6	16.9	17.5	19	19.3	21.4	21.6	21.2	20.6	19.6	20	19.3
1992	18.9	20.1	18.8	19.3	22.2	20.8	21.1	22.4	22.6	21.4	20.4	18.4	20.5
1993	16.7	17.5	19.5	19.3	19.5	21.4	22	21.8	21.9	21.3	18.5	18.2	19.8
1994	16.2	19.3	19	19	20.2	21.5	22	21.7	21.2	21	21.2	20.9	20.3
1995	19.4	18.9	19.9	20.7	20	21.5	22.1	22.4	22.3	22.6	22.8	20.4	21.1
1996	19.6	19	19	19.9	21.3	21.6	22.4	21.5	22.5	21.4	21.3	19.2	20.7
1997	19.8	20.1	21.3	20.6	21.1	22.1	21.9	22.2	23.2	23.6	22.9	20.8	21.6
1998	20.3	21.1	22.8	19.2	20.2	21.3	21.3	22.1	22.4	21.9	20.6	18	20.9
1999	18.7	16.5	18.9	18.6	20.2	20.9	21.7	21.9	22.3	22.4	20.6	18.8	20.1
2000	18.7	18.1	20.4	18.6	19.9	20.5	20.8	21.8	21.1	14.4	18	18.5	19.2
2001	17.8	17.9	19.3	17.7	18.2	19.7	19.6	20.1	21.4	22.8	19.4	21.8	19.6
2002	20.1	19.7	20.2	19	18.6	20.6	21.4	21.5	22.6	22.8	20.9	20.2	20.6
2003	18.3	17.7	19.6	19.4	19.5	21.5	20.9	23.4	22.4	20.6	21	18.8	20.3
2004	17.6	19	18.7	20.1	19.5	20.9	23.3	23.5	21.8	21.3	20	17.2	20.2

Year	J	F	M	A	M	J	JL	A	S	O	N	D	Average
2005	16.1	14.9	20.3	17.8	18.9	20.3	19.8	21.3	21.5	21.8	19.9	17.6	19.2
2006	16	16.7	17.6	19	19.6	21	22.1	23.2	23.2	21.7	21.3	17.4	19.9
2007	17.1	16.9	-	17.7	21	22.4	21.9	21.9	22.2	-	20.1	19.4	20.1
2008	18.6	20	19.6	23.6	20	20.8	21.9	20.7	23.2	-	17.9	-	20.6
2009	17.3	18.6	20.4	19.4	-	-	23.5	22.1	24	22.5	23.1	20.3	21.1
2010	19	19.7	20.9	20.6	20.5	21.2	22.2	22.9	23.1	22.5	20	20.9	21.1
2011	20.7	18.2	19.6	20	24.1	22.2	23.2	22.1	21.6	22.1	20.8	19.9	21.2
2012	17.5	17	20.1	18.7	21	21.3	20.8	21.6	23.3	22.7	21.4	19.4	20.4
2013	18.6	18.7	19.1	19.7	24.6	25.7	29.5	33.8	25.9	24.3	22.3	21.1	23.6
2014	19.9	20	22.7	24.6	27.4	27	28.2	32.3	28.1	29.8	22.9	20.5	25.3
2015	19.3	19.4	22.5	22.4	27.9	26.5	33.5	30.5	29.1	26.7	24.5	24.3	25.6
Average	18.4	18.5	19.7	19.5	20.6	21.4	22.2	22.8	22.9	22.1	20.7	19.5	20.7

Minimum temperature at Essaouira station

Year	J	F	M	A	M	J	JL	A	S	O	N	D	Average
1987	12.4	12.5	13.6	14.9	15.9	17.2	18.3	18.5	19.2	16.6	14.5	13.4	15.6
1988	11.1	12.1	13.4	13.2	15.5	16.8	17.6	18.2	18.7	16.6	14.5	13.4	15.1
1989	9.5	11.9	13.7	14.3	16.4	17.5	18.6	20.4	19.3	19.5	18.5	17.9	16.5
1990	14.6	16.5	15.5	14.7	16.7	17.6	18.2	18.5	19.9	19	16.4	13.9	16.8
1991	10.9	10.6	12.5	12.5	13.4	15.7	17.1	17.9	17.2	16.9	13.5	13.5	14.3
1992	11.3	13.7	14.1	14.7	17.2	17.2	18	18.3	18.2	16.8	13.6	12.3	15.5
1993	9.3	11.2	13.4	14.3	14.9	17.6	18.4	18.1	18.5	16.6	13.6	12.1	14.8
1994	10.1	13.7	14.5	13.6	16.1	17.5	18.5	18.4	17.7	16.9	15.3	13.3	15.5
1995	11.6	12.9	13.9	15.9	16.4	17.1	18.3	18.3	17.9	17.2	16.6	14.6	15.9
1996	14.9	12	13.1	14.6	16.2	18	18.6	17.9	17.8	16	15.1	13.9	15.7
1997	13.4	14.4	14.5	16.2	16.2	17.4	18.2	18.6	19.4	19.1	16.7	14.5	16.6
1998	13.6	15.3	15.1	14.1	15.5	16.8	17.3	18	18.1	16.9	14.6	10.8	15.5
1999	11.6	9.6	12.8	13.6	15.3	16.9	17.2	17.7	18	17.8	14.3	11.5	14.7
2000	10.5	12.4	14.4	13.4	15.7	16.8	17	17.7	17.1	14.4	12.8	12.5	14.6
2001	12.1	11.1	13.8	13.2	13.9	16.2	16.2	16.3	16.9	16.6	13.9	14.6	14.6
2002	12.3	13	13.3	14.1	13.8	15.8	16.5	17	17.7	17.5	15.1	14.2	15

Year	J	F	M	A	M	J	JL	A	S	O	N	D	Average
2003	10.6	11.1	14.2	14.5	15.9	17.3	17.2	19.6	18.5	17.1	14.9	12.9	15.3
2004	11.1	12.6	12.1	14	14.8	16.4	18.3	18.9	17.7	17	13.5	11	14.8
2005	8.3	8.9	13.3	13	14.6	16.6	17.2	17.6	17.6	17.1	16.5	12.1	14.4
2006	10.1	11.5	12.6	14.3	16.1	18.1	19.2	20.9	20.5	18.5	18.4	13.2	16.1
2007	11.9	13	-	14.3	17.6	-	19.7	18.2	18.2	-	14.5	12.9	15.6
2008	12.2	14.8	14.2	14.8	17.2	17.3	18.2	17.9	19.1	-	12.4	-	15.8
2009	9.6	13.4	16.5	13	-	-	18.8	19.1	19.6	17.9	14.1	14.7	15.7
2010	14.6	15	15.5	16.3	16.3	17.2	19.3	19.2	19.7	18.4	13.9	16.2	16.8
2011	14	13.8	14.4	16.7	18	18.5	18.8	19.4	18	17.9	15.3	12.5	16.4
2012	10.8	9.7	14.7	13.6	15.9	17.2	17.3	17.8	19	18.3	15.5	12.4	15.2
2013	11.8	12.1	14.7	15	15.1	16.5	18.1	18.3	18.9	17.2	13.6	10.7	15.2
2014	10.1	10.3	12.2	13.9	16.1	16.7	17.5	17.9	17.9	17.5	14.5	10.2	14.6
2015	9	9	10.6	12.8	15.7	17.2	18.1	18	18.3	17.4	12.3	9.6	14
Average	11.6	12.5	13.9	14.3	15.8	17.1	18	18.4	18.4	17.4	14.9	13.2	15.4

Mean temperature at Essaouira station

Year	J	F	M	A	M	J	JL	A	S	O	N	D	Average
1987	15.6	15.4	16.9	17.6	18.1	19.3	20.2	20.7	21.9	19.1	17.7	16.7	18.2
1988	14.5	15.3	16.6	15.9	17.8	19.1	19.8	20.7	21.6	19.4	17.3	16.1	17.8
1989	13.1	15.1	16.2	16.1	18.2	19	20.1	21.8	20.9	21.3	19.9	19.8	18.4
1990	17.1	18.6	17.4	16.5	18.1	18.9	19.9	19.3	21.8	21	18.7	16.6	18.6
1991	14.6	13.7	14.7	15.2	16.3	17.5	19.2	19.8	19.2	18.7	16.8	16.7	16.9
1992	14.9	16.8	16.5	16.9	19.5	19.1	19.6	20.3	20.5	19.3	16.9	15.2	18
1993	13.1	14.5	16.4	17.1	17.5	19.5	20.1	19.8	20.1	19	16.2	15.1	17.4
1994	13.3	16.3	16.8	16.4	18.3	19.3	19.9	19.9	19.4	18.9	18.1	16.6	17.8
1995	15.2	15.8	16.6	18.1	18	19.5	20.1	20.1	19.7	19.6	19.5	17.2	18.3
1996	17	15.2	16.2	17.3	18.9	19.7	20.2	19.6	20.1	18.6	17.7	16.2	18.1
1997	16.3	17.1	17.9	18.3	18.7	19.8	20	20.3	21.2	21.1	19.5	17.3	19
1998	16.7	17.9	18.5	16.6	17.9	19.2	19.1	19.8	20	18.9	17.5	14.3	18
1999	14.8	13.1	15.7	16	17.6	18.8	19.2	19.6	20	19.8	17.4	14.8	17.2
2000	13.9	15.1	17.2	16.1	17.9	18.5	18.7	19.5	18.9	16.6	15.1	15.3	16.9

Year	J	F	M	A	M	J	JL	A	S	O	N	D	Average
2001	14.8	14.6	16.4	15.5	16	17.8	17.7	18.2	19.1	19.4	16.4	17.3	16.9
2002	15.8	15.6	16.1	16.3	16.2	18	18.7	18.9	19.9	19.9	17.5	16.8	17.5
2003	14.2	14.5	16.6	17	17.7	19.3	18.8	21.2	20.2	18.8	17.3	15.7	17.6
2004	14	15.6	15.4	16.9	17	18.3	20.2	20.8	19.7	18.8	16.7	13.9	17.3
2005	12.2	11.8	16.7	15.5	16.8	18.2	18.4	19.2	19.4	19.1	18.2	14.7	16.7
2006	13.1	14.1	15.1	16.4	17.5	19.4	20.5	21.9	21.8	19.9	20	15.2	17.9
2007	14.6	15	15.5	16.3	19.2	19.2	22.7	20.2	20.8	19	17.7	16.4	18.1
2008	16.2	17.4	17	21.1	18.4	19.2	20.4	19.6	21.2	19.5	15.8	14	18.3
2009	14.4	15.7	18.7	16.6	17.5	19.5	21.2	20.8	22.2	20.6	17.9	18.1	18.6
2010	17.1	17.4	18.5	18.7	18.7	19.6	20.6	20.8	21.5	20.6	17.1	18.7	19.1
2011	17.2	16.4	17	18.5	21.3	20.4	20.9	20.8	19.9	20.1	18.6	16.2	18.9
2012	14.4	14	17.4	16.5	18.9	19.4	19.3	19.9	21.3	20.6	18.8	16.2	18.1
2013	15.3	15.5	17.1	17.6	19.7	21.2	23.7	28	22.2	20.2	17.8	16.3	19.6
2014	15.3	15.1	17	19.2	21.8	21.8	22.6	25.2	23	23.6	19	15.8	20
2015	14.5	13.8	15.6	16.9	21	21	26	23.4	23	21.6	17.5	17.3	19.3
Average	15	15.4	16.7	17	18.2	19.2	20.1	20.6	20.6	19.7	17.8	16.2	18.1

Evapotranspiration at Igrounzar station (mm)

Year	J	F	M	A	M	J	JL	A	S	O	N	D	Total
1987	99.1	97.0	115.4	127.2	139.3	145.0	151.8	147.9	147.7	114.6	120.1	97.8	1503.0
1988	99.2	96.7	117.5	124.3	143.3	146.3	169.0	170.4	138.3	112.5	99.5	96.7	1513.6
1989	98.9	96.1	119.8	121.0	136.9	148.4	158.2	148.8	130.2	120.4	101.3	99.2	1479.2
1990	99.1	96.2	117.5	123.4	140.6	144.8	160.1	160.9	130.7	115.6	100.4	97.3	1486.7
1991	98.7	95.4	115.7	124.0	141.9	153.1	162.8	155.4	132.8	116.3	102.0	98.9	1496.9
1992	99.0	97.5	117.4	129.8	147.4	143.8	161.1	157.7	138.0	116.8	101.8	98.5	1508.9
1993	98.8	96.2	118.1	125.6	138.9	146.1	167.8	153.4	131.5	117.0	99.5	97.6	1490.5
1994	99.2	96.5	117.7	125.4	141.0	152.2	177.3	159.1	134.1	118.5	102.5	98.7	1522.1
1995	99.2	97.5	118.4	126.1	153.7	149.6	169.7	160.2	132.0	122.8	104.5	99.1	1532.6
1996	100.3	96.3	115.3	125.1	143.1	157.1	162.1	154.7	131.0	121.4	103.5	99.1	1509.0
1997	100.6	99.3	118.2	127.8	141.3	147.4	155.9	151.8	133.3	121.9	103.9	98.3	1499.7
1998	100.3	100.2	121.5	125.6	139.3	154.9	166.7	158.4	136.6	122.5	104.1	97.5	1527.6
1999	99.5	95.9	116.7	129.8	146.1	167.3	164.6	159.1	134.4	120.6	101.2	97.7	1532.8

Year	J	F	M	A	M	J	JL	A	S	O	N	D	Total
2000	98.9	99.2	122.2	124.1	144.0	156.2	169.0	158.4	133.6	118.3	101.8	99.1	1524.8
2001	100.5	96.8	121.1	131.1	144.3	156.8	164.2	161.3	150.5	124.4	102.9	100.9	1554.8
2002	100.9	98.7	118.2	125.7	145.3	150.1	162.8	152.5	133.6	124.6	103.6	99.6	1515.7
2003	99.3	96.5	119.0	125.1	151.0	154.0	169.7	158.4	140.7	117.0	104.1	98.6	1533.3
2004	99.7	98.5	117.5	125.1	138.7	154.6	176.0	160.2	141.3	119.1	102.5	99.8	1533.0
2005	101.4	101.7	121.5	129.8	144.3	162.9	186.8	169.6	149.4	124.6	106.3	103.2	1601.7
2006	100.5	97.4	123.6	127.2	142.4	145.8	148.8	143.4	129.5	122.5	108.9	101.9	1491.8
2007	101.4	99.9	120.6	128.9	144.0	149.0	154.7	151.2	135.7	124.4	112.5	102.6	1525.1
2008	103.2	101.1	121.3	128.7	148.4	148.4	161.8	146.2	133.0	122.3	107.9	104.5	1527.0
2009	105.4	105.0	124.2	140.3	146.3	148.4	154.4	144.5	134.1	123.5	104.7	100.9	1531.7
2010	102.0	102.2	127.9	129.4	144.0	149.3	156.9	147.9	136.9	126.1	108.3	107.5	1538.2
2011	108.1	105.0	127.4	134.1	147.1	149.6	155.0	147.9	134.9	126.1	106.9	108.6	1550.5
2012	108.3	103.3	124.2	133.6	154.6	151.9	155.9	147.9	130.7	124.9	109.7	104.1	1549.0
2013	103.8	99.8	125.0	129.1	147.6	149.0	151.2	145.3	134.4	126.1	110.1	104.1	1525.5
2014	105.1	101.9	124.4	131.5	149.8	154.3	165.3	173.3	136.9	125.1	108.1	104.3	1579.9
Average	101.1	98.8	120.3	127.8	144.5	151.3	162.9	155.2	135.9	121.1	105.1	100.6	1524.5

Evapotranspiration Essaouira station (mm)

Year	J	F	M	A	M	J	JL	A	S	O	N	D	Total
1987	102.1	98.4	119.4	126.4	139.8	142.3	147.0	140.8	129.5	117.4	103.7	101.1	1467.7
1988	100.9	98.3	119.0	123.6	139.1	141.8	146.0	140.8	128.8	117.9	103.2	100.4	1459.7
1989	99.7	98.1	118.3	123.9	140.0	141.7	146.6	143.7	127.2	121.8	107.3	106.0	1474.3
1990	104.1	102.7	120.2	124.5	139.8	141.5	146.1	137.6	129.3	121.1	105.3	101.1	1473.2
1991	101.0	96.8	116.4	122.7	136.4	138.6	144.6	138.7	123.6	116.6	102.5	101.2	1439.0
1992	101.3	100.2	118.8	125.2	142.9	141.9	145.5	139.9	126.3	117.8	102.6	99.4	1461.8
1993	99.7	97.5	118.7	125.6	138.6	142.9	146.7	138.7	125.4	117.2	101.7	99.3	1452.0
1994	99.9	99.5	119.3	124.4	140.2	142.4	146.2	139.0	124.0	117.0	104.4	101.1	1457.3
1995	101.7	98.9	119.0	127.4	139.6	142.9	146.7	139.4	124.6	118.3	106.7	101.9	1467.0
1996	103.9	98.3	118.4	125.9	141.5	143.3	147.0	138.3	125.4	116.5	103.8	100.6	1462.7
1997	103.0	100.6	121.1	127.8	141.0	143.6	146.5	139.9	127.9	121.4	106.7	102.0	1481.4
1998	103.5	101.7	122.2	124.7	139.3	142.2	144.3	138.7	125.2	117.0	103.5	98.5	1460.9
1999	101.2	96.4	117.7	123.8	138.7	141.3	144.6	138.3	125.2	118.7	103.3	99.0	1448.2
2000	100.4	98.1	119.9	124.0	139.3	140.6	143.4	138.0	123.0	113.2	100.4	99.5	1439.9

Year	J	F	M	A	M	J	JL	A	S	O	N	D	Total
2001	101.2	97.6	118.7	123.1	135.8	139.1	141.3	135.2	123.4	117.9	102.0	102.0	1437.5
2002	102.4	98.7	118.2	124.3	136.2	139.6	143.4	136.7	125.0	118.9	103.5	101.3	1448.1
2003	100.6	97.5	119.0	125.4	138.9	142.4	143.6	142.1	125.6	116.8	103.2	100.0	1455.3
2004	100.5	98.7	117.3	125.2	137.6	140.2	147.0	141.1	124.6	116.8	102.4	98.1	1449.4
2005	99.2	95.7	119.1	123.1	137.2	140.0	142.8	137.4	124.0	117.4	104.5	98.9	1439.2
2006	99.7	97.2	116.9	124.4	138.6	142.6	147.7	144.0	129.3	118.9	107.6	99.4	1466.3
2007	101.0	98.0	117.4	124.3	142.2	142.2	153.8	139.7	126.9	117.2	103.8	100.8	1467.3
2008	102.9	101.0	119.6	133.8	140.4	142.2	147.5	138.3	127.9	118.1	101.2	98.2	1471.0
2009	100.8	98.8	122.6	124.7	138.6	142.9	149.6	141.1	130.2	120.4	104.1	103.2	1477.0
2010	104.1	101.0	122.2	128.5	141.0	143.1	148.0	141.1	128.6	120.4	102.9	104.1	1485.0
2011	104.2	99.7	119.6	128.1	147.4	145.0	148.8	141.1	125.0	119.3	105.2	100.6	1484.0
2012	100.8	97.1	120.3	124.6	141.5	142.6	144.8	139.0	128.1	120.4	105.5	100.6	1465.1
2013	101.8	98.6	119.8	126.5	143.3	147.1	156.9	163.5	130.2	119.5	103.9	100.7	1511.7
2014	101.8	98.1	119.6	129.6	148.7	148.7	153.5	153.7	132.3	127.3	105.8	100.1	1519.3
2015	100.9	96.9	117.5	125.2	146.6	146.6	164.6	148.2	132.3	122.5	103.5	102.0	1506.8
Year	101.5	98.6	119.2	125.5	140.3	142.4	147.4	141.2	126.8	118.8	103.9	100.7	1466.5

Flow at Igrounzar station (m3/s)

Year	S	O	N	D	J	F	M	A	M	J	JL	A	Average
1979/80	0.07	0.89	0.31	0.26	0.43	0.56	0.77	0.36	0.19	0.13	0.13	0.13	0.35
1980/81	0.15	0.19	1.60	0.55	0.44	0.35	0.14	0.11	0.11	0.13	0.09	0.10	0.33
1981/82	0.10	0.12	0.12	0.14	0.71	0.06	0.23	0.28	0.56	0.08	0.08	0.07	0.21
1982/83	0.08	0.08	0.27	0.15	0.24	0.33	0.16	0.13	0.13	0.13	0.13	0.13	0.16
1983/84	0.13	0.13	0.55	0.06	0.05	0.04	0.07	0.04	0.04	0.03	0.03	0.04	0.10
1984/85	0.04	0.04	0.23	0.04	5.21	0.22	0.13	0.10	0.09	0.27	0.05	0.05	0.54
1985/86	0.04	0.05	0.05	0.11	0.12	0.25	0.49	0.18	0.06	0.07	0.06	0.06	0.13
1986/87	0.06	0.06	0.08	0.07	0.19	0.38	0.30	0.08	0.08	0.08	0.08	0.08	0.13
1987/88	2.70	0.45	0.56	2.16	1.02	0.87	1.03	0.26	0.35	0.16	0.07	0.06	0.81
1988/89	0.06	0.24	2.66	0.30	0.39	0.17	0.23	0.58	0.15	0.10	0.09	0.11	0.42
1989/90	0.10	0.18	0.47	0.51	0.45	0.18	0.29	0.27	0.13	0.11	0.12	0.11	0.24
1990/91	0.11	0.12	0.14	0.56	0.18	1.45	2.76	1.58	0.59	0.35	0.29	0.33	0.70
1991/92	0.18	0.33	0.14	0.34	0.07	0.07	0.04	0.13	0.01	0.02	0.01	0.01	0.11
1992/93	0.01	0.03	0.03	0.08	0.11	0.14	0.08	0.01	0.12	0.03	0.02	0.03	0.06

Year	S	O	N	D	J	F	M	A	M	J	JL	A	Average
1993/94	0.03	0.18	0.42	0.15	0.19	0.26	0.20	0.06	0.06	0.06	0.05	0.05	0.14
1994/95	0.05	0.07	0.06	0.06	0.07	0.22	0.43	0.56	0.04	0.04	0.05	0.04	0.14
1995/96	0.04	0.04	1.08	1.65	9.24	1.96	2.61	1.46	1.26	0.90	0.20	0.18	1.72
1996/97	0.19	0.19	1.21	4.12	5.55	1.93	2.27	1.32	0.42	0.35	0.33	0.30	1.52
1997/98	0.30	0.51	0.61	0.62	0.63	3.12	1.44	0.47	0.36	0.33	0.29	0.29	0.75
1998/99	0.31	0.33	0.33	0.36	0.44	0.43	0.37	0.22	0.24	0.18	0.15	0.39	0.31
1999/00	1.10	0.84	0.24	0.23	0.22	0.21	0.14	0.29	0.13	0.11	0.11	0.11	0.31
2000/01	0.13	0.14	0.15	0.73	0.19	0.13	0.12	0.09	0.08	0.07	0.07	0.07	0.16
2001/02	0.09	0.10	0.11	2.47	0.18	0.16	0.21	0.24	0.15	0.12	0.13	0.13	0.34
2002/03	0.13	0.20	0.49	0.20	0.18	0.16	0.13	0.09	0.07	0.06	0.04	0.07	0.15
2003/04	0.05	0.08	0.32	0.25	0.19	0.24	0.26	0.21	0.21	0.10	0.10	0.10	0.18
2004/05	0.09	0.10	0.11	2.47	0.18	0.16	0.21	0.24	0.15	0.12	0.13	0.13	0.34
2005/06	0.13	0.20	0.49	0.20	0.18	0.16	0.13	0.09	0.07	0.06	0.04	0.07	0.15
2006/07	0.05	0.08	0.32	0.25	0.19	0.24	0.26	0.21	0.21	0.10	0.10	0.10	0.18
2007/08	0.06	0.06	2.43	0.25	0.23	0.16	0.11	0.30	0.51	0.51	0.53	0.55	0.48
2008/09	1.56	2.00	4.07	0.07	0.57	4.70	0.45	0.25	0.18	1.49	0.59	3.57	1.62
Average	0.27	0.27	0.66	0.65	0.93	0.64	0.54	0.34	0.23	0.21	0.14	0.25	0.43

Flow at Zelten station (m3/s)

Year	S	O	N	D	J	F	M	A	M	J	JL	A	Average
1979/80	0.03	0.82	0.01	0.01	0.38	0.83	0.79	0.09	0.05	0.04	0.03	0.03	0.26
1980/81	0.03	0.03	2.38	0.03	0.02	1.27	0.11	0.04	0.04	0.04	0.03	0.03	0.34
1981/82	0.03	0.06	0.03	0.04	1.91	0.03	0.42	0.39	1.83	0.02	0.02	0.01	0.40
1982/83	0.01	0.01	0.56	0.05	0.05	0.38	0.01	0.01	0.01	0.00	0.00	0.00	0.09
1983/84	0.00	0.00	2.71	0.03	0.03	0.03	0.25	0.08	0.03	0.02	0.01	0.01	0.27
1984/85	0.01	0.01	1.97	0.05	6.66	0.09	0.05	0.09	0.02	0.02	0.01	0.01	0.75
1985/86	0.01	0.01	0.01	0.10	0.01	0.48	1.53	0.25	0.03	0.03	0.03	0.03	0.21
1986/87	0.03	0.03	0.09	0.02	0.26	0.51	0.06	0.03	0.03	0.03	0.02	0.02	0.09
1987/88	1.54	0.64	0.89	4.88	2.43	0.82	1.10	0.10	0.35	0.08	0.07	0.07	1.08
1988/89	0.06	0.45	3.25	0.50	0.82	0.07	0.36	0.87	0.03	0.02	0.02	0.02	0.54
1989/90	0.02	0.08	1.45	1.57	0.50	0.14	0.37	0.47	0.05	0.01	0.01	0.01	0.39
1990/91	0.01	0.01	0.01	1.21	0.01	2.80	1.71	0.11	0.07	0.06	0.05	0.06	0.51
1991/92	0.07	0.36	0.01	0.01	0.01	0.02	0.01	0.38	0.01	0.01	0.01	0.01	0.08

Year	S	O	N	D	J	F	M	A	M	J	JL	A	Average
1992/93	0.01	0.01	0.01	0.10	0.33	0.17	0.36	0.04	0.41	0.05	0.33	0.02	0.15
1993/94	0.02	0.33	1.66	0.03	0.10	0.33	0.06	0.03	0.02	0.02	0.02	0.01	0.22
1994/95	0.02	0.07	0.02	0.02	0.02	0.32	1.93	1.42	0.00	0.00	0.00	0.00	0.32
1995/96	0.00	0.06	3.26	8.43	20.82	2.41	6.31	0.22	0.27	0.08	0.05	0.04	3.50
1996/97	0.04	0.04	2.76	7.80	5.43	0.47	1.16	1.57	0.10	0.07	0.06	0.05	1.63
1997/98	0.17	1.82	0.57	0.63	1.45	5.59	0.63	0.14	0.06	0.05	0.04	0.04	0.93
1998/99	0.04	0.04	0.04	0.14	0.27	0.09	0.21	0.02	0.14	0.04	0.03	0.04	0.09
1999/00	0.03	0.68	0.09	0.10	0.07	0.05	0.04	0.32	0.04	0.03	0.03	0.03	0.13
2000/01	0.03	0.03	0.03	1.56	0.11	0.02	0.04	0.02	0.02	0.02	0.02	0.02	0.16
2001/02	0.02	0.02	0.02	3.68	0.01	0.01	0.12	0.37	0.04	0.03	0.02	0.02	0.37
2002/03	0.02	0.02	1.06	0.06	0.03	0.03	0.09	0.05	0.03	0.02	0.02	0.06	0.12
2003/04	0.02	0.22	0.96	0.26	0.13	0.41	0.44	0.14	0.26	0.09	0.02	0.02	0.25
2004/05	0.02	0.02	0.04	0.12	0.04	0.22	0.30	0.04	0.03	0.03	0.03	0.03	0.08
2005/06	0.03	0.03	5.45	0.10	1.18	0.32	0.26	0.59	0.02	0.02	0.01	0.01	0.67
2006/07	0.02	2.94	0.54	0.34	0.53	0.58	0.24	0.37	0.17	0.18	0.18	0.18	0.52
2007/08	0.18	0.18	5.39	0.54	0.87	0.04	0.02	0.02	0.02	0.02	0.08	0.01	0.61
2008/09	0.84	1.18	5.36	0.71	1.35	0.04	0.03	0.02	0.05	0.07	0.05	0.05	0.81
Average	0.11	0.34	1.35	1.10	1.53	0.62	0.63	0.28	0.14	0.04	0.04	0.03	0.52

Débits à la station d'Adamna (m3/s)

Year	S	O	N	D	J	F	M	A	M	J	JL	A	Average
1979/80	0.56	3.05	0.25	0.25	1.28	2.34	3.27	0.23	0.01	0.00	0.00	0.00	0.94
1980/81	0.00	0.02	4.88	0.15	0.08	3.79	0.22	0.01	0.00	0.03	0.00	0.00	0.76
1981/82	0.00	0.07	0.00	0.23	6.91	0.08	1.86	2.90	2.91	0.01	0.00	0.00	1.25
1982/83	0.00	0.00	1.54	0.02	0.01	1.94	0.13	0.00	0.00	0.00	0.00	0.00	0.30
1983/84	0.00	0.00	7.28	0.08	0.00	0.00	0.72	0.14	0.05	0.00	0.00	0.00	0.69
1984/85	0.00	0.00	5.06	0.14	15.75	0.39	0.05	0.13	0.01	0.12	0.00	0.00	1.80
1985/86	0.00	0.00	0.00	0.29	0.66	0.82	2.96	0.85	0.00	0.00	0.00	0.00	0.46
1986/87	0.00	0.00	0.07	0.00	1.21	1.39	0.24	0.00	0.00	0.00	0.00	0.00	0.24
1987/88	2.68	1.41	3.15	14.00	8.21	2.23	3.29	0.09	0.56	0.00	0.00	0.00	2.97
1988/89	0.00	0.66	16.66	0.35	1.32	0.06	0.49	1.83	0.06	0.00	0.00	0.00	1.78
1989/90	0.00	0.38	2.03	2.02	1.00	0.15	0.60	0.72	0.05	0.00	0.00	0.00	0.58
1990/91	0.00	0.00	0.00	3.04	0.58	5.92	7.55	1.06	0.01	0.00	0.00	0.00	1.51

Year	S	O	N	D	J	F	M	A	M	J	JL	A	Average
1991/92	0.00	1.01	0.00	0.29	0.09	0.06	0.04	0.51	0.00	0.00	0.00	0.00	0.17
1992/93	0.00	0.00	0.00	0.13	0.31	0.38	0.32	0.00	0.26	0.00	0.00	0.00	0.12
1993/94	0.00	0.96	3.24	0.04	0.32	0.67	0.12	0.00	0.00	0.00	0.03	0.00	0.45
1994/95	0.00	0.06	0.01	0.00	0.00	1.10	4.80	4.11	0.01	0.00	0.00	0.00	0.84
1995/96	0.00	0.05	5.29	13.12	44.75	5.30	9.82	1.13	0.78	0.85	0.13	0.09	6.78
1996/97	0.11	0.12	4.45	14.74	12.47	2.16	2.45	2.49	0.93	0.65	0.54	0.48	3.47
1997/98	0.63	2.07	1.15	1.11	2.03	12.30	2.76	0.69	0.17	0.05	0.00	0.00	1.91
1998/99	0.00	0.00	0.03	0.43	1.35	0.28	0.92	0.03	0.45	0.00	0.00	0.10	0.30
1999/00	0.05	3.75	0.39	0.44	0.24	0.11	0.00	1.08	0.00	0.00	0.00	0.00	0.50
2000/01	0.00	0.00	0.00	8.36	0.96	0.05	0.03	0.00	0.00	0.00	0.00	0.00	0.78
2001/02	0.04	0.00	0.00	11.30	0.20	0.00	1.49	2.37	0.02	0.00	0.00	0.00	1.28
2002/03	0.00	0.34	5.20	0.70	0.09	0.00	0.30	0.27	0.00	0.00	0.00	0.16	0.59
2003/04	0.00	0.46	3.51	0.39	0.01	0.97	1.11	0.02	0.35	0.00	0.00	0.00	0.57
2004/05	0.00	0.00	0.00	0.28	0.00	0.70	1.11	0.00	0.00	0.00	0.00	0.00	0.17
2005/06	0.00	0.00	13.86	2.39	5.96	0.94	0.11	1.53	0.05	0.00	0.00	0.00	2.07
2006/07	0.00	3.02	1.60	0.43	0.67	0.70	0.06	0.16	0.16	0.00	0.00	0.00	0.57
2007/08	0.00	0.00	3.05	0.33	0.33	0.01	0.00	0.00	0.00	0.00	0.02	0.00	0.31
2008/09	0.87	1.22	8.59	0.28	1.55	9.52	0.82	0.06	0.06	0.55	0.07	0.00	1.97
2009/10	0.76	0.00	0.00	24.09	2.24	12.13	3.32	0.55	0.10	0.00	0.08	0.46	3.64
2010/11	0.00	0.00	5.42	4.56	1.51	0.48	2.17	1.11	2.26	0.24	0.00	0.00	1.48
2011/12	0.00	0.00	0.73	0.30	0.26	0.20	0.01	0.06	0.00	0.00	0.00	0.00	0.13
2012/13	2.02	2.41	2.24	0.59	0.01	0.02	2.09	0.29	0.00	0.00	0.00	0.00	0.81
2013/14	0.63	0.02	0.00	0.00	0.35	0.01	0.01	0.05	0.29	0.00	0.00	0.00	0.11
2014/15	0.00	0.00	2.38	2.30	0.03	0.01	0.01	0.00	0.00	0.00	0.00	0.48	0.43
Avearge	0.16	0.62	3.04	2.51	3.61	1.81	1.59	0.75	0.23	0.08	0.03	0.03	1.20

Annex II
Groundwater level data

Campaign of march 2019: Cenomano-Turonian Aquifer

Sample	X	Y	Z	H	pH	T	EC	Aquifer
	m					°C	µS/cm	
75/52	128124	103181	461	445.2	8.0	18.0	2750	Cenomano-Turonian
89/52	106174	117707	190	178.1	7.4	21.7	2203	Cenomano-Turonian
105/52	138360	98205	604	602.6	7.1	17.3	3646	Cenomano-Turonian
612/52	107407	122209	204	176.2	7.4	20.8	3286	Cenomano-Turonian
613/52	138667	93423	684	674.1	8.0	14.9	1843	Cenomano-Turonian
776/52	141554	95298	637	622.7	7.3	18.8	2173	Cenomano-Turonian
874/52	109190	110628	283	269.9	7.3	20.8	4349	Cenomano-Turonian
883/52	103987	116773	200	165.9	7.1	23.0	2804	Cenomano-Turonian
1112/52	138581	99269	591	555.7	7.5	21.4	1411	Cenomano-Turonian
1209/52	113440	113628	355	-	7.2	23.6	1075	Cenomano-Turonian
1699/52	141573	96319	627	597.5	7.6	20.3	1543	Cenomano-Turonian
O30	130545	101944	500	485.0	7.6	18.0	3389	Cenomano-Turonian
O31	131340	102793	493	485.5	7.5	17.5	1192	Cenomano-Turonian
O33	141474	93754	669	640.3	7.4	19.6	1584	Cenomano-Turonian
O34	132390	100749	526	485.2	7.2	22.2	1261	Cenomano-Turonian
O35	134110	106742	543	518.4	7.8	21.0	862	Cenomano-Turonian
O37	128911	104147	466	453.5	7.2	20.5	4965	Cenomano-Turonian
O39	121773	103695	390	374.3	7.5	20.7	2087	Cenomano-Turonian
O40	119621	106390	347	340.2	7.2	21.0	2149	Cenomano-Turonian
O42	118207	109602	319	291.0	7.7	22.1	2440	Cenomano-Turonian
O46	119814	104010	414	398.9	7.0	22.8	2939	Cenomano-Turonian
O49	110383	116191	222	195.1	7.5	22.7	2148	Cenomano-Turonian
O51	111820	128010	224	173.7	7.2	22.2	2277	Cenomano-Turonian
O52	114269	124836	324	315.1	7.4	21.0	2140	Cenomano-Turonian
O53	103021	119806	190	179.2	7.3	20.8	2657	Cenomano-Turonian
O54	98283	126062	74	63.1	7.6	21.5	2266	Cenomano-Turonian
O55	100532	129964	67	37.4	7.6	21.0	2230	Cenomano-Turonian
O56	94383	125259	11	1.0	7.2	20.7	4277	Cenomano-Turonian
O85	136167	93466	713	701.1	7.1	16.5	1574	Cenomano-Turonian
O90	103393	91167	238	-	8.4	17.8	615	Cenomano-Turonian

Sample	X	Y	Z	H	pH	T	EC	Aquifer
	m					°C	µS/cm	
O105	128503	96158	586	578.9	7.8	21.0	796	Cenomano-Turonian
O106	115169	105125	367	357.0	7.3	19.2	4216	Cenomano-Turonian
O107	117229	100359	444	437.3	7.1	19.5	3690	Cenomano-Turonian
O108	125042	100877	469	455.0	7.8	19.3	1336	Cenomano-Turonian
O109	119343	112497	354	323.3	7.4	20.8	1873	Cenomano-Turonian
O110	125509	113399	411	400.6	7.4	19.2	4370	Cenomano-Turonian
O122	130057	94712	662	655.3	7.6	18.9	882	Cenomano-Turonian
O123	102959	124849	95	-	7.4	22.9	3220	Cenomano-Turonian
O124	113568	115297	264	225.6	7.3	21.5	2650	Cenomano-Turonian
72/52	118004	95743	398	387.4	7.5	19.2	2428	Cenomano-Turonian
809/52	127541	93680	638	629.7	7.8	20.0	736	Cenomano-Turonian
820/52	117336	97635	437	429.7	7.5	21.1	4380	Cenomano-Turonian

Campaign of march 2019: Cenomano-Turonian Aquifer

Sample	X	Y	Z	H	pH	T	EC	Aquifer
	m					°C	µS/cm	
1415/52	113055	96725	370	330.5	7.2	24.0	972	Cenomano-Turonian
O61	118637	93594	408	-	7.1	21.7	2179	Cenomano-Turonian
O62	116879	95278	390	383.4	7.8	18.0	2249	Cenomano-Turonian
O64	110501	94855	313	303.3	7.6	20.3	2199	Cenomano-Turonian
O65	107935	92867	272	257.8	7.7	20.8	2381	Cenomano-Turonian
O66	114500	98776	422	407.4	7.5	22.0	1888	Cenomano-Turonian
O68	107992	96978	400	390.3	7.5	20.2	3842	Cenomano-Turonian
O69	105616	95999	330	325.2	7.4	21.5	4530	Cenomano-Turonian
O73	119124	97847	415	394.4	7.8	19.6	2123	Cenomano-Turonian
O74	119893	100610	436	428.1	7.4	20.8	1559	Cenomano-Turonian
O75	121120	99785	437	417.7	7.5	21.4	1510	Cenomano-Turonian
O78	121875	96049	446	437.9	7.6	20.9	3016	Cenomano-Turonian
O79	120482	96457	426	399.3	7.7	21.4	2500	Cenomano-Turonian
O80	121473	97981	429	411.7	7.2	20.3	5738	Cenomano-Turonian
O125	123518	99423	458	408.2	7.8	21.3	1020	Cenomano-Turonian

Campaign of march 2019: Plio-Quaternary Aquifer

Sample	X	Y	Z	H	pH	T	EC	Aquifer
	m					°C	μS/cm	
3/51	81472	93666	7	-2.9	9.2	21.3	2511	Plio-Quaternary
11/51	80383	96193	3	-1.2	8.0	17.3	12250	Plio-Quaternary
15/51	85890	97935	65	56.8	7.6	19.5	1322	Plio-Quaternary
21/51	89582	91439	128	99.9	7.3	22.6	4840	Plio-Quaternary
27/51	95370	91109	201	170.3	7.7	21.7	880	Plio-Quaternary
28/51	97284	91810	234	184.6	7.6	22.2	947	Plio-Quaternary
105/51	99400	100885	115	103.5	7.5	22.5	1991	Plio-Quaternary
140/51	87205	103776	60	43.6	7.9	19.7	2091	Plio-Quaternary
148/51	85703	102084	58	43.5	7.5	20.8	1559	Plio-Quaternary
149/51	85100	105800	36	-1.7	7.4	22.6	3386	Plio-Quaternary
261/51	96540	99238	118	72.5	7.2	23.4	2099	Plio-Quaternary
272/51	97195	100703	105.5	76.0	7.4	21.0	1750	Plio-Quaternary
327/51	89220	88690	124	96.0	7.5	21.9	3800	Plio-Quaternary
O2	91918	94633	142	57.9	7.8	25.0	1839	Plio-Quaternary
O4	97352	101259	102	79.3	7.5	20.7	1729	Plio-Quaternary
O5	91853	102137	83	54.4	7.7	20.6	1678	Plio-Quaternary
O6	91193	102500	70	54.2	7.3	20.5	1811	Plio-Quaternary
O7	90976	101554	75	53.8	7.6	21.4	1333	Plio-Quaternary
O91	90829	97430	102	61.9	7.7	23.1	2985	Plio-Quaternary
O94	81369	93593	4	-0.7	7.8	21.0	2284	Plio-Quaternary
O96	83000	93735	21	14.0	7.9	20.9	1702	Plio-Quaternary
O98	97273	101093	100	-	8.2	18.1	1751	Plio-Quaternary
O99	85578	105624	13	-	9.1	24.1	2626	Plio-Quaternary
O111	87675	91861	112	79.9	7.1	23.1	2757	Plio-Quaternary

Campaign of march 2019: Plio-Quaternary Aquifer

Sample	X	Y	Z	H	pH	T	EC	Aquifer
	m					°C	µS/cm	
O112	94027	95124	161	100.8	-	-	-	Plio-Quaternary
O113	87063	95467	101	82.6	7.8	19.3	9641	Plio-Quaternary
O126	93744	93784	151	95.7	-	-	-	Plio-Quaternary
O127	91965	98689	102	-	7.6	22.4	2663	Plio-Quaternary
O128	96120	100431	110	-	-	-	-	Plio-Quaternary

Campaign of march 2019: Barremian-Aptian Aquifer

Sample	X	Y	Z	H	pH	T	EC	Aquifer
	m					°C	µS/cm	
P5	89504	77758	244	-	7.4	21.4	1687	Barremian-Aptian
P11	85483	73677	271	252.8	7.7	22.8	1240	Barremian-Aptian
173/51	91073	77100	289	263.4	7.6	22.6	1608	Barremian-Aptian
175/51	93600	74914	351	337.0	7.5	20.9	1571	Barremian-Aptian
176/51	96737	76130	423	413.9	7.9	18.5	1700	Barremian-Aptian
181/51	83495	77133	161	159.5	7.6	18.8	2051	Barremian-Aptian
209/51	80229	73441	141	137.5	7.4	20.7	1318	Barremian-Aptian
208/51	80513	72537	221	216.6	7.5	18.3	1950	Barremian-Aptian
216/51	83750	80350	174	-	7.8	22.2	1783	Barremian-Aptian
217/51	85015	73957	253	238.7	8.0	20.1	1367	Barremian-Aptian
480/51	86908	78386	253	156.0	7.4	23.8	1786	Barremian-Aptian
M74	95250	75315	406	402.6	7.4	16.9	1303	Barremian-Aptian
M84	88000	79900	239	214.3	7.3	22.4	3433	Barremian-Aptian
O14	103564	77103	529	522.4	7.4	18.2	3880	Barremian-Aptian
O17	89662	76734	261	258.2	7.1	20.8	1994	Barremian-Aptian
O19	78995	80733	1	-	8.1	19.0	1977	Barremian-Aptian
O20	82222	81119	82	-	7.4	23.2	2562	Barremian-Aptian
O22	82807	81381	100	75.5	7.3	22.7	2874	Barremian-Aptian
O23	84686	80911	208	149.2	-	-	-	Barremian-Aptian
O129	104713	77013	536	-	7.5	22.8	1613	Barremian-Aptian

Campaign of march 2019: Hautrevian Aquifer

Sample	X	Y	Z	H	pH	T	EC	Aquifer
	m					°C	µS/cm	
163/52	93398	63491	164	153,5	7,3	22,0	1350	Hautrevian
P9	90126	63897	143	-	7,4	24,0	1735	Hautrevian
O24	89239	63810	123	117,4	7,9	18,0	1799	Hautrevian
O25	87764	64270	148	-	7,2	23,5	1836	Hautrevian
O26	89651	63823	135	-	7,4	24,6	1708	Hautrevian
O28	92680	63541	160	-	7,3	24,8	1749	Hautrevian
O29	94921	64380	195	-	8,1	21,4	1130	Hautrevian
O102	89177	64188	156	148,4	7,2	21,9	1601	Hautrevian
O115	98271	68747	335	325,7	7,5	22,8	2405	Hautrevian
O117	94198	68475	287	277,2	7,7	22,8	1113	Hautrevian

Campaign of march 2019: Hautrevian Aquifer

Sample	X	Y	Z	H	pH	T	EC	Aquifer
	m					°C	µS/cm	
O118	90605	67791	267	257,5	8,2	21,9	687	Hautrevian
O120	89536	64080	179	174,6	7,1	21,7	1589	Hautrevian

Campaign of may 2018: Cenomano-Turonian Aquifer

Sample	X	Y	Z	H	pH	T	EC	Aquifer
	m					°C	µS/cm	
54/43	103100	124800	96	-	7.2	22.4	3363	Cenomano-Turonian
75/52	128124	103181	461	445.8	7.9	17.9	2196	Cenomano-Turonian
89/52	106174	117707	190	178.7	7.5	22.6	1925	Cenomano-Turonian
105/52	138360	98205	604	602.0	7.7	17.0	3991	Cenomano-Turonian
108/52	123518	99423	461	411.8	8.8	21.4	986	Cenomano-Turonian
612/52	107407	122209	204	176.2	7.3	21.6	3984	Cenomano-Turonian
613/52	138667	93423	684	674.1	7.9	16.2	1747	Cenomano-Turonian
648/52	132420	101017	524	485.0	7.3	22.0	1248	Cenomano-Turonian
776/52	141554	95298	637	620.4	7.5	20.3	1571	Cenomano-Turonian
874/52	109190	110628	283	269.9	7.6	21.6	4372	Cenomano-Turonian
883/52	103987	116773	200	166.1	7.2	23.4	2769	Cenomano-Turonian

Sample	X	Y	Z	H	pH	T	EC	Aquifer
	m					°C	µS/cm	
1112/52	138581	99269	591	555.8	8.1	21.0	1350	Cenomano-Turonian
1699/52	141573	96319	627	599.1	7.5	20.7	1966	Cenomano-Turonian
O30	130545	101944	500	484.1	7.7	18.5	2801	Cenomano-Turonian
O31	131340	102793	493	487.4	7.8	18.4	1198	Cenomano-Turonian
O33	141474	93754	669	640.9	7.7	20.5	1624	Cenomano-Turonian
O34	132390	100749	526	485.6	7.6	23.2	1163	Cenomano-Turonian
O35	134110	106742	543	518.8	8.1	20.4	833	Cenomano-Turonian
O37	128911	104147	466	454.1	7.3	20.4	4802	Cenomano-Turonian
O39	121773	103695	390	374.1	7.7	20.6	2429	Cenomano-Turonian
O40	119621	106390	347	341.3	7.5	21.7	2170	Cenomano-Turonian
O41	120676	105816	412	392.4	7.8	22.9	2214	Cenomano-Turonian
O42	118207	109602	319	290.9	8.4	22.4	2359	Cenomano-Turonian
O46	119814	104010	414	405.0	7.2	23.1	3256	Cenomano-Turonian
O49	110383	116191	219	192.1	7.5	23.0	2200	Cenomano-Turonian
O51	111820	128010	224	173.5	7.4	21.8	2198	Cenomano-Turonian
O52	114269	124836	324	315.0	7.3	21.7	2152	Cenomano-Turonian
O53	103021	119806	190	179.1	7.3	22.3	2793	Cenomano-Turonian
O54	98283	126062	74	63.7	7.7	21.2	2216	Cenomano-Turonian
O55	100532	129964	67	37.6	7.7	20.8	1650	Cenomano-Turonian
O56	94383	125259	11	1.4	7.3	20.4	4062	Cenomano-Turonian
O58	116706	110366	306	297.8	7.9	21.9	2141	Cenomano-Turonian
O84	129882	102550	483	466.2	7.6	21.5	1694	Cenomano-Turonian
O85	136167	93466	713	701.5	7.8	18.5	1297	Cenomano-Turonian
O105	128503	96158	586	579.0	7.9	20.4	809	Cenomano-Turonian
O106	115169	105125	367	357.7	8.2	19.7	4133	Cenomano-Turonian
O107	117229	100359	444	437.6	7.6	19.8	3664	Cenomano-Turonian

Campaign of may 2018: Cenomano-Turonian Aquifer

Sample	X	Y	Z	H	pH	T	EC	Aquifer
	m					°C	μS/cm	
O108	125042	100877	469	457.3	8.8	19.3	1386	Cenomano-Turonian
O109	119343	112497	354	323.6	8.5	21.0	1600	Cenomano-Turonian
O110	125509	113399	411	401.2	8.8	19.5	5041	Cenomano-Turonian
72/52	118004	95743	398	388.0	9.2	18.7	2224	Cenomano-Turonian
809/52	127541	93680	638	629.3	7.8	20.4	778	Cenomano-Turonian
820/52	117336	97635	437	429.8	8.1	21.4	4538	Cenomano-Turonian
1209/52	113440	95628	355	-	7.7	24.6	1155	Cenomano-Turonian
1415/52	113057	96725	370	331.6	7.9	24.3	990	Cenomano-Turonian
O61	118637	93594	408	-	8.6	21.5	3164	Cenomano-Turonian
O62	116879	95278	390	383.9	9.2	18.1	2320	Cenomano-Turonian
O64	110501	94855	313	303.7	8.8	20.7	2184	Cenomano-Turonian
O65	107935	92867	272	262.3	7.9	21.2	2122	Cenomano-Turonian
O66	114500	98776	422	409.4	8.6	21.9	1734	Cenomano-Turonian
O68	107992	96978	400	391.7	8.9	20.6	2615	Cenomano-Turonian
O69	105615	96001	337	331.7	8.6	21.7	4473	Cenomano-Turonian
O73	119124	97847	415	394.9	9.2	20.0	2146	Cenomano-Turonian
O74	119893	100610	436	428.5	8.5	20.7	1539	Cenomano-Turonian
O75	121120	99785	437	417.6	8.3	21.3	1559	Cenomano-Turonian
O77	121985	96309	447	437.2	7.8	19.2	6845	Cenomano-Turonian
O78	121875	96049	446	437.4	7.5	20.7	3200	Cenomano-Turonian
O79	120482	96457	426	399.4	7.8	20.5	2536	Cenomano-Turonian
O80	121473	97981	429	411.6	7.5	20.3	5769	Cenomano-Turonian
O88	118419	93635	404	394.2	8.5	21.6	3830	Cenomano-Turonian
O81	108234	92667	275	-	8.7	21.9	2194	Cenomano-Turonian
O90	103393	91167	238	-	9.6	19.5	601	Cenomano-Turonian

Campaign of may 2018: Plio-Quaternary Aquifer

Sample	X	Y	Z	H	pH	T	EC	Aquifer
	m					°C	µS/cm	
11/51	80383	96193	3	-1,1	8,4	17,6	9744	Plio-Quaternary
15/51	85890	97935	65	56,9	7,8	19,8	1557	Plio-Quaternary
21/51	89582	91439	128	99,9	7,4	23,3	4933	Plio-Quaternary
27/51	95370	91109	201	170,25	7,8	22,2	916	Plio-Quaternary
28/51	97284	91810	234	184,6	7,6	23,3	1082	Plio-Quaternary
105/51	99400	100885	115	103,6	7,5	22,7	2187	Plio-Quaternary
125/51	93741	93786	151	94	8,0	26,3	2716	Plio-Quaternary
140/51	87205	103776	60	43,5	7,7	20,3	2163	Plio-Quaternary
148/51	85703	102084	58	43,5	7,5	21,2	1602	Plio-Quaternary
149/51	85100	105800	36	-1,7	7,4	23,1	3482	Plio-Quaternary
272/51	97195	100703	105,5	76,9	7,5	22,0	1957	Plio-Quaternary
327/51	89220	88690	124	96,6	7,7	21,9	3608	Plio-Quaternary
O2	91918	94633	132	47,7	7,9	25,2	1960	Plio-Quaternary
O4	97352	101259	102	79,7	7,5	21,3	1900	Plio-Quaternary

Campaign of may 2018: Plio-Quaternary Aquifer

Sample	X	Y	Z	H	pH	T	EC	Aquifer
	m					°C	µS/cm	
O5	91853	102137	83	54.3	7.5	22.1	1773	Plio-Quaternary
O6	91193	102500	70	54.1	7.3	21.7	2176	Plio-Quaternary
O7	90976	101554	75	53.8	7.8	22.1	1258	Plio-Quaternary
O8	91990	97737	106	-	7.9	20.5	2731	Plio-Quaternary
O91	90829	97430	102	62	7.6	23.2	3034	Plio-Quaternary
O94	81369	93593	4	-0.5	7.4	20.7	3408	Plio-Quaternary
O96	83000	93735	21	14.3	8.1	20.7	1842	Plio-Quaternary
O111	87675	91861	112	79.8	7.2	23.6	2794	Plio-Quaternary
O112	94027	95124	161	101	-	-	-	Plio-Quaternary
O113	87063	95467	101	84.6	8.1	21.3	6716	Plio-Quaternary
O98	97273	101093	100	-	8.2	20.7	1896	Plio-Quaternary
O99	85578	105624	13	-	8.7	25.8	2965	Plio-Quaternary

Campaign of may 2018: Barremian-Aptian Aquifer

Sample	X	Y	Z	H	pH	T	EC	Aquifer
	m					°C	µS/cm	
P5	89504	77758	244	-	7.5	19.4	1641	Barremian-Aptian
P11	85483	73677	271	253.5	7.5	22.4	1050	Barremian-Aptian
M74	95250	75315	406	402.6	7.3	17.0	1431	Barremian-Aptian
M84	88000	79900	239	214.2	7.2	22.5	3530	Barremian-Aptian
173/51	91073	77100	289	263.3	7.6	21.8	1619	Barremian-Aptian
175/51	93600	74914	351	336.6	7.8	20.4	1559	Barremian-Aptian
176/51	96737	76130	423	414.1	7.6	19.0	1694	Barremian-Aptian
181/51	83495	77133	161	159.3	7.6	19.6	2218	Barremian-Aptian
208/51	80513	72537	221	216.5	7.5	18.0	2054	Barremian-Aptian
209/51	80229	73441	141	137.4	7.2	21.3	1491	Barremian-Aptian
216/51	83750	80350	174	-	7.7	22.8	1917	Barremian-Aptian
217/51	85015	73957	253	239.4	8.3	19.7	751	Barremian-Aptian
480/51	86908	78386	253	-	7.2	18.0	1884	Barremian-Aptian
O14	103564	77103	529	524.4	7.3	18.0	4409	Barremian-Aptian
O17	89662	76734	261	258.4	7.2	20.1	1899	Barremian-Aptian
O19	78995	80733	1	-	8.1	19.3	1951	Barremian-Aptian
O20	82222	81119	82	-	7.3	23.3	2649	Barremian-Aptian
O22	82807	81381	100	75.4	7.4	22.6	2916	Barremian-Aptian
O23	84686	80911	208	149.3	7.6	23.5	744	Barremian-Aptian
O114	103850	77481	220	-	7.3	20.8	1963	Barremian-Aptian

Campaign of may 2018: Hautrevian Aquifer

Sample	X	Y	Z	H	pH	T	EC	Aquifer
	m					°C	µS/cm	
P5	89504	77758	244	-	7.5	19.4	1641	Hauterivian
P11	85483	73677	271	253.5	7.5	22.4	1050	Hauterivian
M74	95250	75315	406	402.6	7.3	17.0	1431	Hauterivian

Campaign of may 2018: Hautrevian Aquifer

Sample	X	Y	Z	H	pH	T	EC	Aquifer
	m					°C	µS/cm	
163/51	93398	63491	164	153,4	7,3	22,1	1221	Hauterivian
P9	90126	63897	143	-	7,4	23,9	1787	Hauterivian
O24	89239	63810	123	117,5	8,0	18,3	1754	Hauterivian
O25	87764	64270	148	-	7,1	24,0	1991	Hauterivian
O26	89651	63823	135	-	7,3	24,3	1803	Hauterivian
O28	92680	63541	160	-	7,2	23,6	1897	Hauterivian
O29	94921	64380	195	-	8,1	18,1	1094	Hauterivian
O102	89177	64188	156	148,5	7,2	21,6	1754	Hauterivian
O115	98271	68747	335	326,8	7,7	22,1	1461	Hauterivian
O116	94413	68601	287	264,3	7,9	22,1	3688	Hauterivian
O117	94198	68475	287	278,8	7,7	22,6	1131	Hauterivian
O118	90605	67791	267	259,8	8,1	21,6	668	Hauterivian
O119	90798	68298	288	276,4	8,3	21,6	3270	Hauterivian
O120	89536	64080	179	175,2	7,1	21,1	1731	Hauterivian

Campaign of may 2017: Cenomano-Turonian Aquifer

Sample	X	Y	Z	H	pH	T	EC	Aquifer
	m					°C	µS/cm	
54/43	103100	124800	96	-	7.1	22.2	3014	Cenomano-Turonian
75/52	128124	103181	461	445.4	7.8	18.6	2107	Cenomano-Turonian
89/52	106174	117707	190	179.5	7.3	22.2	1962	Cenomano-Turonian
105/52	138360	98205	604	602.5	7.3	18.8	2707	Cenomano-Turonian
612/52	107407	122209	204	176.8	7.4	21.9	3274	Cenomano-Turonian
613/52	138667	93423	684	674.2	7.9	18.4	1200	Cenomano-Turonian
648/52	132420	101017	524	485.3	7.3	22.5	1153	Cenomano-Turonian
776/52	141554	95298	637	621	7.2	20.0	1421	Cenomano-Turonian
824/52	115524	105982	354	340.5	7.6	20.4	3700	Cenomano-Turonian
874/52	109190	110628	283	270	7.4	21.5	3935	Cenomano-Turonian
883/52	103987	116773	200	166.6	7.1	23.4	2424	Cenomano-Turonian
1112/52	138581	99269	591	555.8	7.7	21.5	1175	Cenomano-Turonian
1699/52	141573	96319	627	599.6	7.2	20.7	1808	Cenomano-Turonian

Sample	X	Y	Z	H	pH	T	EC	Aquifer
	m					°C	µS/cm	
1871/52	123872	113403	380	-	7.0	25.1	1856	Cenomano-Turonian
O30	130545	101944	500	485.9	7.4	19.9	2413	Cenomano-Turonian
O31	131340	102793	493	488.6	7.7	17.9	1025	Cenomano-Turonian
O32	129367	103090	474	458.3	7.1	20.7	1589	Cenomano-Turonian
O33	141474	93754	669	640.8	7.6	21.2	1348	Cenomano-Turonian
O34	132390	100749	526	485.7	7.3	23.8	1110	Cenomano-Turonian
O36	130728	104484	483	455	8.0	19.9	2100	Cenomano-Turonian
O37	128911	104147	466	454.2	7.2	20.7	4659	Cenomano-Turonian
O38	125031	100629	469	456	7.3	21.3	1007	Cenomano-Turonian
O39	121773	103695	390	375	7.4	20.7	2224	Cenomano-Turonian
O40	119621	106390	347	341.3	7.1	21.8	1876	Cenomano-Turonian
O41	120676	105816	412	393	7.7	22.7	2044	Cenomano-Turonian

Campaign of may 2017: Cenomano-Turonian Aquifer

Sample	X	Y	Z	H	pH	T	EC	Aquifer
	m					°C	µS/cm	
O42	118207	109602	319	291,1	7,8	22,6	1910	Cenomano-Turonian
O45	117229	100359	444	437,9	7,6	18,7	2811	Cenomano-Turonian
O46	119814	104010	414	405,5	6,9	22,6	2907	Cenomano-Turonian
O47	125504	113395	411	401,4	7,2	19,9	3961	Cenomano-Turonian
O48	119336	112498	335	303,4	7,4	20,6	1640	Cenomano-Turonian
O49	110383	116191	219	193,7	-	-	-	Cenomano-Turonian
O51	111820	128010	224	173,8	7,4	23,1	2003	Cenomano-Turonian
O52	114269	124836	324	314,9	7,2	21,8	1908	Cenomano-Turonian
O53	103021	119806	190	180,3	7,4	22,1	2436	Cenomano-Turonian
O54	98283	126062	74	63,8	7,7	21,7	1806	Cenomano-Turonian
O55	100532	129964	67	38,1	7,2	21,8	3245	Cenomano-Turonian
O56	94383	125259	11	1,64	7,3	20,9	3620	Cenomano-Turonian
O82	107823	112585	233	188,8	7,2	23,6	2387	Cenomano-Turonian
O83	116706	110366	306	299,9	7,1	22,3	1742	Cenomano-Turonian
O84	129882	102550	483	467,2	7,2	21,6	1578	Cenomano-Turonian
O85	136167	93466	713	701,7	7,6	19,0	1341	Cenomano-Turonian

O86	110681	116060	222	195,1	7,4	23,0	1962	Cenomano-Turonian
O87	128508	96144	572	564,2	7,6	20,6	635	Cenomano-Turonian
72/52	118004	95743	398	388,8	7,3	19,9	1884	Cenomano-Turonian
108/52	123518	99423	461	411,9	7,7	22,9	903	Cenomano-Turonian
809/52	127541	93680	638	629,7	7,8	20,3	666	Cenomano-Turonian
820/52	117336	97635	437	430	7,5	21,0	3836	Cenomano-Turonian
1415/52	113057	96725	370	332,1	7,3	24,1	881	Cenomano-Turonian
O59	118067	94404	404	382,3	7,8	20,7	3324	Cenomano-Turonian
O60	117368	91734	389	374,2	8,1	20,2	1043	Cenomano-Turonian
O61	118637	93594	408	-	7,4	29,3	4462	Cenomano-Turonian
O62	116879	95278	390	384	8,0	19,1	1857	Cenomano-Turonian
O63	111270	95118	321	309,8	7,1	21,6	6776	Cenomano-Turonian
O64	110501	94855	313	304,4	7,6	20,5	1765	Cenomano-Turonian
O65	107935	92867	272	262,3	7,2	22,0	1822	Cenomano-Turonian
O66	114500	98776	422	409,7	7,5	21,8	1553	Cenomano-Turonian
O68	107992	96978	400	392	7,5	21,3	2752	Cenomano-Turonian
O69	105615	96001	337	331,8	7,5	21,9	4135	Cenomano-Turonian
O73	119124	97847	415	395,1	7,9	20,5	1827	Cenomano-Turonian
O74	119893	100610	436	429,2	7,5	21,2	1241	Cenomano-Turonian
O75	121120	99785	437	417,7	7,4	21,6	1297	Cenomano-Turonian
O77	121985	96309	447	437,4	7,6	19,3	5423	Cenomano-Turonian
O78	121875	96049	446	437,9	7,7	20,8	2715	Cenomano-Turonian
O79	120482	96457	426	400,1	7,7	20,8	2251	Cenomano-Turonian
O80	121473	97981	429	411,6	6,9	21,2	4970	Cenomano-Turonian
O88	118419	93635	404	394,2	7,2	22,4	3514	Cenomano-Turonian
O89	108234	92667	275	-	7,7	23,0	1699	Cenomano-Turonian
O90	103393	91167	238	-	8,5	24,6	550	Cenomano-Turonian

Campaign of may 2017: Plio-Quaternary Aquifer

Sample	X	Y	Z	H	pH	T	EC	Aquifer
	m					°C	μS/cm	
15/51	85890	97935	65	57.4	7.5	18.9	724	Plio-Quaternary
11/51	80383	96193	3	-1	7.6	18.9	7555	Plio-Quaternary
21/51	89582	91439	128	99.8	7.3	22.9	4226	Plio-Quaternary
27/51	95370	91109	201	170.3	7.8	22.9	762	Plio-Quaternary
28/51	97284	91810	234	184.6	7.7	23.4	926	Plio-Quaternary
53/51	92700	104180	73	58.8	7.4	20.1	1110	Plio-Quaternary
105/51	99400	100885	115	103.6	7.5	22.4	1836	Plio-Quaternary
125/51	93741	93786	151	94	7.6	25.0	2550	Plio-Quaternary
140/51	87205	103776	60	43.7	7.9	20.2	1859	Plio-Quaternary
148/52	85703	102084	58	43.6	7.5	21.2	1453	Plio-Quaternary
149/51	85100	105800	36	-1.6	7.5	22.9	3173	Plio-Quaternary
261/51	96540	99238	118	72.3	7.2	24.2	2023	Plio-Quaternary
272/51	97195	100703	105.5	76.4	7.8	21.6	1757	Plio-Quaternary
327/51	89220	88690	124	97.1	7.7	22.2	3066	Plio-Quaternary
O2	91918	94633	132	48.5	7.8	25.4	1771	Plio-Quaternary
O4	97352	101259	102	78.5	7.7	20.7	1552	Plio-Quaternary
O5	91853	102137	83	54.5	7.7	22.4	1558	Plio-Quaternary
O6	91193	102500	70	54.4	7.4	21.7	1935	Plio-Quaternary
O7	90976	101554	75	54.1	8.0	21.5	1151	Plio-Quaternary
O8	91990	97737	106	-	7.8	22.0	2333	Plio-Quaternary
O9	91106	96507	105	62.5	7.7	23.1	2835	Plio-Quaternary
O91	90829	97430	102	62.2	7.6	23.1	2866	Plio-Quaternary
O92	87653	91800	101	68.6	7.1	23.0	2429	Plio-Quaternary
O93	81472	93666	6	-	7.3	23.0	2049	Plio-Quaternary
O94	81369	93593	4	-0.5	7.4	21.4	2913	Plio-Quaternary
O95	85087	102022	58	36.5	7.6	21.2	1298	Plio-Quaternary
O96	83000	93735	21	14.3	8.0	20.9	1772	Plio-Quaternary

Campaign of may 2017: Barremian-Aptian Aquifer

Sample	X	Y	Z	H	pH	T	EC	Aquifer
	m					°C	µS/cm	
176/51	96737	76130	423	414.4	7.6	19.4	1470	Barremian-Aptian
M74	95250	75315	406	402.9	7.4	17.8	1087	Barremian-Aptian
175/51	93600	74614	351	336.7	7.5	20.9	1306	Barremian-Aptian
173/51	91073	77100	289	263.75	7.6	22.3	1334	Barremian-Aptian
217/51	85015	73957	253	240.1	8.1	20.0	549	Barremian-Aptian
P11	85483	73677	271	253.5	7.3	22.5	926	Barremian-Aptian
209/51	80229	73441	141	137.6	7.2	21.6	1324	Barremian-Aptian
208/51	80513	72537	221	216.5	7.4	19.1	1642	Barremian-Aptian
181/51	83495	77133	161	159.5	7.5	20.8	1885	Barremian-Aptian
224/51	89577	76991	256	250.7	7.0	21.6	2073	Barremian-Aptian
P5	89504	77758	244	-	7.4	22.2	1427	Barremian-Aptian
M86	89322	78410	234	210.4	7.2	22.1	2065	Barremian-Aptian

Campaign of may 2017: Barremian-Aptian Aquifer

Sample	X	Y	Z	H	pH	T	EC	Aquifer
	m					°C	µS/cm	
M84	88000	79800	239	214.4	7.4	21.9	2982	Barremian-Aptian
480/51	86908	78386	253	-	7.4	23.3	1481	Barremian-Aptian
216/51	83750	80350	174	-	7.6	23.0	1670	Barremian-Aptian
214/51	79740	75462	98	-	7.7	23.9	3392	Barremian-Aptian
O14	103564	77103	529	525.2	7.4	18.3	3195	Barremian-Aptian
O15	104796	76619	541	-	7.6	22.9	1929	Barremian-Aptian
O16	99688	76843	465	459.6	7.1	20.1	1589	Barremian-Aptian
O17	89662	76734	261	258.2	7.1	20.9	1747	Barremian-Aptian
O19	78995	80733	1	-	8.0	20.4	1678	Barremian-Aptian
O20	82222	81119	82	-	7.2	23.4	2254	Barremian-Aptian
O22	82807	81381	100	76.5	7.1	23.8	3884	Barremian-Aptian
O23	84686	80911	208	149.4	7.6	23.4	667	Barremian-Aptian
O100	83087	82130	211	-	7.8	23.0	2715	Barremian-Aptian

Campaign of may 2017: Hautrivian Aquifer

Sample	X	Y	Z	H	pH	T	EC	Aquifer
	m					°C	µS/cm	
191/51	88419	64291	131	-	7.2	24.0	1661	Hautrevian
P9	90126	63897	143	-	7.4	24.3	1685	Hautrevian
163/51	93398	63491	164	154.4	7.2	23.3	1165	Hautrevian
O24	89239	63810	123	117.4	7.9	19.4	1641	Hautrevian
O25	87764	64270	148	-	6.9	24.0	1787	Hautrevian
O26	89651	63823	135	-	7.2	24.8	1681	Hautrevian
O27	89157	64079	150	146.1	7.1	22.1	1518	Hautrevian
O28	92680	63541	160	-	7.2	24.6	1751	Hautrevian
O29	94921	64380	195	-	8.4	23.0	1134	Hautrevian
O101	89958	63511	130	123.1	7.8	21.3	2130	Hautrevian
O102	89177	64188	156	148.4	7.2	21.5	1509	Hautrevian
O103	88707	64298	152	-	7.0	22.9	1554	Hautrevian
O104	84836	65179	110	-	6.9	22.9	2203	Hautrevian

Campaign of april 2016: Cenomano-Turonian Aquifer

Sample	X	Y	Z	H	pH	T	EC	Aquifer
	m					°C	µS/cm	
54/43	103100	124800	96	-	7.1	23.2	3100	Cenomano-Turonian
75/52	128124	103181	461	446	7.7	18.5	2050	Cenomano-Turonian
89/52	106174	117707	190	179.3	7.4	21.2	1933	Cenomano-Turonian
105/52	138360	98205	604	602.5	7.6	20.2	3950	Cenomano-Turonian
612/52	107407	122209	204	177	7.3	20.8	3150	Cenomano-Turonian
613/51	138667	93423	684	674.3	7.5	18.5	1516	Cenomano-Turonian
648/52	132420	101017	524	487.5	7.3	22.1	1249	Cenomano-Turonian
776/52	141554	95298	637	621.9	7.4	19.2	1300	Cenomano-Turonian
824/52	115524	105982	354	340.5	7.3	19.4	4300	Cenomano-Turonian

Campaign of april 2016: Cenomano-Turonian Aquifer

Sample	X	Y	Z	H	pH	T	EC	Aquifer
	m					°C	µS/cm	
874/52	109190	110628	283	270.4	7.3	23.0	4150	Cenomano-Turonian
883/43	103987	116773	200	166.5	7.2	24.0	2550	Cenomano-Turonian
1112/52	138581	99269	591	556	7.8	21.0	1188	Cenomano-Turonian
1503/52	115077	111000	279	259	7.1	23.4	2550	Cenomano-Turonian
1699/52	141573	96319	627	601.35	7.7	20.7	1800	Cenomano-Turonian
1871/52	123872	113403	380	-	7.1	23.7	1800	Cenomano-Turonian
O30	130545	101944	500	486.1	7.2	19.5	2190	Cenomano-Turonian
O31	131340	102793	493	488.7	7.8	16.4	493	Cenomano-Turonian
O32	129367	103090	474	458.4	7.2	20.4	1590	Cenomano-Turonian
O33	141474	93754	669	641.8	7.3	20.5	1518	Cenomano-Turonian
O34	132390	100749	526	485.7	7.3	22.3	1202	Cenomano-Turonian
O35	134110	106742	543	519.2	7.5	19.8	803	Cenomano-Turonian
O36	130728	104484	483	456	7.3	19.9	2400	Cenomano-Turonian
O37	128911	104147	466	454.2	7.2	20.5	5100	Cenomano-Turonian
O38	125031	100629	469	456	7.3	21.2	1093	Cenomano-Turonian
O39	121773	103695	390	375.2	7.3	20.7	2500	Cenomano-Turonian
O40	119621	106390	347	341.4	7.2	20.9	1890	Cenomano-Turonian
O41	120676	105816	412	393.7	7.5	23.2	2050	Cenomano-Turonian
O42	118207	109602	319	291.6	7.7	22.0	1954	Cenomano-Turonian
O43	116855	111363	285	266.8	-	-	-	Cenomano-Turonian
O45	117229	100359	444	438	7.5	18.0	3250	Cenomano-Turonian
O46	119814	104010	414	405.6	6.9	22.1	3050	Cenomano-Turonian
O47	125504	113395	411	401.6	7.1	19.6	4920	Cenomano-Turonian
O48	119336	112498	335	303.4	7.5	20.9	1883	Cenomano-Turonian
O49	110383	116191	219	193.7	7.4	23.3	1894	Cenomano-Turonian
O50	102823	112355	266	161	7.4	21.2	1281	Cenomano-Turonian
O51	111820	128010	224	173.9	7.2	22.1	2020	Cenomano-Turonian
O52	114269	124836	324	315	7.2	21.6	2090	Cenomano-Turonian
O53	103021	119806	190	180.5	7.4	22.3	2400	Cenomano-Turonian
O54	98283	126062	74	63.6	7.5	21.9	2200	Cenomano-Turonian
O55	100532	129964	67	38.3	7.8	19.6	3150	Cenomano-Turonian

Sample	X	Y	Z	H	pH	T	EC	Aquifer
	m					°C	µS/cm	
O56	94383	125259	11	2	7.4	20.5	4450	Cenomano-Turonian
O57	100817	118478	162	110.1	7.2	20.7	2150	Cenomano-Turonian
O58	116706	110366	306	299.9	6.9	21.6	2100	Cenomano-Turonian
72/52	118004	95743	398	388.8	7.4	19.0	1926	Cenomano-Turonian
108/52	123510	99414	461	412	7.4	21.6	947	Cenomano-Turonian
809/52	127541	93680	638	630.5	7.3	20.3	714	Cenomano-Turonian
816/52	121300	98063	426	402.1	-	-	-	Cenomano-Turonian
820/52	117336	97635	437	430.2	7.5	20.7	4510	Cenomano-Turonian
1209/52	113440	95628	355	-	7.4	24.3	1051	Cenomano-Turonian
1415/52	113057	96725	370	337.8	7.6	23.4	914	Cenomano-Turonian
2099/52	114487	93961	347	-	7.5	24.2	929	Cenomano-Turonian
O59	118067	94404	404	382.4	-	-	-	Cenomano-Turonian

Campaign of april 2016: Cenomano-Turonian Aquifer

Sample	X	Y	Z	H	pH	T	EC	Aquifer
	m					°C	µS/cm	
O60	117368	91734	389	375	7.4	20.2	1204	Cenomano-Turonian
O61	118637	93594	408	400.15	7.5	20.5	4500	Cenomano-Turonian
O62	116879	95278	390	384.5	7.7	18.0	2120	Cenomano-Turonian
O63	111270	95118	321	310.6	7.1	21.2	7600	Cenomano-Turonian
O64	110501	94855	313	307	7.6	20.0	2000	Cenomano-Turonian
O65	107935	92867	272	262.3	7.5	20.7	1753	Cenomano-Turonian
O66	114500	98776	422	410	7.3	21.5	1696	Cenomano-Turonian
O67	108785	97949	468	343	7.0	19.3	3395	Cenomano-Turonian
O68	107992	96978	400	392.4	7.6	20.3	3600	Cenomano-Turonian
O69	105615	96001	337	331.7	7.6	22.0	4900	Cenomano-Turonian
O71	112972	97169	375	333.8	7.5	22.7	874	Cenomano-Turonian
O72	119147	97040	406	-	7.4	21.0	1227	Cenomano-Turonian
O73	119124	97847	415	395.2	7.7	19.2	1992	Cenomano-Turonian
O74	119893	100610	436	429.3	7.4	20.8	1490	Cenomano-Turonian
O75	121120	99785	437	418	7.6	21.5	1227	Cenomano-Turonian
O76	119267	99793	434	417.3	7.5	22.8	1693	Cenomano-Turonian

Sample	X	Y	Z	H	pH	T	EC	Aquifer
	m					°C	µS/cm	
O77	121985	96309	447	437.57	7.3	19.3	5800	Cenomano-Turonian
O78	121875	96049	446	437.8	7.0	20.8	3300	Cenomano-Turonian
O79	120482	96457	426	400.2	7.3	20.8	2460	Cenomano-Turonian
O80	121473	97981	429	412.3	6.9	21.5	5450	Cenomano-Turonian
O81	108234	92667	275	-	8.2	21.7	1276	Cenomano-Turonian
O70	102821	92177	230	-	8.0	22.6	539	Cenomano-Turonian

Campaign of june 2015: Plio-Quaternary Aquifer

Sample	X	Y	Z	H	pH	T	EC	Aquifer
	m					°C	µS/cm	
3/51	81472	93666	7	0.7	7.6	21.2	2270	Plio-Quaternary
11/51	80383	96193	3	-0.9	7.8	21.5	5210	Plio-Quaternary
15/51	85890	97935	65	53.0	7.8	22.9	2970	Plio-Quaternary
27/51	95370	91109	201	171.8	7.6	22.2	626	Plio-Quaternary
28/51	97284	91810	234	184.7	8.0	23.3	965	Plio-Quaternary
53/51	92700	104180	73	57.1	7.8	20.9	1716	Plio-Quaternary
103/51	94830	102206	91	64.8	8.1	22.2	2010	Plio-Quaternary
105/51	99402	100883	114	102.9	7.9	22.3	2210	Plio-Quaternary
125/51	93741	93786	152	95.4	7.8	25.0	2290	Plio-Quaternary
137/51	86733	94515	81	61.6	7.8	21.4	3090	Plio-Quaternary
138/51	88289	92860	105	79.2	7.8	21.8	7840	Plio-Quaternary
140/51	87205	103776	60	43.6	8.0	21.0	2118	Plio-Quaternary
148/51	85703	102084	58	43.7	8.0	21.1	1650	Plio-Quaternary
149/51	85100	105800	36	-1.6	7.9	22.8	3250	Plio-Quaternary
327/51	89220	88690	124	98.4	7.8	22.3	2150	Plio-Quaternary
O1	94941	95890	153	95.0	7.5	25.0	3850	Plio-Quaternary
O2	91918	94633	132	52.0	7.8	24.8	1924	Plio-Quaternary

Campaign of june 2015: Plio-Quaternary Aquifer

Sample	X	Y	Z	H	pH	T	EC	Aquifer
	m					°C	µS/cm	
O3	91146	93802	134	14.0	7.7	23.1	4060	Plio-Quaternary
O4	97352	101259	102	80.1	7.8	21.3	1720	Plio-Quaternary
O5	91853	102137	83	54.6	7.8	23.7	1715	Plio-Quaternary
O6	91193	102500	70	54.4	7.8	21.8	1795	Plio-Quaternary
O7	90976	101554	75	54.0	8.2	21.9	1348	Plio-Quaternary
O8	91990	97737	106	63.3	7.9	24.2	2520	Plio-Quaternary
O9	91106	96507	105	63.0	7.9	24.5	2980	Plio-Quaternary
O10	89582	91439	128	100.0	7.5	22.9	4260	Plio-Quaternary
O11	88284	95263	102	69.0	8.1	22.5	1135	Plio-Quaternary
O12	85901	97934	59	50.1	7.5	20.6	3540	Plio-Quaternary

Campaign of june 2015: Barremian-Aptian Aquifer

Sample	X	Y	Z	H	pH	T	EC	Aquifer
	m					°C	µS/cm	
173/51	91073	77100	289	263.8	7.9	22.0	1351	Barremian-Aptian
175/51	93600	74614	351	341.2	7.8	20.3	1530	Barremian-Aptian
176/51	96737	76130	423	414.2	7.4	22.3	1776	Barremian-Aptian
181/51	83495	77133	161	159.7	7.7	22.4	2120	Barremian-Aptian
208/51	80513	72537	221	216.5	7.8	18.8	2090	Barremian-Aptian
209/51	80229	73441	141	137.8	7.8	21.6	1430	Barremian-Aptian
214/51	79740	75462	98	98.0	7.6	21.7	3580	Barremian-Aptian
216/51	83750	80350	174	-	7.7	23.6	1820	Barremian-Aptian
217/51	85015	73957	253	240.6	8.2	19.9	490	Barremian-Aptian
224/51	89577	76991	256	251.0	7.5	22.1	2330	Barremian-Aptian
480/51	86908	78386	253	253.0	7.6	24.2	1799	Barremian-Aptian
M84	88000	79900	239	215.0	7.2	22.0	3250	Barremian-Aptian
M86	89322	78410	234	210.3	7.6	22.3	1750	Barremian-Aptian
M74	95250	75315	407	404.0	7.7	20.3	1280	Barremian-Aptian
P5	89504	77758	244	-	7.9	22.7	1365	Barremian-Aptian
P11	85483	73677	271	253.5	7.7	22.5	966	Barremian-Aptian
O14	103564	77103	529	525.8	7.5	21.0	3650	Barremian-Aptian

Sample	X	Y	Z	H	pH	T	EC	Aquifer
	m					°C	µS/cm	
O15	104796	76619	541	-	7.2	25.2	1640	Barremian-Aptian
O16	99688	76843	465	460.5	7.4	21.4	1700	Barremian-Aptian
O17	89662	76734	261	258.4	7.5	22.0	2040	Barremian-Aptian
O18	81259	78882	133	80.0	8.0	24.2	1291	Barremian-Aptian
O19	78995	80733	1	-	8.1	21.2	1875	Barremian-Aptian
O20	82222	81119	82	-	7.5	24.7	2640	Barremian-Aptian
O21	82816	81418	101	76.0	8.1	23.9	2400	Barremian-Aptian
O22	82807	81381	100	77.0	7.9	22.2	3400	Barremian-Aptian
O23	84686	80911	208	149.6	8.0	23.0	624	Barremian-Aptian

Campaign of june 2015: Hauterivian Aquifer

Sample	X	Y	Z	H	pH	T	EC	Aquifer
	m					°C	µS/cm	
163/51	93398	63491	164	154.8	7.7	25.0	1090	Hauterivian
191/51	88419	64291	131	-	7.5	24.7	1720	Hauterivian
P9	90126	63897	143	-	7.7	24.6	1720	Hauterivian
O24	89239	63810	123	117.5	7.7	21.2	1940	Hauterivian
O25	87764	64270	148	-	7.4	25.1	1870	Hauterivian
O26	89651	63823	135	-	7.5	25.0	1660	Hauterivian
O27	89157	64079	154	150.4	7.7	24.4	1660	Hauterivian
O28	92688	63541	160	-	7.5	24.5	1880	Hauterivian
O29	94944	64350	224	-	8.1	23.2	1270	Hauterivian

Campaign of october 2009: Plio-Quaternary Aquifer

Sample	X	Y	Z	H	pH	T	EC	Aquifer
	m					°C	µS/cm	
103/51	94820	102170	99	76.5	21	7.3	1671	Plio-Quaternary
133/51	87800	98800	70	32	22	7.2	2550	Plio-Quaternary
138/51	88289	92860	105	104	21	7.3	3520	Plio-Quaternary
272/51	97195	100703	105.5	105.5	20	7.2	2180	Plio-Quaternary
3/51	81472	93666	7	14	19	7.4	2130	Plio-Quaternary
B5	90290	102260	102	54	19	7.4	2249	Plio-Quaternary

Sample	X	Y	Z	H	pH	T	EC	Aquifer
	m					°C	µS/cm	
B7	95150	104490	97	69.2	20	7.25	770	Plio-Quaternary
B9	93410	102680	114	67	19	7.4	1763	Plio-Quaternary
M33	91150	102300	78	49	20	7.4	2040	Plio-Quaternary
M61	91200	100750	90	56	23	7.5	1720	Plio-Quaternary
149/51	85100	105800	36	2.8	22	6.7	3160	Plio-Quaternary
15/51	85890	97935	65	63	15.5	7.1	3370	Plio-Quaternary
21/51	89582	91439	128	61.6	20	7	3780	Plio-Quaternary

Campaign of october 2007: Plio-Quaternary Aquifer

Sample	X	Y	Z	H	pH	T	EC	Aquifer
	m					°C	µS/cm	
380/51	89900	91494	135	184.00	7.60	25.8	2530	Plio-Quaternary
457/52	90700	96700	110	148.42	7.65	26.9	1930	Plio-Quaternary
829/52	87100	111200	692	16.30	7.45	19.8	547	Plio-Quaternary
327/51	89200	88700	128	96.00	7.10	24.0	2270	Plio-Quaternary
128/51	93300	99500	120	37.00	7.20	22.4	1700	Plio-Quaternary
Privé	93750	105000	84	41.00	6.90	23.5	2430	Plio-Quaternary
346/51	97500	101350	108	300	6.8	27	1920	Plio-Quaternary
389/52	91100	96600	107	54	7.15	24.9	4670	Plio-Quaternary

Campaign of october 2007: Cenomano-Turonian Aquifer

Sample	X	Y	Z	H	pH	T	EC	Aquifer
	m					°C	µS/cm	
1503/52	115100	111000	276	256	6.90	20.8	2092	Cenomano-Turonian
ES02	117500	105400	425	350	7.28	22.0	2600	Cenomano-Turonian
75/52	128124	103181	464	457.8	7.24	20.0	1500	Cenomano-Turonian
605/52	130400	102000	496	494.3	7.50	17.4	998	Cenomano-Turonian
648/52	132450	101050	521	489	7.39	21.9	1065	Cenomano-Turonian
1112/52	138600	99250	594	559.5	7.69	21.3	994	Cenomano-Turonian
105/52	138350	98250	608	608	7.64	17.4	3880	Cenomano-Turonian
776/52	141700	95600	637	631.8	7.60	18.3	1600	Cenomano-Turonian
1699/52	141500	96300	627	-	7.11	21.5	2750	Cenomano-Turonian

Sample	X	Y	Z	H	pH	T	EC	Aquifer
	m					°C	µS/cm	
883/52	104000	116500	194	169.5	6.90	26.6	2500	Cenomano-Turonian
89/52	106174	117707	196	188.5	6.90	22.8	2800	Cenomano-Turonian
54/52	103100	124800	95	95	6.75	22.2	3100	Cenomano-Turonian
89/52	103650	117900	182	182	6.65	24.8	2700	Cenomano-Turonian
874/52	109250	110600	282	273.64	7.35	24.4	2540	Cenomano-Turonian
612/52	107500	122200	203	178	7.35	22.2	2970	Cenomano-Turonian
1576/52	120250	112700	370	-	7.80	23.2	900	Cenomano-Turonian
ES34	143400	98400	595	588	7.10	22.1	1900	Cenomano-Turonian
ES35	141000	85700	877	877	7.65	26.4	3740	Cenomano-Turonian
ES36	120250	112350	365	277	7.40	25.0	1220	Cenomano-Turonian
1871/52	123850	113400	380	-	7.00	26.2	2300	Cenomano-Turonian
1415/52	112972	97169	364	334.4	7.15	24.4	966	Cenomano-Turonian
ES28	117336	97635	429.75	334.75	7.10	25.8	1400	Cenomano-Turonian
72/52	118025	95756	398	392	7.35	23.5	1500	Cenomano-Turonian
677/52	121750	89450	485	482.35	7.10	22.8	1500	Cenomano-Turonian
1690/52	118000	91100	441	351	6.90	24.4	1450	Cenomano-Turonian
2099/52	114487	93961	353	343.5	7.15	24.6	1232	Cenomano-Turonian
ES65	107992	96988	409	405.7	6.85	29.5	1810	Cenomano-Turonian

Campaign of march 1997: Barremian-Aptian Aquifer

Sample	X	Y	Z	H	pH	T	EC	Aquifer
	m					°C	µS/cm	
173/51	91073	77100	289	277.8	-	20	1119	Barremian-Aptian
175/51	93600	74614	351	346.28	-	20	1106	Barremian-Aptian
176/51	96737	76130	423	420	-	22	1743	Barremian-Aptian
181/51	83495	77133	161	160	-	19	1986	Barremian-Aptian
208/51	80513	72537	221	217.5	-	18	5184	Barremian-Aptian
209/51	80229	73441	141	140.4	-	21	2169	Barremian-Aptian
214/51	79740	75462	98	98	-	22	4498	Barremian-Aptian
216/51	83750	80350	174	174	-	23	1668	Barremian-Aptian
217/51	85015	73957	253	244.55	-	18.7	316	Barremian-Aptian

Campaign of march 1997: Barremian-Aptian Aquifer

Sample	X	Y	Z	H	pH	T	EC	Aquifer
	m					°C	µS/cm	
224/51	89577	76991	256	253.3	-	21	3190	Barremian-Aptian
M84	88000	79900	239	231.3	-	21.8	1867	Barremian-Aptian
M86	89322	78410	234	213	-	21.3	1401	Barremian-Aptian
M74	95250	75315	407	404.8	-	18.2	1341	Barremian-Aptian
P5	89504	77758	244	235.6	-	21.7	950	Barremian-Aptian
P11	85483	73677	271	256	-	20.5	763	Barremian-Aptian
213/51	79250	76225	154	153.15	-	26	4906	Barremian-Aptian
215/51	84100	76550	157	156	-	20.5	1746	Barremian-Aptian
395/51	83800	81500	155.4	119.4	-	-	-	Barremian-Aptian
M85	89400	79100	258	202	-	22	2488	Barremian-Aptian
P3	90200	77750	260	241.6	-	21	1031	Barremian-Aptian
P4	89000	78950	230	204	-	22	1062	Barremian-Aptian

Campaign of march 1997: Hauterivian Aquifer

Sample	X	Y	Z	H	pH	T	EC	Aquifer
	m					°C	µS/cm	
163/52	93398	63491	164	139.8	-	23.2	1153	Hauterivian
165/51	94198	68475	287	281.3	-	-	-	Hauterivian
187/51	90798	68298	288	282.86	-	21	2807	Hauterivian
P9	90126	63897	143	143	-	20.5	3376	Hauterivian
198/51	98271	68747	335	328.69	-	21.5	1967	Hauterivian
161/51	94700	63550	175	166.4	-	24	1740	Hauterivian
190/51	88950	64200	132	121.4	-	21	2297	Hauterivian
195/51	85125	64050	91.6	89.9	-	17	3444	Hauterivian
P1	89200	63800	160	158.6	-	-	-	Hauterivian
P6	90500	67850	240	237.8	-	20.8	1314	Hauterivian
P7	92200	67700	340	338	-	21	3403	Hauterivian
M92	94300	66000	318	298.9	-	22.5	4636	Hauterivian
P10	88950	64250	130	130	-	23	2013	Hauterivian
191/51	88000	64300	130	130	-	23	2121	Hauterivian
M91	87700	63950	118	115.4	-	22	1964	Hauterivian

Campaign of december 1995: Cenomano-Turonian Aquifer

Sample	X	Y	Z	H	pH	T	EC	Aquifer
	m					°C	µS/cm	
1	115500	108500	365	335.85	-	-	-	Cenomano-Turonian
824/52	115600	106150	360	347.8	-	18	2600	Cenomano-Turonian
3	114600	107450	335	320.75	-	-	-	Cenomano-Turonian
1045/52	113400	105800	375	343.87	-	20	2230	Cenomano-Turonian
6	115200	101750	430	419	-	-	-	Cenomano-Turonian
1049/52	117150	101600	430	405.5	-	20	804	Cenomano-Turonian
93/52	120000	104800	350	375	-	20	1410	Cenomano-Turonian
80/52	122100	104200	365	392.2	-	19.5	1460	Cenomano-Turonian

Campaign of december 1995: Cenomano-Turonian Aquifer

Sample	X	Y	Z	H	pH	T	EC	Aquifer
	m					°C	µS/cm	
20	122800	102400	405	404.75	-	-	-	Cenomano-Turonian
75/52	128200	103750	465	460.5	-	18	1080	Cenomano-Turonian
794/52	128800	104000	475	447.5	-	17.5	795	Cenomano-Turonian
23	129200	103150	476	454.85	-	18	700	Cenomano-Turonian
24	130900	104350	483	470.9	-	-	-	Cenomano-Turonian
926/52	131500	104800	500	468	-	20	1040	Cenomano-Turonian
796/52	134000	106500	545	528	-	19.5	352	Cenomano-Turonian
792/52	131450	102600	495	489.9	-	18	531	Cenomano-Turonian
898/52	131550	102150	494	486	-	16	567	Cenomano-Turonian
907/52	130700	101300	502	485	-	20	765	Cenomano-Turonian
664/52	130000	101600	498	489.82	-	20	780	Cenomano-Turonian
107/52	125250	100500	460	461	-	18.5	752	Cenomano-Turonian
806/52	128900	95700	585	579.7	-	19	528	Cenomano-Turonian
47	127250	99500	496	495.7	-	21	716	Cenomano-Turonian
807/52	130650	98600	515	533.1	-	21	1020	Cenomano-Turonian
648/52	131600	101200	502	468.8	-	21	616	Cenomano-Turonian
789/52	137750	98800	610	589.8	-	20	2200	Cenomano-Turonian
105/52	138600	98400	600	623	-	15	2010	Cenomano-Turonian
52	138900	97600	623	610	-			Cenomano-Turonian

Sample	X	Y	Z	H	pH	T	EC	Aquifer
	m					°C	µS/cm	
776/52	142100	95850	630	629.5	-	18.5	788	Cenomano-Turonian
55	142000	94000	672	654.95	-			Cenomano-Turonian
59	138150	93600	700	699.8	-	19	1160	Cenomano-Turonian
83/52	117400	100700	440	427	-	-	-	Cenomano-Turonian
7	115550	98800	440	409	-	-	-	Cenomano-Turonian
11	118300	96400	400	403.1	-	-	-	Cenomano-Turonian
13	118200	95700	400	395.65	-	-	-	Cenomano-Turonian
813/52	118250	95150	410	392	-	-	-	Cenomano-Turonian
15	118100	94450	392	391.4	-	-	-	Cenomano-Turonian
16	118800	95350	405	391.7	-	-	-	Cenomano-Turonian
820/52	117500	97900	390	436	-	16	382	Cenomano-Turonian
108/52	123750	99100	460	427.35	-	-	-	Cenomano-Turonian
816/52	121500	98500	430	404.5	-	-	-	Cenomano-Turonian
822/52	120000	101000	436	447.4	-	20.5	759	Cenomano-Turonian
36	119100	99700	430	391	-	-	-	Cenomano-Turonian
821/52	119400	98150	416	405.5	-	-	-	Cenomano-Turonian
38	120700	97250	424	397	-	-	-	Cenomano-Turonian
39	120750	96800	430	401	-	-	-	Cenomano-Turonian
40	121600	96100	450	418.58	-	-	-	Cenomano-Turonian
41	122150	96450	458	446.9	-	-	-	Cenomano-Turonian
43	121850	95900	465	449.7	-	-	-	Cenomano-Turonian
805/52	126150	99250	519	501.6	-	21	990	Cenomano-Turonian

Campaign of june 1995: Plio-Quaternary Aquifer

Sample	X	Y	Z	H	pH	T	EC	Aquifer
	m					°C	µS/cm	
3/51	81472	93666	7	3.8	-	19	2550	Plio-Quaternary
11/51	80383	96193	3	-1.8	-	18	4830	Plio-Quaternary
15/51	85890	97935	65	47.6	-	-	-	Plio-Quaternary
27/51	95370	91109	201	156.9	-	21	2000	Plio-Quaternary
105/51	99402	100883	114	105.1	-	-	-	Plio-Quaternary
125/51	93741	93786	152	90.5	-	24	3330	Plio-Quaternary

Sample	X	Y	Z	H	pH	T	EC	Aquifer
	m					°C	µS/cm	
138/51	88289	92860	105	79.8	-	21	3960	Plio-Quaternary
140/51	87205	103776	60	50.3	-	19	2700	Plio-Quaternary
148/51	85703	102084	58	14.3	-	-	-	Plio-Quaternary
149/51	85100	105800	36	-2.3	-	22	3580	Plio-Quaternary
327/51	89220	88690	124	95.8	-	21.5	1870	Plio-Quaternary
134/51	91990	97737	106	67.3	-	-	-	Plio-Quaternary
13/51	86225	102800	60	32.6	-	-	-	Plio-Quaternary
20/51	88150	96050	92	66.3	-	-	-	Plio-Quaternary
33/51	96800	96750	164	82.2	-	21	2340	Plio-Quaternary
93/51	92370	101900	98	66.7	-	21.5	2150	Plio-Quaternary
101/51	94570	101850	100	69.9	-	-	-	Plio-Quaternary
106/51	100600	100550	118	108.6	-	-	-	Plio-Quaternary
116/51	100650	96000	200	178	-	22	2610	Plio-Quaternary
128/51	93250	98250	120	65	-	-	-	Plio-Quaternary
129/51	90275	102950	66	50.4	-	-	-	Plio-Quaternary
131/51	91800	99600	97	69.2	-	-	-	Plio-Quaternary
132/51	89750	98500	99	60.6	-	15.5	2580	Plio-Quaternary
260/51	96600	100750	115	78.5	-	20.5	2090	Plio-Quaternary
261/51	96420	99250	124	89.9	-	23	2000	Plio-Quaternary
272/51	97170	100000	105.5	79.3	-	20.5	2280	Plio-Quaternary
278/51	90800	103400	72	57.7	-	-	-	Plio-Quaternary
376/51	95350	88650	270	221.4	-	-	-	Plio-Quaternary

Campaign of september 1990: Plio-Quaternary Aquifer

Sample	X	Y	Z	H	pH	T	EC	Aquifer
	m					°C	µS/cm	
3/51	81472	93666	7	2.4	8.05	20	3104	Plio-Quaternary
11/51	80383	96193	3	-1.03	8.31	19	1274	Plio-Quaternary
15/51	85890	97935	65	60.15	7.73	16	4434	Plio-Quaternary
27/51	95370	91109	201	169.52	-	-	-	Plio-Quaternary
28/51	97284	91810	234	184.65	7.94	23	3991	Plio-Quaternary
53/51	92700	104180	73	58.33	-	-	-	Plio-Quaternary

Sample	X	Y	Z	H	pH	T	EC	Aquifer
	m					°C	µS/cm	
103/51	94830	102206	91	62.55	-	-	-	Plio-Quaternary
105/51	99402	100883	114	102.73	8.08	22	1850	Plio-Quaternary
125/51	93741	93786	152	94.55	8.01	25	4212	Plio-Quaternary
137/51	86733	94515	81	62.2	8.06	22	4101	Plio-Quaternary

Campaign of september 1990: Plio-Quaternary Aquifer

Sample	X	Y	Z	H	pH	T	EC	Aquifer
	m					°C	µS/cm	
138/51	88289	92860	105	79.86	7.8	21.5	5654	Plio-Quaternary
140/51	87205	103776	60	50.21	8.16	19.5	2328	Plio-Quaternary
148/51	85703	102084	58	25.65	8.2	21	1197	Plio-Quaternary
149/51	85100	105800	36	-2.67	8.25	22	4268	Plio-Quaternary
327/51	89220	88690	124	91.15	7.81	22	4711	Plio-Quaternary
134/51	91990	97737	106	67.4	-	-	-	Plio-Quaternary
21/51	89582	91439	128	100.81	7.66	20	5654	Plio-Quaternary
20/51	87750	95925	92	66.48	7.88	21	3547	Plio-Quaternary
33/51	97000	97000	150	86	7.9	22	2993	Plio-Quaternary
90/51	93450	103700	88	70.1	8.37	20.5	1796	Plio-Quaternary
91/51	94050	102750	86	62.9	-	-	-	Plio-Quaternary
93/51	92300	101950	96	66.9	-	-	-	Plio-Quaternary
101/51	94575	101850	100	71	8.4	21	1674	Plio-Quaternary
104/51	97400	99750	115	78.2				Plio-Quaternary
116/51	100725	96000	200	178.62	7.9	22.5	3048	Plio-Quaternary
117/51	100500	98450	180	136.42	8	22	1219	Plio-Quaternary
127/51	93750	97250	125	73.99	7.95	19.5	4545	Plio-Quaternary
128/51	93250	98200	120	73.67	-	-	-	Plio-Quaternary
129/51	90275	102950	66	51.42	-	-	-	Plio-Quaternary
131/51	91400	99300	97	69.3	8.1	18	1252	Plio-Quaternary
132/51	89300	98300	99	60.6	8.55	15	3104	Plio-Quaternary
147/51	82900	94650	35	16.94	8.51	20	1208	Plio-Quaternary
272/51	97170	100000	105.5	76.4	8.55	21	1452	Plio-Quaternary
278/51	90800	103400	72	59.26	-	-	-	Plio-Quaternary

Sample	X	Y	Z	H	pH	T	EC	Aquifer
	m					°C	µS/cm	
324/51	87500	103400	80	47.15	-	-	-	Plio-Quaternary
376/51	95350	88650	270	222.65	8.09	21.5	1773	Plio-Quaternary
377/51	97350	90350	252	238.8	8.08	20.5	2017	Plio-Quaternary

Campaign of august 1976: Barremian-Aptian Aquifer

Sample	X	Y	Z	H	pH	T	EC	Aquifer
	m					°C	µS/cm	
173/51	91073	77100	289	272.21	-	-	-	Barremian-Aptian
175/51	93600	74914	351	330.42	-	-	-	Barremian-Aptian
176/51	96737	76130	423	423	-	-	-	Barremian-Aptian
181/51	83495	77133	161	159.6	-	-	-	Barremian-Aptian
209/51	80229	73441	141	137.18	-	-	-	Barremian-Aptian
208/51	80513	72537	221	215.8	-	-	-	Barremian-Aptian
216/51	83750	80350	174	170.65	-	-	-	Barremian-Aptian
205/51	78850	72500	162	159.93	-	-	-	Barremian-Aptian
207/51	78750	72500	120	118.53	-	-	-	Barremian-Aptian
210/51	80200	73450	100	98.33	-	-	-	Barremian-Aptian
213/51	79250	76225	154	151.5	-	-	-	Barremian-Aptian
215/51	84100	76550	157	155.9	-	-	-	Barremian-Aptian

Campaign of august 1976: Hautrivian Aquifer

Sample	X	Y	Z	H	pH	T	EC	Aquifer
	m					°C	µS/cm	
163/52	93398	63491	164	149.85	-	-	-	Hauterivian
165/51	94198	68475	287	278.55	-	-	-	Hauterivian
192/51	94413	68601	287	281.55	-	-	-	Hauterivian
187/51	90798	68298	288	283.25	-	-	-	Hauterivian
161/51	94700	63550	175	168.9	-	-	-	Hauterivian
166/51	94600	68600	307	291.05	-	-	-	Hauterivian
167/51	94600	64450	303.75	296.52	-	-	-	Hauterivian
188/51	92100	68200	333	329.93	-	-	-	Hauterivian
190/51	88950	64200	132	132	-	-	-	Hauterivian

Sample	X	Y	Z	H	pH	T	EC	Aquifer
	m					°C	µS/cm	
193/51	87450	63600	110	104.42	-	-	-	Hauterivian
194/51	96750	63750	85	85	-	-	-	Hauterivian
195/51	85125	64050	91.6	84.33	-	-	-	Hauterivian
222/51	84900	64200	98	92.03	-	-	-	Hauterivian

About the author

Pr. BAHIR Mohammed

Graduate from Mohammadia School of engineers in 1980, got a PhD in 2002.
Full Professor at Cadi Ayyad University of Marrakesh.
Affiliated to Mohammed VI Polytechnic University, International Water Research Institute (IWRI) in Ben Guerir.
Director of the Department of Geology, Ecole Normale Supérieure, Cadi Ayyad University of Marrakesh.
Fields of interest: Hydrogeolgy, Isotopic Hydrology , Hydrochimie, Environment, Geophysics.

Scientific impact :
Scopus https://www.scopus.com/authid/detail.uri?authorId=6505780720
iDorcid http://orcid.org/0000-0003-0041-9832o
Google Scholar https://scholar.google.fr/citations?user=VUa78DUAAAAJ&hl=fr

About the book

This book is a compilation of hydrogeological, hydro-geochemical, isotopic and climatic data over 40 years in the Essaouira basin. The latter includes eight aquifers out of the 80 that are dispersed throughout the country. The impact of climate change in Morocco has been evaluated for this basin to see the prospects of the state of the resource both on the quantitative and qualitative levels. This study extends from 1980 to 2022 and includes the most severe periods of drought that Morocco has experienced, including 1995, the driest year of the last century. It synthesizes my research work, from the end of studies project at the Mohammadia School of Engineering (1979/1980) to the theses I supervised in 1991, 1993, 1997, 2001, 2009, 2014, 2020 and 2022.